MITIGATION OF NONLINEAR IMPAIRMENTS FOR ADVANCED OPTICAL MODULATION FORMATS

Carsten Behrens

A thesis submitted to University College London for the degree of
Doctor of Philosophy (Ph.D.)
in Electronic and Electrical Engineering

Department of Electronic and Electrical Engineering
University College London

August 2012

I, Carsten Behrens confirm that the work presented in this thesis is my own. Where information has been derived from other sources, I confirm that this has been indicated in this thesis.

To my parents, my sister and to Julia

ABSTRACT

Optical fibre networks form the backbone of the global communication infrastructure but are currently experiencing an unprecedented level of stress due to more and more bandwidth-hungry applications. In an effort to address this and avoid a so-called *capacity crunch*, research groups around the world have focused their attention on more spectrally-efficient modulation formats, to increase available capacity at a competitive cost. However, the drive towards higher- order modulation formats leads to greater transmission impairments, reducing the maximum distance over which increased capacity can be provided.

The thesis describes the research work carried out to investigate the achievable transmission distances when using higher order modulation formats together with digital backpropagation (DBP). DBP is a digital signal processing (DSP) algorithm, capable of compensating for deterministic nonlinear impairments by inverting the fibre channel. Single-channel and wavelength-division-multiplexed (WDM) transmission has been investigated in experiment and simulation for a variety of polarisation-division-multiplexed (PDM) modulation formats: binary-phase-shift-keying (PDM-BPSK), quadrature-phase-shift-keying (PDM-QPSK), 8-phase-shift-keying (PDM-8PSK), 8-quadrature amplitude modulation (PDM-8QAM), 16-quadrature amplitude modulation (PDM-16QAM) and polarisation-switched QPSK (PS-QPSK).
Record transmission distances were achieved in WDM transmission experiments with PDM-BPSK, PS-QPSK and PDM-QPSK at 42.9Gbit/s as well as for PDM-8PSK and PDM-8QAM at 112Gbit/s, over the most common fibre type: standard single mode fibre (SSMF) and the most common amplification solution: erbium doped fibre amplifiers (EDFA). For the first time, nonlinear compensation has been compared experimentally for different modulation formats and a fixed-complexity DBP algorithm. Its use led to increased benefit for more spectrally efficient modulation formats.
Computer simulations were used to explore the upper bounds of achievable performance improvement with DBP, using an algorithm with unconstrained complexity. Furthermore, DBP was investigated for varying symbol rates and channel spacings to investigate trade-offs with respect to the digital receiver bandwidth.

It was shown that even though DBP is computationally expensive, it can achieve significant improvements in transmission reach and BER performance. The results presented in this thesis, can be applied to the design of future optical transmission systems.

ACKNOWLEDGEMENTS

First and foremost I would like to thank my supervisor Prof. Polina Bayvel for having given me the opportunity to pursue my PhD at the Optical Networks Group at UCL. I'm deeply grateful for the excellent guidance and steadfast support I received during this time. Her continued interest and incredible patience in face off closing deadlines helped me to explore limits I was previously unaware of and gain the maximum out of my time at the Optical Networks Group.

I would equally like to thank my other two supervisors for their support: Dr. Robert Killey for the help with the numerical simulations and discussions on nonlinear transmission effects and Dr. Seb Savory for his expertise on digital signal processing and coherent communication systems.

I also thank Dr. Sergeys Makoveys, Dr. David Millar and Domaniç Lavery not only for their always professional help without which a large proportion of this work would not have been possible, but for their friendship, which I'm deeply grateful for. In particular, I thank Sergey for providing the data for 112Gbit/s PDM-16QAM transmission in section 4.4 and introducing me to Pinot Noir – a truly excellent vine, David for countless fruitful discussions on highly sophisticated topics like four-dimensional modulation formats and the quality of English football players and Domaniç for his unwavering support during the experiments and an introduction to particle theory.

I would also like to thank Dr. Benn Thomsen for his help in the lab and numerous lessons in physics, Dr. Jose Mendinueta for his help with Linux related issues as well as Dr. Yannis Benlachtar for discussions on OFDM systems. I would like to acknowledge funding provided by Huawei Technologies and the European Commission's FP7 BONE project.

I could not finish without thanking Julia Klemm for her encouragement and patience during all these years. Her understanding and support contributed a great deal to the completion of this work. Finally, I would like to thank my parents Evelyn and Manfred Behrens and my sister Susan for their care and love during this period of my life.

CONTENTS

LIST OF FIGURES

Chapter 1

Chapter 2

Chapter 3

Chapter 4

Chapter 5

Chapter 6

Chapter 7

LIST OF TABLES

Chapter 1

Chapter 2

Chapter 3

Chapter 4

Chapter 5

Chapter 1

INTRODUCTION

1.1 Maximising Capacity in Optical Transport Networks

Global communication infrastructure based on optical networks is essential for the economic and cultural development of modern societies. The computer networks that form the basis of this infrastructure are interconnected by optical fibres [1], which provide a high bandwidth whilst being immune to electro-magnetic interference and, therefore, a cost effective solution to transmit large amounts of information.

Up until recently most optical transmission systems, terrestrial or submarine, were operating at line rates of 10 or 40Gbit/s based on direct-detection on-off-keying (OOK) or differential-detection phase-shift keying (DPSK). In both cases the electrical signal is modulated onto a laser carrier, transmitted in the optical domain and converted back into the electrical domain. The traditional form of detection has been incoherent square law detection with a photodiode, which leads to the loss of the absolute phase-, as well as polarization information. As a consequence, linear transmission impairments (see section 2.1) such as chromatic dispersion and PMD have to be compensated in the optical domain with dispersion compensating fibre (DCF) along the link and by optical filter compensators at the receiver. Furthermore, OOK and DPSK are binary modulation formats, encoding only a single bit per symbol. This comparatively low spectral efficiency limits the capacity per wavelength channel to the modulation speed and the electrical bandwidth of transmitter and receiver electronics (current commercially available optical modulators and photodiodes have bandwidths of ~30GHz [2] and ~100GHz [3], respectively).

Following the invention of the EDFA in 1987 [4] it became possible to amplify vast wavelength regions (in silica typically 30nm) around transmission wavelengths of

commercially available lasers (C-, L- and S- band – see section 2.1.1) in a cost effective way. This triggered the widespread implementation of wavelength-division-multiplexed (WDM) systems, which fill up the available optical bandwidth with WDM channels in order to increase system capacity. This technology guaranteed that increasing capacity demands could be met for more than a decade.

However, with the advent of broadband internet access and the smart phone in recent years, bandwidth-hungry multi-media applications such as social networking pages or video on demand have become ubiquitous. Consequently, internet traffic continues to grow at a nearly exponential pace (see Figure 1), exposing current backhaul and core networks to an unprecedented level of stress. The search for a solution to the predicted "capacity crunch" [5] led to a renewed interest in alternative approaches to system design, including the use of higher-order modulation formats, enabled by coherent detection.

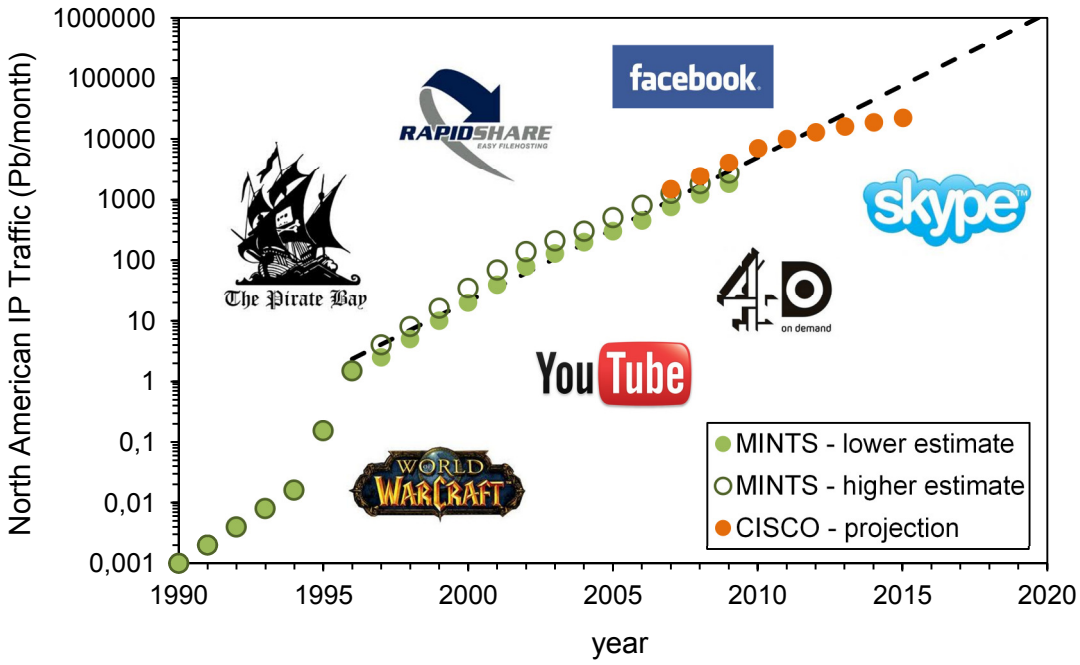

Figure 1: Exponential internet traffic growth over the last two decades and important drivers [6, 7]. IP traffic doubles nearly every 16 months

Although the coherent optical receiver was subject of much research in the late 1980s and early 1990s, no significant progress had been made until 2007. However, after the burst of the Dot-Com bubble in 2000 and because the arrival of 40Gbit/s systems proved slower than expected, the emphasis on reducing the cost per bit grew, necessitating the use of lower bandwidth components and research into the coherent systems intensified again. The result of this research effort is the digital coherent

receiver, which allows detecting in-phase and quadrature components of both polarisations and, therefore, instantly doubles the available capacity and spectral efficiency. Furthermore, it provides access to the entire optical field in the digital domain, which allows compensating for linear impairments of the optical channel by employing powerful DSP algorithms (see section 3.3). Virtually unlimited amounts of chromatic dispersion and PMD can now be compensated digitally allowing for significant cost reductions [8], because dispersion compensating modules, optical filter compensators and half the number of the EDFAs per link could be saved. Another advantage is the resultant reduction of inter-channel nonlinear effects due to the averaging out of nonlinear distortion, arising from the high values of accumulated dispersion in the absence of optical dispersion compensation. In addition, coherent detection offers better scaling characteristics at increased line rates compared to alternative solutions such as differential direct-detection, and increased flexibility, because of its ability to select a wide range of wavelength channels by tuning the local oscillator. However, DSP algorithms require a significant number of logic gates when implemented on an application specific integrated circuit (ASIC) in complementary metal oxide semiconductor technology (CMOS) as demonstrated by Sun et al. [9] (20 million gates in 90nm CMOS). Under these circumstances power dissipation becomes an important figure of merit ([9]: 21W for the ASIC and 140W for the entire transceiver card).

Probably the most important advantage of coherent detection is the ability to detect higher-order modulation formats such as PDM-QPSK [10], PDM-8PSK [11], PDM-8QAM [12], PDM-16QAM [13] and PDM-36QAM [14]. These modulation formats use all the possible degrees of freedom offered by an optical wave to encode information, employing IQ-modulators to access in-phase and quadrature components in both polarisations [15], utilising the available bandwidth much more efficiently than binary modulation formats and, therefore, allowing to boost capacity without the requirement for installing new fibre. Figure 2 shows the overall capacity of the most important optical transmission system experiments of the last decade. Interestingly, maximum available capacity doubles every 18 months and is almost able to keep up with IP traffic growth that doubles every 16 months as shown in Figure 1. In 2004 the first high-capacity QPSK demonstrations were reported (initially employing balanced detection [16]), achieving similar capacities to previous lab experiments using only binary modulation formats [17]. QPSK dominated high capacity systems for 5 years, when 8QAM entered the scene for the first time matching the available capacity of QPSK systems. Since then, further increases of capacity have only been possible by resorting

to even more spectrally efficient formats like 36QAM and 128QAM. Note that a capacity of 305Tb/s has recently been demonstrated by using PDM-QPSK and a 19-core fibre [18]. However, in this work only transmission in a single fibre core is considered, neglecting spatial-division-multiplexing (SDM).

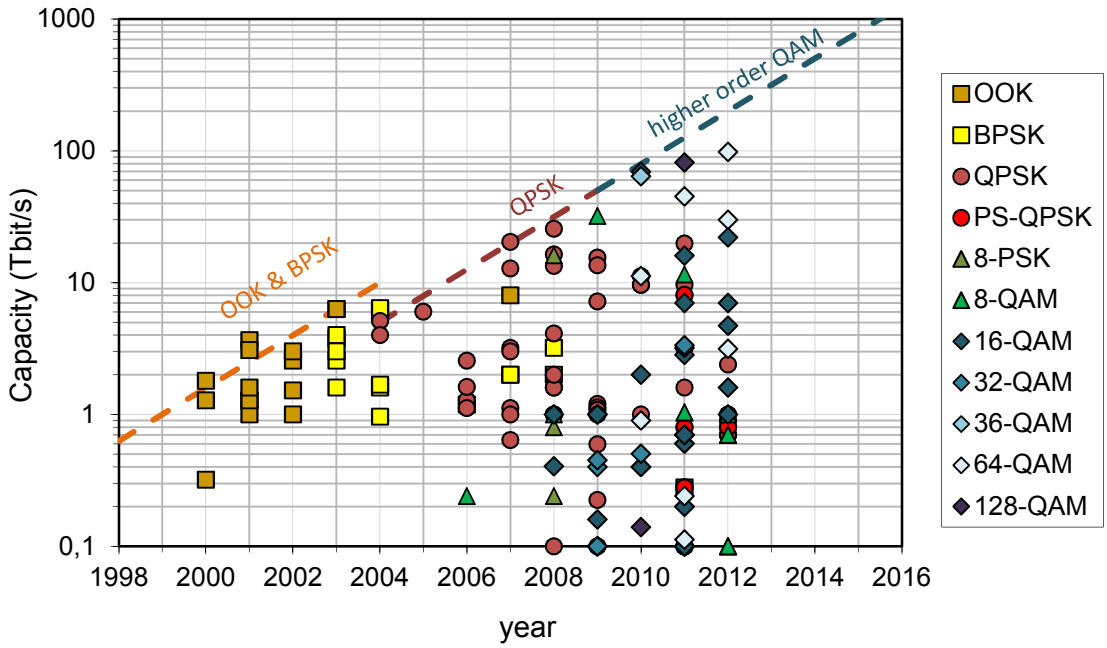

Figure 2: The maximum capacity of experimental optical communication systems has doubled every 18 months for more than a decade.

The use of denser constellation diagrams renders higher-order modulation formats more susceptible to circularly-symmetric Gaussian noise as generated by EDFAs along the transmission link. Even though the launch power per wavelength channel can be increased to improve the signal-to-noise ratio at the receiver, transmission is limited by nonlinear distortions due to the Kerr effect, which have a more severe impact on higher-order modulation formats. As a consequence transmission reach is inevitably sacrificed at the expense of increased capacity, when using more spectrally efficient modulation formats, as opposed to e.g. DPSK. Figure 3 illustrates this dilemma by showing the capacity distance product of the most important transmission experiments since the year 2000. Whilst capacity doubles every 1.5 years as found in Figure 2, equivalent capacity distance product doubles only every ~5 years, indicating that the increased capacity can only be delivered over much shorter distances.

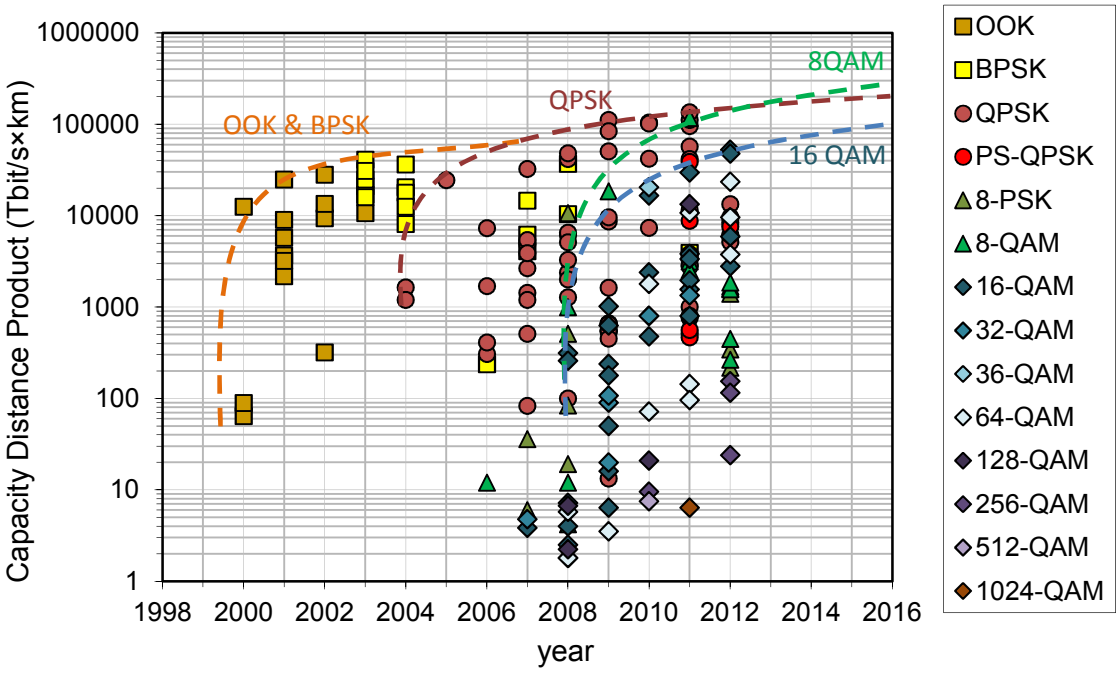

Figure 3: Achieved capacity distance product for experimental optical communication systems during the last decade. Capacity distance product doubles only every 5 years due to nonlinear limitations.

So, the most pressing question of current optical communications research is: how to maximise the transmission reach, whilst increasing the capacity of current optical transport networks by using spectrally-efficient modulation formats? The search for the answers to this question formed the basis of this PhD research.

While ASE-noise cannot be compensated for due to its random nature, nonlinear distortions through the Kerr effect are deterministic and, therefore, predictable. Receiver-based nonlinear compensation can be performed in the digital domain by deploying powerful DSP algorithms, such as digital backpropagation (DBP), which has recently been proposed to overcome nonlinear impairments by emulating the inverse optical channel response [19-21].

The research described in this PhD thesis focused on the investigation of DBP. The aim was to quantify possible transmission reach improvements for a variety of higher-order modulation formats. Even though WDM transmission has previously been restricted by the ITU to fixed channel spacings, typically 50GHz and 100GHz, it is foreseeable that this traditional solution will be surpassed by the adoption of a new *flexigrid* approach in the near future [22]. Thus, the thesis research was not restricted to the ITU-grid, but considered the transmission performance and DBP improvement for reduced frequency spacings and symbol-rates. Several DBP regimes were considered, ranging from a fixed complexity per distance solution, which has been experimentally investigated to ideal multi-channel backpropagation with high

complexity studied by means of extensive computer simulations. It is worthwhile to note that transmitter side nonlinear compensation has also been demonstrated [23]. However, with the advent of the digital coherent receiver it is beneficial to place the compensation entirely at the receiver to reduce the overall system complexity and maintain flexibility in the face of varying channel conditions, avoiding the necessity to loop back information to the transmitter.

The rest of the thesis is organised as follows:

Chapter 2 details the theory of the optical channel by describing linear transmission distortions such as attenuation, chromatic dispersion, PMD and ASE noise as well as nonlinear transmission distortions, such as SPM, XPM, FWM, XPolM and Gordon-Mollenhauer noise. The split-step Fourier method, combined with the waveplate model, serves as a model of optical fibre transmission and is described in this chapter.

Chapter 3 describes the transmitter and receiver structures and DSP algorithms for chromatic dispersion compensation, equalisation and phase recovery of PDM-BPSK, PS-QPSK, PDM-QPSK, PDM-8PSK, PDM-8QAM and PDM-16QAM. Additionally, it includes a section about receiver based digital backpropagation with a literature review on the topic.

Chapter 4 describes long-haul and ultra-long haul transmission results obtained for the aforementioned modulation formats in experiment and simulation. After a description of the experimental setup, the simulation environment developed in MATLAB, in the course of the PhD research, is described. Both back-to-back and ultra-long-haul single-channel and WDM transmission results for PDM-BPSK, PS-QPSK and PDM-QPSK at a line rate of 42.9Gbit/s are described. Back-to-back and long haul single channel and WDM transmission results of 112Gbit/s PS-QPSK, PDM-QPSK, PDM-8PSK, PDM-8QAM and PDM-16QAM are presented with and without DBP, supported by simulation results for both back-to-back and over the longest transmission distances achieved.

Chapter 5 presents simulation results on the nonlinear transmission performance of previously investigated modulation formats at varying symbol rates and wavelength spacings, whilst keeping the spectral efficiency constant for every modulation format. In this chapter the system is assumed to be unconstrained in terms of algorithm complexity and optimum settings for the DBP algorithm are investigated. In the following, two scenarios for DBP are compared: central channel DBP and a fixed bandwidth approach covering 100GHz of the optical spectrum.

Finally, conclusions are drawn in Chapter 6. These are based on the obtained results described in chapter 4 and 5 and potential research fields for future work are discussed. The Appendix describes a perturbation approach to the nonlinear Schrödinger equation which provides an analytical estimation of the influence of intra channel four-wave mixing.

1.2 Key achievements

The following original contributions to the field of optical communications have been made in the course of this research:

- Section 4.3 outlines the first experimental demonstration of the 4-dimensional modulation format PS-QPSK for optical long-haul transmission at 42.9Gbit/s [24] . PS-QPSK was compared to PDM-QPSK and PDM-BPSK at the same bit rate, achieving record transmission distances for all three modulation formats on standard single mode fibre employing EDFA amplification [25, 26].

- Section 4.4 and 5.4 describes work that demonstrated for the first time that higher order modulation formats experience a higher gain from digital backpropagation by means of computer simulations [27, 28] and in lab experiments investigating the transmission characteristics of several higher order modulation formats [29, 30] [31, 32]. As part of this work, record transmission distances have been achieved for PDM-8PSK and PDM-8QAM on standard single mode fibre employing EDFA amplification [31]. Furthermore, PS-QPSK was demonstrated for the first time at a line rate of 112Gbit/s with and without the use of digital backpropagation [30]. The experimental investigation has been carried with the help of several colleagues: D. Lavery, S. Makovejs and D.S. Millar, while S. Hellerbrand has contributed to computer simulations in [29].

- Chapter 5 describes a detailed simulation study focussed on investigating the trade-off between inter- and intra-channel nonlinearities for a wide range of modulation formats [33, 34]. Furthermore, trade-offs between the two dominant factors limiting digital backpropagation: nonlinear signal-ASE interactions and uncompensated inter-channel nonlinearity are investigated for the first time in a fair comparison.

1.3 List of publications

1) D. Lavery, D.S. Millar, **C. Behrens**, B.C. Thomsen and S.J. Savory, "**Benefits of Reduced Bandwidth Electronics for Mitigating Backreflections in a Bidirectional 10Gbit/s Coherent WDM-PON**", submitted to the *European Conference of Optical Communications 2012*, Amsterdam, Netherlands, (2012)

2) **C. Behrens**, D. Lavery, R.I. Killey, S.J. Savory and P.Bayvel, "**Long-haul WDM transmission of PDM-8PSK and PDM-8QAM with nonlinear DSP**", *Proc. Optical Fiber Communication Conference 2012*, OM3A, Los Angeles, USA, (2012).

3) D. Lavery, **C. Behrens**, S.J. Savory, **"On the Impact of Backreflections in a Bidirectional 10 Gbit/s Coherent WDM-PON"**, *Proc. Optical Fiber Communication Conference 2012*, OTh1F.3, Los Angeles, USA, (2012).

4) D. Lavery, **C. Behrens**, S. Makovejs, D.S. Millar, R.I. Killey, S.J. Savory and P.Bayvel, "**Long-Haul Transmission of PS-QPSK at 100 Gb/s Using Digital Backpropagation**", *Photon. Technol. Lett.*, 24(3), pp. 176-178, (2011).

5) **C. Behrens**, D. Lavery, D.S. Millar, S. Makovejs, B.C. Thomsen, R.I. Killey, S.J. Savory and P.Bayvel, "**Ultra-long-haul transmission of 7×42.9Gbit/s PS-QPSK and PM-BPSK**", *Opt. Express*, 19(26), pp. B581-B586, (2011).

6) D. Lavery, **C. Behrens** and S.J. Savory, "**A Comparison of Modulation Formats for Passive Optical Networks**", *Opt. Express*, 19(26), pp. B836-B841, (2011).

7) **C. Behrens**, D. Lavery, D.S. Millar, S. Makovejs, B.C. Thomsen, R.I. Killey, S.J. Savory and P.Bayvel, "**Ultra-long-haul transmission of 7×42.9Gbit/s PS-QPSK and PM-BPSK**", *Proc. European Conference of Optical Communications 2011*, Mo.2.B.2, Geneva, Switzerland (2011); (Winner of the Best Student Paper Award ECOC 2011)

8) D. Lavery, **C. Behrens** and S.J. Savory, "**A Comparison of Modulation Formats for Passive Optical Networks**", *Proc. European Conference of Optical Communications 2011,* Tu.5.C.5, Geneva, Switzerland (2011).

9) **C. Behrens**, S. Makovejs, R.I. Killey, S.J. Savory, M. Chen and P.Bayvel, "**Pulse-shaping vs. Digital Backpropagation in 224Gbit/s PDM-16QAM Transmission**", *Opt. Express*, 19(14), pp. 12879-12884, (2011).

10) **C. Behrens**, R.I. Killey, S.J. Savory, M. Chen and P. Bayvel, "**Nonlinear Transmission Performance of Higher Order Modulation Formats**", *Photon. Technol. Lett.*, 23(6), pp. 377-379, (2011).

11) D.S. Millar, D. Lavery, S. Makovejs, **C. Behrens**, B.C. Thomsen, P. Bayvel and S.J. Savory, "**Generation and long-haul transmission of polarization-switched QPSK at 42.9 Gb/s**", *Opt. Express*, 19(10), pp. 9296-9302, (2011).

12) **C. Behrens**, R.I. Killey, S.J. Savory, M. Chen and P.Bayvel, "**Benefits of digital backpropagation in coherent QPSK and 16QAM fibre links**", *Proc. of SPIE 2010*, 7988, Article 79880S, (2011).

13) R.I. Killey and **C. Behrens**, "**Shannon's theory in nonlinear systems**", *Journal of Modern Optics*, 58(1), pp. 1-10, (2011).

14) **C. Behrens**, R.I. Killey, S.J. Savory, M. Chen and P. Bayvel, "**Nonlinear Distortion in Transmission of Higher Order Modulation Formats**", *Photon. Technol. Lett.*, 22(15), pp 1111-1113, (2010).

15) **C. Behrens**, R.I. Killey, S.J. Savory, M. Chen and P.Bayvel, "**Benefits of digital backpropagation in coherent QPSK and 16QAM fibre links**", *Proc. Asia Communications and Photonics Conference and Exhibition 2010*, pp. 359–360, Shanghai, China (2010).
(Winner of the Best Student Paper Award ACP 2010)

16) **C. Behrens**, R.I. Killey, S.J. Savory, M. Chen and P.Bayvel, "**Fibre Nonlinearities in WDM-Systems with Reduced Channel-Spacing and Symbol-Rate**", *Proc. European Conference of Optical Communications 2010*, poster P4.20, Torino, Italy (2010).

17) D.S. Millar, S. Makovejs, **C. Behrens**, S. Hellerbrand, R.I. Killey, P. Bayvel and S.J. Savory, "**Mitigation of Fiber Nonlinearity using a Digital Coherent Receiver**", *J. Sel. Top. Quantum Electron.*, 16(5), pp. 1217-1226, (2010).

18) S. Makovejs, D.S. Millar, D. Lavery, **C. Behrens**, R.I. Killey, S.J. Savory and P. Bayvel, "**Characterization of long-haul 112Gbit/s PDM-QAM-16 transmission with and without digital nonlinearity compensation**", *Opt. Express*, 18(12), pp. 12939-12947), (2010).

19) **C. Behrens**, R.I. Killey, S.J. Savory, M. Chen and P.Bayvel, "**Reducing the Impact of Intrachannel Nonlinearities by Pulse-Width Optimisation in Multi-level Phase-Shift-Keyed Transmission**", *Proc. European Conference of Optical Communications 2009*, paper 10.4.1, Vienna, Austria (2009).

20) P. Bayvel, **C. Behrens**, R.I. Killey, S. Makovejs, D.S. Millar and S.J. Savory, "**Coherent Electronic Compensation Techniques for Long-Haul Optical Fibre Transmission – Opportunities and Challenges**", *Proc. European Conference of Optical Communications 2009*, paper 10.7.2, Vienna, Austria (2009).

1.4 References

[1] K. C. Kao and G. A. Hockham, "Dielectric-Fibre Surface Waveguides for Optical Frequencies," *Proceedings of the Institution of Electrical Engineers-London,* vol. 113, pp. 1151-&, 1966.

[2] Fujitsu Optical Components Ltd. (2011, November). Available: http://jp.fujitsu.com/group/foc/downloads/services/100gln/ln100gdpqpsk-e-111102.pdf

[3] u2t photonics. (2012, April). Available: http://www.u2t.de/products/xpdv4120r

[4] R. J. Mears, L. Reekie, I. M. Jauncey, and D. N. Payne, "Low-Noise Erbium-Doped Fiber Amplifier Operating at 1.54-Mu-M," *Electronics Letters,* vol. 23, pp. 1026-1028, Sep 10 1987.

[5] A. Chraplyvy, "The coming capacity crunch," in *Proc. 35th European Conference on Optical Communication ECOC 2009*, Vienna, 2009, p. Mo1.0.2.

[6] University of Minnesota. (2009, August). *Minnesota Internet Traffic Studies (MINTS)*. Available: http://www.dtc.umn.edu/mints/home.php

[7] Cisco Visual Networking Index. (2011, June). Available: http://www.cisco.com/en/US/solutions/collateral/ns341/ns525/ns537/ns705/ns827/white_paper_c11-481360_ns827_Networking_Solutions_White_Paper.html

[8] S. J. Savory, G. Gavioli, V. Mikhailov, R. I. Killey, and P. Bayvel, "Ultra Long-Haul QPSK Transmission using a Digital Coherent Receiver," in *Proc. Digest of the IEEE LEOS Summer Topical Meetings*, 2007, pp. 13-14.

[9] H. Sun, K.-T. Wu, and K. Roberts, "Real-time measurements of a 40 Gb/s coherent system," *Optics Express,* vol. 16, pp. 873-879, 2008.

[10] M. Salsi, H. Mardoyan, P. Tran, C. Koebele, E. Dutisseuil, G. Charlet, and S. Bigo, "155x100Gbit/s coherent PDM-QPSK transmission over 7200km," in *Proc. 35th European Conference on Optical Communication ECOC 2009*, 2009, p. PD2.5.

[11] J. Yu, X. Zhou, M.-F. Huang, Y. Shao, D. Qian, T. Wang, M. Cvijetic, P. Magill, L. Nelson, M. Birk, S. Ten, H. B. Matthew, and S. K. Mishra, "17 Tb/s (161x114 Gb/s) PolMux-RZ-8PSK transmission over 662 km of ultra-low loss fiber using C-band EDFA amplification and digital coherent detection," in *Proc. 34th European Conference on Optical Communication ECOC 2008*, 2008.

[12] X. Zhou, J. Yu, M.-F. Huang, T. S. Y., P. Magill, M. Cvijetic, L. Nelson, M. Birk, G. Zhang, S. Ten, H. B. Mattew, and S. K. Mishra, "32Tb/s (320x114Gb/s) PDM-RZ-8QAM transmission over 580km of SMF-28 ultra-low-loss fiber," in *Proc. Conference on Optical Fiber Communication and the National Fiber Optic Engineers Conference OFC/NFOEC 2009*, 2009.

[13] A. H. Gnauck, P. J. Winzer, S. Chandrasekhar, X. Liu, B. Zhu, and D. W. Peckham, "10 x 224-Gb/s WDM Transmission of 28-Gbaud PDM 16-QAM on a

50-GHz Grid over 1200km of Fiber," in *Proc. Conference on Optical Fiber Communication OFC '10*, 2010, p. PDPB.

[14] X. Zhou, J. Yu, M. Huang, Y. Shao, T. Wang, L. Nelson, P. Magill, M. Birk, P. I. Borel, D. W. Peckham, and R. Lingle, "64-Tb/s (640 x 107-Gb/s) PDM-36QAM transmission over 320km using both pre- and post-transmission digital equalization," in *Proc. Conference on Optical Fiber Communication and the National Fiber Optic Engineers Conference OFC/NFOEC 2010*, 2010, p. PDPB9.

[15] S. Shimotsu, S. Oikawa, T. Saitou, N. Mitsugi, K. Kubodera, T. Kawanishi, and M. Izutsu, "Single Side-Band Modulation Performance of a LiNbO3 Integrated Modulator Consisting of Four-Phase Modulator Waveguides," *Photonics Technology Letters,* vol. 13, pp. 364-366, April 2001.

[16] N. Yoshikane and I. Morita, "160 % Spectrally-Efficient 5.12 Tb/s (64x85.4 Gb/s RZ DQPSK) Transmission without Polarisation Demultiplexing," in *Proc. 30th European Conference on Optical Communication ECOC 2004*, 2004.

[17] G. Charlet, J.-C. Antona, S. Lanne, and S. Bigo, "From 2,100 km to 2,700 km distance using phase-shaped binary transmission at 6.3 Tbit/s capacity," in *Proc. Conference on Optical Fiber Communication and the National Fiber Optic Engineers Conference OFC/NFOEC 2003*, 2003, pp. 329-330.

[18] J. Sakaguchi, B. J. Puttnam, W. Klaus, Y. Awaji, N. Wada, A. Kanno, T. Kawanishi, K. Imamura, H. Inaba, K. Mukasa, R. Sugizaki, T. Kobayashi, and M. Watanabe, "19-core fiber transmission of 19x100x172-Gb/s SDM-WDM-PDM-QPSK signals at 305Tb/s," 2012, p. PDP5C.1.

[19] X. Li, X. Chen, G. Goldfarb, E. Mateo, I. Kim, F. Yaman, and G. Li, "Electronic post-compensation of WDM transmission impairments using coherent detection and digital signal processing," *Optics Express,* vol. 16, pp. 880-888, 2008.

[20] E. Ip and J. M. Kahn, "Compensation of dispersion and nonlinear effects using digital backpropagation," *Journal of Lightwave Technology,* vol. 26, pp. 3416-3425, 2008.

[21] G. Goldfarb, M. G. Taylor, and G. Li, "Experimental Demonstration of Fiber Impairment Compensation Using the Split-Step Finite-Impulse-Response Filtering Method," *Photonics Technology Letters,* vol. 20, pp. 1887-1889, 2008.

[22] O. Gerstel, M. Jinno, A. Lord, and S. J. B. Yoo, "Elastic optical networking: a new dawn for the optical layer?," *Communications Magazine, IEEE,* vol. 50, pp. s12-s20, 2012.

[23] K. Roberts, C. Li, L. Strawczynski, M. O'Sullivan, and I. Hardcastle, "Electronic precompensation of optical nonlinearity," *Photonics Technology Letters,* vol. 18, pp. 403-405, 2006.

[24] D. S. Millar, D. Lavery, S. Makovejs, C. Behrens, B. C. Thomsen, P. Bayvel, and S. J. Savory, "Generation and long-haul transmission of polarization switched QPSK at 42.9Gbit/s," *Optics Express,* vol. 19, pp. 9296-9302, 2011.

[25] C. Behrens, D. Lavery, D. S. Millar, S. Makovejs, B. C. Thomsen, R. I. Killey, S. J. Savory, and P. Bayvel, "Ultra-long-haul transmission of 7x42.9Gbit/s PS-QPSK and PM-BPSK," in *Proc. ECOC 2011*, Geneva, 2011, p. Mo.2.B.2.

[26] C. Behrens, D. Lavery, D. S. Millar, S. Makovejs, B. C. Thomsen, R. I. Killey, S. J. Savory, Bayvel, and P., "Ultra-long-haul transmission of 7x42.9Gbit/s PS-QPSK and PM-BPSK," *Optics Express,* vol. 19, pp. B581-B586, 2011.

[27] C. Behrens, R. I. Killey, S. J. Savory, M. Chen, and P. Bayvel, "Benefits of digital backpropagation in coherent QPSK and 16QAM fibre links," in *Communications and Photonics Conference and Exhibition (ACP), 2010* Shanghai, 2010, pp. 359-360.

[28] C. Behrens, R. I. Killey, S. J. Savory, M. Chen, and P. Bayvel, "Benefits of digital backpropagation in coherent QPSK and 16QAM fibre links," *Proc. of SPIE,* p. 79880S, 2011.

[29] D. S. Millar, S. Makovejs, C. Behrens, S. Hellerbrand, R. I. Killey, P. Bayvel, and S. J. Savory, "Mitigation of Fiber Nonlinearity using a Digital Coherent Receiver," *Journal of Selected Topics in Quantum Electronics,* vol. 16, pp. 1217-1226, 2010.

[30] D. Lavery, C. Behrens, S. Makovejs, D. S. Millar, R. I. Killey, S. J. Savory, and P. Bayvel, "Long-Haul Transmission of PS-QPSK at 100 Gb/s Using Digital Backpropagation," *Photonics Technology Letters,* vol. 24, pp. 176-178, February 2012.

[31] C. Behrens, D. Lavery, R. I. Killey, S. J. Savory, and P. Bayvel, "Long-haul WDM transmission of PDM-8PSK and PDM-8QAM with nonlinear DSP," in *Proc. Conference on Optical Fiber Communication and the National Fiber Optic Engineers Conference OFC/NFOEC 2012*, Los Angeles, 2012, p. OMA3A.4.

[32] S. Makovejs, D. S. Millar, D. Lavery, C. Behrens, V. Mikhailov, G. Gavioli, Killey, R.I., Savory, S.J., and P. Bayvel, "Characterization of long-haul 112Gbit/s PDM-QAM-16 transmission with and without digital nonlinearity compensation," *Optics Express,* 2010.

[33] C. Behrens, R. I. Killey, S. J. Savory, M. Chen, and P. Bayvel, "Fibre Nonlinearities in WDM-Systems with Reduced Channel-Spacing and Symbol-Rate," in *Proc. 36th European Conference on Optical Communication ECOC 2010*, 2010, p. P4.20.

[34] C. Behrens, R. I. Killey, S. J. Savory, M. Chen, and P. Bayvel, "Nonlinear Transmission Performance of Higher Order Modulation Formats," *Photonics Technology Letters,* vol. 23, pp. 377-379, 2011.

Chapter 2

THEORY OF OPTICAL FIBRE TRANSMISSION

This chapter presents the theory of the optical channel as well as the most important effects impairing transmission over it. After explaining linear impairments such as attenuation, chromatic dispersion, polarisation mode dispersion and ASE-noise, the attention of the reader is drawn to nonlinear impairments, which are caused by the Kerr effect.

2.1 Linear effects

This section focuses on effects which act linearly on the optical field, namely the attenuation, chromatic dispersion, polarisation mode dispersion and ASE-noise.

2.1.1 Attenuation

The simplest propagation equation for optical fibres takes only loss into account:

$$\frac{\partial A}{\partial z} + \frac{\alpha}{2} A = 0 \qquad (1)$$

A denotes the optical field, while α is the attenuation constant which describes the loss-characteristics of the fibre. A typical value of α for standard single mode fibres at 1550nm is around 0.046 km^{-1} corresponding to 0.2 dB/km ($\alpha_{dB} = 10 \log_{10}(e) \cdot \alpha \approx 4.34 \cdot \alpha$).

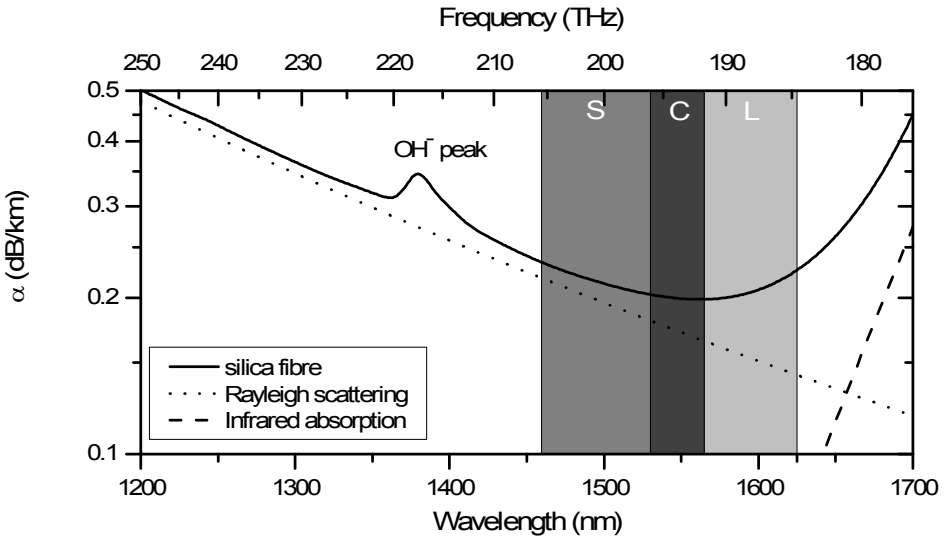

Figure 4: Loss profile of a typical standard mode fibre as a function of wavelength and frequency. S- (1460-1530nm), C- (1530-1565nm) and L-transmission bands (1565-1625nm) are highlighted.

The loss profile of an optical fibre is wavelength-dependent as shown in Figure 4. Major loss mechanisms are material absorption as well as Rayleigh scattering. Material absorption includes electronic resonances in the ultraviolet region and molecular resonances in the far-infrared region. Furthermore, impurities such as the OH ion cause vibrational resonances leading to absorption peaks such as around 1390nm. Rayleigh scattering stems from density fluctuations of the fused silica which results in fluctuations of the local refractive index. These intrinsic fluctuations cause the light to be scattered, especially at lower wavelengths. Additional loss mechanisms include micro- and macro-bending losses and the phosphorous absorption peak [1].

The International Telecommunication Union (ITU) has defined several transmission bands for the single mode fibre [2]. The most important ones lie around the attenuation minimum as shown in Figure 4: the S-band (short-wavelength) from 1460 to 1530nm, the C-band (conventional) from 1530 to 1565nm and the L-band (long-wavelength) from 1565 to 1625nm. The most prominent out of the three mentioned bands is the C-band since conventional erbium doped fibre amplifier (EDFA) provide amplification around 1545nm – right in the middle of the C-band.

2.1.2 Chromatic Dispersion

If equation (1) is extended with the propagation constant $\beta(\omega)$ it yields the linear Schrödinger equation (LSE). For convenience, β can be expanded around the carrier frequency into a Taylor series, which is truncated after the 3rd term [3]:

$$\frac{\partial A}{\partial z} + \frac{\alpha}{2}A + \beta_1 \frac{\partial A}{\partial t} + \frac{i}{2}\beta_2 \frac{\partial^2 A}{\partial t^2} - \frac{1}{6}\beta_3 \frac{\partial^3 A}{\partial t^3} = 0 \quad \textbf{(2)}$$

Here β_1 is related to the group velocity v_G and, therefore, determines at what speed the envelope of an optical pulse moves along the fibre:

$$\beta_1 = \frac{1}{v_G} = \frac{1}{c}\left(n + \omega \frac{dn}{d\omega}\right) \quad \textbf{(3)}$$

with c being the speed of light in vacuum, n the linear refractive index and ω the optical frequency. β_2 is the group-velocity dispersion (GVD) parameter, which is responsible for the broadening of a propagating pulse:

$$\beta_2 = \frac{1}{c}\left(2\frac{dn}{d\omega} + \omega \frac{d^2 n}{d\omega^2}\right) \quad \textbf{(4)}$$

The dispersion parameter D is defined as the first derivative of β_1 with respect to the optical wavelength λ:

$$D = \frac{d\beta_1}{d\lambda} = -\frac{2\pi c}{\lambda^2}\beta_2 \approx \frac{\lambda}{c}\frac{d^2 n}{d\lambda^2} \quad \textbf{(5)}$$

$\beta_3 = d\beta_2/d\omega$ is denoted as the GVD slope parameter, which is related to the dispersion slope parameter S:

$$S = \frac{d\beta_2}{d\lambda} = -\frac{4\pi c^2}{\lambda^3}\beta_2 + \left(\frac{2\pi c}{\lambda^2}\right)^2 \beta_3 \quad \textbf{(6)}$$

The GVD slope becomes especially important for transmission in the region of zero-dispersion wavelength ($\beta_2 = 0$).

For the sake of simplicity one might consider a modified version of equation (2). A retarded time frame $T = t - z/v_G$ is introduced, which moves with the signal at the group velocity eliminating β_1 from the equation. Furthermore, the influence of the GVD slope can be neglected considering standard single-mode fibres (SMF) or other types with sufficiently high GVD:

$$\frac{\partial A}{\partial z} + \frac{\alpha}{2}A + \frac{i}{2}\beta_2 \frac{\partial^2 A}{\partial T^2} = 0 \quad \textbf{(7)}$$

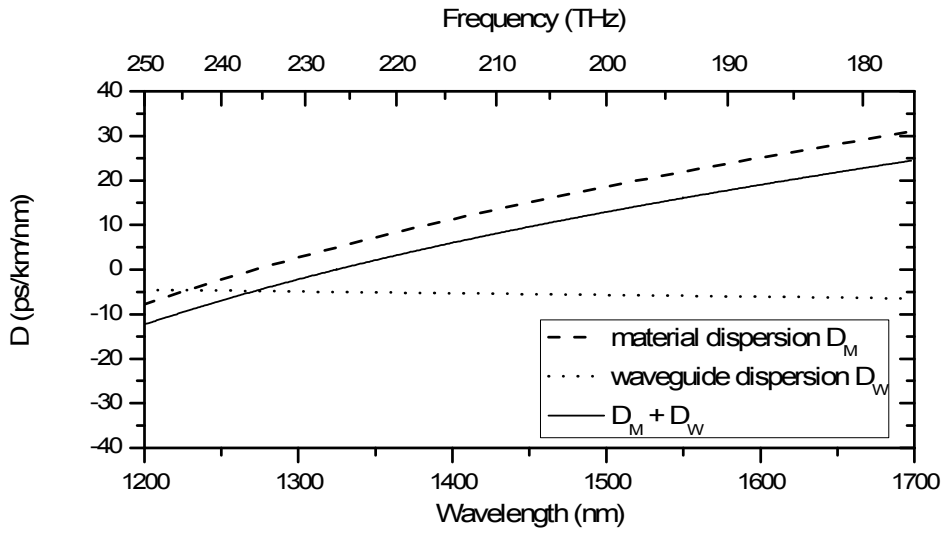

Figure 5: Dispersion characteristic of a typical standard single mode fibre as a function of wavelength and frequency. Material and waveguide dispersion influence the fibre dispersion.

The overall dispersion profile of an optical fibre is determined by the material dispersion D_M and by the waveguide dispersion D_W. In the case of standard single mode fibre the summation of those two parameters gives the dispersion profile shown in Figure 5, with the zero dispersion wavelength at 1324 nm and D=16ps/km/nm at 1550 nm. While the material dispersion cannot be changed for silica fibres, the waveguide dispersion can be modified since it depends on the effective refractive index, which is determined by the index profile of the fibre. By changing the index profile, different fibres such as dispersion compensating fibre (DCF) with D=-80ps/km/nm and non-zero dispersion shifted fibre (NZDSF) with D=4ps/km/nm can be manufactured. Note that low dispersion fibres like e.g. dispersion shifted fibre (DSF) facilitate nonlinear mixing processes due to better phase matching conditions along the propagation path.

2.1.3 Polarisation Mode Dispersion

Single-mode fibres support the transmission of two polarisation-modes that are orthogonal to each other. Temperature fluctuations and random birefringence due to mechanical stress cause the states-of-polarisation (SOP) and, therefore, the group velocity to vary with time and across the full length of the fibre [4]. The typical length scale over which the SOP variation occurs ranges from hundreds of metres up to a few kilometres. Mathematically, one can define modal birefringence, B_m as:

$$B_m = \frac{|\beta_x - \beta_y|\lambda}{2\pi} = |n_x - n_y| \qquad (8)$$

with n_x and n_y being the effective refractive index of both modes and β_x and β_y the equivalent propagation constants. The axis with larger group velocity is usually denoted as the fast axis while the axis with smaller group velocity is referred to as the slow axis.

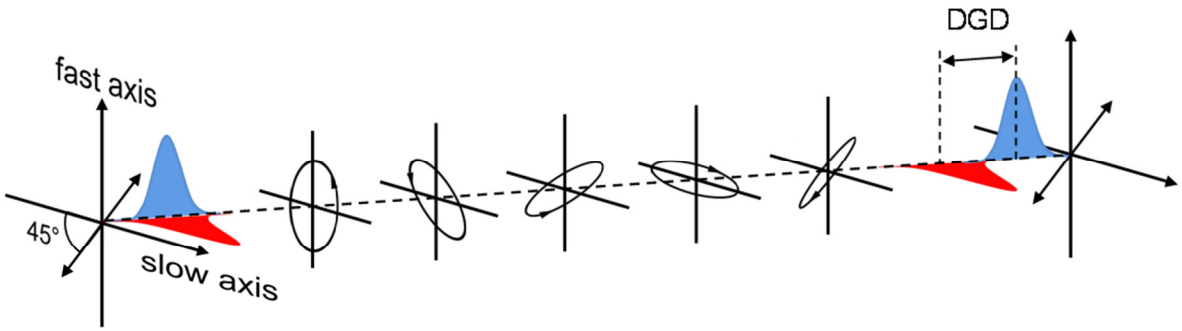

Figure 6: Random birefringence and resulting differential group delay for a pulse, which is launched into the fibre at a 45° with respect to the slow axis.

Consider a linearly polarised pulse, which is launched into a fibre at a 45 degree (pi/4 rad) angle with respect to the slow axis as shown in Figure 6. In this case, the pulse excites two orthogonal modes of equal power, one in the slow axis and one in the fast axis. Whilst propagating along the fibre the energy splits randomly between these two polarisation states and the receiver detects two pulses; one in each polarisation. The difference between the arrival-times of the two pulses is denoted as differential group delay $\Delta\tau$ (DGD) and exhibits a Maxwellian distribution around the mean DGD-value $\langle\Delta\tau\rangle$. The mean DGD scales with the square root of the fibre length and is directly related to the PMD parameter of the fibre, which typically varies between 0.01 and 0.5ps/$\sqrt{\text{km}}$:

$$\langle\Delta\tau\rangle = PMD \cdot \sqrt{L} \tag{9}$$

Note, that DGD is also referred to as first order polarisation mode dispersion (PMD), whereas second order PMD designates the frequency-dependence of DGD, which introduces additional signal distortion. Section 2.3 describes how statistical PMD can be modelled to simulate optical transmission systems.

2.1.4 ASE-noise

The dominant noise source in optical transmission systems is introduced by the EDFA (Erbium-Doped-Fibre-Amplifier), which is used to compensate for fibre loss as shown in Figure 7. Population inversion inside the EDFA leads to stimulated emission and amplification of the incoming signal. Unfortunately this process is associated with spontaneous emission, which generates ASE-noise (amplified-spontaneous-emission)

[5]. ASE-noise can be modelled as independent and identically distributed (i.i.d.) Gaussian random processes with zero mean, which impacts real and imaginary part of the optical signal in both polarisations. Considering the constellation of a modulation format, ASE leads to a symmetrical spread of the symbol points. Therefore the ASE-noise tolerance of a modulation format is dominated by the closest Euclidian distance between two symbol-points in the constellation.

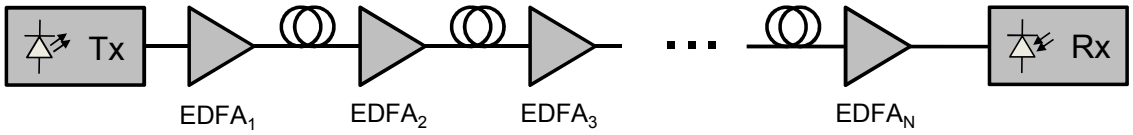

Figure 7: Schematic of an optical transmission link with EDFAs compensating for the fibre loss.

The noise power P_N added by an EDFA within the optical bandwidth B is given as follows:

$$P_{ASE} = 2n_{sp}(G-1)h\vartheta B \tag{10}$$

With G being the amplifier gain, h Plancks constant, ϑ the carrier frequency and n_{sp} the spontaneous emission factor which is related to the amplifiers noise figure NF:

$$n_{sp} = \frac{NF \cdot G}{2(G-1)} \tag{11}$$

The noise figure NF is defined as the ratio between input signal-to-noise-ratio (SNR) and output signal-to-noise ratio:

$$NF = \frac{SNR_{in}}{SNR_{out}} = \frac{P_{Sig}/P_N}{G \cdot P_{Sig}/(P_{ASE}+P_N)} \tag{12}$$

In optical communications the signal quality is usually expressed in terms of the optical signal to noise ratio (OSNR). The OSNR normalises the signal power to the signal bandwidth B_{Sig} and relates it to the ASE noise in both polarisations within a reference bandwdith B_{Ref} (usually 0.1nm or 12.5GHz):

$$OSNR = \frac{B_{Sig}}{2B_{Ref}} SNR \tag{13}$$

Assuming that the entire loss of the preceding span is ideally compensated by the following EDFA $\left(G = \alpha L_{Span}\right)$, the overall noise figure NF_{Link} of transmission systems with N spans and repeated EDFA amplification (see Figure 7) can be expressed as follows:

$$NF_{Link} = 1 + N\left(\alpha L_{Span} \cdot NF - 1\right) \tag{14}$$

Equation (14) illustrates the trade-off between the number of EDFAs N and the span length L_{Span} by showing that it is possible to reduce the overall noise figure of the link NF_{Link} with smaller EDFA spacing.

2.2 Nonlinear effects

By extending equation (7) to include nonlinear propagation effects, we obtain the nonlinear Schrödinger equation (NLSE) [3]:

$$\frac{\partial A}{\partial z} + \frac{\alpha}{2}A + \frac{i}{2}\beta_2 \frac{\partial^2 A}{\partial T^2} = i\gamma |A|^2 A \tag{15}$$

The refractive index of an optical fibre consists of a linear part n and a nonlinear part n_2, which depends on the optical intensity in the fibre (Kerr effect):

$$\tilde{n} = n + n_2 |A|^2 \tag{16}$$

The nonlinearity coefficient γ in equation (15) is related to n_2 and the effective core area A_{eff} by:

$$\gamma = \frac{n_2\, \omega}{c\, A_{eff}} \tag{17}$$

Typical values of γ range from 5 $W^{-1}km^{-1}$for DCF over 1.5 $W^{-1}km^{-1}$ for NZDSF to 1.2 $W^{-1}km^{-1}$ for SMF and 0.6 $W^{-1}km^{-1}$ for pure silica core large effective area fibre (PSCF).

We now decompose the optical field A in equation (7) into three interacting field-components A_0, A_1 and A_2, each describing a different WDM-channel with $\Delta\beta$ describing the phase relationship between them. To illustrate the influence of nonlinearity we restrict ourselves to small-signal distortions, and separate equation (7) into three coupled equations e.g. for WDM-channel A_0 [6]:

$$\frac{\partial A_0}{\partial z} + \frac{\alpha}{2}A_0 + \frac{i}{2}\beta_2 \frac{\partial^2 A_0}{\partial T^2} = \underbrace{i\gamma |A_0|^2 A_0}_{\text{SPM}} + \underbrace{2i\gamma (|A_1|^2 + |A_2|^2) A_0}_{\text{XPM}} + \underbrace{i\gamma \sum_{l,m\neq 0} A_l A_m A_{l+m}^* exp(i\Delta\beta z)}_{\text{FWM}} \tag{18}$$

Each nonlinear contribution on the right hand side describes a different nonlinear effect, depending on which WDM-channels are involved. In case of self-phase modulation (SPM), the nonlinear phase shift caused by the power of the WDM-channel

itself is considered, while cross-phase modulation (XPM) describes the nonlinear phase shift induced by the optical power of neighbouring channels. Four-wave mixing (FWM) describes a mixing process between WDM channels satisfying $k = l + m - n$.In equation (18) the focus lies on frequency components falling on WDM-channel $k = 0$, so that n can be set equal to $l + m$. In the following we shall concentrate on the first nonlinear term describing SPM.

2.2.1 Self-phase modulation (SPM)

If we assume single channel propagation as in section 4.3.2, 4.4.2 and 5.1 (no XPM and FWM as defined in equation (18)) and neglect chromatic dispersion, the solution to equation (18) has the following form:

$$A(z,T) = A(0,T)\exp\left(-\frac{\alpha}{2}z\right) exp(i\phi_{SPM}) \quad \textbf{(19)}$$

describing the exponential decay of the waveform due to fibre-loss, and the nonlinear phase-distortion ϕ_{SPM} due to the self-phase-modulation (SPM). The phase shift acquired due to SPM is dependent on the intensity profile of the waveform and is proportional to the optical power:

$$\phi_{SPM}(z,T) = \gamma L_{eff}|A|^2 \quad \textbf{(20)}$$

Furthermore, ϕ_{SPM} scales with L_{eff}, which takes into account the exponential decay of the power profile:

$$L_{eff} = \frac{1-\exp(-\alpha L)}{\alpha} \approx \frac{1}{\alpha} \quad \text{(for sufficiently long fibres)} \quad \textbf{(21)}$$

Note, that in absence of chromatic dispersion SPM does not change the pulse shape, while the interaction of SPM with dispersion results in pulse distortion due to PM-IM conversion of the phase distortion ϕ_{SPM}. In the latter case, the time dependant nonlinear phase shift induces carrier frequency fluctuations, which are referred to as chirp:

$$\delta\omega(T) = -\frac{\partial\phi_{SPM}(T)}{\partial T} \quad \textbf{(22)}$$

The chirp generates new frequency components leading to spectral broadening in dispersive media, increasing for fast pulse rise times since the shape of $\phi_{SPM}(T)$ is proportional to the pulse shape. In a response to the SPM phase shift the leading edge

of the pulses experiences a frequency reduction (red shift) and the trailing edge a frequency increase (blue shift). This is the property which is exploited in soliton systems, which aim at balancing the phase shift induced by chromatic dispersion with the nonlinear phase shift of SPM to achieve transmission with spatially invariant pulse shapes.

To gain insight into the SPM behaviour in the case of significant pulse overlap during transmission in single-mode fibre links without dispersion compensating fibre, we decompose the optical field A into three interacting field-components, similarly to equation (18). A_0, A_1 and A_2, now describes pulses of the same wavelength channel in the time domain with $\Delta\beta$ describing the phase relationship between them. Again, we can separate equation (18) into three coupled equations e.g. for A_0:

$$\frac{\partial A_0}{\partial z} + \frac{\alpha}{2}A_0 + \frac{i}{2}\beta_2\frac{\partial^2 A_0}{\partial T^2} = \underbrace{\underbrace{i\gamma|A_0|^2A_0}_{\text{ISPM}} + \underbrace{2i\gamma(|A_1|^2+|A_2|^2)A_0}_{\text{IXPM}} + \underbrace{i\gamma\sum_{l,m\neq 0} A_lA_mA_{l+m}^* exp(i\Delta\beta z)}_{\text{IFWM}}}_{\text{SPM}} \quad \textbf{(23)}$$

This mathematical trick helps us to separate SPM into intra-channel self-phase-modulation (ISPM), intra-channel cross-phase-modulation (IXPM) and intra-channel four-wave-mixing (IFWM), depending on which pulses are involved when generating a contribution to the nonlinear phase shift.

To illustrate the influence of SPM, Figure 8 (a) shows two Gaussian pulses at 160Gbit/s before and after transmission over one 80 km span of SMF. The average pulse power is 1 W to facilitate nonlinear distortions and chromatic dispersion and fibre loss is ideally compensated after transmission. It can be seen that ISPM and IXPM cause a spreading of the original pulses as described earlier, while IFWM generates ghost pulses (see Figure 8 (b)). The analytical solution based on perturbation analysis outlined in section 7.1 [7, 8] accurately predicts the generation of 1st order ghost pulses, but does not take into account 2nd order ghost pulses which are due to the interaction between a 1st order ghost pulse and an original pulse.

Note that ISPM and IXPM only depend on the intensity of the overlapping pulse, while the IFWM distortion includes the phase-information of neighbouring pulses. This has some interesting implications for RZ-phase-shift keyed transmission, where ISPM and IXPM do not impair the signal in a data-dependant manner, since the distortion is the

same for every pulse. Furthermore, the impact of IFWM reduces with the pulse-width as shown in section 7.1, but increases with symbol-rate (see section 5.1).

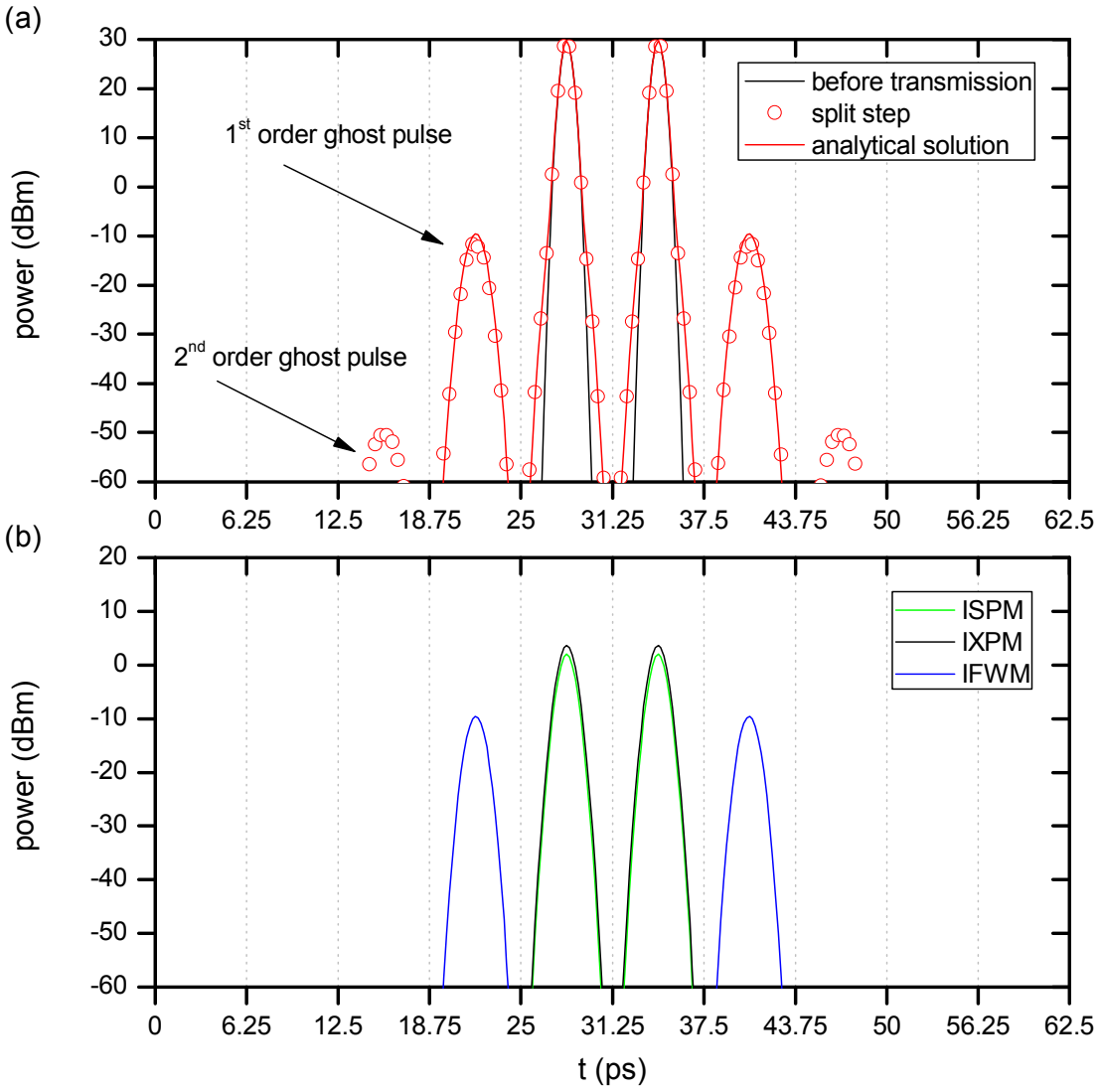

Figure 8: Two Gaussian pulses spaced 6.25 ps after transmission over an 80 km SMF span. Average pulse power is 1 W to facilitate the influence of nonlinearities. Figure (a) shows comparison between analytical solution based on the perturbation analysis and split-step Fourier method and (b) shows separate contributions of ISPM, IXPM and IFWM to the nonlinear distortion [9].

Let us now consider polarisation multiplexed transmission of a single wavelength channel. In this case we have to change equation (7) to:

$$\frac{\partial A_X}{\partial z} + \frac{\alpha}{2}A_X + \frac{i}{2}\beta_2\frac{\partial^2 A_X}{\partial T^2} = i\gamma\left(|A_X|^2 + \frac{2}{3}|A_Y|^2\right)A_X + \frac{i\gamma}{3}A_X^* A_Y^2 exp(-2i\Delta\beta z) \qquad \textbf{(24)}$$

where A_X and A_Y correspond to the optical fields in X- and Y-polarisation. The last term on the right hand side is due to the degenerate four-wave-mixing (FWM - section 2.2.3) between the two polarisations. In case of random polarisation evolution like

experienced in transmission fibre, the phase-mismatch between both polarizations $\Delta\beta$ is very high and the contribution averages out to zero. Therefore, we can reduce the nonlinear phase shift incident on the X-polarisation to:

$$\phi_{NL}(z,T) = \gamma L_{eff}\left(|A_X|^2 + \frac{2}{3}|A_Y|^2\right) \quad \textbf{(25)}$$

where the nonlinear phase shift ϕ_{NL} now splits into two parts: SPM as discussed earlier and a second term, which is called degenerate XPM depending on the intensity profile of the orthogonal polarisation.

Note that at high symbol-rates SPM has been found to be the dominant nonlinearity in transmission systems investigated in this work (non-dispersion-managed transmission systems employing SMF) [10]. Under these conditions nonlinear compensation of SPM is particularly beneficial as demonstrated in section 4.4.3 and 5.4 .

2.2.2 Cross-phase modulation (XPM)

By analogy to self-phase-modulation, cross-phase modulation is also a result of a nonlinear phase-shift in an optical field. With SPM, the phase shift in an optical signal is due to time-dependent power fluctuations in the wavelength channel itself. XPM, in contrast, covers the influence of the nonlinear phase shift induced by an orthogonal polarisation (polarisation multiplex) or neighbouring wavelength channels (wavelength division multiplex).

Referring to the second term on the right hand side of equation (18), one can find an expression for the nonlinear phase shift due to two neighbouring channels A_2 and A_3 :

$$\begin{aligned}\phi_{XPM}(z,T) = \gamma L_{eff} 2\Bigg(&\int_0^{\mathrm{z}} \left|A_2(0,T+d_{sp}z')\exp\left(\frac{i}{2}\beta_2\omega_2^2 z'\right)\right|^2 \mathrm{dz}' \\ &+ \int_0^{\mathrm{z}} \left|A_3(0,T+d_{sp}z')\exp\left(\frac{i}{2}\beta_2\omega_3^2 z'\right)\right|^2 \mathrm{dz}'\Bigg)\end{aligned} \quad \textbf{(26)}$$

This expression can be generalised to express the nonlinear phase shift induced on central channel A_{s} due to XPM, by summing up the contributions of all neighbouring WDM-channels:

$$\phi_{XPM}(z,T) = \gamma L_{eff} 2\sum_{p\neq 1}\int_0^{\mathrm{z}} \left|A_{\mathrm{p}}(0,T+d_{sp}z')\exp\left(\frac{i}{2}\beta_2\omega_p^2 z'\right)\right|^2 \mathrm{dz}' \quad \textbf{(27)}$$

Due to the different group velocities of each WDM-channel the symbol-patterns of the interacting channels walk-off from the central channel as displayed in Figure 9. This effect is described by the walk-off parameter d_{sp}:

$$d_{sp} \approx D \cdot (\lambda_s - \lambda_p) \tag{28}$$

A higher walk-off parameter helps decorrelate XPM contributions along the transmission link and reduces the variance of the XPM distortion as illustrated in section 5.3. Equation (27) shows, that ϕ_{XPM} depends on the power profile of the adjacent channels and is therefore, similarly to SPM, stronger within the effective length of the fibre. Furthermore, the nonlinear phase shift depends on the accumulated dispersion of the interfering channel. Since the peak to average power ratio of a signal is generally smaller for larger values of accumulated dispersion, it is justified to say that highly dispersed channels induce less severe XPM-distortions.

However, even if the impact of XPM can be reduced by using non-dispersion-managed transmission links and SMF with high GVD (D=16ps/km/nm), XPM still has a palpable influence on the transmission performance (see section 4.3.3 and 4.4.3), especially at lower symbol rates (see section 5.3 and reference [10]). Under these conditions nonlinear compensation of XPM is particularly effective as shown in section 5.5.

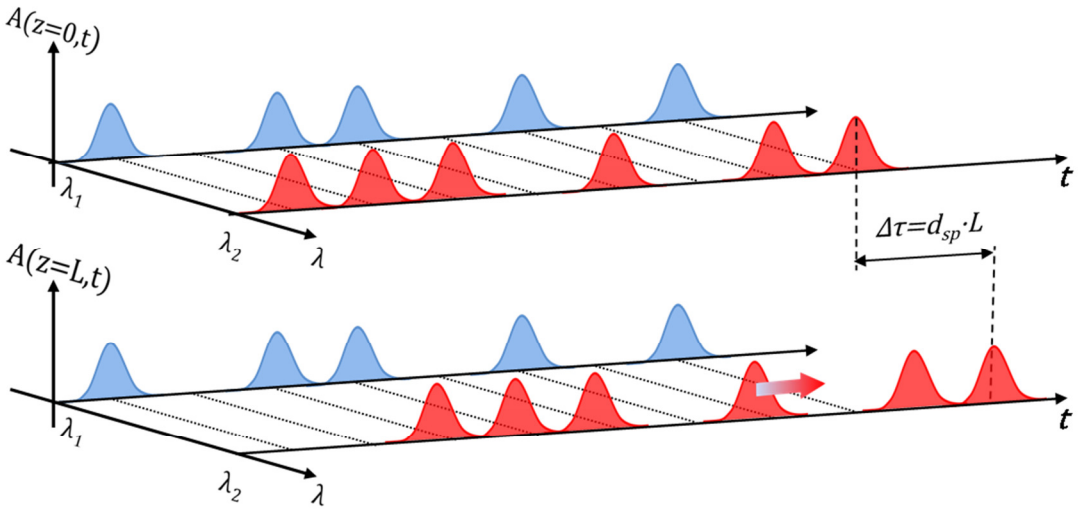

Figure 9: Walk-off between two WDM channels at wavelength λ_1 and λ_2 after propagation over the distance L.

2.2.3 Four-wave mixing (FWM)

FWM is a result of the Kerr effect where optical fields of different frequencies ω interact and generate new frequency components $\omega_l = -\omega_i + \omega_j + \omega_k$. If any two frequencies

are equal, degenerate FWM occurs as indicated by the third term on the right-hand side of equation (18).

In order to understand FWM one can generalise equation (18), neglecting the influence of SPM, XPM and chromatic dispersion. The power loss of the input signals due to FWM is considered negligible and only determined by the fibre attenuation. Furthermore, the optical fields are assumed to be time-independent (CW) with $A(z) = A_0 exp(-\alpha z/2)$. Under these assumptions, the evolution of the l-th field $A_l(z)$ can be described by a nonlinear coupled wave-equation [11]:

$$\frac{dA_l(z)}{dx} + \frac{\alpha}{2}A_l(z) = i\frac{\gamma}{3}\sum_{ijk} d_l A_i^*(z)A_j(z)A_k(z)\exp(i\Delta\beta z) \quad \textbf{(29)}$$

where d_l denotes the degeneracy factor with $d_l = (1,3,6)$ for three, two or no identical frequencies, respectively. Similarly to XPM, the distortion due to FWM is calculated as the sum of all possible permutations Σijk from frequency component i, j and k. $\Delta\beta$ is the phase mismatch between the propagation constant β_l of A_l (see equation (3)) and the combination of the other frequency components involved:

$$\Delta\beta = -\beta_i + \beta_j + \beta_k - \beta_l. \quad \textbf{(30)}$$

However, the FWM efficiency depends on the local dispersion and can be minimised by high local dispersion increasing $\Delta\beta$. Therefore, FWM can be neglected when the channel wavelengths lie far away from the zero-dispersion wavelength, which is the case for the fibre used throughout this work: SMF as well as NZDSF.

2.2.4 Cross Polarisation Modulation (XPolM)

In WDM-systems with sufficient walk-off (e.g. after a 80km SMF span a 28GBd WDM channel will have walked off from its neighbour spaced 50GHz away by more than 14 symbol slots), the intensity envelope of the signal varies rapidly due to colliding pulses. XPM introduces a different nonlinear phase shift in each polarisation depending on the temporal power envelope of both polarisations (see equation (25)). As a consequence, the state of polarisation (SOP) fluctuates depending on the signal itself as it propagates along the fibre [12]:

$$\frac{d\mathbf{s}}{dz} = \gamma \begin{pmatrix} s_1 \\ s_2 \\ \frac{s_3}{3} \end{pmatrix} \times \mathbf{s} \quad \textbf{(31)}$$

s is the Stokes vector with its components $s_1 = |A_X|^2 - |A_Y|^2$, $s_2 = 2\,Re(A_X A_Y{}^*)$ and $s_3 = 2\,Im(A_X A_Y{}^*)$ and γ is nonlinear coefficient of the fibre. Figure 10 shows how group velocity differentials affect the evolution of the SOP in the WDM transmission systems. As an example, three polarised WDM-channels are launched into a fibre at wavelengths λ_1, λ_2 and λ_3 (Figure 10 (a)). The SOP of every pulse depends on the SOPs of temporarily aligned pulses in neighbouring channels, as indicated in Figure 10 (b). Figure 10 (c) illustrates the effect of walk-off between the WDM channels due to different group velocities. After propagation over the distance Δz, different pulses overlap in time leading to another XPolM induced change of SOP for every pulse.

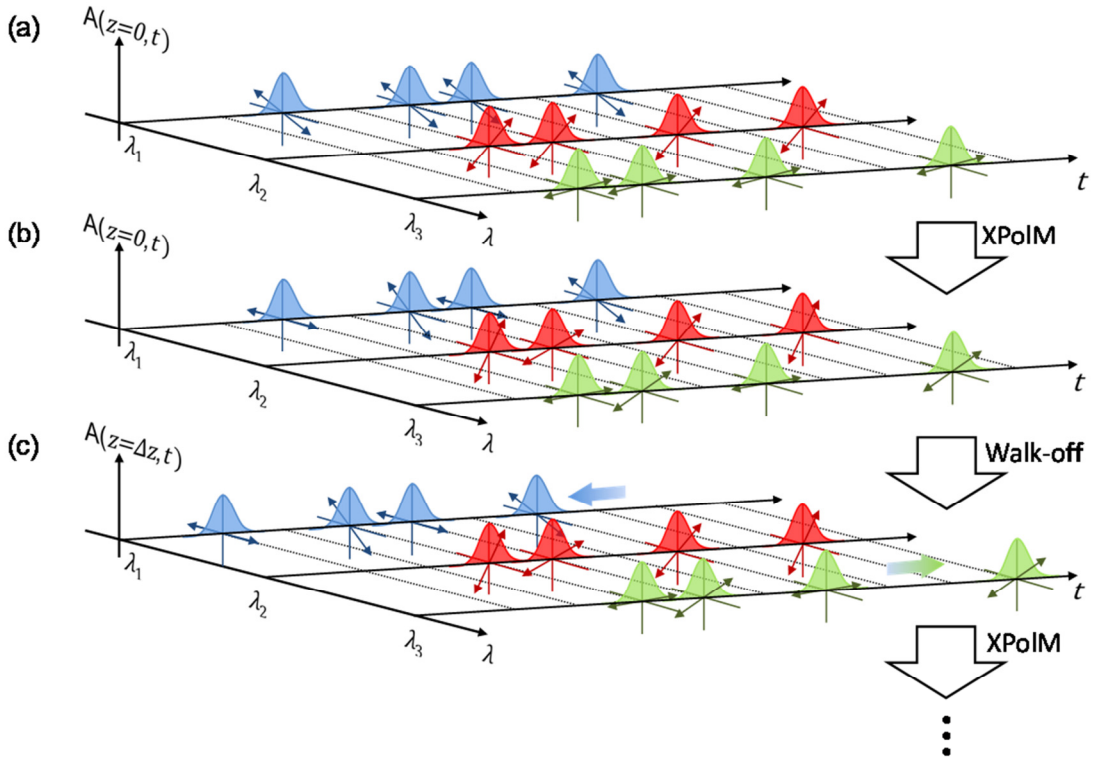

Figure 10: Interaction between XPolM and walk-off due to different group velocities. Three polarised WDM-channels are shown before being launched into a fibre (a) and after XPolM has acted on them (b). The induced polarisation rotation depends on, which pulses of the relevant WDM-channels overlap in time. Different group velocities cause the channels to walk-off from each other (c), leading to overlap between different pulses and the SOP to be scattered again [12].

Considering chromatic dispersion induced pulse-spreading and random polarisation rotations due to PMD, this nonlinear polarisation scattering leads to depolarisation of the signal [13]. XPolM is particularly harmful in polarisation multiplexed systems, since the SOP is scattered on a much faster time scale than an adaptive equaliser would be able to cope with, even though symbols of a particular WDM-channel might still have the same degree of correlation.

Note that, Bononi et al. [10] found that for non-dispersion-managed links employing SMF (as in this work) the severity of XPolM is similar to XPM and both distortions dominate the transmission regime at lower symbol rates (see section 5.3).

2.2.5 Gordon-Mollenauer effect

Nonlinear Phase Noise (NLPN) (or Gordon-Mollenauer-noise [14]) is noise, that is present in amplified optical transmission links. Due to the Kerr nonlinearity intensity fluctuations induced by ASE-noise (generated by the amplifiers along the link, as described in section 2.1.4 on ASE) are converted into phase-noise. NLPN has a probability density distribution of the sum of a Gaussian random variable and a non-central chi-square random variable with two degrees of freedom [15].

Nonlinear phase noise is particularly damaging in long-distance transmission and can lead to significant distortions of the constellation diagram [16, 17]. In the case of optically compensated transmission, partial re-alignment of the pulses will lead to a bean-shaped distortion of the constellation diagram, while uncompensated transmission usually results in a symmetrical spread of a constellation point.

Note, that nonlinear phase noise is included in all simulations by adding noise power with a Gaussian distribution after each EDFA. Therefore, we can ensure that all the nonlinear interactions between signal and ASE-noise during transmission have been taken into account.

2.3 Split-step Fourier algorithm

In section 2.2 the nonlinear Schrödinger equation is given describing wave propagation in nonlinear media. Unfortunately, the analytical solution for equation (19) is known only for a few cases, such as zero dispersion. Therefore, a general numerical solution has been developed for the solution of the full transmission system with all its parameters. A technique most commonly used is the split-step Fourier algorithm [18].

The split-step Fourier method calculates numerically a solution of a set of coupled differential equations, usually referred to as coupled nonlinear Schrödinger equation (CNLSE). It can be derived for X and Y-polarisation from equation (24) without the nonlinear term for the degenerate four-wave mixing:

$$\frac{\partial A_X}{\partial z}+\frac{\alpha}{2}A_X+\frac{i}{2}\beta_2\frac{\partial^2 A_X}{\partial t^2}-\frac{1}{6}\beta_3\frac{\partial^3 A_X}{\partial t^3}=i\gamma\left(|A_X|^2+\frac{2}{3}|A_Y|^2\right)A_X \quad (32)$$

$$\frac{\partial A_Y}{\partial z}+\frac{\alpha}{2}A_Y+\frac{i}{2}\beta_2\frac{\partial^2 A_Y}{\partial t^2}-\frac{1}{6}\beta_3\frac{\partial^3 A_Y}{\partial t^3}=i\gamma\left(|A_Y|^2+\frac{2}{3}|A_X|^2\right)A_Y \quad (33)$$

By introducing the linear operator $\widehat{D}$ and the nonlinear operator $\widehat{N}$, each equation can be written in the following form:

$$\frac{\partial A}{\partial z}=\left(\widehat{D}+\widehat{N}\right)A \quad (34)$$

$\widehat{D}$ describes the effect of chromatic dispersion and dispersion slope and $\widehat{N}$ includes the Kerr nonlinearity in the same polarisation and crosstalk from the orthogonal polarisation as well as attenuation:

$$\widehat{D}=-\frac{i}{2}\beta_2\frac{\partial^2}{\partial t^2}+\frac{1}{6}\beta_3\frac{\partial^3}{\partial t^3} \quad (35)$$

$$\widehat{N}=i\gamma\left(\left|A_{\parallel}\right|^2+\frac{2}{3}|A_{\perp}|^2-\frac{\alpha}{2}\right) \quad (36)$$

Although, chromatic dispersion and nonlinearity act together along the full length of the optical fibre, the split-step Fourier method assumes that nonlinear and linear effects can be separated over a small distance Δh. It has been shown that the split-step Fourier method is a very good numerical approximation of fibre propagation if Δh is small enough (as rule of thumb: the maximum nonlinear phase shift $\Delta h \cdot \widehat{N}$ should stay below 0.05 radians). As a consequence, one can split the fibre into sections of length Δh and, iteratively, calculate the complex field at the output of each section $A(z+\Delta h,t)$ from the values at the input $A(z,t)$ (see Figure 11).

$$A(z+\Delta h,t)\approx exp\left(\Delta h\widehat{D}\right)exp\left(\Delta h\widehat{N}\right)A(z,t) \quad (37)$$

In equation (37) the dispersion operator is first applied and then the nonlinearity operator. The accuracy of the split-step algorithm was explored by the Baker-Campbell-Hausdorff formula [19] for the two operators $\widehat{N}$ and $\widehat{D}$. The error is found to be of the order of Δh^2 as indicated in [20].

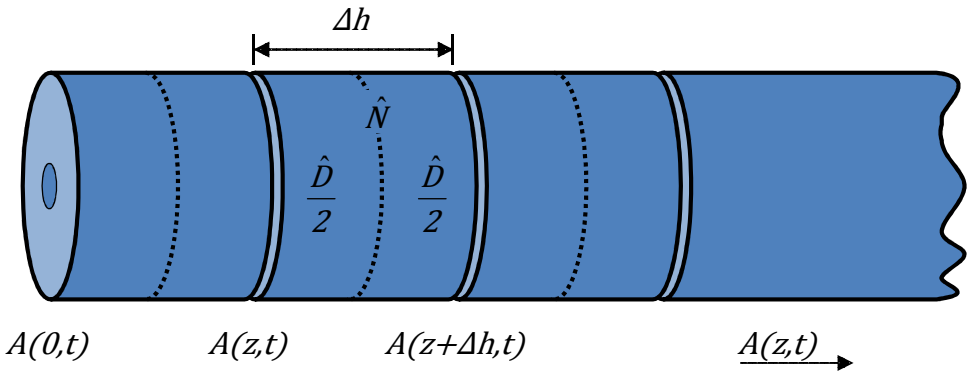

Figure 11: Principle of the split-step Fourier algorithm to obtain an approximate solution of the nonlinear Schrödinger equation for the propagation of the optical field $A(z,t)$

A modification with higher accuracy of the order Δh^3 is the symmetrical split-step Fourier method illustrated in Figure 11. Here the nonlinear operator $\hat{\mathrm{N}}$ is applied between two identical blocks of dispersion $\hat{\mathrm{D}}/2$.

The effect of PMD is taken into account, by using the waveplate model [16] to simulate random phase shifts and energy coupling between the two polarisation states. This approach has also been followed in the work described in this thesis. Similar to the split-step Fourier method, the whole fibre is divided into small segments (waveplates) of equal length Δh, which are assumed to have constant birefringence. A commonly used value for the waveplate length Δh is 100m, but at least 100 segments to obtain the right statistical behaviour. The fast and slow axis of the birefringent transmission in each waveplate and with it the velocities of light along these axes remain unchanged. As a result the DGD is modelled as being constant within Δh, which can be expressed by the transfer matrix:

$$\mathbf{B}_i(\omega) = \begin{bmatrix} exp\left(-i\omega\frac{\Delta\tau_p}{2}\right) & 0 \\ 0 & exp\left(i\omega\frac{\Delta\tau_p}{2}\right) \end{bmatrix} \tag{38}$$

The DGD per waveplate $\Delta\tau_p$ can be related to the PMD parameter of the whole fibre using the following equation [21]:

$$\Delta\tau_p = PMD \cdot \sqrt{L} \cdot \sqrt{\frac{3\pi}{8N}} = \langle\Delta\tau\rangle \cdot \sqrt{\frac{3\pi}{8N}} \tag{39}$$

Here, L is the fibre length, PMD denotes the PMD parameter, $\langle\Delta\tau\rangle$ stands for the mean DGD of the whole fibre, and N the number of waveplates.

The random variations in the axis of the two orthogonally polarised fibre modes along the fibre are described by a random rotation of the polarisation axes and by a random phase shift at the beginning of each waveplate described by the matrices $\mathbf{C}_i$ and $\mathbf{D}_i$, respectively. These matrices are given by:

$$\mathbf{C}_i = \begin{bmatrix} exp\left(-i\frac{\varphi}{2}\right) & 0 \\ 0 & exp\left(i\frac{\varphi}{2}\right) \end{bmatrix} \quad (40)$$

$$\mathbf{D}_i = \begin{bmatrix} \cos(\theta) & -\sin(\theta) \\ \sin(\theta) & \cos(\theta) \end{bmatrix} \quad (41)$$

φ and θ denote random phase and polarisation angles, respectively, which are uniformly distributed in $[-\pi; \pi]$.

By putting these three matrices together, the optical field $\mathbf{A}_i^{out}(\omega)$ at the output of a segment number i can be related to the input optical field $\mathbf{A}_i^{in}(\omega)$ in frequency domain by a 2x2 complex transfer matrix $\mathbf{U}_i(\omega)$ according to:

$$\mathbf{A}_i^{out}(\omega) = \mathbf{B}_i \cdot \mathbf{C}_i \cdot \mathbf{D}_i \cdot \mathbf{A}_i^{in}(\omega) = \mathbf{U}_i(\omega) \cdot \mathbf{A}_i^{in}(\omega), \quad \text{with } \mathbf{A} = \begin{bmatrix} A_X \\ A_Y \end{bmatrix} \quad (42)$$

To cover all different physical effects described previously with numerical simulations the waveplate model must be incorporated into the split-step Fourier method. This is done by setting the length of a step in the split-step Fourier method, so it corresponds to the length of a waveplate.

2.4 Summary

This chapter discussed the optical channel as described by the nonlinear Schrödinger equation (NLSE) as well as additional distortions such as amplified spontaneous emission noise (ASE) and polarisation mode dispersion (PMD). Initially linear distortions are described starting with attenuation, chromatic dispersion and PMD. ASE-noise is described as another linear distortion adding white Gaussian noise to a signal in an amplified optical transmission link. Subsequently, the nonlinear term of the NLSE is investigated under the condition of single channel transmission, isolating three different terms: intra-channel self-phase modulation (ISPM), intra-channel cross phase modulation (IXPM) and intra-channel four-wave mixing (IFWM). Assuming wavelength division multiplexed transmission, additional nonlinear terms named cross phase modulation (XPM) and four wave mixing(FWM) are discussed, while cross polarisation modulation (XPolM) is present in polarisation multiplexed transmission systems. After

the interaction between ASE and nonlinearity termed Gordon-Mollenhauer noise is added to the list of nonlinear distortions, the split-step Fourier model and the waveplate model are described, which are used to model optical transmission in computer simulations presented in this work.

The following chapter describes the generation and detection of higher order modulation formats in next generation high speed optical networks. The transmitter architecture for phase shift keyed modulation and quadrature amplitude modulation as well as for polarisation switched QPSK is discussed. Coding schemes such as Gray coding and differential coding are examined in the context of higher order modulation formats. The phase and polarisation diverse coherent receiver is introduced, detailing digital signal processing algorithms for chromatic dispersion compensation, nonlinear compensation, adaptive equalisation and phase recovery.

2.5 References

[1] S. S. Walker, "Rapid Modeling and Estimation of Total Spectral Loss in Optical Fibers," *Journal of Lightwave Technology,* vol. 4, pp. 1125-1131, Aug 1986.

[2] "Optical system design and engineering - Supplement 39," Internation Telecommunication Union2008.

[3] G. P. Agrawal, *Nonlinear Fiber Optics*: Academic Press, 1995.

[4] G. J. Foschini and C. D. Poole, "Statistical theory of polarization dispersion in single mode fibers," *Journal of Lightwave Technology,* vol. 9, pp. 1439-1456, 1991.

[5] E. Desurvire, *Erbium-Doped Fiber Amplifiers - Principles and Applications*: John Wiley & Sons, Inc., 1994.

[6] P. J. Winzer and R.-J. Essiambre, "Advanced Optical Modulation Formats," *Proceedings of the IEEE,* vol. 94, pp. 952-985, 2006.

[7] A. Lau, S. Rabbani, and J. M. Kahn, "On the Statistics of Intrachannel Four-Wave Mixing in Phase-Modulated Optical Communication Systems," *Journal of Lightwave Technology,* vol. 26, pp. 2128-2135, 2008.

[8] K.-P. Ho, *Phase Modulated Optical Communication Systems*: Springer, 2005.

[9] S. Randel, "Analyse faseroptischer Übertragungssysteme mit Wellenlängenmultiplex bei 160 Gbit/s Kanaldatenrate," PhD thesis, Elektrotechnik und Informatik, TU Berlin, Berlin, 2005.

[10] A. Bononi, P. Serena, N. Rossi, and D. Sperti, "Which is the Dominant Nonlinearity in Long-haul PDM-QPSK Coherent Transmissions?," in *Proc. ECOC 2010*, Turin, Italy, 2010, p. Th.10.E.1.

[11] K. O. Hill, D. C. Johnson, B. S. Kawasaki, and R. I. MacDonald, "CW three-wave mixing in single-mode optical fiber," *Journal of Applied Physics,* vol. 49, pp. 5098-5106, 1978.

[12] M. Karlsson and H. Sunnerud, "Effects of nonlinearities on PMD-induced system impairments," *Journal of Lightwave Technology,* vol. 24, pp. 4127--4137, November 2006.

[13] M. Winter, C. A. Bunge, D. Setti, and K. Petermann, "A Statistical Treatment of Cross-Polarization Modulation in DWDM System," *Journal of Lightwave Technology,* vol. 27, pp. 3739-3751, September 2009.

[14] J. P. Gordon and L. F. Mollenauer, "Phase noise in photonic communications systems using linear amplifiers," *Optics Letters,* vol. 15, p. 1351, 1990.

[15] K.-P. Ho, "Probability density of nonlinear phase noise," *Journal of the Optical Society of America B,* vol. 20, pp. 1875-1879, 2003.

[16] F. Curti, B. Daino, G. De Marchis, and F. Matera, "Statistical treatment of the evolution of the principil states of polarization in single-mode fibers," *Journal of Lightwave Technology,* vol. 8, pp. 1162-1166, 1990.

[17] P. Serena, N. Rossi, and A. Bononi, "PDM-iRZ-QPSK vs. PS-QPSK at 100Gbit/s over dispersion-managed links," *Optics Express,* vol. 20, pp. 7895-7900, March 2012.

[18] R. A. Fisher and W. K. Bischel, "The Role of Linear Dispersion in Plane-Wave Self-Phase Modulation," *Applied Physics Letters,* vol. 23, p. 661, 1973.

[19] G. H. Weiss and A. A. Maradudin, "The Baker-Hausdorff Formula and a Problem in Crystal Physics," *Journal of Mathematical Physics,* vol. 3, pp. 771-777, Jul.-Aug. 1962.

[20] D. S. Millar, S. Makovejs, C. Behrens, S. Hellerbrand, R. I. Killey, P. Bayvel, and S. J. Savory, "Mitigation of Fiber Nonlinearity using a Digital Coherent Receiver," *Journal of Selected Topics in Quantum Electronics,* vol. 16, pp. 1217-1226, 2010.

[21] C. D. Poole and D. L. Favin, "Polarization-mode dispersion measurements based on transmission spectra through a polarizer," *Journal of Lightwave Technology,* vol. 12, pp. 917-929, 1994.

Chapter 3

TRANSCEIVER-ARCHITECTURE AND LITERATURE REVIEW

The previous chapter discussed the optical channel as described by the coupled nonlinear Schrödinger equation, including linear and nonlinear distortions that occur when information is transmitted over this channel. The present chapter continues with the description of transmitter and digital coherent receiver architecture for a variety of spectrally efficient modulation formats.

Initially, several transmitters are described, which have to convert bits (binary information) into symbols (which are defined by a certain symbol alphabet) and modulate these symbols on the complex optical field. The symbol alphabet of phase-shift keyed modulation formats such as BPSK, QPSK and 8PSK is restricted to the optical phase, while quadrature amplitude modulation formats such as 8QAM and 16QAM use distinct levels in inphase and quadrature component of the optical field to encode information. Polarisation shift QPSK expands the symbol space to the polarisation of the optical field by introducing correlation between the orthogonal polarisations in a single mode fibre. After elaborating on channel coding schemes, such as gray-coding and differential coding, the principle of operation of the digital coherent receiver is explained and digital signal processing algorithms are described.

3.1 Transmitter

3.1.1 M-PSK

A large proportion of the installed optical communication infrastructure is based on intensity modulation and direct detection (IMDD) employing low cost directly modulated lasers and photodiodes. However, IMDD systems have a ~3dB lower receiver

sensitivity compared to e.g. binary phase shift keying (BPSK). BPSK encodes 1 bit/symbol in two phase states with a phase difference of π as depicted in the constellation diagram (representation of symbols in the complex plane of the optical field) in Figure 12 (b). It can be generated by using a Mach Zehnder interferometer (MZI), which consists of two nested phase modulators. These phase modulators are used to manipulate the relative phase between the two branches and to achieve either constructive or destructive interference at the output. The MZI is driven in push-pull-mode (one of the phase modulators is driven with the inverse data pattern to reduce the required driving voltage) around its zero-transmission point, to achieve a relative phase of π radians (see Figure 12).

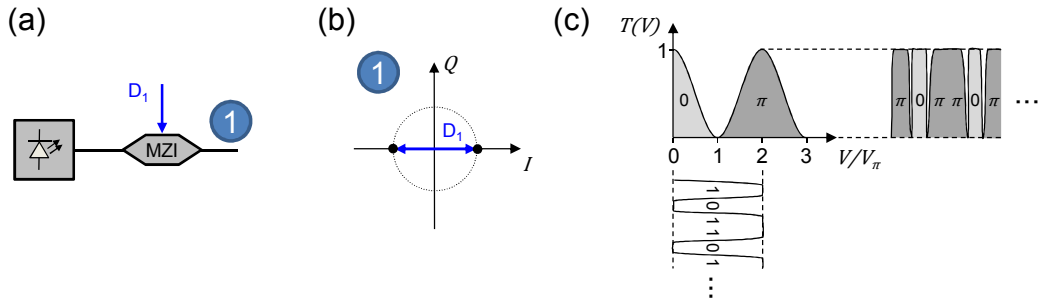

Figure 12: (a) A Mach Zehnder interferometer (MZI) is used to generate a BPSK constellation (b). (c) Power transfer function of a standard MZI: a binary data sequence with a voltage swing of $2 \cdot V_\pi$, biased at the null transmission point generates an output waveform with varying optical phase.

For an ideal, lossless push-pull MZI the transfer function displayed in Figure 12 (c) can be written as follows:

$$T(V) = \frac{A_{out}}{A_{in}} = \left\{exp\left(j\frac{\pi}{2}\frac{V}{V_\pi}\right) - exp\left(-j\frac{\pi}{2}\frac{V}{V_\pi}\right)\right\} = cos\left(\frac{\pi}{2}\frac{V}{V_\pi}\right) \quad \textbf{(43)}$$

Here is V the electrical driving voltage and V_π the voltage to achieve a phaseshift of π.

One of the first multilevel formats adapted for optical communications was differential-quaternary-phase-shift-keying ((D)QPSK) [1], containing 4 phase states separated by a phase distance of π/2 rad (see Figure 13 (b)). (D)QPSK encodes 2bits/symbol and is often generated by two nested MZI, each of which is driven by a binary electrical signal with an amplitude of $2V_\pi$ biased at the zero transmission point. One of the optical outputs is then phase shifted by π/2 rad and combined with the other signal (see Figure 13). In recent literature, this transmitter structure is denoted as an IQ-modulator, because one MZI modulates the inphase-, whereas the other is encoding the quadrature-component of the signal.

8PSK encodes 3bits/symbol with 8 phase-states [2, 3], equally spaced with a phase difference of π/4 rad (see Figure 13 (b)). It can be generated by using a QPSK transmitter followed by a phase-modulator, which shifts the phase between 0 and π/4 rad (see Figure 13). Note, that it is possible to encode 16 different phase states and obtain 16PSK if an 8PSK transmitter is preceded by an additional phase-modulator shifting the signals phase between 0 and π/8 rad.

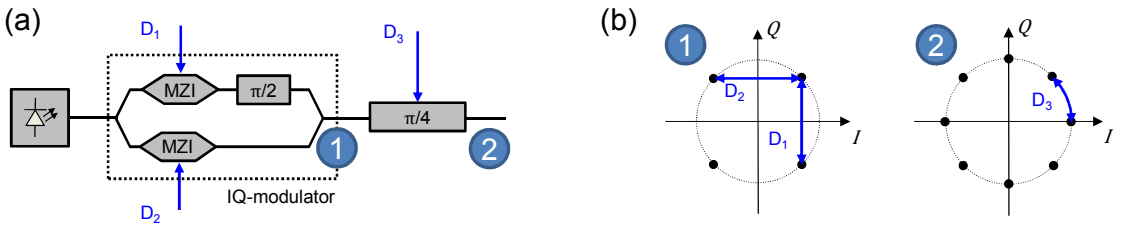

Figure 13: (a) An IQ-modulator is used to generate a QPSK constellation. Inserting a phase modulator into the optical path, shifting the phase between 0 and $\pi/4$, it is possible to obtain 8PSK. (b) Shows the resulting constellation diagrams of QPSK on the left and 8PSK on the right.

3.1.2 8QAM

A format which is widely known in wireless transmission for showing optimum power efficiency in 2-dimensional channels limited by additive white Gaussian noise is 8-quadrature amplitude modulation (8QAM) [4]. 8QAM encodes 3bits/symbol on two intensity rings, each of which contains 4 phase-states (Figure 14 (c) 1 and 4). Both rings are offset, in phase, by π/4 rad and the intensity ratio between the rings is $(1+\sqrt{3})/\sqrt{2}$, so that every symbol on the inner ring has 4 nearest neighbours. 8QAM can be generated by an IQ-modulator followed by a phase modulator [5] or by two serial IQ-modulators [6].

In the first case, one arm of the IQ-modulator is driven by $2V_\pi$ around the zero transmission point, whereas the driving voltage for the other arm is reduced to $0.3464 \cdot 2V_\pi$ and phaseshifted by π/4 rad (Figure 14 (a)). A subsequent phase modulator shifting the phase by π/2 rad according to a third data signal gives the desired constellation diagram.

Figure 14 (b) shows how 8QAM can be generated with 2 IQ-modulators. The first modulator generates a standard QPSK constellation, while the second IQ modulator has one arm fixed at $0.3464 \cdot V_\pi$ and a phase shift of π/4 rad and the other arm driven over a voltage range $2V_\pi$.

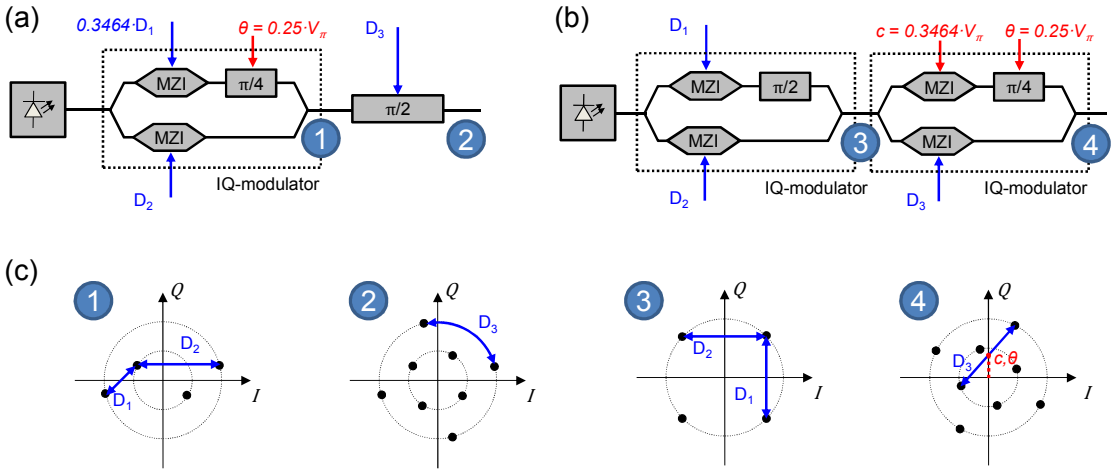

Figure 14: (a) shows the generation of 8QAM by using an IQ-modulator with a subsequent phase modulator. Equally, 8QAM can be generated by using two serial IQ-modulators. (c) depicts constellation diagrams for both transmitter architectures.

Note that, the format called staggered 8-APSK, which was introduced by [7] is equivalent to 8QAM. This format was generated by combining an intensity-modulated signal with a phase-shifted CW-laser obtaining staggered BASK initially. The following IQ-modulator is driven to modulate QPSK and eventually transforms staggered BASK into staggered 8-APSK/8QAM.

3.1.3 16QAM

Another modulation format that has been widely used in the microwave regime, and that is becoming increasingly popular in optical communications is 16 quadrature-amplitude-modulation (16QAM) encoding 4bits/symbol. This modulation scheme has this name, because it is modulated by 2 amplitude-modulated carriers that are phase-shifted by π/2 rad, hence in quadrature. Note, that QPSK modulated by an IQ-modulator is also a QAM-format (i.e. 4QAM), in a very strict sense.

To generate 16QAM, the IQ-modulator must be driven by electrical 4-level-signals [8], which is difficult to obtain because current high speed electrical driving circuitry is optimised for binary signals and state of the art arbitrary waveform generators have low electrical bandwidths (Tektronix: 6GHz). However, these driving signals can be generated at a decent symbol rate by superimposing two binary data streams as shown in Figure 15 (a). Winzer et al. [9] used this technique combined with a 2-bit DAC to improve the quality of the driving signals. Note that the signals levels can be equally spaced and driven over the linear region of the modulator's transfer function (Figure 15 (b)) or can be predistorted to exploit the full swing of the modulator. In the latter case the inner rings of the format will have a worse SNR than the outer ring, because the

nonlinear region of the transfer function suppresses the translation of electrical noise into the optical domain.

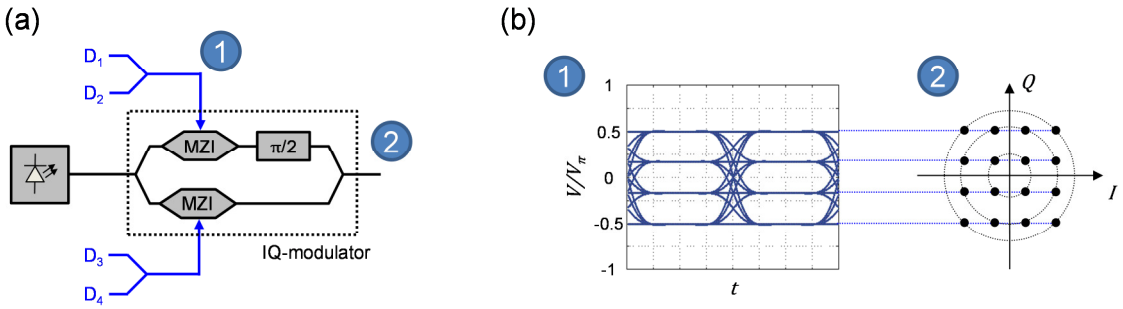

Figure 15: To generate 16QAM with a single IQ-modulator (a), 4-level driving signals are required (b), which can be obtained by combining two binary data sequences in power combiner.

To overcome the need to generate multi-level driving signals, transmitters that operate with bi-level drive containing 2 nested IQ-modulators for QAM-16 have been investigated [10, 11]. Apart from reduced requirements for the electrical circuitry, both QPSK constellations can take advantage of noise suppression capabilities of the nonlinear part of the transfer function.

3.1.4 PS-QPSK

An optical wave offers 4 degrees of freedom (2 quadratures in 2 polarizations) and recent work has addressed the question of the optimum modulation format for this higher dimensional channel [12, 13]. After solving a 4-dimensional sphere packing problem, Karlsson and Agrell [12] arrived at a modulation format that provides an asymptotic sensitivity gain of 1.76 dB over BPSK - polarization-switched QPSK (PS-QPSK). PS-QPSK provides maximum power efficiency by transmitting a QPSK symbol in one polarization at a time, with the resultant spectral efficiency limits of 3 bit/s/Hz.

To generate PS-QPSK both arms of an IQ-modulator can be driven over $2V_\pi$ to obtain QPSK. The IQ-modulator is followed by a polarisation switching stage consisting of two parallel Mach-Zehnder modulators (MZMs) (Figure 16 (a)). The MZMs are driven between 0 and V_π with inverse data patterns to block one or the other polarisation to generate the PS-QPSK.

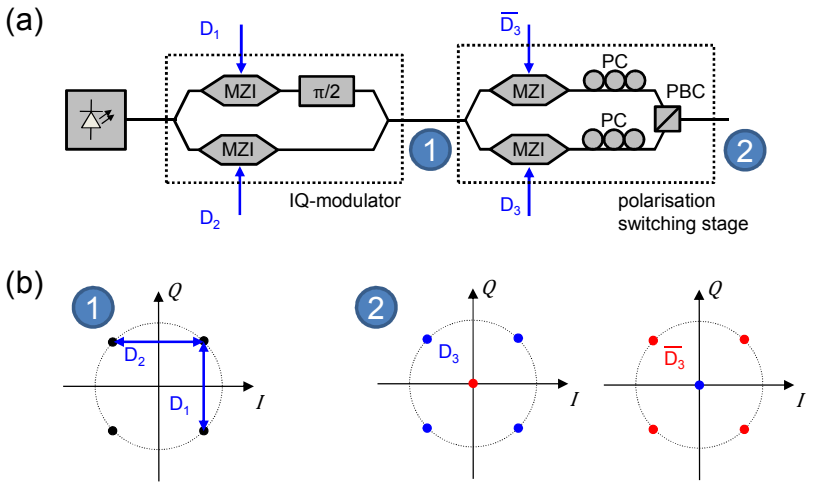

Figure 16: (a) shows a dual stage PS-QPSK transmitter, consisting of an IQ-modulator and a polarisation switching stage. (b) depicts constellation diagrams before and after the polarisation switching stage, with D_3 determining which polarisation the QPSK-constellation is mapped to.

Another way to generate PS-QPSK is to use an IQ-modulator for each polarisation and precode the driving signals, so that a QPSK symbol is only present in one polarisation at the time[13]. This configuration offers the possibility to transmit either polarisation multiplexed QPSK with 4 bits/symbol and fall back on PS-QPSK with 3 bits/symbol when the channel condition worsens [14].

Note, that all of the previously described modulation formats can be generated with a 'software'-defined transmitter [15]. This transmitter uses digital-to-analogue converters (DACs) that generate appropriate driving signals to run two IQ-modulators, one for each polarisation.

3.2 Coding

This section describes channel coding techniques such as Gray coding and differential coding. Gray coding minimises the bit error rate by ensuring that the nearest neighbouring symbols have a Hamming distance of 1, while differential coding prevents error bursts in presence of cycle slips introduced by the phase recovery and is applied in Chapter 5. Note that neither Gray- nor differential coding ads redundancy to the signal and therefore none of the codes have the ability to correct for errors. For forward error correction (FEC) purposes the ITU has standardised a (255,239) Reed-Solomon code with 255 bits out of which 239 carry payload information [16].

3.2.1 Gray-Coding

Under the assumption that the transmission channel is limited by additive white Gaussian noise the symbol error rate will be dominated by errors from the nearest neighbouring symbol. Therefore it is useful to map the bits to the constellation so that only one bit changes between neighbouring symbols resulting in a Hamming distance of only 1. As a consequence, a symbol error will most likely be associated with a single bit-error, even when M bits per symbol are encoded, leading to bit error probability of $p_{Bit} = p_{Symbol}/M$.

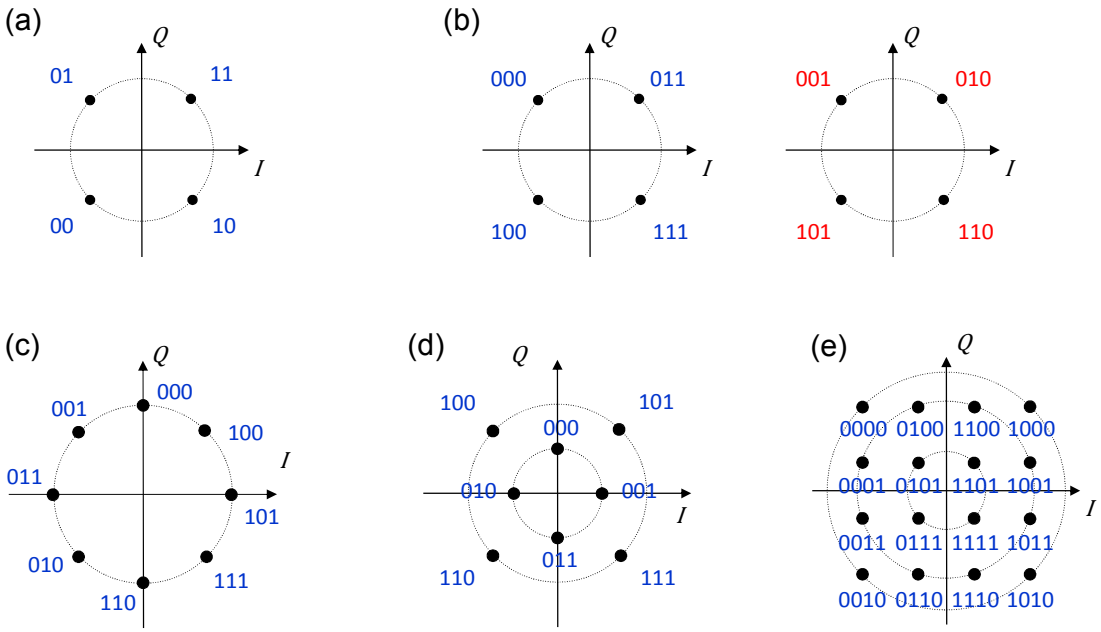

Figure 17: Optimum bit to symbol mapping for (a) QPSK, (b) PS-QPSK, (c) 8-PSK, (d) 8QAM and (e) 16QAM

Figure 17 shows optimum bit to symbol mapping for (a) QPSK, (b) PS-QPSK, (c) 8-PSK, (d) 8QAM and (e) 16QAM. Every constellation is Gray coded, apart from 8QAM, which cannot be Gray coded because the inner symbols have 4 nearest neighbours and only 3 bits to code. Consequently, 8QAM has been coded so that 3 out of the 4 nearest neighbours are Gray coded [17].

3.2.2 Differential Coding

In a differentially coded phase shift keyed (PSK) signals the bit information is not stored in terms of an absolute phase value but in the relative phase difference between adjacent symbols. This coding scheme is required to be able to detect a PSK signal with a delay line interferometer, which converts the phase difference between adjacent symbols into intensity. However, due to its ability of mitigating catastrophic error

propagation due to cycle slips it has been widely adopted in coherent detection, too. Note that differential encoding always reduces receiver sensitivity, since two adjacent symbols have to be evaluated to extract the information and therefore only half the amount of noise can be tolerated.

The differentially pre-coded driving signal, needed to generate DBPSK, is obtained by passing the NRZ data-sequence through an XOR-gate, combining every original bit a_k with its coded predecessor I_{k-1}:

$$I_k = a_k \oplus I_{k-1} \tag{44}$$

In case of differential QPSK (DQPSK) the pre-coding function is given as follows[18]:

$$\begin{aligned} I_k &= \overline{a_k \oplus b_k} \cdot \overline{b_k \oplus I_{k-1}} + (a_k \oplus b_k) \cdot (b_k \oplus Q_{k-1}) \\ Q_k &= \overline{a_k \oplus b_k} \cdot \overline{b_k \oplus Q_{k-1}} + (a_k \oplus b_k) \cdot \overline{b_k \oplus I_{k-1}} \end{aligned} \tag{45}$$

with a_k and b_k denoting the original bits and Q_k as well as I_k the pre-coder output driving the IQ-modulator. Furthermore, $\oplus$ and $\overline{\ }$ symbolise XOR- and NOT function, respectively.

Differentially coded polarisation switched QPSK is precoded using equation (44) for DQPSK with the 3rd bit determining which polarisation the QPSK constellation is mapped to. Differential 8PSK and 16PSK is usually pre-coded in a similar way, however with significantly more complex pre-coding functions. The interested reader is referred to [19] for 8PSK and [20] for 16PSK, where functions describing the driving signals for IQ-modulator and subsequent phase modulators are given. As mentioned earlier the BER in differentially coded PSK systems is a factor of 2 higher than in standard gray-coded systems. For 8QAM and 16QAM-formats, differential coding was employed by dividing the constellation into 4 quadrants and coding the most significant bits to identify those quadrants, while the least significant bits are rotational invariant [17]. Note that by differentially coding 8QAM and 16QAM BERs deteriorate by a factor of 1.45 and 1.625, respectively, compared to optimum bit to symbol mapping as described in section 3.2.1.

3.3 Coherent Detection

In a phase and polarisation diverse coherent receiver, the transmitted signal interferes inside an optical hybrid with a LO-signal provided by another CW-Laser (see Figure 18) converting both quadratures of X- and Y- polarisation into the electrical domain. LO- and transmit laser are impacted with phase noise, which can be modelled with a

Gaussian distribution of the variance $\sigma^2 = 2\pi \cdot \Delta\vartheta \cdot dt$ with $\Delta\vartheta$ representing the laser linewidth. Typical laser linewidths range from ~100kHz, corresponding to commercially available external cavity lasers (ECL), up to a few MHz for a conventional DFB laser. The LO laser is usually free running within ~1GHz of the optical frequency of the transmit laser, which is referred to as intradyne detection. In this case, the remaining frequency offset is compensated digitally e.g. by applying a higher order nonlinearity to the signal and estimating the offset from the spectrum. Considering the transfer function of a single polarization coherent receiver employing asymmetric 3x3 fibre couplers, which is given below, it becomes clear, that the coherent receiver translates the full information of the optical field into the electrical domain by generating currents proportional to real- and imaginary parts of the optical field:

$$\begin{bmatrix} i_I(t) \\ i_Q(t) \end{bmatrix} = 0.2 \cdot \begin{vmatrix} E_{in}(t) + (-1+j) \cdot E_{LO} \cdot \exp\left(-j\left({}^{3}/_{4}\right)\pi\right) \\ E_{in}(t) \cdot (-1+j) + E_{LO} \cdot \exp\left(-j\left({}^{3}/_{4}\right)\pi\right) \end{vmatrix}^2 \tag{46}$$

$$= \sqrt{2} \cdot 0.4 \cdot \begin{pmatrix} Re(E_{in}(t) \cdot {E_{LO}}^*) \\ Im(E_{in}(t) \cdot {E_{LO}}^*) \end{pmatrix} + 0.2 \cdot \begin{pmatrix} |E_{in}(t)|^2 + 2 \cdot |E_{LO}|^2 \\ 2 \cdot |E_{in}(t)|^2 + |E_{LO}|^2 \end{pmatrix}$$

The second terms contribution can be eliminated by a DC-block, when the LO power is sufficiently higher than the signal power, or a pair of balanced photo-diodes can be used instead of single ended detection. For further details see [21] and [22].

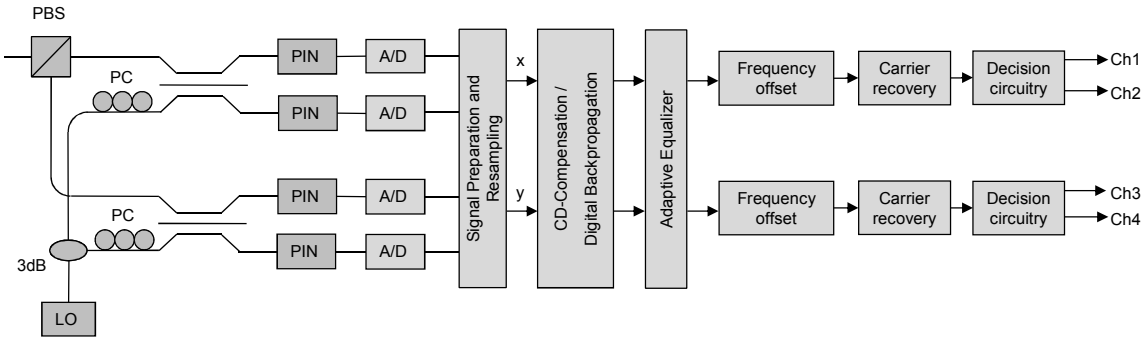

Figure 18: Coherent receiver using a fibre coupler as 90˚ hybrid, chromatic dispersion compensation, equalisation, digital phase recovery and differential decoding

After converting the information about the optical field into the electrical domain, the signal is digitised by analogue-to-digital converters (ADCs), deskewed and resampled at twice the symbol-rate to prepare it for subsequent digital signal processing. Figure 18 shows the following DSP blocks which consist of chromatic dispersion compensation, CMA equaliser, digital carrier recovery and differential decoding of the signal.

3.3.1 Chromatic Dispersion Compensation

The compensation of chromatic dispersion in commercial systems is mostly done in the time domain by employing a finite-impulse-response (FIR) filter. Therefore we shall continue with this time-domain approach [23].

The following partial differential equation describes the propagation of an optical wave $\mathrm{A}(\mathrm{z},\mathrm{t})$ inside a fibre, assuming only chromatic dispersion is present:

$$\frac{\partial A(z,t)}{\partial z} = j\frac{D\lambda^2}{4\pi c}\frac{\partial^2 A(z,t)}{\partial t^2} \tag{47}$$

Equation (47) can be solved in the frequency domain by $\mathrm{H}(\mathrm{z},\omega)$, which is then translated back into the time domain to obtain the impulse response $\mathrm{h}(\mathrm{z},\mathrm{t})$:

$$H(z,\omega) = exp\left(-j\frac{D\lambda^2}{4\pi c}\omega^2\right) \Leftrightarrow h(z,t) = \sqrt{\frac{c}{jD\lambda^2 z}}exp\left(j\frac{\pi c}{D\lambda^2 z}t^2\right) \tag{48}$$

To compensate for chromatic dispersion we have to invert the sign of D, which results in the impulse response of the compensating-filter:

$$\tilde{h}(z,t) = \sqrt{\frac{jc}{D\lambda^2 z}}exp\left(-j\frac{\pi c}{D\lambda^2 z}t^2\right) \tag{49}$$

$\tilde{h}(z,t)$ is infinite in duration, non-causal and it passes all frequencies for a finite sampling frequency, introducing aliasing. To apply this impulse response in an FIR-filter, we approximate the continuous time impulse response with a sampled impulse response which can be implemented using a tapped delay-line (Figure 19). Additionally, the impulse response is truncated to an odd number of taps, with the following tap-weights:

$$a_n = \sqrt{\frac{jcT^2}{D\lambda^2 z}}exp\left(-j\frac{\pi cT^2}{D\lambda^2 z}n^2\right) \qquad \text{for } -\left\lfloor\frac{N}{2}\right\rfloor \le n \le \left\lfloor\frac{N}{2}\right\rfloor \text{ with } N = 2\left\lfloor\frac{|D|\lambda^2 z}{2cT^2}\right\rfloor + 1 \tag{50}$$

If we assume a transmission system similar to the one investigated in Chapter 5 (1000km SSMF with D =16ps/km/nm operating at 28Gbd) an FIR filter with 401 taps would be required to compensate for all of the accumulated chromatic dispersion in the link.

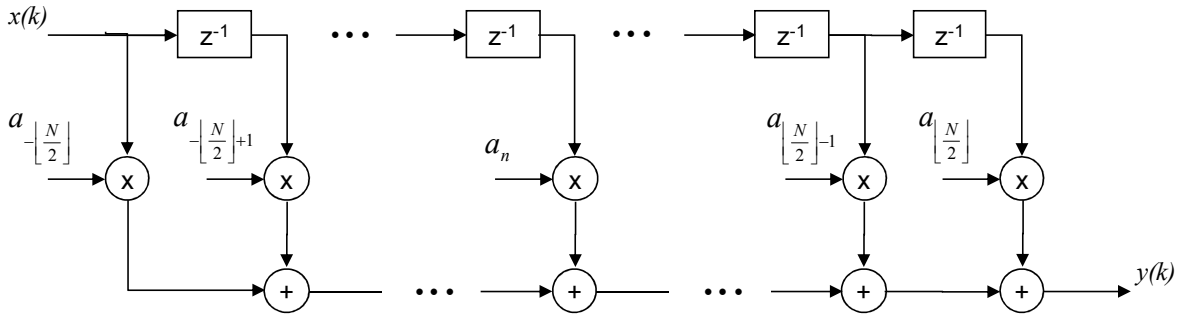

Figure 19: Structure of a FIR-filter for compensating for chromatic dispersion in the time domain

Note, that filter properties like group-delay ripple can heavily impact the performance, especially of short filters. Therefore, a frequency domain compensation approach is used in all simulations to avoid the additional degradation. The sampled instance of the signal is transformed into the frequency domain using a Fast-Fourier-Transform(FFT), then multiplied by the inverse of the channel (compare equation (48)):

$$\widetilde{H}(z,\omega) = \exp\left(j\frac{D\lambda^2}{4\pi c}\omega^2\right) \tag{51}$$

and finally translated back into the time domain.

3.3.2 Digital Backpropagation

Digital backpropagation is a nonlinear compensation scheme which exploits the knowledge about the physical channel and tries to invert it. An electrical field propagating in an optical fibre is most commonly described by the coupled nonlinear Schrödinger equation (CNLSE) [24], which does not account for the effect of randomly varying birefringence along the fibre (see section 2.3 equation (32) and (33)). However, the Manakov equation averages over random polarisation fluctuations and has been shown to accurately model transmission over the length scales important for optical communications [25]. In contrast to the CNLSE, the Manakov equation assumes that fibre nonlinearity acts equally on both polarizations, since the birefringence scatters the state of polarization on a much smaller length scale than the nonlinear length. In the following we use the Manakov equation (52) as the basis for the digital backpropagation algorithm:

$$\begin{aligned}\frac{\partial}{\partial z}E_X &= -\frac{\alpha}{2}E_X + \frac{j\beta_2}{2}\frac{\partial^2}{\partial t^2}E_X - j\gamma\frac{8}{9}(|E_X|^2 + |E_Y|^2)E_X \\ \frac{\partial}{\partial z}E_Y &= -\frac{\alpha}{2}E_Y + \frac{j\beta_2}{2}\frac{\partial^2}{\partial t^2}E_Y - j\gamma\frac{8}{9}(|E_Y|^2 + |E_X|^2)E_Y\end{aligned} \tag{52}$$

with α denoting the fibre attenuation coefficient, β_2 the chromatic dispersion coefficient and γ the nonlinear coefficient as well as X and Y for the two orthogonal polarizations. Since there is no analytical solution to this equation, the split-step method has to be applied to find an approximate solution for the inverse channel. Consequently, equation (52) can be split up into a linear and nonlinear part.

$$\frac{\partial \mathbf{E}}{\partial z} = \left(\widehat{D} + \widehat{N}\right)\mathbf{E} \tag{53}$$

With $\mathbf{E} = [E_{\mathrm{X}} \quad E_{\mathrm{Y}}]^{\mathrm{T}}$ describing the optical field in both polarizations, $\widehat{D}$ the effect of chromatic dispersion and $\widehat{N}$ describing the Kerr effect as well as the attenuation of the fiber:

$$\widehat{D} = \frac{j\beta_2}{2}\frac{\partial^2}{\partial t^2} \tag{54}$$

$$\widehat{N} = -j\gamma\frac{8}{9}\mathbf{E}^{\mathbf{H}}\mathbf{E} - \frac{\alpha}{2} \tag{55}$$

For sufficiently small step size h the solution to equation (53) can be approximated by:

$$\mathbf{E}(z+h,T) \approx \exp\left(\widehat{D}\frac{h}{2}\right)\exp\left(\widehat{N}h_{eff}\right)\exp\left(\widehat{D}\frac{h}{2}\right)\mathbf{E}(z,T) \tag{56}$$

where $h_{eff} = (1-\exp(-\alpha h))/\alpha$ denotes the effective length of the step size. In equation (56) the symmetrical split-step method has been applied, resulting in higher accuracy by splitting up the dispersive step into two equal steps [5]. Note that the symmetrical split-step method increases the complexity when implemented in hardware, in this work; however, we accept this additional complexity to investigate the maximum achievable performance by digital backpropagation.

The dispersive step is performed in the frequency domain by inverting the frequency response of a dispersive fibre:

$$\widehat{D}(\omega) = -j\frac{\beta_2}{2}\omega^2 \tag{57}$$

while the nonlinear step is performed in the time domain applying an inverse nonlinear phase shift proportional to the total power in both polarisations:

$$\widehat{N}(t) = -j\gamma\varphi\frac{8}{9}(|E_Y|^2 + |E_X|^2)P_{in}10^{\left(-\left[\frac{s}{n}-1\right]\frac{\alpha L}{10}\right)} \tag{58}$$

Here φ is a variable that converges with increasing number of steps towards 1, but has to be optimised for a realistic number of steps. P_{in} denotes the launch power at the beginning of each span, while $10^{\left(-\left[\frac{s}{n}-1\right]\frac{\alpha L}{10}\right)}$ accounts for the varying power profile along the span, with n being the number of steps per span, s the index of the step within a span, L the span length in km and α the fibres loss coefficient in dB/km. Although, digital backpropagation requires an oversampling of 3 samples per symbol to account for spectral broadening during the nonlinear step [26], we consider 2 samples per symbol which has been demonstrated to achieve impressive performance improvements [27], whilst relaxing hardware requirements. Note that, during the course of this work Du and Lowery [28] demonstrated that similar performance can be achieved with 2 samples per symbol backpropagation by suppressing aliasing effects with a low pass filter applied to the estimated nonlinear phase shift.

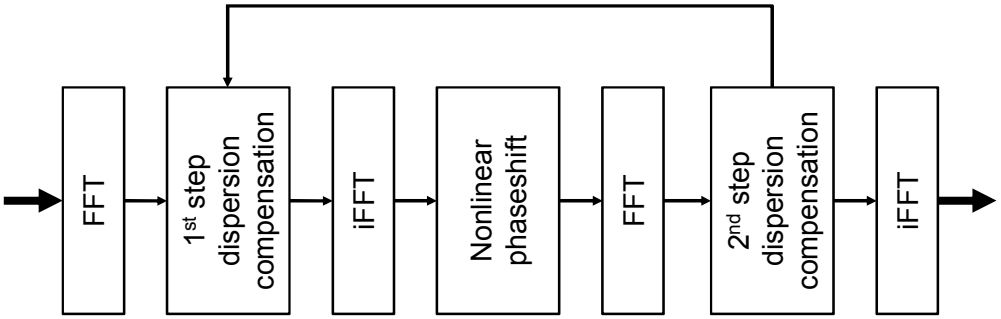

Figure 20: Block Diagram of Digital Backpropagation

The symmetric split step method for digital backpropagation is implemented as shown in the signal flow model of Figure 20 and replaces the block compensating for chromatic dispersion in standard digital coherent receivers. In Chapter 4 we will restrict ourselves to compensating only for intra-channel nonlinearities, which means that digital backpropagation will only be performed on the central channel. Nevertheless it is, possible to detect and backpropagate neighbouring channels as well [27, 29] and therefore compensate for intra-channel nonlinearities such as self-phase modulation (SPM) and inter-channel nonlinearities such as cross phase modulation (XPM) given that sufficient electrical receiver bandwidth is available. An investigation of multiple channel DBP solutions is presented in section 5.5.

3.3.3 Experimental Demonstrations of Digital Backpropagation

In light of the coming “capacity crunch” [30], it is essential to provide increased optical transport capacity by using spectrally more efficient modulation formats. Unfortunately, higher order modulation formats suffer from increased OSNR requirements as well as a

higher susceptibility to nonlinear distortions, restricting the reach over which increased capacity can be provided. One potential solution to increase transmission reach is to compensate for deterministic nonlinear distortions by digitally backpropagating portions of the received spectrum, as introduced in the previous section.

Table 1: Experimental demonstrations of Digital Backpropagation to compensate for intra-channel nonlinearities in a WDM environment. Publications resulting from this work are highlighted in grey.

YEAR	MODULATION FORMAT	LINE RATE	NUMBER OF CHANNELS	CHANNEL SPACING	PERFORMANCE IMPROVEMENT
2009 [31]	PDM-QPSK	112 Gbit/s	19	100 GHz	2dBQ
2009 [32]	PDM-QPSK	112 Gbit/s	40	100 GHz	1.7dBQ
2009 [33]	PDM-QPSK	112 Gbit/s	72	50 GHz	0.25dBQ
2010 [34]	PDM CO-OFDM	224 Gbit/s	7	50 GHz	0.5dBQ
2010 [35]	PDM-QPSK	112 Gbit/s	10	50 GHz	3% reach
2010 [35]	PDM-QPSK	112 Gbit/s	10	100 GHz	24% reach
2011 [36]	PDM-16-QAM	224 Gbit/s	3	50 GHz	10% reach
2011 [37]	PDM-16-QAM	112 Gbit/s	3	50 GHz	24% reach
2011 [38]	PDM CO-OFDM	448 Gbit/s	3	80 GHz	25% reach
2011 [39]	PDM CO-OFDM	111 Gbit/s	10	??? GHz	25% reach (1.3dBQ)
2011 [40]	PDM-QPSK	112 Gbit/s	40	100 GHz	1.3dBQ
2011 [41]	PDM-QPSK	224 Gbit/s	40	100 GHz	1.2dBQ
2011 [42]	PDM-QPSK, NRZ aggressors	112 Gbit/s	80	50 GHz	0.9dBQ
2011 [43]	PDM-QPSK	112 Gbit/s	40	100 GHz	1.6dBQ
2012 [44]	PDM-8-QAM	112 Gbit/s	7	50 GHz	17.8% reach
2012 [44]	PDM-8-PSK	112 Gbit/s	7	50 GHz	20% reach
2012 [44]	PDM-QPSK	112 Gbit/s	7	50 GHz	19.6% reach

Table 1 shows recent experimental results employing digital backpropagation to compensate for intra-channel nonlinearities. All these experiments have in common that a single channel (or band of subcarriers in case of OFDM) is coherently detected after being propagated in a WDM environment. The received portion of the spectrum is then digitally backpropagated to increase margin or transmission reach as detailed in the last column. Whilst DBP can lead to modest performance improvements of +2dBQ [31] (increase in Q^2-factor in dB: $Q^2 = 20\,log\left(\sqrt{2}\,erfcinv(2 \cdot BER)\right)$ – inverse of

equation (70)) or +24% transmission reach [35] when a coarse frequency grid of 100GHz is used, it is limited when the frequency spacing is reduced. In case of a 50GHz spacing, the improvement of transmission performance has been limited to less than 1dBQ [33, 34, 42] or small increases in transmission reach of +3% [35]. However, recent investigations, which are part of this work, have revealed that transmission reach can be increased by ~20% even on a 50GHz grid [44].

Table 2: Experimental demonstrations of full field Digital Backpropagation in a single channel environment (*all 3 channels are backpropagated)

YEAR	MODULATION FORMAT	LINE RATE	NUMBER OF CHANNELS	CHANNEL SPACING	PERFORMANCE IMPROVEMENT
2008 [27]*	BPSK	6 Gbit/s	3	7 GHz	121% reach
2009 [45]	PDM CO-OFDM	111 Gbit/s	1		13% reach
2009 [29]*	PDM-BPSK	12 Gbit/s	3	7 GHz	16dBQ
2009 [46]	PDM-QPSK	42.7 Gbit/s	1		33% reach
2009 [46]	PDM-QPSK	85.4 Gbit/s	1		50% reach
2010 [47]	PDM CO-OFDM	61.7 Gbit/s	1		2.2dBQ
2010 [35]	PDM-QPSK	112 Gbit/s	1		46% reach
2011 [48]	PDM-QPSK	42.7 Gbit/s	1		1.6dBQ
2011 [48]	PDM-16-QAM	85.4 Gbit/s	1		1dBQ
2011 [37]	PDM-16-QAM	112 Gbit/s	1		67% reach
2011 [36]	PDM-16-QAM	224 Gbit/s	1		12% reach
2011 [39]	PDM CO-OFDM	111 Gbit/s	1		13.3% reach (0.5dBQ)
2011 [49]	PDM-QPSK	43 Gbit/s	1		1.9dBQ
2012 [50]	PS-QPSK	112 Gbit/s	1		20.7% reach
2012 [44]	PDM-8-QAM	112 Gbit/s	1		69.7% reach
2012 [44]	PDM-8-PSK	112 Gbit/s	1		59.3% reach
2012 [44]	PDM-QPSK	112 Gbit/s	1		31.6% reach

It has been demonstrated that at least 7-9 WDM channels have to be transmitted to capture all XPM distortions that restrict the efficiency of the DBP algorithm and reliably assess the performance under WDM conditions [36, 51]. Consequently, the improvement of up to ~25% increase in reach obtained for 3 channel PDM-16QAM [37] and PDM CO-OFDM [38] might be significantly reduced when adding additional WDM

channels. Polarisation mode dispersion has been found to limit the efficiency of DBP depending on the ratio between symbol slot and differential group delay (DGD) up to 2dBQ for single carrier and 6dBQ for OFDM transmission [51]. In practice however, DGD is expected to be as small as 0.1 ps/$\sqrt{\text{km}}$ leading only to a negligible walk-off of ~0.12×symbol slot in case of 28GBd transmission over 2000km. Even under high PMD conditions DBP has been demonstrated to be effective [42].

In the absence of uncompensated inter channel nonlinearities the performance improvement gained from DBP is much higher as detailed in Table 2, which shows recent experimental results employing DBP to the entire transmitted optical field. Under these circumstances the DBP algorithm has been found to be largely limited by non-deterministic nonlinear signal-ASE interactions [52]. Nevertheless, Goldfarb [51] and Yaman [29] demonstrated an impressive increase of +121% transmission reach and a performance improvement of 16dBQ, under the condition that a very low symbol rate is used and all 3 transmitted WDM channels can be fitted into the electrical bandwidth of a single coherent receiver to be digitally backpropagated. Furthermore it has been found that higher order modulation formats show an increased benefit for modulation formats when comparing increase in transmission reach of +67% for PDM-16QAM [37] as well as +69.7% and +59.3% for PDM-8QAM and PDM-8PSK [44] on one side to +31.6% PDM-QPSK [44] and +20.7% for PS-QPSK [50] on the other side. Similar conclusions have been drawn as a result of simulation studies comparing PDM-QPSK and PDM-16QAM transmission [53] and multilevel QAM formats [54].

The optimum number of computational DBP steps has been shown to be related to the spectral width of the received signal (symbol rate) and the chromatic dispersion parameter of the fibre [53]. Up to a symbol rate of 28GBd 1 step per transmitted span is widely established as providing a good trade-off between algorithm complexity and performance improvement [31, 32, 45, 48, 55]. However, at higher symbol rates such as 56GBd more steps per span are necessary to provide optimum performance as demonstrated in [41]. In an attempt to reduce complexity of the DBP algorithm, the correlation of the nonlinear distortion incident on neighbouring symbols has been exploited by filtering the calculated nonlinear phase shift [28]. This method has been implemented in the frequency domain [28] as well as in the time domain [40] reducing the number of required steps by 75% without sacrificing performance.

3.3.4 Alternative nonlinear compensation schemes

Alternative solutions for nonlinear equalisation have been investigated in the last decade mainly with the focus on reduced complexity. A particular low complexity solution is a data dependant *nonlinear phase shift* at the receiver, which can be regarded as digital backpropagation with a single step per link. This compensation method has been investigated in the analogue [56] and digital domain [57], along with the introduction of non-rectangular decision boundaries based on a priori knowledge of the transmission link [58]. All of these approaches exploit the fact that optically compensated transmission links produce non circular symmetric nonlinear distortions ("bean" shape constellation diagrams), which can be easily equalised. However, in uncompensated transmission, distortion statistics tend to be circular symmetric [59], rendering this approach ineffective.

Maximum-likelihood sequence estimation (MLSE) has been found to be the optimum nonlinear decoder in presence of deterministic distortions such as chromatic dispersion and intra-channel nonlinearities [60]. It is based on finding the most likely transmitted sequence by computing the cross-correlations between a set of expected sequences and the received one. The MLSE is usually implemented with the Viterbi algorithm [61] in which case the computational complexity scales with M^N where M is the symbol alphabet and N the memory length related to the pulse spreading. Since modern coherent systems omit optical dispersion compensation and increased amounts of accumulated dispersion have been shown to reduce inter-channel nonlinear distortions, a high pulse spreading is the consequence and MLSE would incur an unacceptable complexity burden. Nevertheless, reduced complexity MLSE has been demonstrated for uncompensated 10.7Gbit/s IMDD transmission and high memory length [62] and in the case of reduced memory length due to optically compensated transmission [63]. Note that even though MLSE has been implemented for coherent detection of 112Gbit/s PDM-QPSK in [64], it is used to reduce ISI due to aggressive filtering and not capable of compensating for large amounts of nonlinearity, since the memory introduced by chromatic dispersion is compensated separately.

Another approach to the compensation for deterministic nonlinearities is the *maximum a posteriori probability* (MAP) detector, which exploits the pattern dependency of nonlinear distortions. A training sequence is sent across the channel to initialise a look up table at the receiver with statistical distributions of a certain memory length. Similarly to MLSE, the pattern with the highest correlation is chosen as the MAP decision, but minimising the symbol error rate rather than the probability of a sequence

error as in case of MLSE [65]. Notable performance improvements have been demonstrated recently in lab experiments [66, 67] and in simulation [68], albeit at the expense of significant DSP complexity.

Volterra series transfer functions have initially been investigated to increase the speed of fibre transmission simulations [69]. These types of nonlinear transfer functions based on a generalisation of the Taylor series have recently attracted much interest, because they allow to design nonlinear filters which are capable of compensating for nonlinear distortions[70-72]. However, adequate DBP algorithms outperform nonlinear Volterra equalisers designed with the focus on low complexity [72].

The transmitter side equivalent to digital backpropagation is *electronic predistortion*, which requires digital-to-analogue converters (DACs) and signal processing capabilities at the transmitter [73-75]. In the case of coherent detection an ASIC would be required at the receiver for the adaptive equaliser, which may render the concentration of all DSP at the receiver the more economical solution instead of an additional ASIC at the transmitter.

3.3.5 Equalisation

Multiple-input-multiple-output (MIMO) systems are widely used in optical communications [23] to combat multipath propagation effects such as polarisation-mode-dispersion (PMD). This structure, which is sometimes referred to alternatively as a butterfly structure, is implemented in this work and consists of four FIR filters ($\mathbf{h}_{xx}$, $\mathbf{h}_{xy}$, $\mathbf{h}_{yx}$ and $\mathbf{h}_{yy}$) as displayed in Figure 21. These filters have to include adaptive taps, due to the time dependant nature of PMD. The transfer function of the sample $x_{out}(k)$, which depends on the input samples $x_{in}(k)$ and $y_{in}(k)$, is given here:

$$x_{out}(k) = \mathbf{h}_{xx}^{T}\boldsymbol{x}_{in} + \mathbf{h}_{xy}^{T}\boldsymbol{y}_{in} = \sum_{m=0}^{M-1} h_{xx}(m)x_{in}(k-m) + h_{xy}(m)y_{in}(k-m) \qquad \textbf{(59)}$$

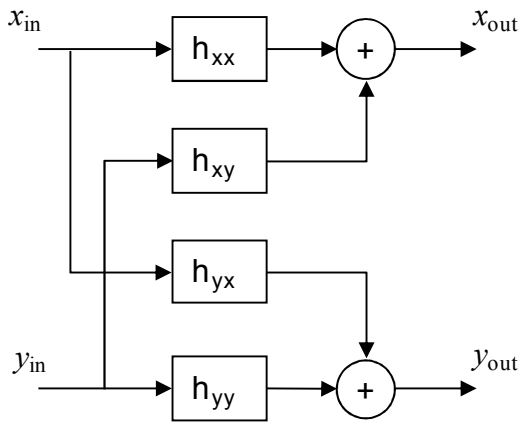

Figure 21: Butterfly structure to compensate for polarisation-mode-dispersion

Generally, an adaptive equaliser, as described in the previous paragraph, tries to estimate the Jones-matrix of the channel and apply the inverse of it to the signal. Additionally, it emulates a matched filter and therefore compensates for linear distortions incurred by filtering, leading to an optimisation of the receiver sensitivity. An adaptive equaliser is also capable of compensating for chromatic dispersion. However splitting up PMD- and chromatic dispersion compensation is desirable, since it leads to a much smaller footprint of the DSP. If we assume a transmission system similar to the one investigated in Chapter 5 (1000km SSMF with a PMD-coefficient of 0.1ps/$\sqrt{\text{km}}$), the mean DGD adds up to 3.2ps which is in case of 28Gbd less than 0.1×symbol spacing resulting in 3 taps to be sufficient to track the mean DGD as opposed to more than 400 taps for chromatic dispersion compensation. Since PMD shows a Maxwellian distribution around the mean DGD-value, we use 15 equaliser taps in this work, which is sufficient to track most of the random polarisation rotations experienced in the system.

To adapt the taps to the changing channel conditions, different update-algorithms are necessary depending on the properties of the modulation format. The following paragraphs focus on the details of the equaliser algorithms, which have been implemented as part of this work for PDM-BPSK, PDM-QPSK, PDM-8PSK, PDM-8QAM, PDM-16QAM and PS-QPSK.

In case of PDM-QPSK and PDM-8PSK, we implement the constant modulus algorithm (CMA, [76]), which exploits the fact that the symbols lie on intensity rings, i.e. have a constant modulus. The updating algorithms are given in equation (60), with the step size parameter μ, the polarisation dependant error-signals (e_x, e_y) and the complex conjugates of the input sequences ($\mathbf{x}_{in}^*$, $\mathbf{y}_{in}^*$).

$$\begin{aligned}
\mathbf{h}_{xx} &\rightarrow \mathbf{h}_{xx} + \mu e_x x_{out}(k)\mathbf{x}_{in}^* \\
\mathbf{h}_{xy} &\rightarrow \mathbf{h}_{xy} + \mu e_x x_{out}(k)\mathbf{y}_{in}^* \\
\mathbf{h}_{yx} &\rightarrow \mathbf{h}_{yx} + \mu e_y y_{out}(k)\mathbf{x}_{in}^* \\
\mathbf{h}_{yy} &\rightarrow \mathbf{h}_{yy} + \mu e_y y_{out}(k)\mathbf{y}_{in}^*
\end{aligned} \tag{60}$$

The input samples have to be normalised to unit power to determine the error signals e_x and e_y (Figure 22). The equaliser tries to minimise the amplitudes of e_x and e_y in a mean squares sense to converge on the inverse Jones matrix of the channel. However, in case of 8QAM and 16QAM one has to decide to which radius the current symbol belongs to, before being able to calculate an error signal. The set of error signals of this so called radially directed equaliser (RDE) are shown in Figure 22 (a) and (b) [77]. The step size parameter starts at 0.1 and then gradually decreases to 0.01 to ensure safe convergence.

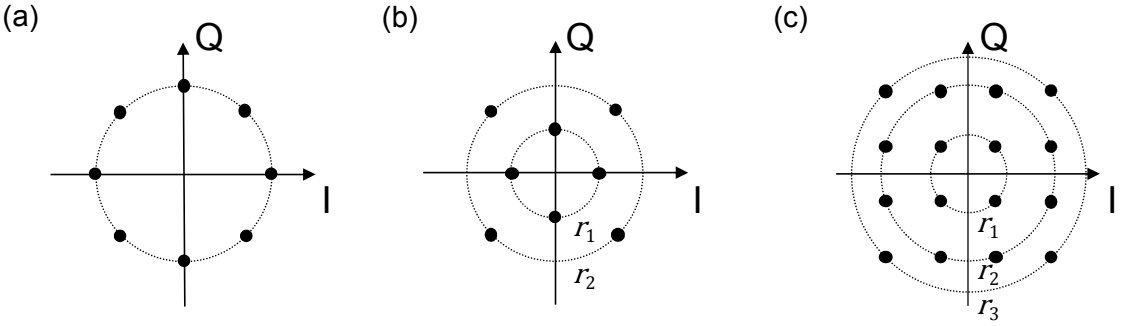

(a)

$$e_x = 1 - |x_{out}|^2$$

$$e_y = 1 - |y_{out}|^2$$

(b)

$$e_x = \begin{cases} |r_1|^2 - |x_{out}|^2 \\ |r_2|^2 - |x_{out}|^2 \end{cases}$$

$$e_y = \begin{cases} |r_1|^2 - |y_{out}|^2 \\ |r_2|^2 - |y_{out}|^2 \end{cases}$$

(c)

$$e_x = \begin{cases} |r_1|^2 - |x_{out}|^2 \\ |r_2|^2 - |x_{out}|^2 \\ |r_3|^2 - |x_{out}|^2 \end{cases}$$

$$e_y = \begin{cases} |r_1|^2 - |y_{out}|^2 \\ |r_2|^2 - |y_{out}|^2 \\ |r_3|^2 - |y_{out}|^2 \end{cases}$$

Figure 22: Constellation diagrams of 8PSK, 8QAM and 16QAM, with equivalent error signals.

For PDM-BPSK a decision directed equaliser can help to improve convergence with respect to just using the standard CMA. After preconvergence with the CMA and frequency offset removal the receiver moves into a decision directed mode, similarly to the equaliser implemented for PDM-QPSK in [21]. In this case the outputs $x_{out}(k)$ and $y_{out}(k)$ of the butterfly structure displayed in Figure 21 are combined with an additional phase correction term, resulting in new output values: $X(k) = \exp(-j\varphi_x(k))x_{out}(k)$ and $Y(k) = \exp(-j\varphi_y(k))y_{out}(k)$. The updating algorithms in (60) turn into:

$$\begin{aligned}\mathbf{h}_{xx} &\rightarrow \mathbf{h}_{xx} + \mu e_x \exp(j\varphi_x)\mathbf{x}_{in}^* \\ \mathbf{h}_{xy} &\rightarrow \mathbf{h}_{xy} + \mu e_x \exp(j\varphi_x)\mathbf{y}_{in}^* \\ \mathbf{h}_{yx} &\rightarrow \mathbf{h}_{yx} + \mu e_y \exp(j\varphi_y)\mathbf{x}_{in}^* \\ \mathbf{h}_{yy} &\rightarrow \mathbf{h}_{yy} + \mu e_y \exp(j\varphi_y)\mathbf{y}_{in}^*\end{aligned} \quad (61)$$

With the corresponding error functions for each polarisation:

$$\begin{aligned}e_x &= \mathrm{sgn}(\mathrm{Re}\{X\}) - X \\ e_y &= \mathrm{sgn}(\mathrm{Re}\{Y\}) - Y\end{aligned} \quad (62)$$

Where $\mathrm{sgn}(\mathrm{Re}\{X\})$ denotes the sign of the real part of the relevant symbol. The estimated phase values, averaged over the N following symbols, can be written as:

$$\begin{aligned}\varphi_x &= \frac{1}{\mathrm{N}}\arg\sum_{\mathrm{i}=1}^{\mathrm{N}} \mathrm{sgn}(\mathrm{Re}\{X_i\}) \cdot X_i \\ \varphi_y &= \frac{1}{\mathrm{N}}\arg\sum_{\mathrm{i}=1}^{\mathrm{N}} \mathrm{sgn}(\mathrm{Re}\{Y_i\}) \cdot Y_i\end{aligned} \quad (63)$$

In the case of PS-QPSK a polarisation switch CMA is used to ensure convergence [78]. A decision based on the energy of the symbol enables to identify the polarisation with the QPSK constellation. This polarisation is then equalised with a standard CMA-equaliser, forcing the symbol to the radius $R = 1$, while the other polarisations energy is being minimised with $R = 0$. The resulting error functions are shown in equation (64):

$$\begin{aligned}e_x &= R_x - |x_{out}|^2 \\ e_y &= R_y - |y_{out}|^2\end{aligned} \quad (64)$$

Additionally, for every modulation format the bit-error rate is monitored to prevent the equaliser from converging on the same polarisation, in which case the equaliser is re-initialised with a different tap weight until it has converged correctly.

3.3.6 Carrier Phase Recovery

Digital phase estimation is used to recover the signal's carrier phase. A widely used carrier phase recovery scheme for PSK signals such as BPSK, QPSK and 8PSK is the feed forward M^{th} power phase estimation [4] (or Viterbi and Viterbi algorithm [79]), which has been implemented as part of the coherent receiver model in the research described in this thesis. The received complex samples are first raised to the M^{th} power

to eliminate the phase modulation (Figure 23). Afterwards the k[th] symbol $x(k)$ is added to its N predecessors and successors to average the estimated phase in order to combat the influence of noise. The argument divided by M leads to a phase estimate $\varphi'(k)$ for $x(k)$:

$$\varphi'(k) = \frac{1}{M} \cdot \arg\left(\frac{1}{2\mathrm{N}+1} \sum_{\mathrm{l}=-\mathrm{N}}^{\mathrm{N}} x(k+l)^{\mathrm{M}} \right) \tag{65}$$

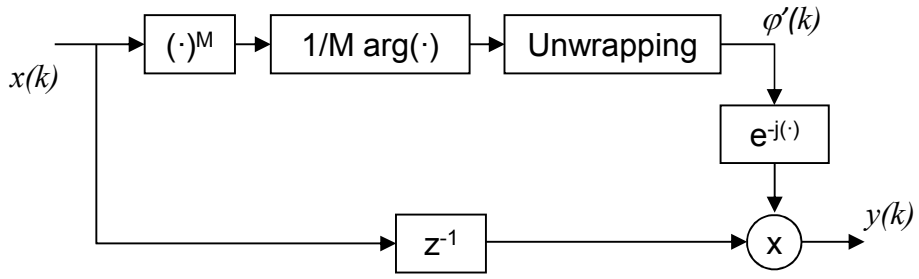

Figure 23: carrier recovery using the M[th] power scheme

Generally, this averaging can be seen as a low-pass filtering with the number of taps determining the bandwidth of the filter. Therefore, the optimum block-length $2 \cdot N + 1$ depends on the amount of noise that has been picked up by the signal and the symbol-rate, since a lower symbol-rate leads to a larger phase walk-off between neighbouring symbols, increasing the laser phase noise variance $\sigma^2 = 2\pi \cdot \Delta\vartheta \cdot T_S$. The estimated phase must be unwrapped to combat cycle-slips (90 degree phase jumps) that arise from the signals phase ambiguity in presence of severe phase noise or ASE noise. Furthermore, differential encoding can be employed to increase resilience towards cycle slips even more and avoid fatal error bursts.

To recover the phase of a polarisation switched QPSK the M[th] power phase estimator has to be slightly modified. The two parallel signal streams of a PS-QPSK signal, one in each polarisation, can be collapsed to a single QPSK stream by making decisions on the energy in each symbol slot. The resulting QPSK signal can then be processed with the standard M[th] power scheme and the phase can be recovered [78].

Since QAM-modulation is not restricted to the optical phase alone, the M[th] power algorithm as introduced above, is not suitable for this kind of modulation. Therefore, in this work, a decision directed phase-locked loop [77] has been used to track the phase in case of 8QAM and 16QAM modulation. As shown in Figure 24, the PLL calculates the error between $y(\mathrm{k})$ and the corresponding hard-decision $y'(\mathrm{k})$:

$$e(k) = y(k) - y'(k) \quad \textbf{(66)}$$

The decision boundaries were set, assuming phase-noise to be the dominant distortion at this stage [80]. The error-information is used to update the phase estimate for the following symbol:

$$\varphi(k+1)' = \varphi(k)' - \mu \,\mathrm{Im}\{y(k)e^*(k)\} \quad \textbf{(67)}$$

where * denotes the complex conjugate and μ is the step size parameter, which was set to 0.1 [77]. Finally, the estimated phase is then applied to the next symbol $y(k+1) = x(k+1) \cdot \exp(-\mathrm{j}\,\varphi(k+1)')$.

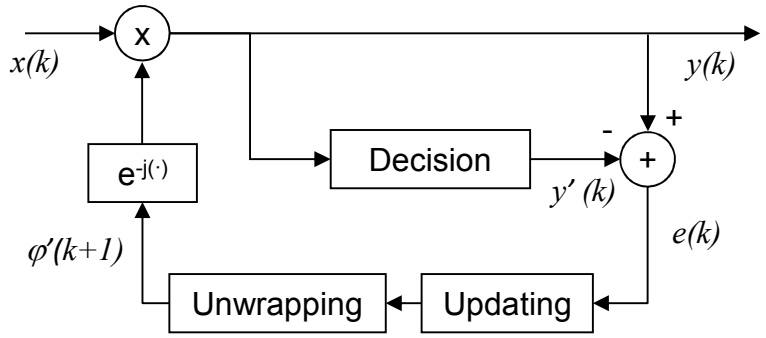

Figure 24: Decision-directed carrier recovery

3.4 Summary

This chapter described transmitter and receiver structures of next generation high speed optical transmission systems. Initially the generation of higher order phase shift keyed modulation formats (e.g. QPSK and 8PSK), higher order quadrature amplitude modulation formats (e.g. 8QAM and 16QAM) and polarisation switched QPSK is discussed. Coding schemes such as Gray coding, which minimises the bit error probability for a given symbol error rate and differential coding, which minimises the bit error rate in presence of cycle slips as introduced by digital phase estimation are explained for higher order modulation formats. Subsequently the digital coherent receiver is explained using the example of single ended detection. Digital signal processing algorithms compensating for a variety of distortions are detailed, starting with FIR filtering to compensate for chromatic dispersion. The digital backpropagation algorithm (DBP) is introduced as a means to compensate for nonlinear distortions of the optical channel. After the available literature on DBP is reviewed, recent progress in the field is highlighted focussing on achieved performance improvements by compensating for intra-channel nonlinearities (partial field DBP) and full field DBP. Additionally, alternative approaches to compensate for nonlinearities such as maximum

likelihood sequence estimation (MLSE), maximum a posteriori detection (MAP) and Volterra equalisers are investigated. The chapter concludes by describing adaptive equalisers to compensate for PMD, polarisation rotations and the linear frequency response of the channel as well as phase recovery algorithms for higher order modulation formats.

The next chapter examines long-haul and ultra-long-haul transmission of higher order modulation formats in single channel and WDM configurations. Line rates of 42.9Gbit/s and 112Gbit/s per wavelength channel are investigated by using a recirculating loop with standard single mode fibre and EDFA amplification and phase and polarisation diverse coherent detection. The impact of receiver based DBP is assessed for a fixed complexity per distance (1 step per span) and a wide range of modulation formats. Experimental results are backed up with extensive computer simulations.

3.5 References

[1] R. A. Griffin and A. C. Carter, "Optical differential quadrature phase-shift key (oDQPSK) for high capacity optical transmission," in *Proc. Conference on Optical Fiber Communication and the National Fiber Optic Engineers Conference OFC/NFOEC 2002*, 2002, pp. 367-368.

[2] M. Seimetz, L. Molle, D.-D. Gross, B. Auth, and R. Freund, "Coherent RZ-8PSK Transmission at 30Gbit/s over 1200km Employing Homodyne Detection with Digital Carrier Phase Estimation," in *Proc. 33st European Conference on Optical Communication ECOC 2007*, 2007.

[3] M. Serbay, C. Wree, and W. Rosenkranz, "Experimental investigation of RZ-8DPSK at 3 x 10.7 Gb/s," in *Proc. 18th Annual Meeting of the IEEE Lasers and Electro-Optics Society LEOS 2005*, 2005, pp. 483-484.

[4] J. D. Proakis and M. Salehi, *Digital Communications*: McGraw-Hill, 2008.

[5] X. Zhou, J. Yu, and P. Magill, "Cascaded two-modulus algorithm for blind polarization de-multiplexing of 114-Gb/s PDM-8-QAM optical signals," in *Proc. Conference on Optical Fiber Communication and the National Fiber Optic Engineers Conference OFC/NFOEC 2009*, 2009, pp. 1-3.

[6] R. Cigliutti, E. Torrengo, G. Bosco, N. P. Caponio, A. Carena, V. Curri, P. Poggiolini, Y. Yamamoto, T. Sasaki, and F. Forghieri, "Transmission of 9 x 138 Gb/s Prefiltered PM-8QAM Signals Over 4000 km of Pure Silica-Core Fiber," *Journal of Lightwave Technology,* vol. 29, pp. 2310-2318, August 2011.

[7] N. Kikuchi, K. Mandai, and S. Sasaki, "Experimental Demonstration of Incoherent Optical Multilevel Staggered-APSK (Amplitude- and Phase-Shift Keying) Signaling," in *Proc. Conference on Optical Fiber communication/National Fiber Optic Engineers Conference OFC/NFOEC 2008*, 2008, pp. 1-3.

[8] K.-P. Ho and H.-W. Cuei, "Generation of arbitrary quadrature signals using one dual-drive Modulator," *Journal of Lightwave Technology,* vol. 23, pp. 764-770, 2005.

[9] P. J. Winzer, A. H. Gnauck, C. R. Doerr, M. Margarini, and L. L. Buhl, "Spectrally Efficient Long-Haul Optical Networking Using 112-Gb/s Polarization-Multiplexed 16-QAM," *Journal of Lightwave Technology,* vol. 28, pp. 547-556, February 2010.

[10] S. Makovejs, D. S. Millar, V. Mikhailov, G. Gavioli, R. I. Killey, S. J. Savory, and P. Bayvel, "Novel Method of Generating QAM-16 Signals at 21.3 Gbaud and Transmission Over 480 km," *Photonics Technology Letters,* vol. 22, pp. 36-38, 2010.

[11] T. Sakamoto, A. Chiba, and T. Kawanishi, "50-Gb/s 16 QAM by a quad-parallel Mach-Zehnder modulator," in *Proc. 33th European Conference on Optical Communication ECOC 2007*, 2007.

[12] M. Karlsson and E. Agrell, "Which is the most power efficient modulation format in optical links?," *Optics Express,* vol. 17, pp. 10814-10819, 2009.

[13] E. Agrell and M. Karlsson, "Power-Efficient Modulation Formats in Coherent Transmission Systems," *Journal of Lightwave Technology,* vol. 27, pp. 5115-5126, 2009.

[14] J. Renaudier, O. Bertran Pardo, H. Mardoyan, M. Salsi, P. Tran, E. Dutisseuil, G. Charlet, and S. Bigo, "Experimental Comparison of 28Gbaud Polarization Switched- and Polarisation Division Multiplexed- QPSK in WDM long-haul Transmission," in *Proc. ECOC 2011*, Geneva, 2011, p. Mo.2.B.3.

[15] W. Freude, R. Schmogrow, B. Nebendahl, D. Hillerkuss, J. Meyer, M. Dreschmann, M. Huebner, J. Becker, C. Koos, and J. Leuthold, "Software-Defined Optical Transmission," *2011 13th International Conference on Transparent Optical Networks (Icton),* 2011.

[16] ITU-T. (2004). *Recommendation G.975 (10/00)*. Available: http://www.itu.int/rec/T-REC-G.975-200010-I/en

[17] E. Ip and J. M. Kahn, "Feedforward Carrier Recovery for Coherent Optical Communications," *Journal of Lightwave Technology,* vol. 25, pp. 2675-2692, 2007.

[18] K.-P. Ho, *Phase Modulated Optical Communication Systems*: Springer, 2005.

[19] C. Kim and G. Li, "Direct-detection optical differential 8-level phase-shift keying (OD8PSK) for spectrally efficient transmission," *Opt. Express,* vol. 12, pp. 3415-3421, 2004.

[20] M. Seimetz, M. Noelle, and E. Patzak, "Optical Systems With High-Order DPSK and Star QAM Modulation Based on Interferometric Direct Detection," *Journal of Lightwave Technology,* vol. 25, pp. 1515-1530, 2007.

[21] S. J. Savory, G. Gavioli, R. I. Killey, and P. Bayvel, "Electronic compensation of chromatic dispersion using a digital coherent receiver," *Optics Express,* vol. 15, pp. 2120-2126, 2007.

[22] E. Ip, A. P. T. Lau, D. J. F. Barros, and J. M. Kahn, "Coherent detection in optical fiber systems," *Optics Express,* vol. 16, pp. 753-791, 2008.

[23] S. J. Savory, "Digital filters for coherent optical receivers," *Optics Express,* vol. 16, pp. 804-817, 2008.

[24] G. P. Agrawal, *Nonlinear Fiber Optics*: Academic Press, 1995.

[25] C. R. Menyuk, "Application of multiple-length-scale methods to the study of optical fiber transmission," *Journal of Engineering Mathematics,* vol. 36, pp. 113-136, 1999.

[26] E. Ip and J. M. Kahn, "Compensation of dispersion and nonlinear effects using digital backpropagation," *Journal of Lightwave Technology,* vol. 26, pp. 3416-3425, 2008.

[27] G. Goldfarb, M. G. Taylor, and G. Li, "Experimental Demonstration of Fiber Impairment Compensation Using the Split-Step Finite-Impulse-Response Filtering Method," *Photonics Technology Letters,* vol. 20, pp. 1887-1889, 2008.

[28] L. B. Du and A. J. Lowery, "Improved single channel backpropagation for intra-channel fiber nonlinearity compensation in long-haul optical communication systems," *Optics Express,* vol. 18, pp. 17075-17088, August 2010.

[29] F. Yaman and G. Li, "Nonlinear Impairment Compensation for Polarization-Division Multiplexed WDM Transmission Using Digital Backward Propagation " *Photonics Journal,* vol. 1, pp. 144-152, August 2009.

[30] A. Chraplyvy, "The coming capacity crunch," in *Proc. 35th European Conference on Optical Communication ECOC 2009*, Vienna, 2009, p. Mo1.0.2.

[31] S. Oda, T. Tanimura, T. Hoshida, C. Ohshima, H. Nakashima, Z. Tao, and J. C. Rasmussen, "112 Gb/s DP-QPSK transmission using a novel nonlinear compensator in digital coherent receiver," in *Proc. Conference on Optical Fiber Communication OFC 2009*, 2009, pp. 1-3.

[32] T. Tanimura, T. Hoshida, S. Oda, T. Tanaka, C. Oshima, Z. Tao, and J. C. Rasmussen, "Systematic Analysis on Multi-Segment Dual-Polarisation Nonlinear Compensation in 112Gb/s DP-QPSK Coherent Receiver," in *Proc. 35th European Conference on Optical Communication ECOC 2009*, Vienna, 2009, p. 9.4.5.

[33] G. Charlet, M. Salsi, P. Tran, M. Bertolini, H. Mardoyan, J. Renaudier, O. Bertran-Pardo, and S. Bigo, "72x100Gb/s Transmission over Transoceanic Distance, Using Large Effective Area Fiber, Hybrid Raman-Erbium Amplification and Coherent Detection," in *Proc. National Fiber Optic Engineers Conference*, 2009, p. PDPB6.

[34] X. Liu, S. Chandrasekhar, B. Zhu, P. J. Winzer, and D. W. Peckham, "7x224-Gb/s WDM Tranmission of Reduced-Guard-Interval CO-OFDM with 16-QAM Subcarrier Modulation on a 50-GHz Grid over 2000 km of ULAF and Five ROADM Passes," in *Proc. 36th European Conference on Optical Communication ECOC 2010*, Torino, 2010, p. Tu.3.C.2.

[35] S. J. Savory, G. Gavioli, E. Torrengo, and P. Poggiolini, "Impact of Interchannel Nonlinearities on a Split-Step Intrachannel Nonlinear Equalizer," *Photonics Technology Letters,* vol. 22, pp. 673 - 675, May 2010.

[36] C. Behrens, S. Makovejs, R. I. Killey, S. J. Savory, M. Chen, and M. Bayvel, "Pulse-shaping versus digital backpropagation in 224Gbit/s PDM-16QAM transmission," *Optics Express,* vol. 19, pp. 12879-12884, 2011.

[37] S. Makovejs, "High-speed optical fibre transmission using advanced modulation formats," PhD thesis, Electrical and Electronic Engineering, University College London, London, 2011.

[38] X. Liu, S. Chandrasekhar, B. Zhu, P. J. Winzer, A. H. Gnauck, and D. W. Peckham, "448-Gb/s Reduced-Guard-Interval CO-OFDM Transmission Over 2000 km of Ultra-Large-Area Fiber and Five 80-GHz-Grid ROADMs," *Journal of Lightwave Technology,* vol. 29, pp. 483-489, February 2011.

[39] E. Yamazaki, A. Sano, T. Kobayashi, E. Yoshida, and Y. Miyamoto, "Mitigation of Nonlinearities in Optical Transmission Systems," in *Proc. Conference on*

Optical Fiber Communication and the National Fiber Optic Engineers Conference OFC/NFOEC 2011, Los Angeles, 2011, p. OThF1.

[40] L. Li, Z. Tao, L. Dou, W. Yan, S. Oda, T. Tanimura, T. Hoshida, and J. C. Rasmussen, "Implementation Efficient Nonlinear Equalizer Based on Correlated Digital Backpropagation," in *Proc. Conference on Optical Fiber Communication and the National Fiber Optic Engineers Conference OFC/NFOEC 2011*, Los Angeles, 2011, p. OWW3.

[41] M. Salsi, O. Bertran-Pardo, J. Renaudier, W. Idler, H. Mardoyan, P. Tran, G. Charlet, and S. Bigo, "WDM 200Gb/s Single Carrier PDM-QPSK Transmission over 12,000km," in *Proc. 37th European Conference on Optical Communication ECOC 2011*, Geneva, 2011, p. Th.13.C.5.

[42] T. Tanimura, S. Oda, T. Hoshida, L. Li, Z. Tao, and J. C. Rasmussen, "Experimental Characterisation of Nonlinearity Mitigation by Digital Back Propagation and Nonlinear Polarization Crosstalk Canceller under High PMD condition," in *Proc. Conference on Optical Fiber Communication and the National Fiber Optic Engineers Conference OFC/NFOEC 2011*, Los Angeles, 2011, p. JWA20.

[43] W. Yan, Z. Tao, L. Dou, L. Li, S. Oda, T. Tanimura, T. Hoshida, and J. C. Rasmussen, "Low Complexity Digital Perturbation Back-propagation," in *Proc. European Conference on Optical Communications ECOC 2011*, Geneva, 2011, p. Tu.3.A.2.

[44] C. Behrens, D. Lavery, R. I. Killey, S. J. Savory, and P. Bayvel, "Long-haul WDM transmission of PDM-8PSK and PDM-8QAM with nonlinear DSP," in *Proc. Conference on Optical Fiber Communication and the National Fiber Optic Engineers Conference OFC/NFOEC 2012*, Los Angeles, 2012, p. OMA3A.4.

[45] E. Yamazaki, H. Masuda, A. Sano, T. Yoshimatsu, T. Kobayashi, E. Yoshida, Y. Miyamoto, R. Kudo, K. Ishihara, M. Matsui, and Y. Takatori, "Multi-staged Nonlinear Compensation in Coherent Receiver for 16340-km Transmission of 111-Gb/s No-Guard-Interval Co-OFDM," in *Proc. 35th European Conference on Optical Communication ECOC 2009*, 2009.

[46] D. S. Millar, S. Makovejs, V. Mikhailov, R. I. Killey, P. Bayvel, and S. J. Savory, "Experimental Comparison of Nonlinear Compensation in Long-Haul PDM-QPSK Transmission at 42.7 and 85.4 Gb/s," in *Proc. 35th European Conference on Optical Communication ECOC 2009*, 2009.

[47] L. Du, B. Schmidt, and A. Lowery, "Efficient Digital Backpropagation for PDM-CO-OFDM Optical Transmission Systems," in *Proc. Conference on Optical Fiber Communication and the National Fiber Optic Engineers Conference OFC/NFOEC 2010*, 2010, p. OTuE2.

[48] D. S. Millar, S. Makovejs, C. Behrens, S. Hellerbrand, R. I. Killey, P. Bayvel, and S. J. Savory, "Mitigation of Fiber Nonlinearity using a Digital Coherent Receiver," *Journal of Selected Topics in Quantum Electronics,* vol. 16, pp. 1217-1226, 2010.

[49] T. Yoshida, T. Sugihara, H. Goto, T. Tokura, K. Ishida, and T. Mizuochi, "A Study on Statistical Equalization of Intra-channel Fiber Nonlinearity for Digital

Coherent Optical Systems," in *Proc. European Conference on Optical Communications ECOC 2011*, Geneva, 2011, p. Tu.3.A.1.

[50] D. Lavery, C. Behrens, S. Makovejs, D. S. Millar, R. I. Killey, S. J. Savory, and P. Bayvel, "Long-Haul Transmission of PS-QPSK at 100 Gb/s Using Digital Backpropagation," *Photonics Technology Letters,* vol. 24, pp. 176-178, February 2012.

[51] E. Ip, "Nonlinear Compensation Using Backpropagation for Polarization-Multiplexed Transmission," *Journal of Lightwave Technology,* vol. 28, pp. 939-951, March 2010.

[52] D. Rafique and A. D. Ellis, "The Impact of Signal-ASE Four-Wave Mixing in Coherent Transmission Systems," in *Proc. Conference on Optical Fiber Communication and the National Fiber Optic Engineers Conference OFC/NFOEC 2011*, 2011, p. OthO2.

[53] C. Behrens, R. I. Killey, S. J. Savory, M. Chen, and P. Bayvel, "Benefits of digital backpropagation in coherent QPSK and 16QAM fibre links," in *Communications and Photonics Conference and Exhibition (ACP), 2010* Shanghai, 2010, pp. 359-360.

[54] D. Rafique, J. Zhao, and A. D. Ellis, "Digital back-propagation for spectrally efficient WDM 112 Gbit/s PM m-ary QAM transmission," *Optics Express,* vol. 19, pp. 5219-5224, March 2011.

[55] S. Makovejs, E. Torrengo, D. Millar, R. Killey, S. Savory, and P. Bayvel, "Comparison of pulse shapes in a 224Gbit/s (28Gbaud) PDM-QAM16 long-haul transmission experiment," in *Proc. Conference on Optical Fiber Communication and the National Fiber Optic Engineers Conference OFC/NFOEC 2011*, Los Angeles, 2011, p. OMR5.

[56] C. Xu and X. Liu, "Postnonlinearity compensation with data driven phase modulators in phase-shift keying transmission," *Optics Letters,* vol. 27, pp. 1619-1621, September 2002.

[57] K. Kikuchi, "Electronic Post-compensation for Nonlinear Phase Fluctuations in a 1000-km 20-Gbit/s Optical Quadrature Phase-shift Keying Transmission System Using the Digital Coherent Receiver," *Optics Express,* vol. 16, pp. 889-896, 2008.

[58] K.-P. Ho and J. M. Kahn, "Electronic compensation technique to mitigate nonlinear phase noise," *Photonics Technology Letters,* vol. 22, pp. 779-783, 2004.

[59] A. Carena, G. Bosco, V. Curri, P. Poggiolini, M. Tapia Taiba, and F. Forghieri, "Statistical Characterization of PM-QPSK Signals after Propagation in Uncompensated Fiber Links," in *Proc. European Conference on Optical Communications ECOC 2010*, Torino, 2010, p. P4.07.

[60] G. D. Forney, "Maximum-likelihood sequence estimation of digital sequences in the presence of intersymbol interference"," *Transactions on Information Theory,* vol. IT-18, pp. 363-378, May 1972.

[61] G. D. Forney, "The Viterbi algorithm," *Proceedings of the IEEE,* vol. 61, pp. 268-278, March 1973.

[62] S. J. Savory, Y. Benlachtar, R. I. Killey, P. Bayvel, G. Bosco, P. Poggiolini, J. Prat, and M. Omella, "IMDD Transmission over 1,040 km of Standard Single-Mode Fiber at 10Gbit/s using a One-Sample-per Bit Reduced-Complexity MLSE Receiver," in *Proc. Conference on Optical Fiber Communication and the National Fiber Optic Engineers Conference OFC/NFOEC 2007*, 2007, p. OThK2.

[63] S. Chandrasekhar and A. H. Gnauck, "Performance of MLSE Receiver in a Dispersion-Managed Multispan Experiment at 10.7Gb/s Under Nonlinear Transmission," *Photonics Technology Letters,* vol. 18, pp. 2448-2450, December 2006.

[64] J. X. Cai, Y. Cai, C. R. Davidson, A. Lucero, H. Zhang, D. G. Foursa, O. V. Sinkin, W. W. Patterson, A. Philipetskii, G. Mohs, and N. S. Bergano, "20 Tbit/s Capacity Transmission Over 6,860 km," in *Proc. Conference on Optical Fiber Communication and the National Fiber Optic Engineers Conference OFC/NFOEC 2011*, Los Angeles, 2011, p. PDPB4.

[65] J. G. Proakis, "Adaptive Equalization for TDMA Digital Mobile Radio," *IEEE Transactions on Vehicular Technology,* vol. 40, pp. 333-341, May 1991.

[66] J.-X. Cai, Y. Cai, C. R. Davidson, D. G. Foursa, A. Lucero, O. Sinkin, W. Patterson, A. Pilipetskii, G. Mohs, and N. S. Bergano, "Transmission of 96x100-Gb/s Bandwidth-Constrained PDM-RZ-QPSK Channels With 300% Spectral Efficiency Over 10610 km and 400% Spectral Efficiency Over 4370 km," *Journal of Lightwave Technology* vol. 29, pp. 491-497, February 2011.

[67] Y. Cai, D. G. Foursa, C. R. Davidson, J. X. Cai, O. Sinkin, M. Nissov, and A. Philipetskii, "Experimental Demonstration of Coherent MAP Detection for Nonlinearity Mitigation in Long-Haul Transmissions," in *Proc. Conference on Optical Fiber Communication and the National Fiber Optic Engineers Conference OFC/NFOEC 2010*, 2010, p. OTuE1.

[68] J. Zhao and A. D. Ellis, "Performance Improvement Using a Novel MAP Detector in Coherent WDM Systems," in *Proc. 34th European Conference on Optical Communication ECOC 2008*, 2008, p. Tu.1.D.2.

[69] K. V. Peddanarappagari and M. Brandt-Pearce, "Volterra series approach for optimizing fiber-optic communications system designs," *Journal of Lightwave Technology,* vol. 16, pp. 2046-2055, 1998.

[70] Y. Gao, F. Zhang, L. Dou, Z. Chen, and A. Xu, "Intra-channel nonlinearities mitigation in pseudo-linear coherent QPSK transmission systems via nonlinear electrical equaliser," *Optics Communications,* vol. 282, pp. 2421-2425, March 2009.

[71] F. P. Guiomar, J. D. Reis, A. L. Teixeira, and A. N. Pinto, "Mitigation of intra-channel nonlinearities using a frequency-domain Volterra series equaliser," *Optics Express,* vol. 20, pp. 1360-1368, January 2012.

[72] Z. Pan, B. Châtelain, M. Chagnon, and D. V. Plant, "Volterra Filtering for nonlinearity impairment mitigation in DP-16QAM and DP-QPSK fiber optic communication systems," in *Proc. Conference on Optical Fiber Communication and the National Fiber Optic Engineers Conference OFC/NFOEC 2011*, Los Angeles, 2011, p. JThA40.

[73] K. Roberts, C. Li, L. Strawczynski, M. O'Sullivan, and I. Hardcastle, "Electronic precompensation of optical nonlinearity," *Photonics Technology Letters,* vol. 18, pp. 403-405, 2006.

[74] R. Waegemans, S. Herbst, L. Hohlbein, P. Watts, P. Bayvel, C. Fuerst, and R. I. Killey, "10.7 Gb/s electronic predistortion transmitter using commercial FPGAs and D/A converters implementing real-time DSP for chromatic dispersion and SPM compensation," *Optics Express,* vol. 17, pp. 8630-8640, May 2009.

[75] C. Weber, J. K. Fischer, C. A. Bunge, and K. Petermann, "Electronic Precompensation of Intrachannel Nonlinearities at 40 Gb/s," *Photonics Technology Letters,* vol. 18, pp. 1759-1761, August 2006.

[76] D. Godard, "Self-Recovering Equalization and Carrier Tracking in Two-Dimensional Data Communication Systems," *Transactions on Communications,* vol. 28, pp. 1867-1875, 1980.

[77] I. Fatadin, D. Ives, and S. J. Savory, "Blind Equalization and Carrier Phase Recovery in a 16-QAM Optical Coherent System," *Journal of Lightwave Technology,* vol. 27, pp. 3042-3049, 2009.

[78] D. S. Millar and S. J. Savory, "Blind Adaptive Equalization of Polarization Switched QPSK Modulation," *Optics Express,* vol. 19, pp. 8533-8538, 2011.

[79] A. Viterbi and A. Viterbi, "Nonlinear estimation of PSK-modulated carrier phase with application to burst digital transmission," *Transactions on Information Theory,* vol. 29, pp. 543-551, 1983.

[80] E. Ip and J. M. Kahn, "Carrier synchronization for 3- and 4-bit-per-symbol optical transmission," *Journal of Lightwave Technology,* vol. 23, pp. 4110-4124, 2005.

Chapter 4

COHERENT TRANSMISSION AT 40 AND 100GBIT/S

As outlined in Chapter 1, next generation optical transport networks have to operate at higher bit rates to meet future capacity demands without sacrificing transmission reach. In this chapter the investigation of maximum transmission distances is described for a wide range of modulation formats, spectrally more efficient compared to on-off keying (OOK), employing digital coherent detection at net bit rates of 40Gbit/s and 100Gbit/s.

Firstly, transmission at 42.9Gbit/s was considered comparing polarisation-multiplexed binary-phase-shift-keying (PDM-BPSK), which is currently the most promising option for transpacific transmission at 40Gbit/s encoding 2bit/symbol [1], to quadrature-phase-shift-keying (PDM-QPSK) encoding 4bit/symbol. For the first time these formats are compared experimentally, in single channel and WDM regimes, with polarisation switched QPSK (PS-QPSK) encoding 3bit/symbol. PS-QPSK has been found to provide a 1.76dB asymptotic sensitivity gain over PDM-BPSK and PDM-QPSK by solving a 4-dimensional sphere packing problem [2]. This makes it the most power efficient modulation format available in the 4-dimensional optical channel (2 quadratures in 2 polarisations) [2, 3].

In the next step, the investigation is extended to spectrally more efficient modulation formats of 8-phase-shift-keying (PDM-8PSK) and 8-quadrature-amplitude-modulation (PDM-8QAM) as well as 16-quadrature-amplitude-modulation (PDM-16QAM), encoding 6 and 8bit/symbol, whilst capacity is increased to 112Gbit/s. Furthermore, the performance of a nonlinear compensation algorithm with a fixed complexity of 1 computational step per transmitted span (digital backpropagation – see section 3.3.2)

is investigated for 112Gbit/s. Finally, upper bounds on transmission performance with and without digital backpropagation are explored by means of computer simulations.

Figure 25 shows the maximum transmission distances obtained as a consequence of this work with big markers among other lab demonstrations with various modulation formats on a similar link (SSMF and EDFA amplification) as well as the theoretical linear and nonlinear limits [4, 5]. The linear limit was calculated assuming 80 km SSMF spans, EDFA-only amplification (NF=4.5 dB) and a 50 GHz grid with full population of the C-band, while in case of the nonlinear limit, cross phase modulation was assumed to be the dominant nonlinearity. It can be seen that several record transmission distances have been obtained as a result of this work, even though it is to be noted that spectral efficiency can still be increased by an estimated factor of 5 until the nonlinear theoretical limit is reached.

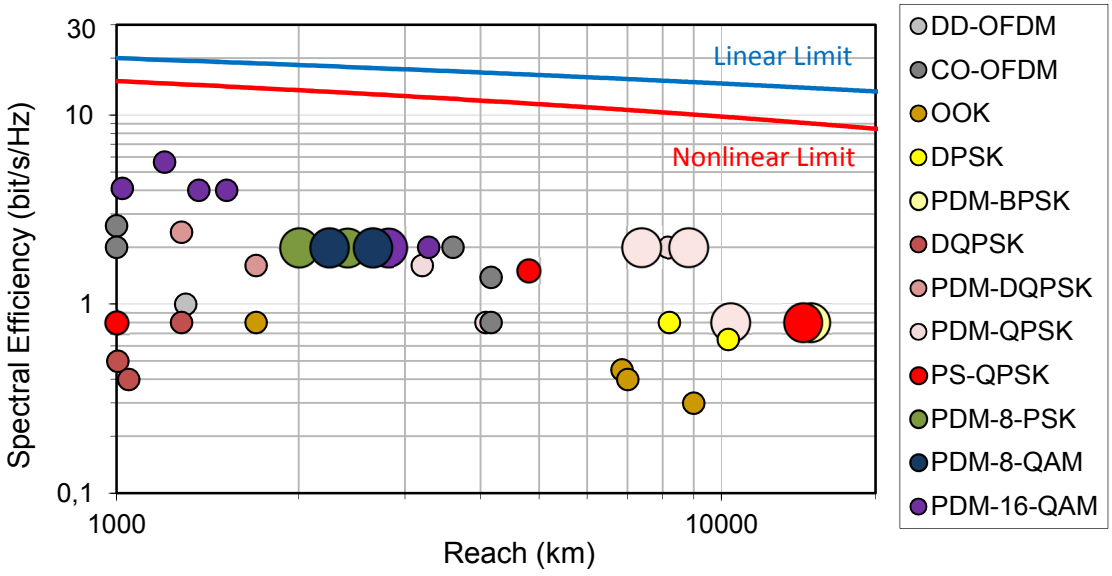

Figure 25: Spectral efficiency versus transmission reach for various WDM-experiments employing a variety of modulation formats on erbium doped fibre amplifier (EDFA) amplified links with standard single mode fibre (SSMF). Big markers denote experimental results obtained as part of this work. The linear limit assumes ASE noise as the only limitation [4], while the nonlinear limit additionally assumes XPM to be the dominant nonlinearity [5].

The author is grateful to Sergeys Makovejs, David Millar and Dominic Lavery for the help with the experiments and for providing experimental data for 112Gbit/s PDM-16QAM.

4.1 Experimental Transmission Setup

4.1.1 Transmitter Setup

This section focuses on the details of the experimental transmitter stages for 42.9Gbit/s PDM-BPSK, PS-QPSK and as well as 112Gbits/s PS-QPSK, PDM-QPSK, PDM-8PSK, PDM-8QAM and PDM-16QAM. An external cavity laser at 1553nm with a linewidth of 100 kHz surrounded by 6 DFB-lasers with 50GHz frequency spacing was used as the signal source throughout the experiments. The driving signals were generated with a 28GHz Anritsu MP1800A pulse-pattern generator (PPG) and amplified with 40GHz SHF 803P amplifiers. Both IQ-modulators used in the experiments were Avanex 792000540 models with a 3dB bandwidth of 26GHz bandwidth (see Figure 26).

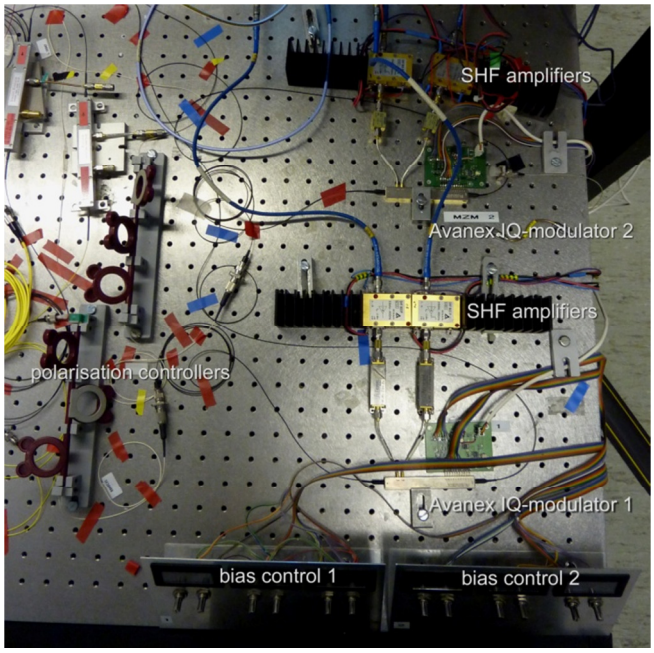

Figure 26: Photograph of the transmitter setup displaying driver amplifiers, IQ-modulators and polarisation controllers.

PDM-BPSK

In the case of PDM-BPSK, the underlying BPSK constellation was generated by driving the two arms of an Avanex IQ-modulator at 21.45GBd with 2^{15}-1 long pseudo-random binary sequences (PRBS) yielding an overall bit rate of 42.9Gbit/s. As shown in Figure 27, the IQ-modulator was followed by a polarization-multiplexing stage with a relative delay 2.4ns (corresponding to 51 symbols). The insets in Figure 27 show the constellation diagram after the IQ modulator as well as after the polarisation multiplexing stage (red: X polarisation, blue: Y polarisation).

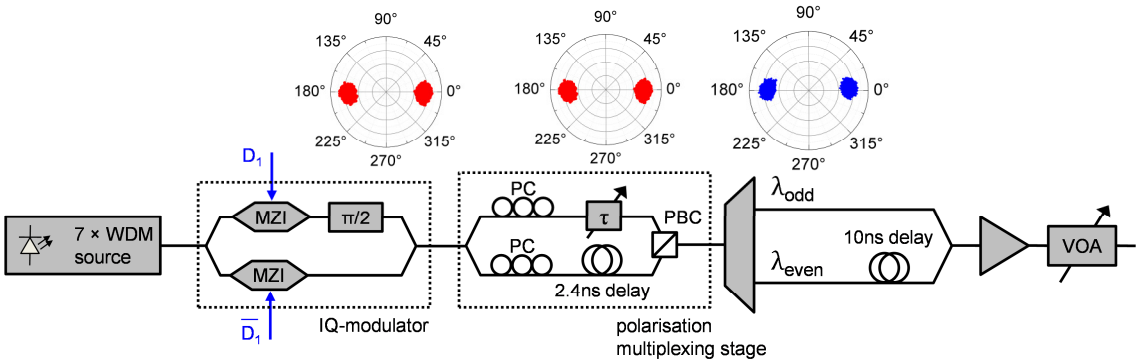

Figure 27: PDM-BPSK transmitter setup with 7 channel WDM source, IQ-modulator, polarisation multiplexing stage and decorrelation stage for odd and even channels. Insets show the constellation diagram after the IQ modulator as well as after the polarisation multiplexing stage (red: X polarisation, blue: Y polarisation).

PS-QPSK

PS-QPSK can encode 3bits per symbol, compared to only 2bits per symbol for PDM-BPSK. To generate it, the IQ-modulator was driven at a symbol rate of 14.3GBd to give 42.9Gbit/s and 37.3GBd to give 112Gbit/s. The two driving signals were modulated with two decorrelated PRBS 15 sequences first to obtain QPSK. Note that in case of 112Gbit/s the driving signals were provided by an Ando AP9950 PPG with a 3dB bandwidth of 40GHz due to the insufficient bandwidth of the Anritsu PPG. The Avanex IQ modulator was followed by a polarization switching stage consisting of two parallel Sumitomo T.MZI1.5-40 40GHz Mach-Zehnder modulators (Figure 28). The MZMs were driven at 14.3GBd (yielding 42.9Gbit/s) or 37.3GBd (yielding 112Gbit/s) with inverse data patterns, to block one or the other polarization, to generate the PS-QPSK format. In Figure 28 the resulting constellation diagrams of the two formats are shown, illustrating the correlation between X- (red) and Y-polarisation (blue) in the case of PS-QPSK, as opposed to no correlation in the case of PDM-BPSK.

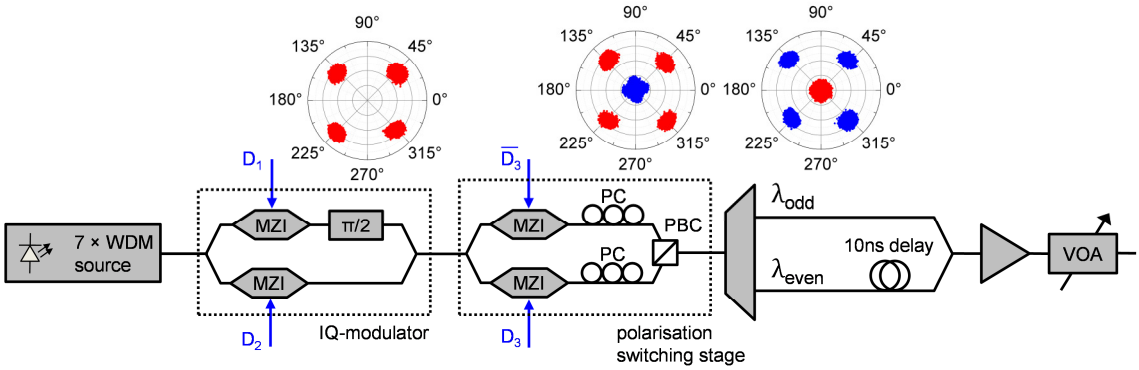

Figure 28: PS-QPSK transmitter setup with laser source, IQ-modulator, polarisation switching stage and decorrelation stage for odd and even channels. Insets show the constellation diagram after the IQ modulator as well as after the polarisation switching stage (red: X polarisation is transmitting, blue: Y polarisation is transmitting).

Figure 29 shows a photograph of the polarisation stage with the splitter at the input, the two MZMs (one in each arm of the switching stage) and the polarisation beam combiner (PBC) at the output of the stage. Polarisation controllers are used to optimise the polarisation state into each MZMs and into the PBS, while the optical delay lines are used to balance the path lengths in each arm so that the pulses in both polarisations are aligned in time.

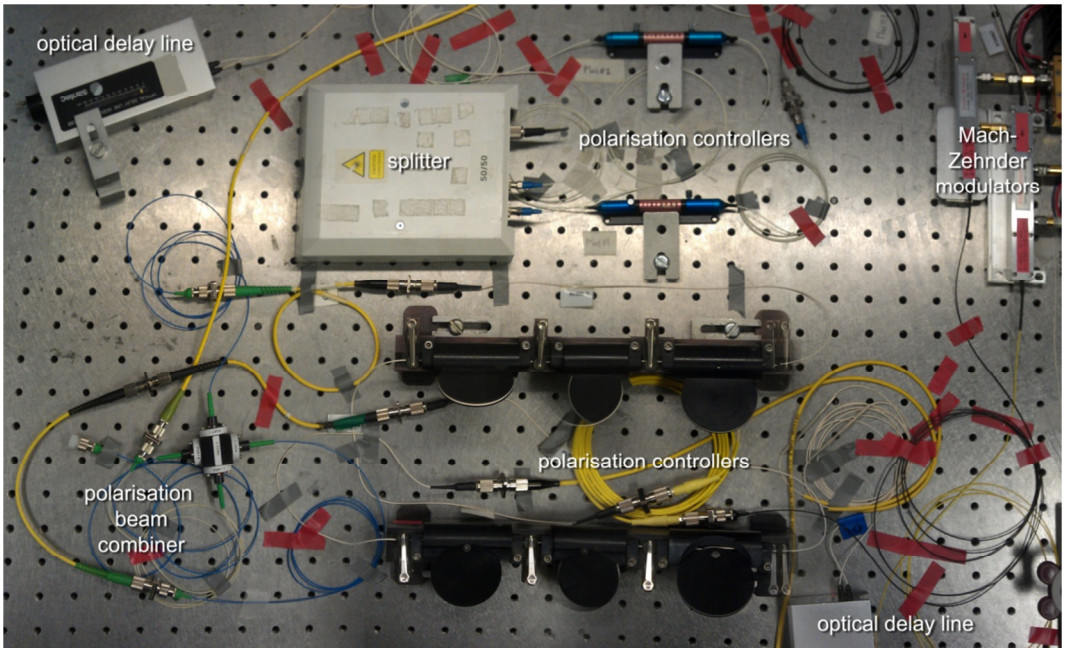

Figure 29: Photograph of the polarisation switching stage showing the splitter, Mach-Zehnder modulators, optical delay line and polarisation controllers, before the signals are recombined with a polarisation beam combiner.

PDM-QPSK

PDM-QPSK can encode 4bits per symbol, 2bits per symbol in each polarisation. Therefore, the Avanex IQ-modulator is driven with two decorellated PRBS 15 sequences, either at 10.7GBd (yielding 42.9Gbit/s) or 28GBd (yielding 112Gbit/s). Similarly to PDM-BPSK, the IQ-modulator is followed by a passive delay line stage to emulate polarisation multiplexing (see Figure 30). The delay is equal to 2.4ns, which corresponds to 26 symbols in case of 42.9Gbit/s and 67 symbols for 112Gbit/s.

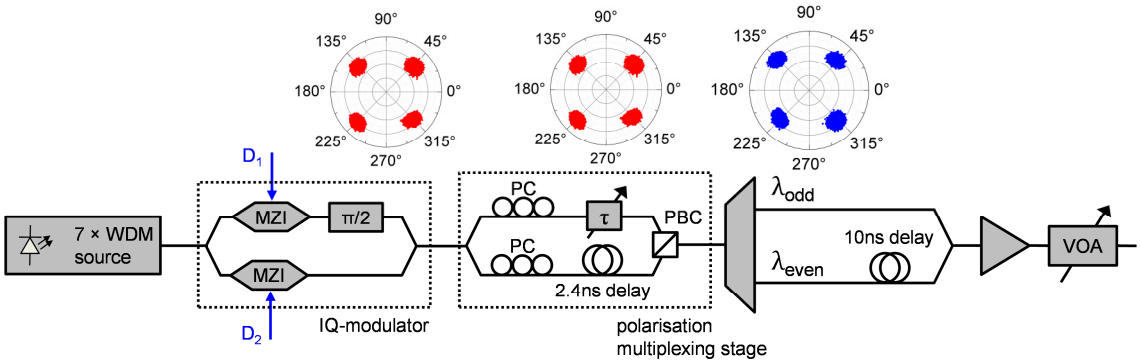

Figure 30: PDM-QPSK transmitter setup with laser source, IQ-modulator, polarisation multiplexing stage and decorrelation stage for odd and even channels. Insets show the constellation diagram after the IQ modulator as well as after the polarisation multiplexing stage (red: X polarisation, blue: Y polarisation).

PDM-8PSK

PDM-8PSK encodes 6bits per symbol and, therefore, the symbol rate, to give an overall bit rate of 112Gbit/s, drops to 18.66GBd, compared to 28GBd for QPSK. An IQ modulator was used to generate a QPSK constellation at 18.66GBd, which was then fed into a phase-modulator, driven with a phase shift of π/4, to generate 8PSK as shown in Figure 31. The relative delay of 2.4ns within the following polarisation multiplexing stage corresponds to a decorrelation length of 45 symbols. The insets in Figure 31 show the detected constellation diagrams after the IQ modulator and after the phase modulator as well as polarisation multiplexing stage.

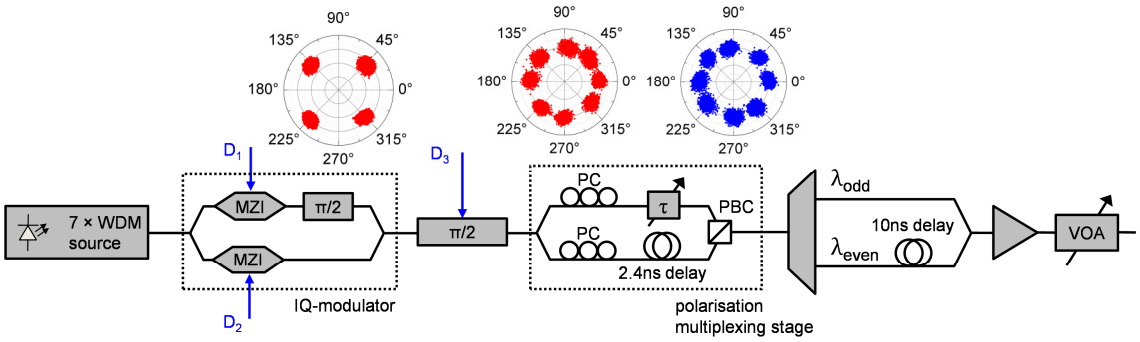

Figure 31: PDM-8PSK transmitter setup with laser source, IQ-modulator, phase modulator, polarisation multiplexing stage and decorrelation stage for odd and even channels. Insets show the constellation diagram after the IQ modulator as well as after the polarisation multiplexing stage (red: X polarisation, blue: Y polarisation).

PDM-8QAM

PDM-8QAM has the same spectral efficiency as PDM-8PSK and, therefore employs, the same symbol rate of 18.66GBd to yield 112Gbit/s. The phase-modulator in the 8PSK setup was replaced with an additional IQ-modulator with one arm driven over

$2 \cdot V_\pi$ while the bias point of the other arm was adjusted as shown in the inset in Figure 32. In this configuration, the QPSK constellation was either mapped to the inner or outer 8QAM circle (see section 3.1.2). Similarly to the PDM-8PSK setup the delay within the polarisation multiplexing stage corresponds to 45 symbols.

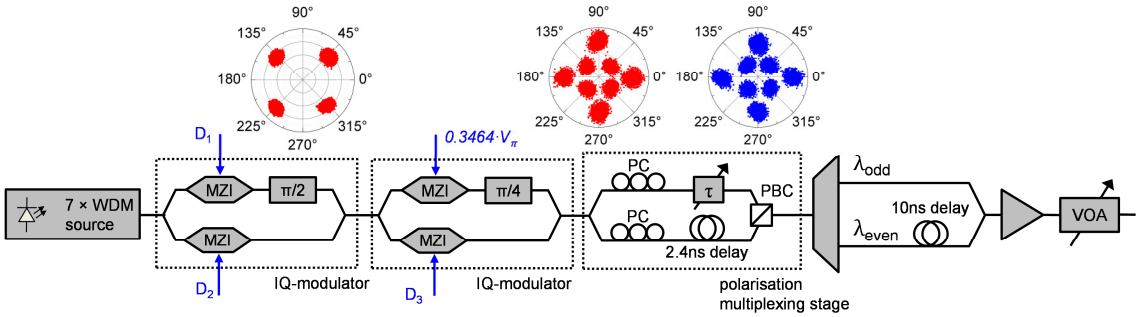

Figure 32: PDM-8QAM transmitter setup with laser source, IQ-modulators, polarisation multiplexing stage and decorrelation stage for odd and even channels. Insets show the constellation diagram after the IQ modulator as well as after the polarisation multiplexing stage (red: X polarisation, blue: Y polarisation).

For each modulation format described till now, odd and even channels were separated with a 50GHz interleaver (3dB bandwidth of 42GHz) and recombined with a relative delay of 10 ns to decorrelate the neighbouring wavelength channels with a 2m long fibre. This decorrelation length corresponds to 214 symbols for PDM-BPSK, 143 symbols for PS-QPSK and 107 symbols for PDM-QPSK in the case of 42.9Gbit/s as well as 280 symbols for PDM-QPSK and 187 symbols for PDM-8PSK and PDM-8QAM at 112Gbit/s. Note that the interleaver stage was not used in the case of 112Gbit/s PS-QPSK, because of a very high implementation penalty obtained, even in the case of the single channel setup, as described in section 4.4.1.

16QAM

The experimental transmitter setup used for PDM-16QAM is slightly different compared to the previously described modulation formats, because rather than modulating 16QAM on the optical carrier, a phase-stabilised fibre interferometer is used to combine two QPSK constellations of varying power to give 16QAM [6]. As a consequence, linewidth requirements for all WDM channels are more stringent than for the previous experiments, as explained below.

The optical source used for the central channel was an external cavity laser (ECL) with a measured linewidth of 100kHz, surrounded by 2 aggressors, both of which were ECLs with linewidths of 700kHz. The central channel and the aggressors were modulated by two separate IQ modulators, driven by binary driving signals with a

PRBS length of 2^{15}-1 to generate a 28GBd-QPSK signal. The I- and Q- components were decorrelated by 500ps (or 7 symbols) by using electrical cables of differing lengths. After amplification, the central channel and the aggressors were decorrelated by several hundreds of symbols with an additional optical fibre and combined in a 50GHz interleaver (3dB bandwidth of 42GHz). To synthesise a 16QAM signal from the original QPSK signal, a phase-stabilised fibre interferometer was used [7], that combines two QPSK constellations with 3dB power difference to yield 16QAM (see Figure 33 (b)). The phase-stabilization was achieved by counter-propagating a portion of the CW light of the source laser in the interferometer and processing an electrical interference product with a feedback circuit to provide a control signal for a phase shifter.

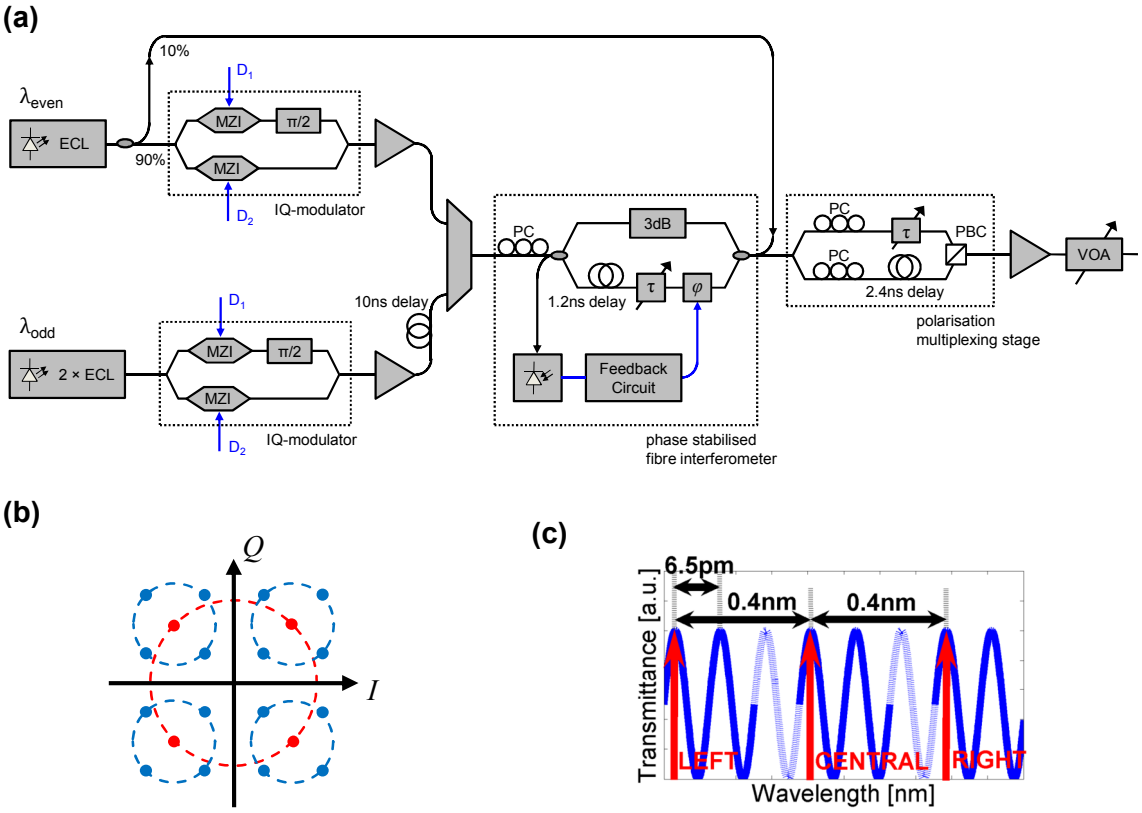

Figure 33: (a) shows an illustration of the PDM-16QAM transmitter setup with laser sources, IQ-modulators, phase stabilised fibre interferometer and polarisation multiplexing stage. (b) shows the constellation diagram after the IQ modulators in red and after fibre interferometer in blue, while (c) shows the transfer function of the fibre interferometer with a free spectral range of 6.5pm.

To ensure that the adjacent WDM channels represent true 16QAM signals, the free spectral range of the interferometer was measured to be 6.5pm. The wavelengths of the two adjacent ECL lasers were then fine-tuned to coincide with the peaks of the interferometer transfer function; this corresponds to the scenario in which two interfering signals are in-phase (hence, yielding a 16-QAM signal – see Figure 33 (b)

and (c)). It must be noted that there is no fundamental limitation of generating more than 3 WDM channels using this technique, providing the source lasers are stable in frequency. For this reason ECLs were used rather than distributed-feedback lasers (only 3 ECLs were used, limited by experimental resources). The two arms of the interferometer were decorrelated by 17 symbols. To obtain a PDM signal, a passive delay-line stage with adjustable states of polarization (PC) for signals in each arm was used; the two signals were decorrelated by 34 symbols and recombined via a polarization beam splitter (PBS). Note that all delay values were sufficient to ensure uniformly distributed symbols per channel and decorrelation between the adjacent channels.

Even though the relative phase between both QPSK constellations has been minimised with the feedback circuit displayed in Figure 33 (a), minimum Euclidian distance decision boundaries were implemented at the receiver to combat remaining modulation distortions and minimise the BER. Figure 34 shows two constellation diagrams, (a) with rectangular decision boundaries and (b) minimum Euclidian distance decision boundaries. In this particular case it has been possible to reduce the BER by more than an order of magnitude (2.0×10^{-3} to 1.0×10^{-4}).

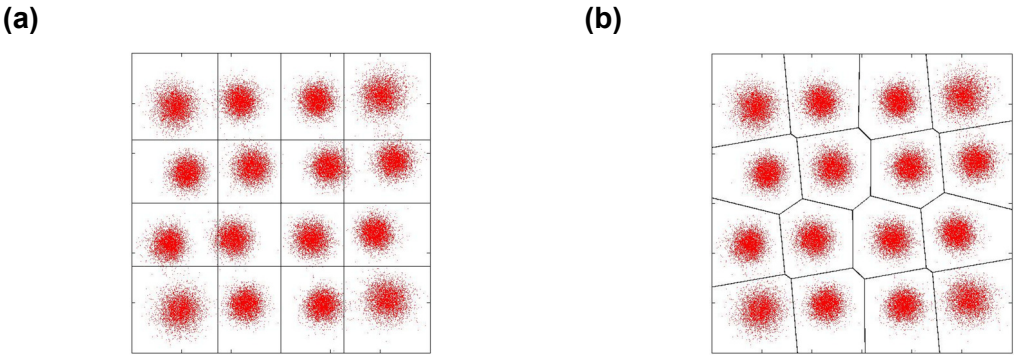

Figure 34: Two different BER calculation methods. (a) With rectangular decision boundaries. (b) With minimum Euclidean distance decision boundaries. Bit error rate is reduced from (a) $2.0\text{x}10^{-3}$ to (b) $1.0\text{x}10^{-4}$ [6].

The eye diagrams for 21.45GBd BPSK, 14.3GBd PS-QPSK and 10.7GBd QPSK, yielding 42.9Gbit/s, were measured and are shown in Figure 35. In the case of BPSK two transitions can be seen; either the neighbouring symbol is the same or its phase differs by 180 degrees and a transition through the origin can be observed. PS-QPSK and QPSK contain the same transitions as BPSK plus a third one to the two nearest neighbours with a phase difference of ±90 degrees.

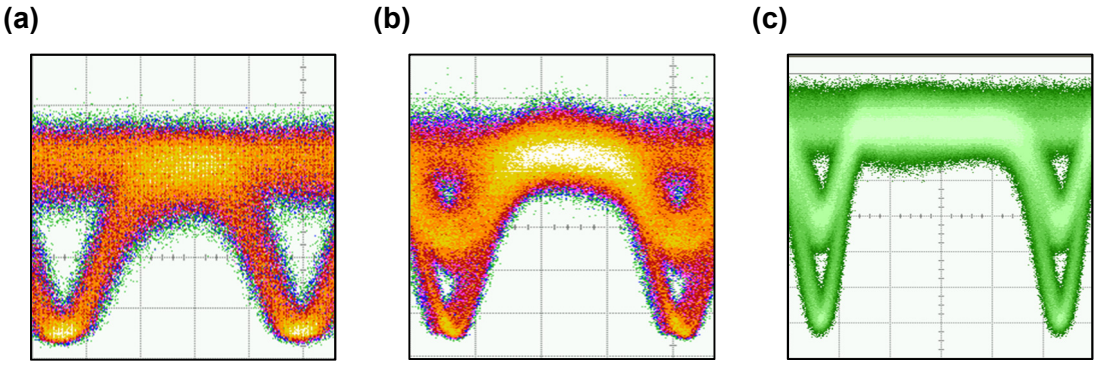

Figure 35: Measured optical eye diagrams at 42.9Gbit/s: (a) 21.45GBd BPSK, (b) 14.3GBd PS-QPSK and (c) 10.7GBd QPSK. ((a): 10ps per division; (b), (c): 20ps per division on the time axis)

Figure 36 shows the measured optical eye diagrams for 37.33GBd PS-QPSK, 28GBd QPSK, 18.66GBd 8PSK, 18.66GBd 8QAM and 14GBd 16QAM yielding 112Gbit/s. PS-QPSK, QPSK and 8PSK show similar eye diagrams, each having three transitions between the symbols. Note that, 8PSK does not show additional transitions in the eye diagram because 4 of the 8 phase states are accessed with a phase modulator, incurring no change in optical intensity. The eye diagram of 8QAM shows its characteristic two intensity levels, while 16QAM has three intensity levels.

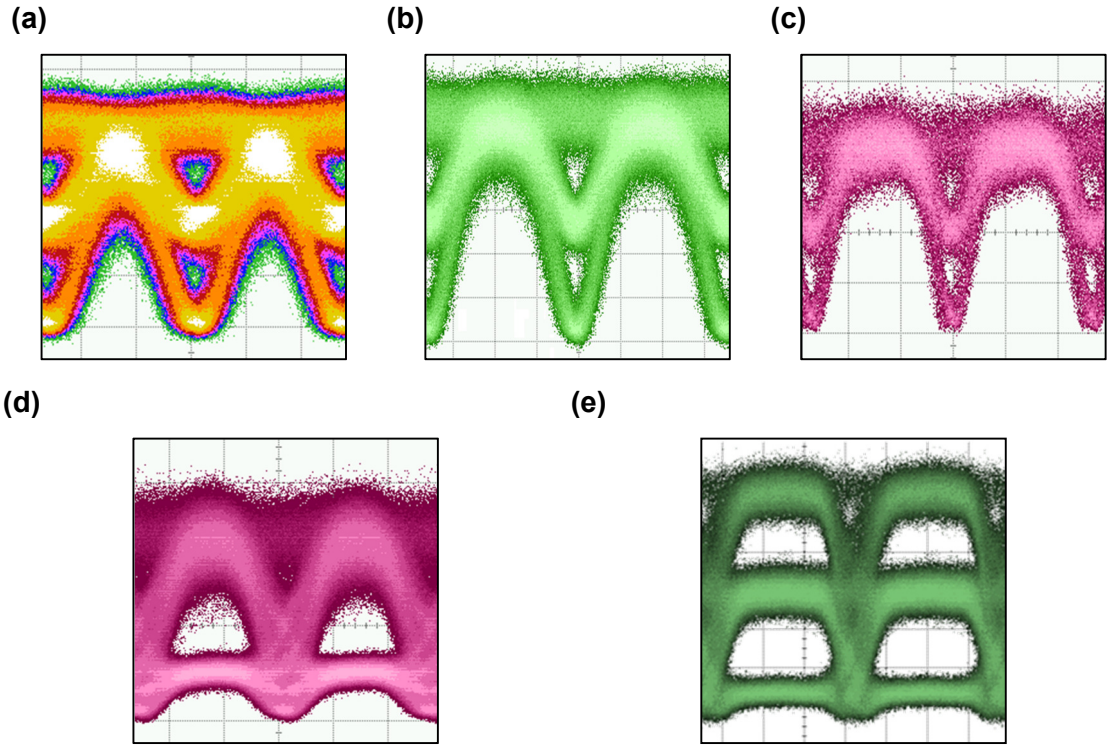

Figure 36: Measured optical eye diagrams at 112Gbit/s: (a) 37.3GBd PS-QPSK, (b) 28GBd QPSK, (c) 18.66GBd 8PSK, 18.66GBd 8QAM and 14GBd 16QAM. ((a), (b):10ps per division; (c)-(e): 20ps per division on the time axis)

4.1.2 Recirculating Loop

The experimental setup used for the all the transmission experiment is shown in Figure 37. After modulation, polarisation multiplexing and WDM synthesis, the resultant WDM signal was launched into a recirculating loop consisting of a single span of 80.2 km single mode fibre (SMF) with a chromatic dispersion of 1347 ps/nm and 15.4 dB loss (the total loop loss was 23.5 dB per recirculation). Erbium-doped fibre amplifiers (EDFAs) with noise figures of ~4.5 dB were used to compensate for the loop loss. Within the loop, gain flattening Mach-Zehnder-type filters (GFF) were used to equalise the WDM signal after each recirculation and reject out of band ASE noise, that would otherwise saturate the EDFAs (for the single-channel experiments a filter with a fixed 100GHz bandwidth was used). In some experiments a loop synchronous polarization controller (LSPC) was used to scramble the state of polarization in the loop and prevent catastrophic build-up of polarisation dependant loss (PDL). When the LSPC was not available a polarisation controller was used to manually equalise PDL by assuring similar BERs in both polarisations. The loop was gated by a pair of acousto-optic modulators (AOM) that were controlled by a signal generator to switch between "loading" and "transmission" state (details can be found in [6]).

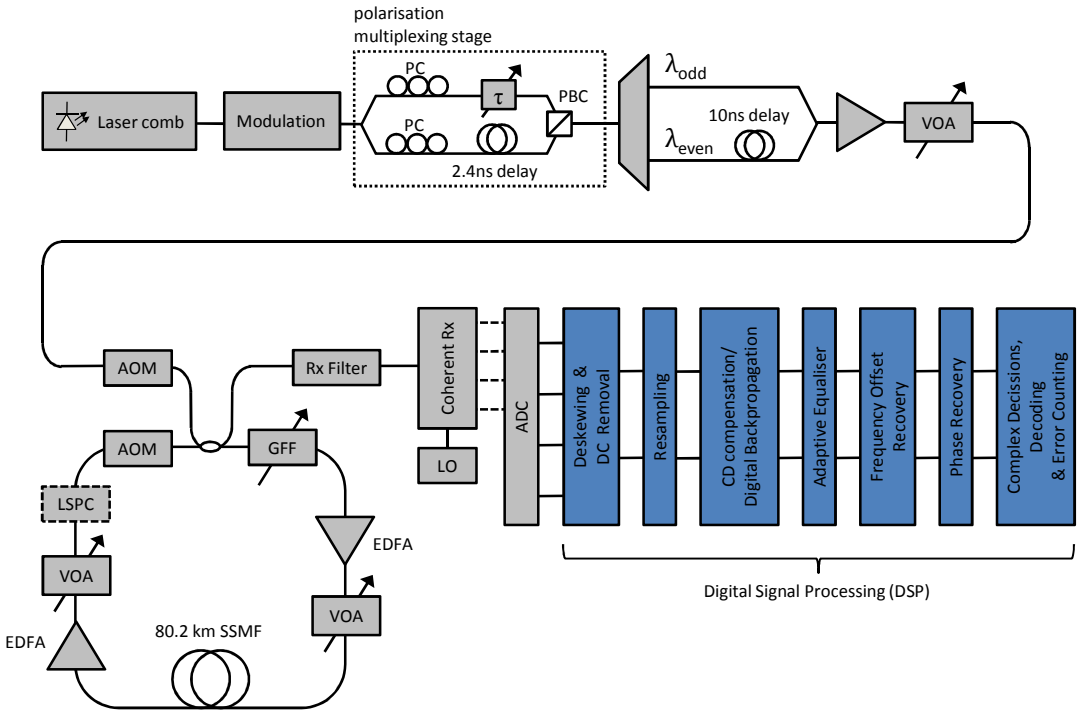

Figure 37: Transmitter setup is shown as a comb source, modulation, polarisation multiplexing stage and channel decorellation. The recirculating loop consists of accousto-optic modulators (AOM) to gate the loop, variable optical attenuators (VOA) and erbium doped fibre amplifiers (EDFA) to overcome losses and balance the loop and a gain flattening filter (GFF) to reject out of band noise. The coherent receiver and local oscillator(LO) is shown including a digital signal processing signal flow diagram.

4.1.3 Receiver

After the desired number of recirculations in the fibre loop, the signal was coupled out and detected with polarization- and phase-diverse coherent receiver. The incoming optical signal was combined with a free running local oscillator (LO) (ECL with 100kHz linewidth) to generate signals proportional to in-phase and quadrature components of the two orthogonal polarizations (see equation (46)). In most experiments four pairs of balanced PIN photo diodes with 32.5GHz electrical bandwidth were used to receive the four quadratures, except for the 16QAM experiment, where single-ended photo diodes with a similar bandwidth were used. However, with a LO-signal ratio in excess of 20dB no performance degradation could be observed, since direct detection terms were adequately suppressed and the strong DC component was filtered out by a DC block. Note that the incoming optical signal was passed through a 100GHz optical filter before detection, to protect the receiver PINs from power surges. A 50GSamples/s Tektronix DPO 72004 digital sampling oscilloscope with an analogue bandwidth of 16.5GHz was used to digitise the signals (see Figure 38).

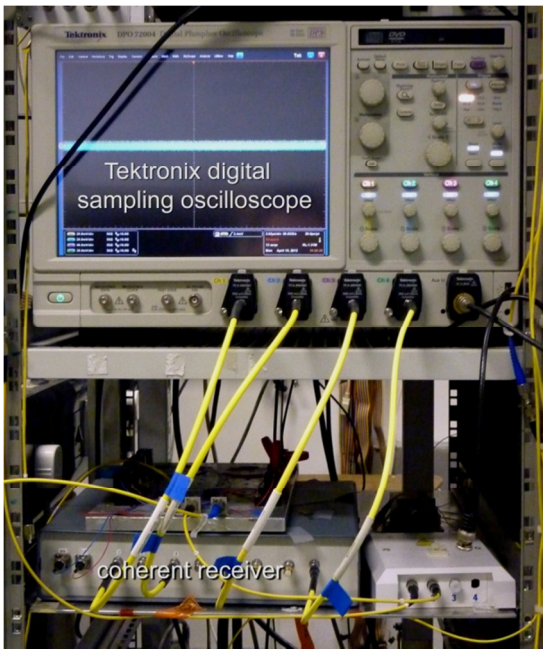

Figure 38: Photograph of coherent receiver containing the optical hybrid and balanced photodiodes, as well as the digital sampling oscilloscope.

Subsequent digital signal processing (DSP) comprises the following modules, as seen in Figure 37. Initially, the signal had to be deskewed to compensate for the different path lengths within the optical hybrid and the receiver. After that the signal was resampled to 2 samples per symbol and chromatic dispersion was compensated in the frequency domain or digital backpropagation has been applied. An adaptive equaliser

was used to estimate the coefficients of the Jones matrix and therefore compensate for polarisation mode dispersion (PMD) and maximise the received SNR. This adaptive equaliser comprises a MIMO structure of 4 FIR filters with adaptive updating of the filter taps as described in section 3.3.5. The updating algorithm is governed by an error signal which is obtained based on the expected modulation format (constant modulus for PSK formats , multiple constellation rings for QAM formats or constant modulus in one polarisation and no power in the other for PS-QPSK). Subsequently, frequency offset recovery has been done by applying a higher order nonlinearity and deduce the frequency offset from the resulting spectrum. Phase recovery has been done either by the Viterbi and Viterbi algorithm [8] for PSK signals, a modified Viterbi and Viterbi algorithm [9] for PS-QPSK and a decision directed PLL [10] as described in 3.3.6. After phase recovery, complex decisions are made and errors are counted.

4.2 Simulation Setup

All experimental results described in the following sections have been guided and verified by transmission simulations, carried out using the simulation software developed in MATLAB. For every set of results, transmitter models have been programmed depending on which modulation format is used (see section 3.1), while the recirculating loop model and the coherent receiver model remains the same (except for the DSP – see section 3.3), similarly to the experiment. Note that the developed models are based on already existent simulation building blocks developed by some of my colleagues (e.g. the split-step Fourier method, EDFA, photodiode). The following approach was used to ensure the best matching of the experimental results and achieve an optimum representation of the physical transmission system.

First, the experimental back-to-back performance was characterised by measuring the BER as a function of the OSNR. The simulation model was then adjusted at the transmitter to match these experimental curves. This adjustment was performed by changing the electrical filter bandwidth of a 5^{th} order Bessel filter which is applied to every electrical driving signal to model bandwidth constraints of the transmitter. Optical eye diagrams were measured with a digital communication analyser (DCA) and matched to the simulated eye diagrams so that rise and fall times corresponded closely to the experimentally obtained eye (see Figure 39). Additionally, electrical noise was added to the driving signals to reflect the finite SNR due to electrical noise sources in the system. In reality, the noise sources are split between transmitter and receiver, however, for simplicity we added the noise only at the transmitter to match the

experimental results. A 2nd order Gaussian optical filter with a 3dB bandwidth of 42GHz was used to model the interleaver frequency response, as shown in Figure 40.

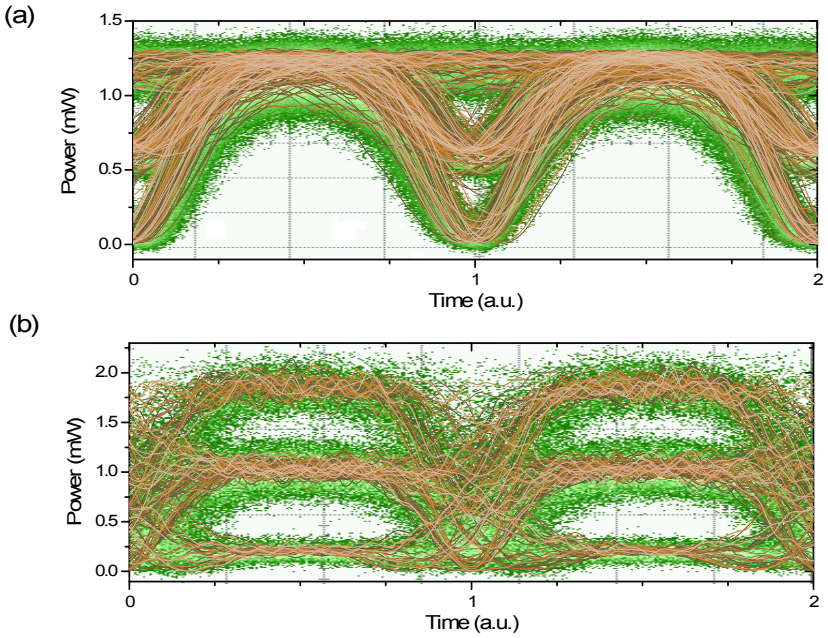

Figure 39: Eye diagrams at the output of the transmitter of (a) QPSK and (b) 16QAM. Green dots denote the measured optical eye, whereas brown traces show the simulated eye.

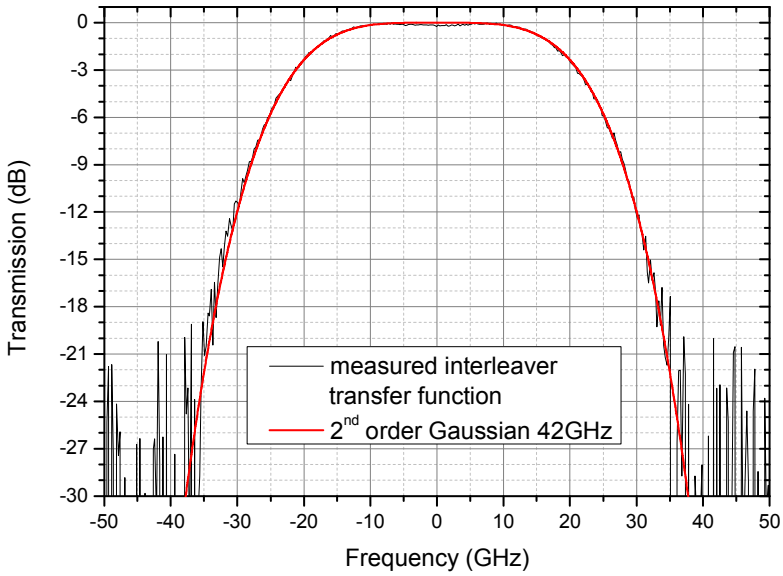

Figure 40: The measured interleaver transfer function could be approximated with a 2nd order Gaussian with 42GHz bandwidth.

As described in the previous chapter, each WDM-channel was modulated with 2^{15} symbols using a different random symbol sequence drawn from a uniform probability

distribution, rendering every symbol equally probable, and all the WDM channels were co-polarised at the transmitter to reflect a worst case scenario. Single channel and WDM propagation has been modelled with 8 and 16 temporal samples per symbol, respectively. This poses a good trade-off between simulation time (a few days per reach curve) and accuracy, since it allows for sufficient bandwidth to accommodate the spectrum and excess bandwidth to cover nonlinearity induced spectral broadening. Note that with high values of accumulated dispersion (as in this thesis) the sequence length might be insufficient and an isolated pulse might interact with itself due to aliasing in the time domain. Although this might lead to an increased level of phase matched nonlinear distortions, agreement between simulation and experiment has been very good, suggesting, that this effect has a negligible impact on the accuracy of transmission simulations. Laser phase noise was modelled as a Wiener process and the transmitter laser linewidth was set to be 100 kHz, similarly to the ECL, which was used as a transmit laser in the experiments.

Table 3: Fibre and link parameters

α [dB/km]	0.19
D [ps/km/nm]	16.87
γ [1/W/km]	1.2
PMD COEFFICIENT [ps/$\sqrt{\text{km}}$]	0.1
SPAN LENGTH [km]	80.2
EDFA NOISE FIGURE [dB]	4.5

To ensure a close fit of the experimental results, the transmission-link pictured in Figure 37 has been modelled as detailed as possible, by making the following assumptions. Each AOM introduced a loss of 3dB, while EDFAs are operated in saturation to give a fixed output power of 17dBm and add noise power to the signal corresponding to a noise figure of 4.5dB. Table 3 shows the parameters used in the simulations corresponding to the experimental values. The signal propagation along the fibre was modelled with the symmetrical split-step Fourier method (step size 100m), which has been extended with the wave-plate model to take polarization mode dispersion into account (see section 2.3). In single channel transmission, the gain flattening filter was modelled as a 2nd order Gaussian filter with adjustable bandwidth to accommodate the full optical spectrum. For WDM transmission however, a brick-wall

filter has been used in simulations to avoid degradation of the outer channels (due to the roll-off and cascaded filtering), which has been tuned out in the experiment.

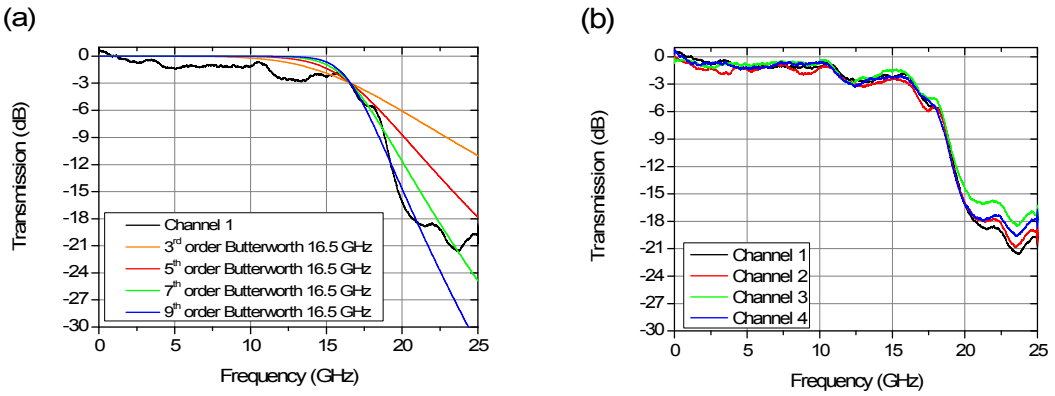

Figure 41: Figure (a) shows frequency response of channel 1 of the digital sampling oscilloscope (DSO) as well as Butterworth filters with a one-sided 3dB bandwidth of 16.5 GHz and varying order. Figure (b) shows frequency responses of channel 1-4 of the DSO.

After transmission, the incoming signal was detected with a phase- and polarization diverse digital coherent receiver. The linewidth of the LO was set to 100 kHz (similarly to the ECL used in the experiment) and a negligible frequency offset between transmitter and LO-laser was assumed. Since the Teleoptix T43G-DPN-DTLNR-xx receiver PINs have a two-sided 3dB bandwidth of 65GHz, the limited receiver bandwidth is dominated by the bandwidth of the ADCs inside the DSO, which we attempted to model with various orders of a Butterworth filter with a two-sided 3dB bandwidth of 33GHz. As can be seen in Figure 41(a) the matching is insufficient, especially in the passband. Therefore the limited receiver bandwidth was modelled with a filter employing measured frequency responses of every channel of the digital sampling oscilloscope used in the experiment (see Figure 41 (b)). Additional quantization noise was added by simulating ADCs with 5 bits of resolution. Subsequent DSP includes chromatic dispersion compensation, equalisation and digital phase estimation as described in section 3.3. Monte-Carlo error counting was performed to determine the BER, which serves as the performance metric to determine the achievable reach at a given launch power.

4.3 Transmission results at 42.9Gbit/s

4.3.1 Back-to-Back measurements

Figure 42, Figure 43 and Figure 44 show back-to-back (BtB) measurements of the BER vs. the optical signal-noise-ratio (OSNR) and corresponding simulation results to match the experimental performance PDM-BPSK, PS-QPSK and PDM-QPSK, respectively. The results are plotted on a double-log scale and fitted linearly to ease comparison

between the formats, as well as against theoretical sensitivity limits as determined by equation (71), (75) and (72).

Single channel PDM-BPSK encodes 2bit/symbol and was, therefore, modulated at 21.45GBd to generate 42.9Gbit/s. Figure 42(a) shows BtB measurements for single channel and WDM configuration, demonstrating implementation penalties of 0.4dB for single channel and 0.6 for WDM at BER=3.8×10^{-3}, which is considerably better than ~1.5dB implementation penalty in a similar setup [11]. The required OSNR at BER=3.8×10^{-3} is 8.3dB in the single channel case and increases to 8.5dB for WDM transmission, which is due to crosstalk induced by neighbouring channels.

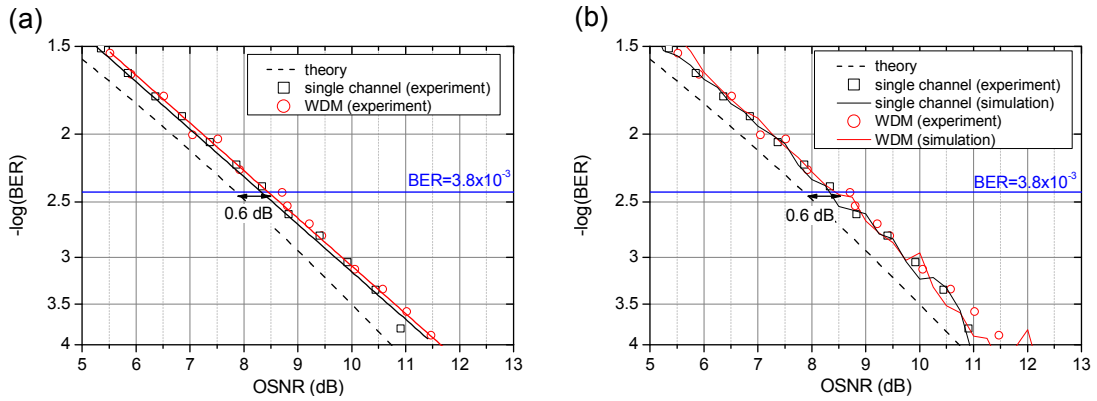

Figure 42: Back to back performance of 42.9Gbit/s PDM-BPSK in single channel and WDM configuration. (a) shows experimental measurements and a linear fit, while (b) displays corresponding simulation results to match the experimental performance.

PS-QPSK encodes 3bit/symbol and is modulated with 14.3Gbd, yielding an overall bit-rate of 42.9Gbit/s. The PS-QPSK transmitter setup incurred an implementation penalty of 0.8dB in the single channel case and 1dB in case of WDM, which is as in the case of PDM-BPSK due to crosstalk from neighbouring channels. It is worth mentioning, that the implementation penalty for the single channel setup can be reduced further to ~0.4dB by using a multi-stage equaliser at the receiver [12]. The required OSNR at BER=3.8×10^{-3} is 7.9dB for the single channel setup and 8.1dB for WDM.

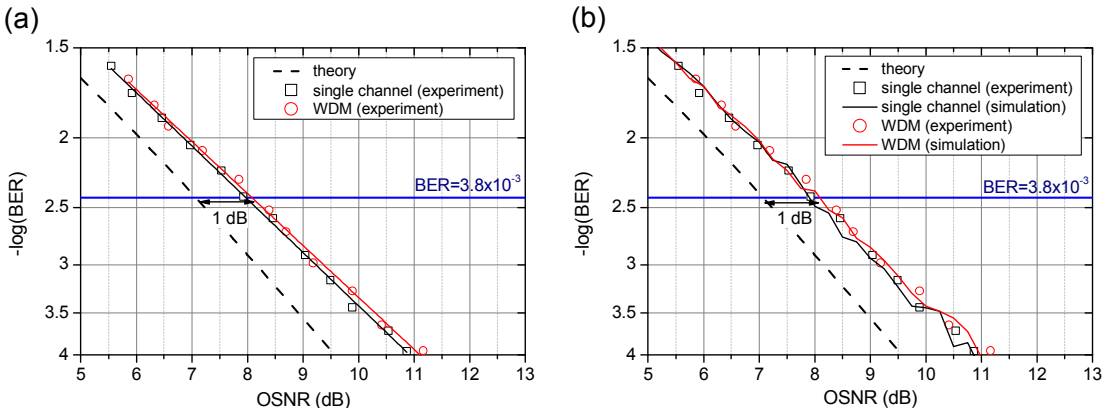

Figure 43: Back to back performance of 42.9Gbit/s PS-QPSK in single channel and WDM configuration. (a) shows experimental measurements and a linear fit, while (b) displays corresponding simulation results to match the experimental performance.

PDM-QPSK encodes 4bit/symbol and was modulated at 10.7GBd. It shows an OSNR of 8.8dB at BER=3.8×10^{-3} for both, single channel and WDM setup. The implementation penalty is 0.9dB in both cases. Note that AT&T and University College Cork [12] demonstrated a reduced implementation penalty of ~0.4dB.

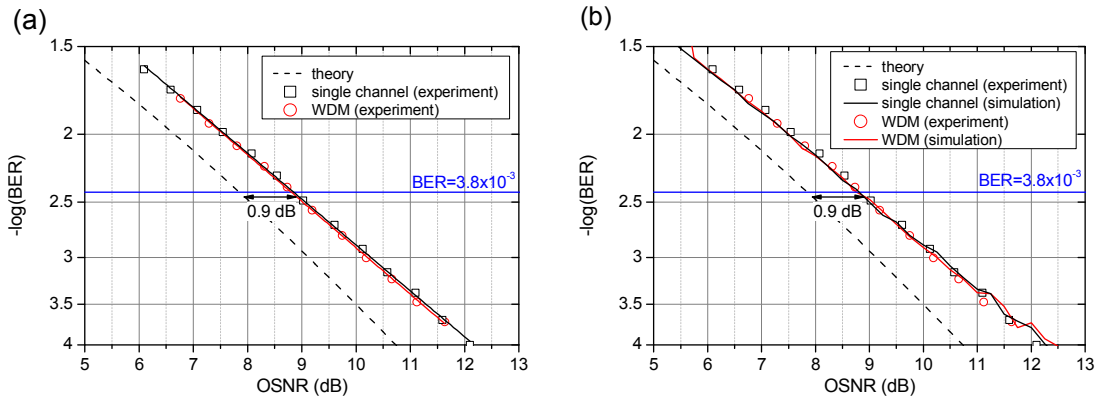

Figure 44: Back to back performance of 42.9Gbit/s PDM-QPSK in single channel and WDM configuration. (a) shows experimental measurements and a linear fit, while (b) displays corresponding simulation results to match the experimental performance.

Considering the WDM setup the different implementation penalties result in a reduction of PS-QPSK's theoretical sensitivity advantage of 0.75dB over PDM-BPSK down to 0.4dB at a BER of 3.8×10^{-3}. However, with 0.7dB at a BER of 3.8×10^{-3}, PS-QPSK retains its sensitivity advantage of 0.75dB over PDM-QPSK as shown in Table 4.

Table 4: required OSNR and implementation penalty for WDM setup of 42.9Gbit/s PDM-BPSK, PS-QPSK and PDM-QPSK @ BER = 3.8×10^{-3}

	PDM-BPSK	PS-QPSK	PDM-QPSK
REQUIRED OSNR (dB)	8.5	8.1	8.8
IMPLEMENTATION PENALTY (dB)	0.6	1	0.9

It is worth noting that excellent agreement between experiment and simulation has been achieved in the back-to-back case, which is an important prerequisite for the following investigation of the transmission characteristics of the three modulation formats at 42.9Gbit/s.

4.3.2 Maximum reach measurements for a single channel system

In this section single-channel transmission performance of PDM-BPSK, PS-QPSK and PDM-QPSK is compared at 42.9Gbit/s. To investigate maximum transmission distances, the modulated signal was launched into the single-span recirculating loop with a span length of 80.24km as described in section 4.1.2. Note that for this set of experiments a loop synchronous polarisation scrambler was not available. However, excessive PDL was equalised manually with a polarisation controller in the loop and by tracking the BER in both polarisations.

After the desired number of recirculations the signal is coupled out and detected with a phase and polarization-diverse coherent receiver using a pair of balanced PINs to receive each quadrature. The local oscillator was an ECL with 100 kHz linewidth whose frequency was tuned to ensure that the frequency offset did not exceed 1GHz. The signal was digitised with a digital sampling oscilloscope with an electrical bandwidth of 16.5 GHz (see Figure 41 (b)) and processed offline. After the signal had been de-skewed, normalised and resampled, chromatic dispersion was compensated digitally. In the case of PDM-BPSK, joint equalisation and phase-recovery was performed in a similar manner to that described in [13], while PDM-QPSK used a standard CMA equaliser, followed by and the Viterbi & Viterbi phase recovery algorithm [8]. For PS-QPSK, a polarization-switched constant modulus algorithm equaliser with least-mean squares updating was used [14], followed by a modified Viterbi & Viterbi phase recovery [9]. All algorithms are described in detail in section 3.3.5 and 3.3.6.

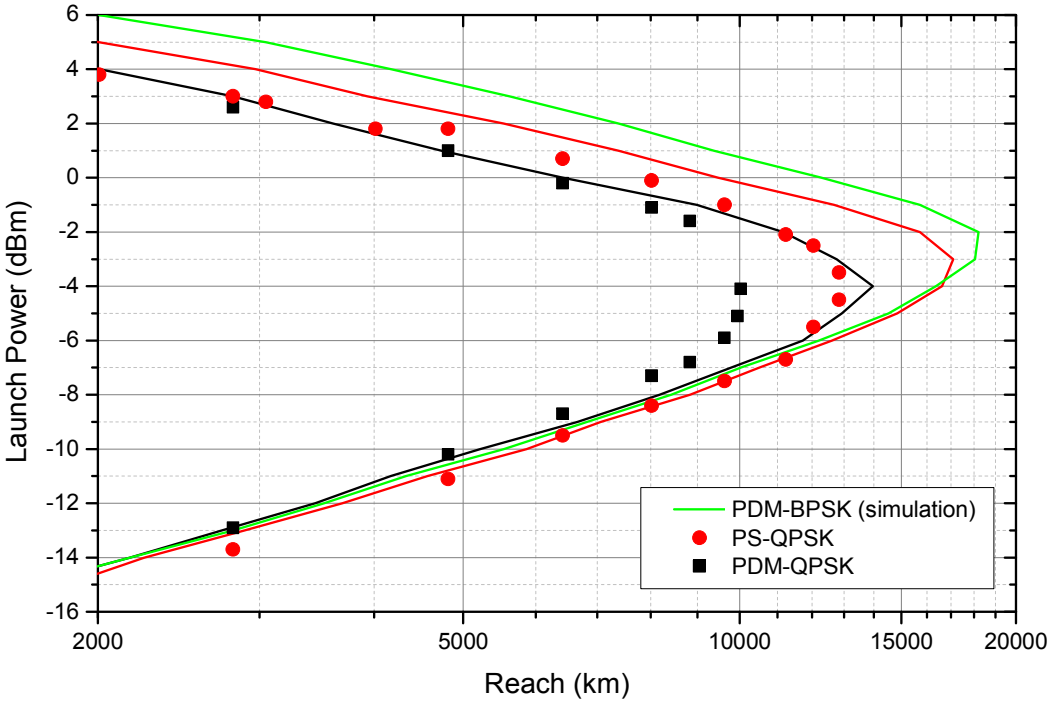

Figure 45: Reach as a function of launch power at BER=3.8×10^{-3} for 42.9Gbit/s single channel PDM-BPSK, PS-QPSK and PDM-QPSK. Markers show experimental results while lines denote simulated performance with equivalent implementation penalty.

Figure 45 shows the achievable transmission distance at BER=3.8×10^{-3} for PDM-BPSK, PS-QPSK and PDM-QPSK as a function of the launch power, varied between -14 and 6dBm. Experimental reach curves of PS-QPSK and PDM-QPSK are shown as symbols, while simulations are shown as lines. Note that, single channel PDM-BPSK was only investigated with simulations due to time constraints.

The experimental results show lower maximum reach than predicted by computer simulations, which can be attributed to inaccuracies such as in the EDFA noise figure and nonlinear fibre coefficient, as well as the absence of a loop synchronous polarization scrambler. Furthermore, the loop had to be rebalanced for each launch power, which could affect the amount of noise added per recirculation. All these effects accumulate with an increased number of recirculations, especially if, as in this case, a single span loop is used. However, experimental results and simulations agree well in the general trends, as well as transmission performance in the linear and nonlinear regimes.

At low launch powers, transmission was limited by ASE-noise added by EDFAs along the link. ASE-noise follows a bi-Gaussian distribution and acts linearly on the optical field (see section 2.1.4), which is why this particular transmission regime is denoted as

the linear regime. The achievable transmission distance depends on the received OSNR, which increases exponentially with launch power. When increasing the launch power beyond a certain value, nonlinear transmission distortions caused by the Kerr effect (see section 2.2) start to dominate the transmission performance. This transmission regime is called the nonlinear transmission regime, because these distortions increase with the square of the launch power.

In the linear transmission regime performance reflects the different values of required OSNR, as described in the previous section (PDM-BPSK: 8.3dB, PS-QPSK: 7.9dB and PDM-QPSK: 8.8dB). This is due to the accumulation of ASE-noise added along the link by EDFAs. As a result an increase in launch power leads to a higher received OSNR leading to 0.4dB penalty PDM-BPSK and the 0.9dB penalty of PDM-QPSK when compared to PS-QPSK.

In the nonlinear transmission regime, PDM-BPSK exhibits a 1dB better performance compared to PS-QPSK, which shows a 1-1.5dB better performance than PDM-QPSK. The same increase in nonlinear performance towards modulation formats with lower spectral efficiency is observed in section 5.1. Although, lower symbol rates lead to an improved nonlinear performance due to reduced pulse overlap and smaller impact of IXPM and IFWM and reduced depolarisation of the signal [15]. However, these effects are masked by a more significant reduction in the Euclidian distance between constellation points (and phase margin in case of BPSK) when choosing modulation formats with higher spectral efficiency such as PDM-QPSK. Given that nonlinear distortions in optically uncompensated transmission with sufficient accumulated dispersion have a circular symmetric Gaussian PDF [16], this dominance becomes even clearer.

Table 5: maximum transmission reach and optimum launch power @ BER=3.8×10^{-3} (simulation results are given in brackets)

	PDM-BPSK	PS-QPSK	PDM-QPSK
MAXIMUM REACH (km)		12838	10030
	(18214)	(17091)	(13961)
OPTIMUM LAUNCH POWER (dBm)		-3.5	-4
	(-2)	(-3)	(-4)

Overall, PDM-BPSK yielded the longest transmission reach with 18,214km at an optimum launch power of -2dBm (see Table 5). PS-QPSK comes second with a

1,120km lower maximum reach of 17,091km at an optimum launch power of -3dBm. PDM-QPSK has a significantly lower maximum transmission distance of 13,961km at -4dBm. These results lead to the conclusion, that the maximum transmission distance was dominated by the nonlinear performance of each modulation format. Although PS-QPSK preserves its inherent sensitivity advantage compared to PDM-BPSK, it exhibited a smaller nonlinear tolerance, due to a reduced phase margin (phase difference between adjacent symbols).

Note that further improvement in nonlinear transmission performance can be achieved for all modulation formats when applying pulse carving at the transmitter [17].

4.3.3 Maximum reach measurements for a WDM system

To characterise the transmission performance of PDM-BPSK, PS-QPSK and PDM-QPSK, 7 WDM channels were launched into a recirculating loop (see section 4.1.2) and the launch power per channel was varied between -14 and 4dBm to determine the maximum transmission distance at BER=3.8×10^{-3}. Figure 46 shows the experimental as well as the simulation results for all three formats.

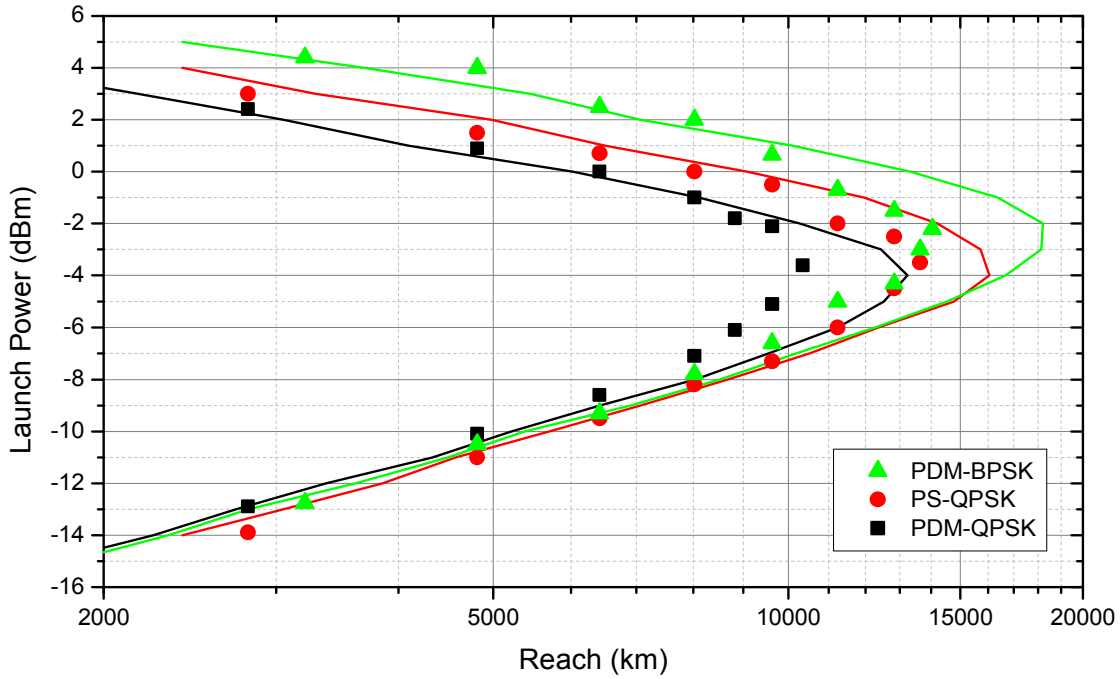

Figure 46: Reach as a function of launch power at BER=3.8×10^{-3} for 42.9Gbit/s WDM transmission of PDM-BPSK, PS-QPSK and PDM-QPSK. Symbols show experimental results while lines denote simulated performance with equivalent implementation penalty.

Despite showing similar optimum launch powers of -3.5dBm, in experiment, and -4dBm in simulation, PS-QPSK clearly outperformed PDM-QPSK with a maximum reach of 13,640 km compared to 10,350km, corresponding to an increase of 30% (28% in simulation). However, PDM-BPSK shows a 1-1.5dB higher optimum launch power, which translated into 14,040km maximum reach, corresponding to an increase of less than 3% compared to PS-QPSK (29% in simulation).

The higher receiver sensitivity of PS-QPSK observed in the back-to-back measurements translates into an increased performance in the linear transmission regime (+0.4dB better with respect to PDM-BPSK and +0.7dB compared to PDM-QPSK), similarly to the single channel experiments in the previous section. In the nonlinear transmission regime, PDM-BPSK was ~1.5 dB more resilient towards nonlinearities than PS-QPSK, in both experiment and simulation (see Figure 46). However, PDM-QPSK showed a similar penalty of ~1.5 dB and 3 dB in the nonlinear region, compared to PS-QPSK and PDM-BPSK, respectively. Interestingly, PDM-BPSK shows the same maximum transmission distance in single channel and WDM simulations. Therefore, it can be concluded that inter-channel nonlinearities are negligible in this case. However, PS-QPSK and PDM-QPSK simulations in Figure 46 show a reduced transmission reach for WDM compared to single channel transmission (by 1,043km and 722km respectively). The reduced influence of cross channel nonlinearities can be attributed to an increased walk-off (relative to the symbol period) as a result of increasing symbol-rates: 10.7GBd for PDM-QPSK, 14.3GBd for PS-QPSK and 21.45GBd for PDM-BPSK can be observed. This increased walk-off helps to average-out XPM contributions from neighbouring WDM channels.

Table 6: maximum transmission reach and optimum launch power @ BER=3.8×10^{-3} (simulation results are given in brackets)

	PDM-BPSK	PS-QPSK	PDM-QPSK
MAXIMUM REACH (km)	14,042	13,640	10,350
	(18,214)	(16,048)	(13,239)
OPTIMUM LAUNCH POWER (dBm)	-2.2	-3.5	-3.6
	(-2)	(-3)	(-4)

Similarly to the single channel experiments, the experimental WDM results show lower maximum reach than predicted by the computer simulations. Furthermore, experimentally obtained maximum transmission distances have been found to be

higher for WDM transmission than in case of single channel transmission. These inconsistencies can be attributed to the absence of a loop synchronous polarization scrambler and small inaccuracies such as e.g. in EDFA noise figure and nonlinear fibre coefficient, which tend to accumulate with increasing transmission distance. A potential source of error present only in the WDM experiments is the loop filter, consisting of a bank of tuneable MZI-filters, which had to be adjusted manually when increasing transmission distance.

In terms of the DSP complexity, it is worth mentioning that the number of FIR-filter taps required to compensate for chromatic dispersion scales with the square of the symbol-rate (see equation (50)). Therefore, PDM-BPSK and PS-QPSK require an approximately 300% and 78% longer FIR-filter compared to PDM-QPSK. For transmission over 170 spans this corresponds to 847 taps for PDM-QPSK, 1507 taps for PS-QPSK and 3389 taps for PDM-BPSK [18], which is equivalent to 1024, 2048 and 4096 taps when ceiled to the nearest power of two for implementation with the 'overlap and save' technique. Furthermore, the lower symbol-rate of PDM-QPSK and PS-QPSK would lead to 100% and 50% lower electrical bandwidth requirements for transmitter and receiver-side electronics compared to PDM-BPSK.

Digital Backpropagation was not investigated at 42.9Gbit/s due to insufficient time. However, the commercial benefit of digital backpropagation is doubtful in this scenario, because for every investigated modulation format the transmission distance achieved without it is more than sufficient for almost all terrestrial and submarine transmission links.

4.4 Transmission results at 112Gbit/s

4.4.1 Back-to-Back Measurements

The back-to-back receiver sensitivities were measured for all modulation formats to determine the intrinsic implementation penalty of the experimental setup. Figure 47 - Figure 51 show the receiver sensitivities, measured and calculated, for 112Gbit/s PS-QPSK, PDM-QPSK, PDM-8PSK, PDM-8QAM and PDM-16QAM. Each figure is divided into two subfigures, (a) shows the results for the single channel and WDM-setup with linear fits to determine excess penalties arising e.g. from coherent crosstalk when adding more channels to the setup, and (b) shows the sensitivity comparison between experiment and simulation. Analytical approximations describing the ideal BER performance as a function of the optical signal-to-noise ratio (OSNR) are described for every modulation format in section 5.1.

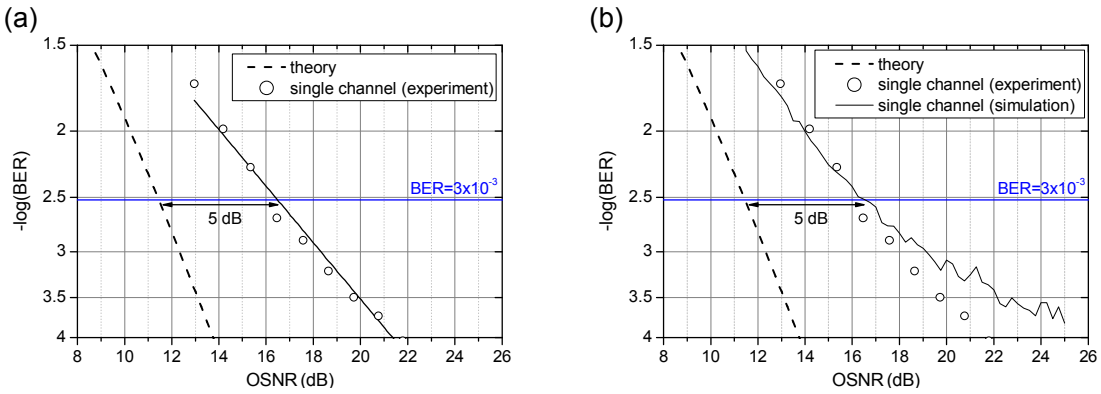

Figure 47: Back-to-back performance of 112Gbit/s single channel PS-QPSK. (a) shows experimental measurements and a linear fit, while (b) displays corresponding simulation results to match the experimental performance.

To obtain 112Gbit/s PS-QPSK it was necessary to modulate the signal at 37.33GBd, because PS-QPSK encodes 3bits/symbol. The Avanex 792000540 IQ-modulators used in all experiments have a two-sided electrical bandwidth of ~26GHz, which heavily limits the achievable receiver sensitivity as shown in Figure 47. This can be justified as follows: Figure 36 (a) shows an optical eye diagram of 37.33GBd PS-QPSK taken after the transmitter, where bandwidth limitations are clearly visible in terms of slow rise- and fall times. Since all additional components in the signal path have sufficient bandwidths for a 37.33GBd signal (Ando AP9950 PPG: 40GHz, SHF 803P amplifiers: 40GHz, Sumitomo T.MZI1.5-40 MZM: 40GHz), the culprit must be the Avanex IQ-modulator. The required OSNR at BER = 3×10^{-3} is 16.5dB and the implementation penalty amounts to 5dB. As a consequence of this high penalty, WDM-transmission has not been investigated for PS-QPSK.

Note that a recent transmission experiment demonstrated that it is possible to bring down the implementation penalty to ~1dB by employing an integrated dual polarisation IQ-modulator with a modulation bandwidth of ~33GHz and a programmable bit pattern generator, which was custom calibrated by the manufacturer [19].

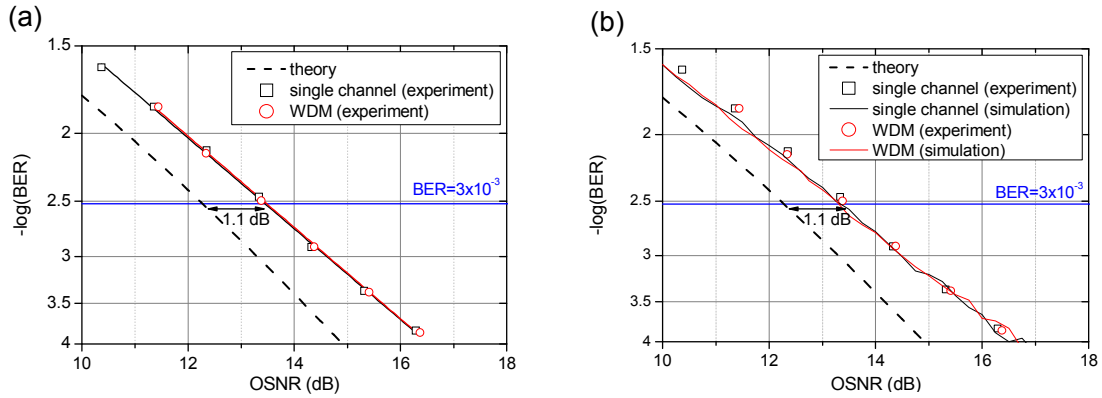

Figure 48: Back to back performance of 112Gbit/s PDM-QPSK in single channel and WDM configuration. (a) shows experimental measurements and a linear fit, while (b) displays corresponding simulation results to match the experimental performance.

Figure 48 shows the receiver sensitivity measurements for 112Gbit/s PDM-QPSK. PDM-QPSK encodes 4bit/symbol which leads to a reduced symbol rate of 28GBd compared to the 37.33GBd for PS-QPSK. The required OSNR at BER = 3×10^{-3} is 13.4dB, leading to an implementation penalty of 1.1dB for single channel and WDM setup. [19] and [20] demonstrated nearly identical implementation penalties of ~1dB for a similar experimental setup.

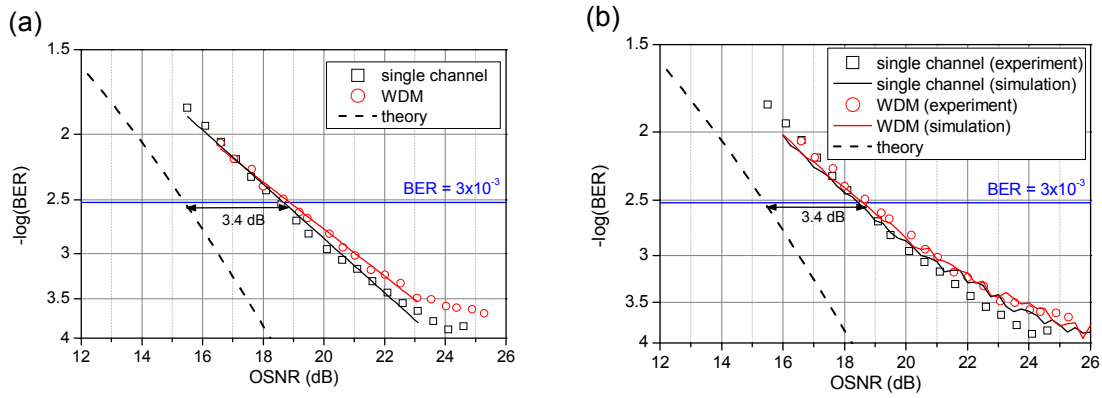

Figure 49: Back to back performance of 112Gbit/s PDM-8PSK in single channel and WDM configuration. (a) shows experimental measurements and a linear fit, while (b) displays corresponding simulation results to match the experimental performance.

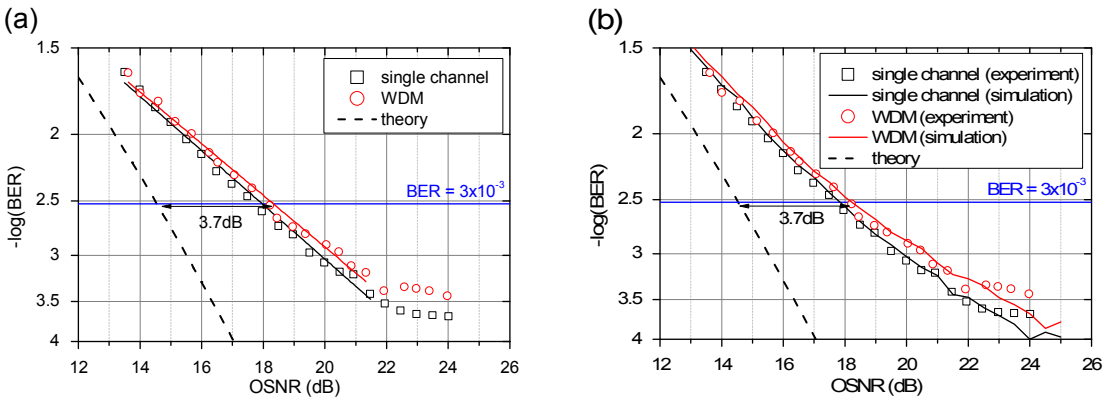

Figure 50: Back to back performance of 112Gbit/s PDM-8QAM in single channel and WDM configuration. (a) shows experimental measurements and a linear fit, while (b) displays corresponding simulation results to match the experimental performance.

Figure 49 and Figure 50 show the measured receiver sensitivities of PDM-8PSK and PDM-8QAM. Both formats encode 6bits/symbol which reduces the symbol rate down to 18.66GBd. Implementation penalty values of 3.2 dB and 3.4 dB were measured for single channel PDM-8PSK and PDM-8QAM at a bit error rate (BER) of 3×10^{-3}. The addition of WDM channels to the signal resulted in penalties of ~0.2dB for PDM-8PSK and ~0.3dB for PDM-8QAM. Even though PDM-QPSK showed the influence of crosstalk induced by neighbouring channels to be negligible at a higher bandwidth of 28GHz, denser modulation schemes such as 8PSK or 8QAM are less resilient even to lower levels of crosstalk. Taking the excess penalty into account it is worth noting that, PDM-8QAM had a required OSNR of 18.3dB at a BER of 3×10^{-3}, corresponding to 3.7dB implementation penalty and PDM-8PSK of 18.9dB, corresponding to 3.4dB implementation penalty. The error floor for both modulation formats is attributed to the modulation distortions stemming from the drift of operating points of the second modulation stage (phase modulator for PDM-8PSK and IQ-modulator for PDM-8QAM).

Previous experiments of 100Gbit/s PDM-8QAM demonstrated single channel implementation penalties of ~3.8dB [21] with a cascade of an IQ-modulator and a phase modulator (see Figure 14 (a)) compared with 3.4dB achieved here. However, the implementation penalty could be further reduced to ~3dB [22] with the same transmitter setup as used here. The single channel implementation penalty for PDM-8PSK was measured as ~3.2dB, which is significantly better than previously demonstrated implementation penalties e.g. 4.4dB in [23].

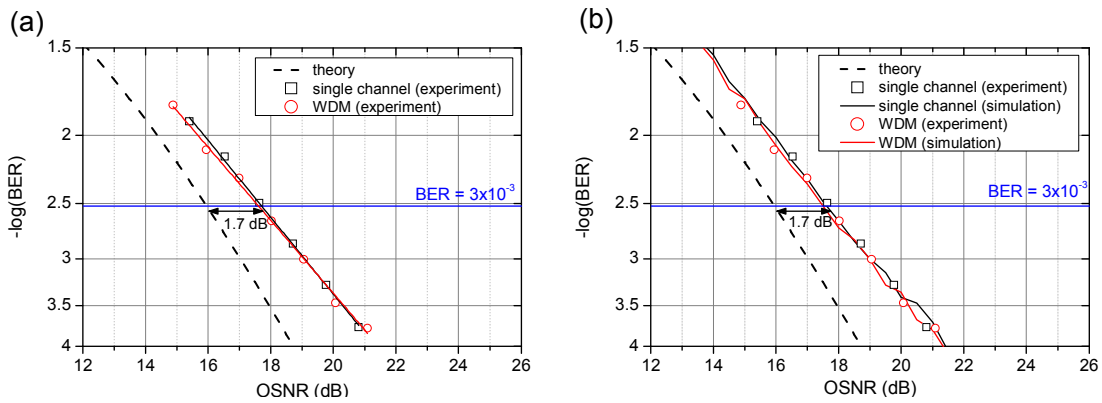

Figure 51: Back-to-back performance of 112Gbit/s PDM-16QAM in single channel configuration. (a) shows experimental measurements and a linear fit, while (b) displays corresponding simulation results to match the experimental performance.

Figure 51 shows the receiver sensitivity of 112Gbit/s PDM-16QAM, which encodes 8bit/symbol and was, therefore, modulated at 14GBd. Due to the noise suppression characteristics of the phase stabilised fibre interferometer transmitter described in the previous section, the required OSNR @ BER = 3×10^{-3} was only 17.7dB, corresponding to an implementation penalty of 1.7dB. Furthermore, the reduced symbol rate leads to a decreased influence of crosstalk induced by neighbouring channels and consequently to the same performance for single channel and WDM setup.

Earlier work on the generation of PDM-16QAM (integrated IQ modulator and 2bit DACs to create multilevel driving signals as described in Figure 15) at 112Gbit/s reported an implementation penalty which had been reduced from ~3.9dB down to ~2.6dB by employing pulse shaping [24], which is still 0.9dB worse than the fibre interferometer approach used in the work described in this thesis.

Focussing on the WDM setup it appears that PDM-QPSK has a 3.1dB lower required OSNR than PS-QPSK, losing its inherent 0.75dB advantage due to the increased implementation penalty of 5dB – see Table 7. Furthermore, PDM-16QAM showed a lower required OSNR of 17.7dB compared to 18.9dB for PDM-8PSK and 18.3dB for PDM-8QAM, even though it has an inherent theoretical penalty of 0.3dB compared to PDM-8PSK and 1.5dB compared to PDM-8QAM (see Figure 59 (b)). This behaviour can be attributed to increased implementation penalties for dual stage transmitter structures, which act as filter cascades increasing ISI and add twice the amount of electrical noise to the signal. Even though the phase stabilised fibre interferometer is also a 2 stage device, it is entirely passive, in the sense, that the second stage is not modulated by an electrical driving signal. Moreover, the reduced symbol rate in the case of PDM-16QAM relaxes bandwidth requirements and reduces ISI. Another

important difference between PDM-16QAM and all other modulation formats is that maximum likelihood decision boundaries have been implemented to combat modulation distortions and improve the BER [25]. When comparing PDM-8QAM and PDM-8PSK one observes that PDM-8QAM preserves 0.6 dB of the theoretical sensitivity advantage of 0.9 dB over PDM-8PSK.

Table 7: required OSNR and implementation penalty for WDM setup of 112Gbit/s PS-QPSK, PDM-QPSK, PDM-8PSK, PDM-8QAM and PDM-16QAM @ BER = 3×10^{-3}

	PS-QPSK (SINGLE CHANNEL)	PDM-QPSK	PDM-8PSK	PDM-8QAM	PDM-16QAM
REQUIRED OSNR (dB)	16.5	13.4	18.9	18.3	17.7
IMPLEMENTATION PENALTY (dB)	5	1.1	3.4	3.7	1.7

It is worth noting that excellent agreement between experiment and simulation has been achieved in all the back-to-back cases, which is an important prerequisite for the following investigation of the transmission characteristics of the three modulation formats at 112Gbit/s.

4.4.2 Maximum reach measurements for a single channel system

In this section, the single channel transmission performances of PS-QPSK, PDM-QPSK, PDM-8PSK, PDM-8QAM and PDM-16QAM are compared at 112Gbit/s. To achieve this the modulated signal was fed into the recirculating loop, coupled out after the desired number of recirculations and detected with a digital coherent receiver, as described in section 4.1. PS-QPSK and PDM-QPSK were processed with the same algorithms described in section 4.1.3, while PDM-8PSK, PDM-8QAM and PDM-16QAM required modified DSP algorithms after the chromatic dispersion compensation stage. For PDM-8PSK a standard CMA equaliser, followed by and the Viterbi & Viterbi phase recovery algorithm [8] was employed, similarly to PDM-QPSK. Quadrature amplitude modulation formats like PDM-8QAM and PDM-16QAM have more than one intensity level and therefore require a radially-directed algorithm for equalisation [10]. For the same reason a decision directed PLL was used to recover the carrier phase of QAM formats. All algorithms are described in detail in section 3.3.5 and 3.3.6.

Figure 52 shows the maximum achievable transmission distance, obtained in experiments and by simulations, at BER=3×10^{-3} for PS-QPSK, PDM-QPSK, PDM-8PSK, PDM-8QAM and PDM-16QAM as a function of the launch power, varied between -10 and 8dBm. The simulations have been conducted with equivalent

implementation penalties to guide the experiments. Agreement between experiment and simulation is generally very good, with the simulation slightly overestimating maximum transmission distance in most cases.

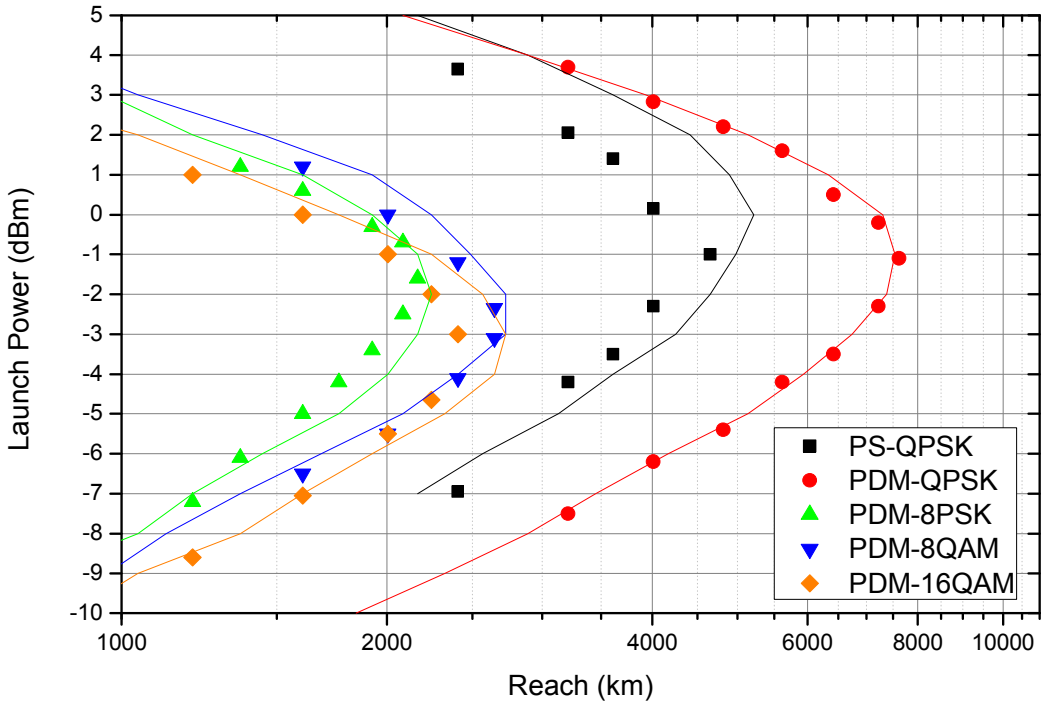

Figure 52: single channel transmission of PS-QPSK, PDM-QPSK, PDM-8PSK, PDM-8QAM and PDM-16QAM at 112Gbit/s without nonlinear compensation. Markers denote experimentally obtained data, whereas lines denote simulation results with equivalent implementation penalty.

In the linear transmission regime, the achievable transmission distance depends on the received OSNR, which increases exponentially with launch power. The difference in required OSNR for all modulation formats displayed in Table 7 can be directly related to the relative performance of modulation formats in the linear regime. Therefore PDM-QPSK performs best in this regime with ~3dB better performance than PS-QPSK. PDM-16QAM shows a penalty of ~1.2dB with respect to PS-QPSK, but performs ~0.7dB better than PDM-8QAM and ~1.3dB better than PDM-8PSK.

As already described in section 4.3.2 and 4.3.3, modulation formats are more susceptible to nonlinear distortions with increased modulation density, which is simply due to reduced phase and amplitude margins. This relation can be clearly observed in the nonlinear transmission regime in Figure 52, where PS-QPSK show a similar nonlinear performance like PDM-QPSK, while PDM-8QAM, PDM-8PSK and PDM-16QAM show a penalty of ~4dB, ~4.7dB and ~5.4dB respectively. The same relationship between constellation density and nonlinear performance is reflected in the optimum launch power, which increases with lower constellation density (Table 8).

But which nonlinear distortions limit transmission under the present circumstances? When transmitting only a single wavelength channel it is possible to eliminate inter-channel nonlinear distortions such as XPM (section 2.2.2) and XPolM (section 2.2.4) which would only be caused by adjacent wavelength channels. Another nonlinearity that can be neglected is FWM, which is due to the relatively high local dispersion which minimises phase matching conditions (section 2.2.3). As a consequence, transmission is limited by the intra-channel nonlinearity SPM, which can be subdivided into ISPM, IXPM and IFWM (see section 2.2.1). ISPM denotes the nonlinear phase shift caused by the pulse itself, while IXPM involves the contribution of isolated neighbouring pulses. IFWM contributes to the nonlinear distortion as a mixing process of the pulse itself and frequency components of two different pulses, generating a fourth frequency component. Modulation formats with an identical pulse shape per slot do not suffer from ISPM and IXPM, since the induced nonlinear phase shift is identical for every slot and can, therefore, easily be mitigated by the phase recovery. This effect is the reason why pulse carving (irrespective of the duty cycle) reduces nonlinear distortions in transmission. Since no pulse carving is implemented for this work, different pulse shapes can be observed in the eye diagrams of Figure 36. Even modulation formats such as PS-QPSK, QPSK and 8PSK, which use only the phase to encode information, exhibit different pulse shapes due to varying transitions between symbols which leads to transmission distortions stemming from ISPM and IXPM. While ISPM contributions start to fade with increasing transmission distance and pulse overlap (due to the reduced pulse peak power), IXPM and IFWM distortions become worse. Another nonlinear distortion increasing with pulse overlap, is depolarisation due to intra channel nonlinearities, which has been reported recently [15]. As a consequence the impact of single channel nonlinearities reduces with reduced symbol rate for a fixed modulation format as described in section 5.1. However, possible benefits due to reduced pulse overlap stemming from lower symbol-rate are more than offset by the reduction in Euclidian distance and, therefore, reduced receiver sensitivity that is associated with more spectrally efficient modulation formats.

Table 8: maximum transmission distance and optimum launch power @ BER=3×10^{-3} in single channel configuration without employing nonlinear compensation (simulation results are given in brackets)

	PS-QPSK	PDM-QPSK	PDM-8PSK	PDM-8QAM	PDM-16QAM
MAXIMUM REACH (km)	4,654	7,623	2,166	2,648	2,407
	(5,216)	(7,543)	(2,245)	(2,728)	(2,728)
OPTIMUM LAUNCH POWER (dBm)	-1	-1.1	-1.6	-2.7	-3
	(0)	(-1)	(-2)	(-2.5)	(-3)

Performance in the linear and nonlinear transmission regime, translated into the maximum transmission distance and optimum launch power, is detailed in Table 8. The maximum transmission distance of PDM-QPSK is 7,623km at -1.1dBm (simulation: 7,543km at -1dBm) compared to 4,654km at -1dBm (simulation: 5,216km at 0dBm) for PS-QPSK. PDM-8QAM shows a higher transmission distance of 2,648km at -2.7dBm (simulation: 2,728km at -2.5dBm) compared to PDM-8PSK with 2,166km at -1.6dBm (simulation: 2,245km at -2dBm). Due to low implementation penalty, PDM-16QAM outperforms PDM-8PSK with 2,407km at -3dBm (simulation: 2,728km at -3dBm).

The impact of digital backpropagation was investigated with 1 computational step per span to compare 112Gbit/s single channel PS-QPSK, PDM-QPSK, PDM-8PSK, PDM-8QAM and PDM-16QAM, whilst maintaining a fixed complexity per distance. The nonlinear compensation algorithm is based on the split step Fourier method employing the Manakov equation (see section 3.3.2) and has been optimised for 10.7GBd signals as part of collaborative work described in [26]. Generally, nonlinear backpropagation algorithms employing a higher number of steps per span are more efficient, especially for signals with a higher symbol rate (broader spectrum) as described in section 5.2. Therefore, the algorithm with a fixed complexity per distance is expected to suffer a penalty with respect to the optimum performance for higher symbol rate signals used here. This penalty is essentially due to pulse spreading and the related change of the waveform within the effective length of the fibre that cannot be approximated by the single sample taken by the backpropagation algorithm. Other limitations of the algorithm are signal-ASE interaction as well as PMD and PDL, which cannot be compensated for due to their nondeterministic nature. Receiver distortions such as the frequency response of the receiver (optical filter, electrical front end ...) and laser phase noise added by the LO affect the received signal, leading to additional distortions after the waveform has been backpropagated.

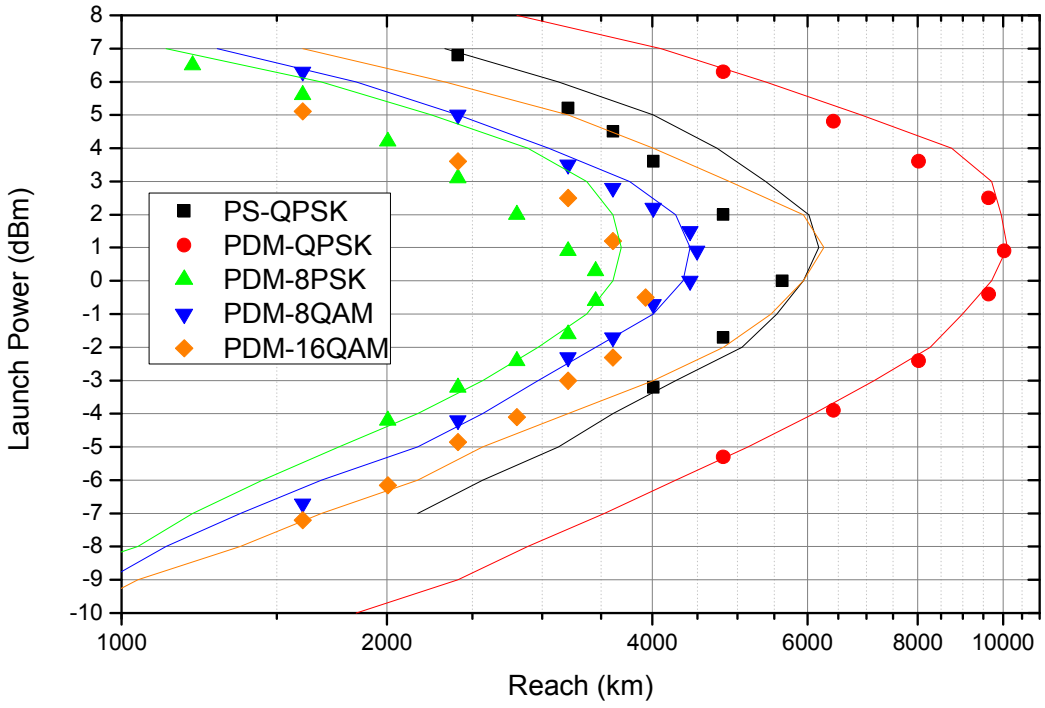

Figure 53: single channel transmission of PS-QPSK, PDM-QPSK, PDM-8PSK, PDM-8QAM and PDM-16QAM at 112Gbit/s with nonlinear compensation. Markers denote experimentally obtained data, whereas lines denote simulation results with equivalent implementation penalty.

Figure 53 shows experimental and simulation results for single channel 112Gbit/s transmission with nonlinear compensation. The maximum transmission distance of PS-QPSK could be extended by +20.7% to 5,617km at 0dBm (simulation: +18.5% to 6,180km at 1dBm) compared to +31.6% increase to 10,030km at 0.9dBm (simulation: +34% to 10,110km at 1dBm) for PDM-QPSK. The greater benefit of digital backpropagation for modulation formats with a higher spectral efficiency is evident when looking at PDM-8QAM, which shows a +69.7% longer transmission distance of 4,493km at 0.9dBm (simulation: +58.8% to 4,333km at 1dBm). Considering that PDM-8PSK has the same spectral efficiency as PDM-8QAM, the increase in maximum reach is similar too: +59.3% to 3,450km at -0.1dBm (simulation: +58.8% to 3,691km at 1dBm). PDM-8QAM outperforms PDM-8PSK in the linear as well as in the nonlinear regime, which results in a 13 span (more than 1,000km) longer transmission reach.

In the case of PDM-16QAM the transmission distance could be increased by +63.4% to 3932km at -0.5dBm (simulation: +129.5% to 6260km at 1dBm). Here, the experiment seems to drastically underestimate the benefit of digital backpropagation, despite very good agreement in the linear transmission regime. This might be due to the fact that it is notoriously difficult to correctly measure absolute power values, and simulations as well as the calibration of the power values have been performed after the experiment.

When no nonlinear compensation is used, it is possible to apply a calibration factor after the measurement (corresponding to an upwards or downwards shift of the whole reach curve) without loss of accuracy. However, digital backpropagation requires a good knowledge of the absolute power value P_{in} to be able to optimise φ for the correct nonlinear phase shift (as in equation (58)):

$$\hat{N}(t) = -j\gamma\varphi\frac{8}{9}(|E_Y|^2 + |E_X|^2)P_{in}10^{\left(-\left[\frac{s}{n}-1\right]\frac{\alpha L}{10}\right)} \quad \textbf{(68)}$$

where L is the span length in km, α the fibres attenuation coeffient in dB/km and s a running variable identifying the current step out of n steps per span. Even though it is possible to trade-off P_{in} vs φ, it is difficult to find a global optimum for φ in face of uncertainty of the absolute power value. Additional factors that affect the stability of the power measurements are: drift of triggering signals to the OSA and the necessity to rebalance the loop depending on distance and input power. For installed systems employing digital backpropagation the accurate knowledge of the launch power is as important as in lab experiments. The more complex loss profile (due to splices, connectors,...) requires a much more careful optimisation of the nonlinear backpropagation algorithm. However, once optimised the digital backpropagation algorithm does not require feedback as long as the loss profile does not change and the launch power stays constant at its optimum value.

Table 9 summarises maximum achievable reach, optimum launch power and the relative benefit of applying digital backpropagation of all modulation formats.

Table 9: maximum transmission distance and optimum launch power @ BER=3×10^{-3} in single channel configuration with nonlinear compensation (simulation results are given in brackets)

	PS-QPSK	PDM-QPSK	PDM-8PSK	PDM-8QAM	PDM-16QAM
MAXIMUM REACH (km)	5,617	10,030	3,450	4,493	3,932
	(6,180)	(10,110)	(3,691)	(4,333)	(6,260)
OPTIMUM LAUNCH POWER (dBm)	0	0.9	-0.1	0.9	-0.5
	(1)	(1)	(1)	(1)	(1)
INCREASE IN MAXIMUM REACH (%)	20.7	31.6	59.3	69.7	63.4
	(18.5)	(34.0)	(64.4)	(58.8)	(129.5)
INCREASE IN OPTIMUM LAUNCH POWER (dB)	1	1	1.5	3.6	2.5
	(1)	(2)	(3)	(3.5)	(4)

4.4.3 Maximum reach measurements for a WDM system

To characterise the transmission performance of PDM-QPSK, PDM-8PSK, PDM-8QAM and PDM-16QAM, 7 WDM channels were launched into a recirculating loop (as described in section 4.1.2) and the launch power per channel was varied between -10 and 4dBm to determine the maximum transmission distance at BER=3×10^{-3}. Figure 46 shows the experimental as well as the simulation results for all four formats.

The higher receiver sensitivity of PDM-QPSK observed in the back-to-back measurements results in an improved performance in the linear transmission regime (4.3dB better with respect to PDM-16QAM, 5.1dB better than PDM-8QAM and 5.5dB better than PDM-8PSK), similar to the single channel experiments in the previous section. In the nonlinear transmission regime, PDM-QPSK is more than 5dB more resilient towards nonlinearities compared to PDM-8QAM and PDM-16QAM, which show similar performance, while PDM-8PSK suffers from a 5.5dB penalty towards PDM-QPSK. Note that due to the limited availability of ECLs, which are required to ensure that neighbouring channels are true 16QAM channels when generated with fibre interferometer (see section 4.1.1), the WDM experiment for 16QAM was carried out with only 3 wavelength channels instead of 7 channels as for all the other modulation formats. To explore the accuracy of these results and extend them, simulations of 3-, 5- and 7-WDM channel systems were conducted to ensure that performance in the nonlinear regime is comparable to the other modulation formats and not skewed due to the lack of XPM contributions from the 4 missing channels. Indeed a 3 channel system would have underestimated nonlinear performance by ~0.25dB compared to a 5 channel system and 0.5dB compared to 7 channels.

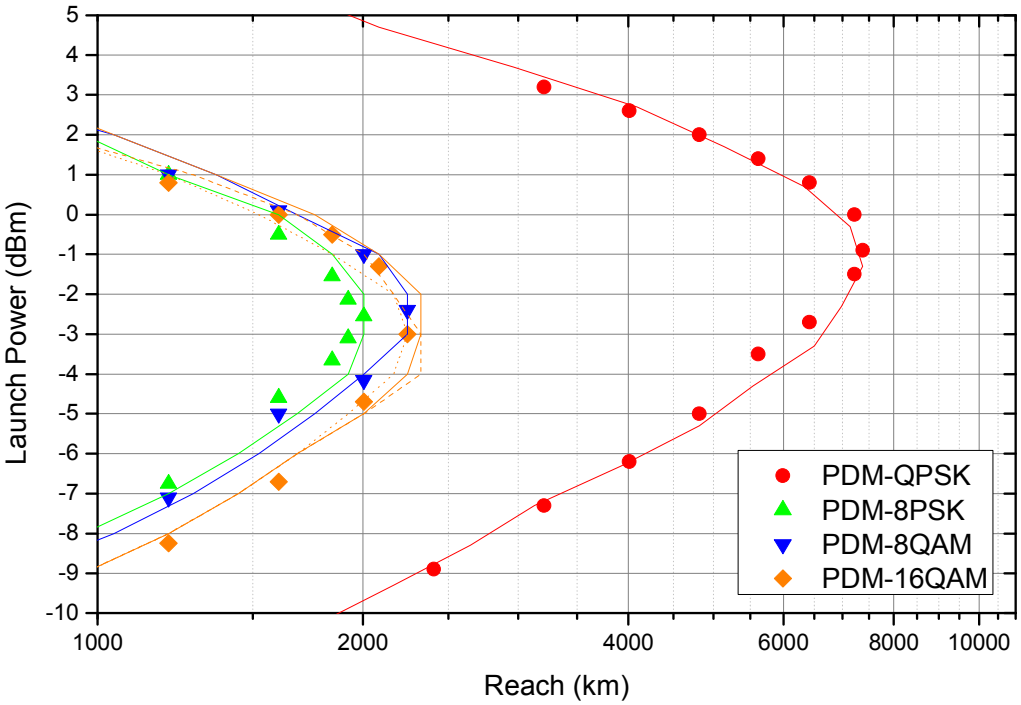

Figure 54: WDM transmission of PDM-QPSK, PDM-8PSK, PDM-8QAM and PDM-16QAM at 112Gbit/s without nonlinear compensation. Markers denote experimentally obtained data, whereas lines denote simulation results with equivalent implementation penalties.
In case of PDM-16QAM a solid line denotes 3 WDM channels, a dashed line 5 WDM channels and a dotted line 7WDM channels.

PDM-QPSK achieved a maximum transmission distance of 7,382km at -0.9dBm (simulation: 7,382km at -1dBm), which is 3 spans less than in the case of a single channel system (simulation: 2 spans). An equally small penalty can be observed when going from single channel to WDM configuration for PDM-8PSK: 2,006km at -2.55dBm, which is 2 spans less than the single channel case (simulation: 3 spans). However, when looking at the relation of maximum transmission distance between single channel and WDM PDM-8QAM the difference is more noticeable: 5 spans (simulation: 6 spans). When comparing 3 and 5 channel WDM transmission of PDM-16QAM to the single channel case the penalty for WDM transmission is only a single span, whilst in case of 7 channel WDM transmission the WDM-penalty increases to 2 spans. Therefore, one could conclude that the influence of inter-channel nonlinearities is weak and the system is largely limited by intra channel nonlinearities. However, XPM contributions are noticeable (especially with formats with a higher peak to average power ratio like 8QAM and 16QAM [27]), even though it might not translate into dramatically reduced reach.

Table 10 summarises achieved maximum transmission distance as well as optimum launch powers for 7 channel WDM transmission of PDM-QPSK, PDM-8PSK, PDM-8QAM and PDM-16QAM at 112Gbit/s.

Table 10: maximum transmission distance and optimum launch power @ BER=3×10^{-3} for 7 WDM channels without employing nonlinear compensation (simulation results are given in brackets)

	PDM-QPSK	PDM-8PSK	PDM-8QAM	PDM-16QAM
MAXIMUM REACH (km)	7,382	2,006	2,247	
	(7,382)	(2,006)	(2,247)	(2,247)
OPTIMUM LAUNCH POWER (dBm)	-0.9	-2.55	-2.4	
	(-1.3)	(-2.5)	(-2.5)	(-3)

As a next step the impact of digital backpropagation was investigated for 112Gbit/s WDM-transmission of PDM-QPSK, PDM-8PSK, PDM-8QAM and PDM-16QAM. Computational complexity per distance was fixed by using a single step per span algorithm, based on the split step Fourier method employing the Manakov equation (see section 3.3.2). As noted earlier this algorithm was optimised as part of collaborative work described in [26]. Additionally to signal-ASE interaction, PMD, PDL, receiver distortions and the insufficient number of steps per span, inter channel nonlinearities affect the efficiency of the digital backpropagation algorithm in a WDM system.

Figure 55 shows experimental and simulation results for WDM transmission with digital backpropagation. The maximum transmission distance of PDM-QPSK could be extended by +19.6% to 8,826km at 0.3dBm (simulation: +26.1% to 9,308km at 1dBm) compared to +20% increase to 2,407km at -1.32dBm (simulation: +28% to 2,568km at -1dBm) for PDM-8PSK. PDM-8QAM shows a +17.8% increased maximum transmission distance of 2,648km at -1dBm (simulation: +21.4% to 2,728km at -1dBm) compared to a 50% increase to 3,370km for 7 channel PDM-16QAM. The reduction of the number of WDM channels gradually increases achievable transmission distance in case of PDM-16QAM to +62% (3,771km) for 5 WDM channels, +75.8% for 3 WDM channels, converging against +129.5% the improvement for single channel transmission with nonlinear compensation. Similarly to the experimental single channel PDM-16QAM data, improvement by digital backpropagation is heavily underestimated for 3 channel WDM transmission to +25% (simulation: +75.8%), which is attributed to difficulties in measuring the optical power as outlined in the previous section.

As expected, the higher benefit of digital backpropagation for modulation formats with a higher spectral efficiency is more pronounced in single channel transmission, but still noticeable in a WDM system. However, uncompensated nonlinear crosstalk from neighbouring channels limits the efficiency of the backpropagation algorithm dramatically and therefore achievable transmission distance.

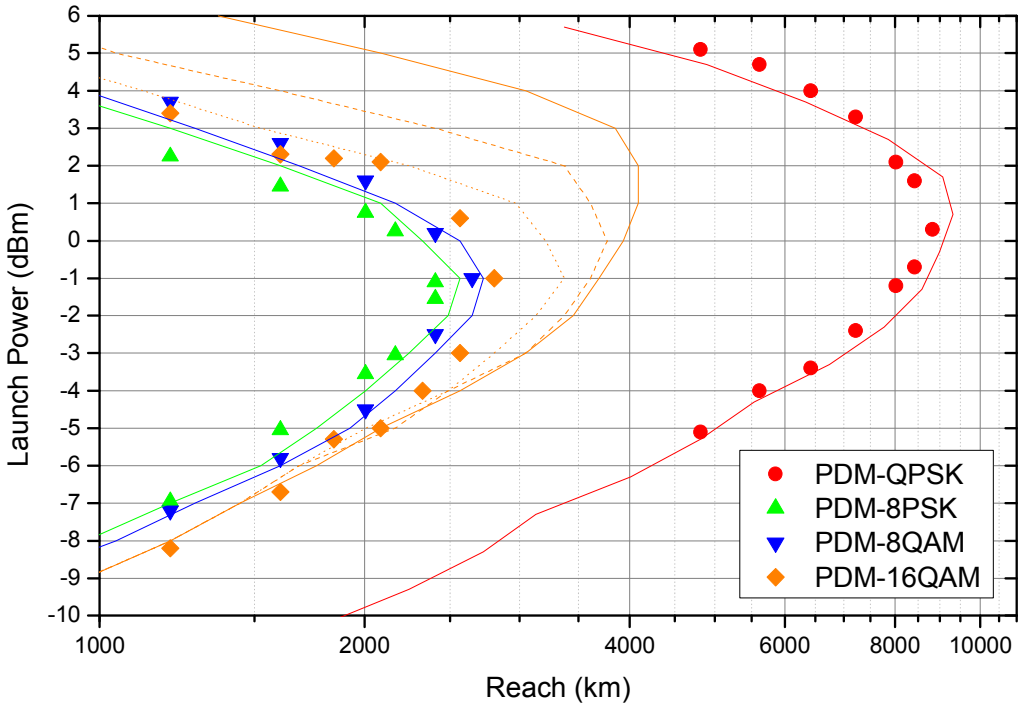

Figure 55: WDM transmission of PDM-QPSK, PDM-8PSK, PDM-8QAM and PDM-16QAM at 112Gbit/s with nonlinear compensation. Markers denote experimentally obtained data, whereas lines denote simulation results with equivalent implementation penalties.
In case of PDM-16QAM a solid line denotes 3 WDM channels, a dashed line 5 WDM channels and a dotted line 7WDM channels.

Table 11 summarises achieved maximum transmission distance, as well as optimum launch powers for 112Gbit/s WDM transmission of PDM-QPSK, PDM-8PSK, PDM-8QAM and PDM-16QAM with digital backpropagation.

Table 11: maximum transmission distance and optimum launch power @ BER=3×10^{-3} for 7 WDM channels with nonlinear compensation (simulation results are given in brackets)

	PDM-QPSK	PDM-8PSK	PDM-8QAM	PDM-16QAM
MAXIMUM REACH (km)	8,826	2,407	2,648	
	(9,308)	(2,568)	(2,728)	(3,370)
OPTIMUM LAUNCH POWER (dBm)	0.3	-1.32	-1	
	(0.7)	(-1)	(-1)	(-1)
INCREASE IN MAXIMUM REACH (%)	19.6	20	17.8	
	(26.1)	(28)	(21.4)	(50)
INCREASE IN OPTIMUM LAUNCH POWER (dB)	1.2	1.23	1.4	
	(2)	(1.5)	(1.5)	(2)

In the following it will be assumed that transmitter and receiver hardware has been integrated in an ASIC. Hardware limitations such as insufficient bandwidth or additional distortions including electrical noise, driving up the implementation penalty of the experimental setup are assumed to be negligible yielding a reduced implementation penalty for a commercial product. Since the increased implementation penalty (especially for PDM-8PSK: 3.4dB, PDM-8QAM: 3.7dB and PS-QPSK: 5dB) will have reduced achievable transmission distance in the previous investigation, the aim of the following simulation study was to explore an upper bound of transmission performance. The simulation setup described in section 4.2 was modified as follows: no electrical noise was added to the driving signals and the electrical bandwidth of transmitter and receiver has been modelled with a 5th order Bessel filter with a bandwidth of 0.8 × symbol-rates.

Figure 56 compares transmission performance of 7 channel WDM transmission with implementation penalty similar to the experiment to an upper performance bound. The reduction in implementation penalty can be easily deduced from the linear transmission performance: PDM-QPSK: -1.1dB PDM-8PSK: -2.2dB, PDM-8QAM: -2.5dB, PDM-16QAM: -0.6dB and in case of PS-QPSK: -3.8dB (comparing to Figure 52). In contrast to the experimental comparison in the previous section, linear performance increases with reduced constellation density, since SNR requirements are reduced as outlined in section 5.1. A similar behaviour can be observed in the nonlinear regime, since it has been shown that nonlinear distortions incident in an uncompensated transmission link with sufficient group velocity dispersion can be approximated by a bi-Gaussian distribution [16]. As a consequence achievable transmission reach increases

exponentially with reduced spectral efficiency (reduced SNR requirements) as shown in Table 12.

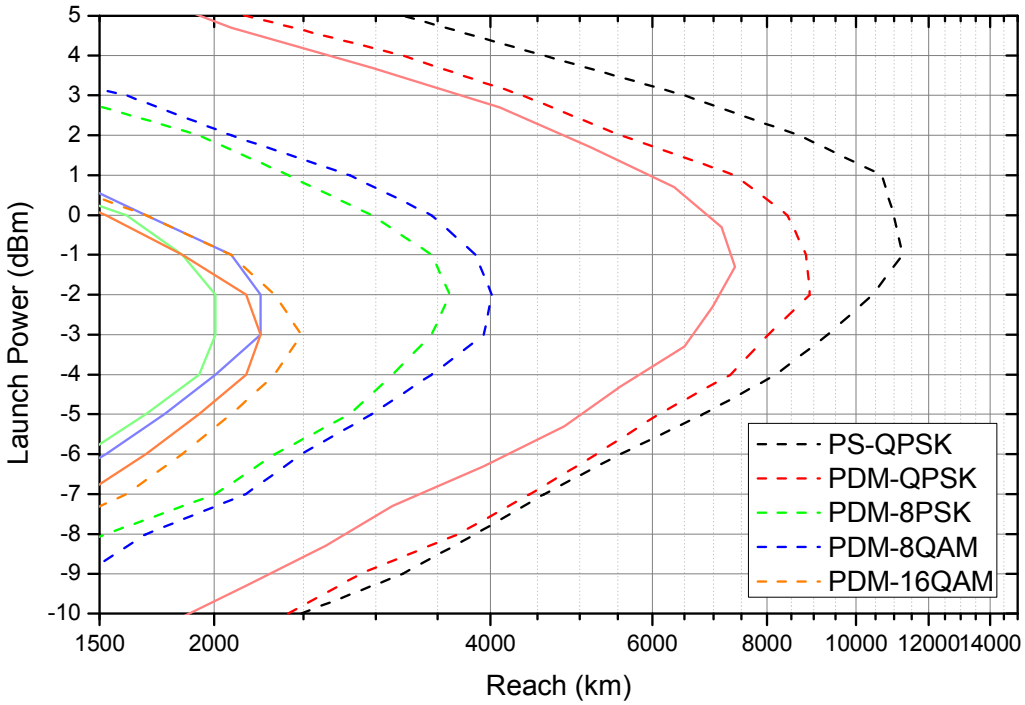

Figure 56: WDM transmission of PDM-QPSK, PDM-8PSK, PDM-8QAM and PDM-16QAM at 112Gbit/s without nonlinear compensation. Solid lines denote simulated systems with implementation penalty equivalent to the experiments (PS-QPSK was not investigated), while dashed lines denote upper bounds on transmission performance.

Figure 57 shows the WDM transmission performance of 112Gbit/s PS-QPSK, PDM-QPSK, PDM-8PSK, PDM-8QAM and PDM-16QAM with applying a 1 step per span digital backpropagation algorithm. Maximum transmission reach could be extended for PS-QPSK by +15.7% to 13,000km, for PDM-QPSK by +35.1% to 12,036km, for PDM-8PSK by +40% to 5,055km compared to +36% increase to 5,456km for PDM-8QAM. PDM-16QAM shows a +51.6% increased maximum transmission distance of 3,771km. That an increased benefit in maximum achievable transmission reach and optimum launch power can be gained (see Table 12), when backpropagating higher order modulation formats is confirmed here again.

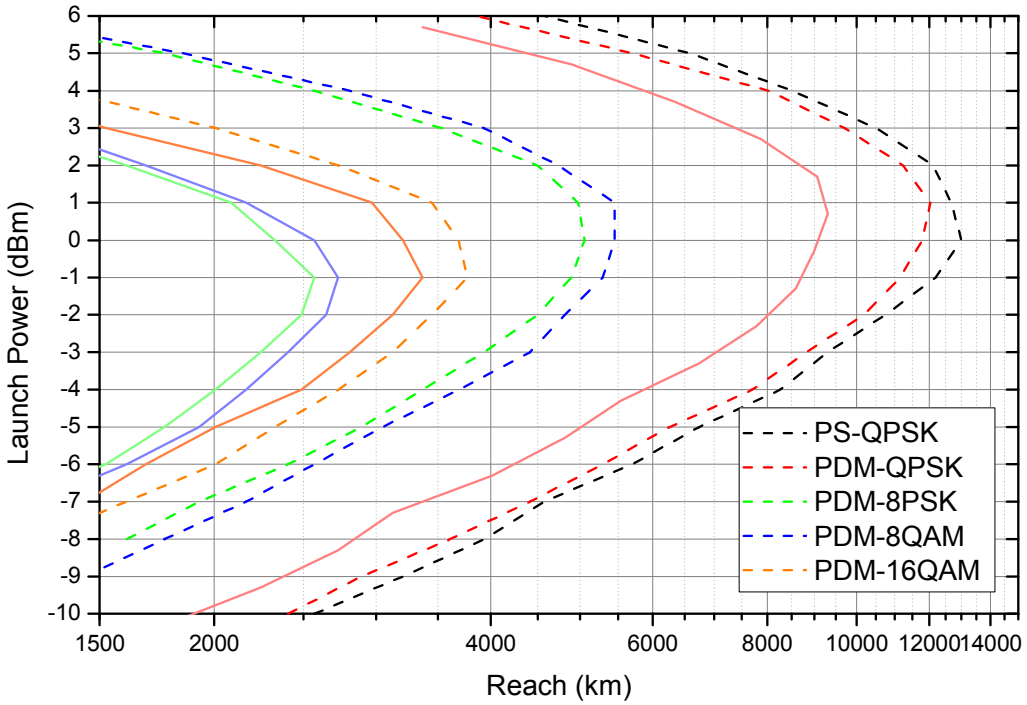

Figure 57: WDM transmission of PDM-QPSK, PDM-8PSK, PDM-8QAM and PDM-16QAM at 112Gbit/s with nonlinear compensation. Solid lines denote simulated systems with implementation penalty equivalent to the experiments, while dashed lines denote upper bounds on transmission performance.

Table 12: maximum transmission distance @ BER=3×10^{-3} for 7 WDM channels with (grey) and without nonlinear compensation (white)

	PS-QPSK	PDM-QPSK	PDM-8PSK	PDM-8QAM	PDM-16QAM
MAXIMUM REACH (km)	11,234	8,907	3,611	4,012	2,487
	13,000	12,036	5,055	5,456	3,771
OPTIMUM LAUNCH POWER (dBm)	-1	-2	-2	-2	-3
	0	1	0	0.5	-1
INCREASE IN MAXIMUM REACH (%)	+15.7	+35.1	+40	+36	+51.6
INCREASE IN OPTIMUM LAUNCH POWER (dB)	+1	+3	+2	+2.5	+4

4.5 Summary

Long-haul and ultra-long-haul transmission of PDM-BPSK, PS-QPSK, PDM-QPSK, PDM-8PSK, PDM-8QAM and PDM-16QAM modulation has been studied at fixed bit rates of 42.9Gbit/s and 112Gbit/s. Single channel and 7 channel WDM-transmission over an uncompensated SMF link employing 80km spans, with EDFA-only amplification and phase and polarization-diverse coherent detection, was investigated experimentally and by means of computer simulations. Linear and nonlinear performance was found to be related to the density of the constellation, since ASE-noise and nonlinear distortions lead to symmetric spread of each constellation point, which can be approximated with a bi-Gaussian distribution in both cases. Consequently, maximum transmission distance increases exponentially when less spectrally efficient modulation formats are employed. Several record transmission distances were achieved for standard single-mode fibre and EDFA amplification at 42.9Gbit/s (14,042km for PDM-BPSK, 13,640km for PS-QPSK and 10,350km for PDM-QPSK) and at 112Gbit/s (7,382km for PDM-QPSK, 2,247km for PDM-8QAM, 2,006km for PDM-8PSK and 2,247km for PDM-16QAM).

A digital backpropagation (DBP) algorithm based on the Manakov equation has been applied to extend the reach of the 112Gbit/s WDM-systems. The complexity of the algorithm has been fixed at 1 step per transmitted span and an increased benefit for the more spectrally efficient modulation formats has been demonstrated. Maximum transmission reach has been extended for PDM-QPSK by 19.6% to 8,826km, for PDM-PSK by 20% to 2,407km, for PDM-8QAM by 17.8% to 2,648km and for PDM-16QAM by 25% to 2,808km.

Table 13 summarises achieved transmission distances and relative improvement gained by applying DBP for all the modulation formats and bit rates that were experimentally investigated in this chapter. The following chapter extends this experimental investigation, which was conducted at fixed bit rates, by computer simulations focussing on fixed symbol rates. Furthermore, DBP will be explored with an optimum number of steps per span for backpropagation of the central channel as well as multi-channel DBP.

Table 13: maximum transmission distance achieved in 7×WDM experiments (PDM-16QAM: 3×WDM) for 42.9Gbit/s and 112Gbit/s. Increased transmission distance by applying a 1 step per span digital backpropagation algorithm is highlighted in grey.

		PDM-BPSK	PS-QPSK	PDM-QPSK	PDM-8PSK	PDM-8QAM	PDM-16QAM
42.9 Gbit/s	MAXIMUM REACH (km)	14,042	13,640	10,350			
112 Gbit/s	MAXIMUM REACH (km)			7,382	2,006	2,247	2,247
				8,826	2,407	2,648	2,808
	INCREASE IN MAXIMUM REACH (%)			+19.6	+20	+17.8	+25

4.6 References

[1] J. Gaudette, J. Sitch, M. Hinds, E. Rivera Hartling, P. Rolle, R. Hadaway, K. Roberts, B. Smith, and D. Veverka, "40Gb/s and 100Gb/s Ultra Long Haul Submarine Systems," in *Proc. SubOptic 2010*, 2010.

[2] M. Karlsson and E. Agrell, "Which is the most power efficient modulation format in optical links?," *Optics Express,* vol. 17, pp. 10814-10819, 2009.

[3] E. Agrell and M. Karlsson, "Power-Efficient Modulation Formats in Coherent Transmission Systems," *Journal of Lightwave Technology,* vol. 27, pp. 5115-5126, 2009.

[4] C. E. Shannon, "A mathematical theory of communication," *Bell Syst. Tech. J.,* vol. 27, 1948.

[5] P. P. Mitra and J. B. Stark, "Nonlinear limits to the information capacity of optical fibre communications," *Nature,* vol. 411, pp. 1027-1030, 2001.

[6] S. Makovejs, "High-speed optical fibre transmission using advanced modulation formats," PhD thesis, Electrical and Electronic Engineering, University College London, London, 2011.

[7] S. Makovejs, D. S. Millar, V. Mikhailov, G. Gavioli, R. I. Killey, S. J. Savory, and P. Bayvel, "Novel Method of Generating QAM-16 Signals at 21.3 Gbaud and Transmission Over 480 km," *Photonics Technology Letters,* vol. 22, pp. 36-38, 2010.

[8] A. Viterbi and A. Viterbi, "Nonlinear estimation of PSK-modulated carrier phase with application to burst digital transmission," *Transactions on Information Theory,* vol. 29, pp. 543-551, 1983.

[9] D. S. Millar, D. Lavery, S. Makovejs, C. Behrens, B. C. Thomsen, P. Bayvel, and S. J. Savory, "Generation and long-haul transmission of polarization switched QPSK at 42.9Gbit/s," *Optics Express,* vol. 19, pp. 9296-9302, 2011.

[10] I. Fatadin, D. Ives, and S. J. Savory, "Blind Equalization and Carrier Phase Recovery in a 16-QAM Optical Coherent System," *Journal of Lightwave Technology,* vol. 27, pp. 3042-3049, 2009.

[11] V. A. J. M. Sleiffer, M. S. Alfiad, van den Borne, D., S. L. Jansen, M. Kushnerov, S. Adhikari, and H. De Waardt, "A Comparison of 43-Gb/s POLMUX-RZ-DPSK and POLMUX-RZ-DQPSK Modulation for Long-Haul Transmission Systems," in *Proc. European Conference on Optical Communications ECOC 2010*, Torino, 2010, p. Mo.2.C.4.

[12] L. E. Nelson, X. Zhou, N. Mac Suibhne, A. D. Ellis, and P. Magill, "Experimental comparison of coherent polarization-switched QPSK to polarization- multiplexed QPSK for 10x100km WDM transmission," *Optics Express,* vol. 19, pp. 10849-10856, May 2011.

[13] S. J. Savory, G. Gavioli, R. I. Killey, and P. Bayvel, "Electronic compensation of chromatic dispersion using a digital coherent receiver," *Optics Express,* vol. 15, pp. 2120-2126, 2007.

[14] D. S. Millar and S. J. Savory, "Blind Adaptive Equalization of Polarization Switched QPSK Modulation," *Optics Express,* vol. 19, pp. 8533-8538, 2011.

[15] A. Mecozzi and F. Matera, "Polarization scattering by intra-channel collisions," *Optics Express,* vol. 20, pp. 1213-1218, January 2012.

[16] A. Carena, G. Bosco, V. Curri, P. Poggiolini, M. Tapia Taiba, and F. Forghieri, "Statistical Characterization of PM-QPSK Signals after Propagation in Uncompensated Fiber Links," in *Proc. European Conference on Optical Communications ECOC 2010*, Torino, 2010, p. P4.07.

[17] C. Behrens, R. I. Killey, S. J. Savory, M. Chen, and P. Bayvel, "Nonlinear Distortion in Transmission of Higher-Order Modulation Formats," *Photonics Technology Letters,* 2010.

[18] S. J. Savory, "Digital filters for coherent optical receivers," *Optics Express,* vol. 16, pp. 804-817, 2008.

[19] M. Noelle, J. K. Fischer, L. Molle, C. Schmidt-Langhorst, D. Peckham, and C. Schubert, "Comparison of 8x112 Gb/s PS-QPSK and PDM-QPSK signals over transoceanic distances," *Optics Express,* vol. 19, pp. 24370-24375, November 2011.

[20] J.-X. Cai, Y. Cai, C. R. Davidson, D. G. Foursa, A. Lucero, O. Sinkin, W. Patterson, A. Pilipetskii, G. Mohs, and N. S. Bergano, "Transmission of 96x100-Gb/s Bandwidth-Constrained PDM-RZ-QPSK Channels With 300% Spectral Efficiency Over 10610 km and 400% Spectral Efficiency Over 4370 km," *Journal of Lightwave Technology* vol. 29, pp. 491-497, February 2011.

[21] X. Zhou and J. Yu, "Multi-Level, Multi-Dimensional Coding for High-Speed and High-Spectral-Efficiency Optical Transmission," *Journal of Lightwave Technology,* vol. 27, pp. 3461-3653, August 2009.

[22] R. Cigliutti, E. Torrengo, G. Bosco, N. P. Caponio, A. Carena, V. Curri, P. Poggiolini, Y. Yamamoto, T. Sasaki, and F. Forghieri, "Transmission of 9 x 138 Gb/s Prefiltered PM-8QAM Signals Over 4000 km of Pure Silica-Core Fiber," *Journal of Lightwave Technology,* vol. 29, pp. 2310-2318, August 2011.

[23] X. Zhou, J. Yu, D. Qian, T. Wang, G. Zhang, and P. D. Magill, "8x114 Gb/s, 25-GHz-spaced, PolMux-RZ-8PSK transmission over 640 km of SSMF employing digital coherent detection and EDFA-only amplification," in *Proc. Conference on Optical Fiber Communication and the National Fiber Optic Engineers Conference OFC/NFOEC 2008*, 2008, p. PDP1.

[24] P. J. Winzer, A. H. Gnauck, C. R. Doerr, M. Margarini, and L. L. Buhl, "Spectrally Efficient Long-Haul Optical Networking Using 112-Gb/s Polarization-Multiplexed 16-QAM," *Journal of Lightwave Technology,* vol. 28, pp. 547-556, February 2010.

[25] S. Makovejs, D. S. Millar, D. Lavery, C. Behrens, V. Mikhailov, G. Gavioli, Killey, R.I., Savory, S.J., and P. Bayvel, "Characterization of long-haul 112Gbit/s PDM-QAM-16 transmission with and without digital nonlinearity compensation," *Optics Express,* 2010.

[26] D. S. Millar, S. Makovejs, C. Behrens, S. Hellerbrand, R. I. Killey, P. Bayvel, and S. J. Savory, "Mitigation of Fiber Nonlinearity using a Digital Coherent Receiver," *Journal of Selected Topics in Quantum Electronics,* vol. 16, pp. 1217-1226, 2010.

[27] D. Rafique, J. Zhao, and A. D. Ellis, "Digital back-propagation for spectrally efficient WDM 112 Gbit/s PM m-ary QAM transmission," *Optics Express,* vol. 19, pp. 5219-5224, March 2011.

Chapter 5

NONLINEAR TOLERANCE WITH VARYING SYMBOL-RATE

As demand for capacity continues to soar and limits to the available optical bandwidth are conceivable, higher order modulation formats become a viable solution to use the available bandwidth more efficiently. However, with increasing constellation density, noise limitations become more stringent as described in section 2.1.4. The investigation in the previous chapter concluded that overall transmission performance and maximum reach strongly depends on linear and nonlinear distortions. Furthermore, nonlinear compensation has been shown to be able to mitigate nonlinear impairments and, therefore, improve transmission reach by up to ~50% even though the complexity of the algorithm in use was constrained to one computational step per span and only the central channel was backpropagated.

In this chapter, the investigation of nonlinear compensation, based on digital backpropagation, is described; the digital compensation was examined without complexity limitations and under the assumption that enough electrical bandwidth is available to backpropagate more than 1 wavelength channel, in order to explore upper bounds of performance improvement. Additionally, this chapter is devoted to investigate nonlinear limitations of higher order modulation formats for varying symbol-rates and channel spacing. In particular, the research focused on the trade-off between inter- channel nonlinearities, such as cross-phase modulation (XPM – section 2.2.1) and intra-channel nonlinearities, such as self-phase-modulation (SPM – section 2.2.2). This trade-off is central to the comparison carried out in the thesis work.

Initially, single channel polarisation-multiplexed transmission at symbol-rates varying from 3.5GBd to 56GBd, without nonlinear compensation is described. The importance

of comparing different symbol-rates in terms of the power spectral density is explained. After obtaining optimum parameters for digital backpropagation based on the Manakov equation, nonlinear compensation of a single channel is applied (as described in section 3.3.2). Subsequently, wavelength division multiplexed (WDM) transmission is investigated with and without optimum backpropagation of the central channel and up to 16 channels given a fixed receiver bandwidth. Finally, the potential increase in maximum transmission distance as a result of applying central channel backpropagation is examined.

5.1 Single Channel Transmission Performance

To investigate the relative contributions of intra- and inter-channel nonlinear effects to the nonlinear penalties, polarization multiplexed single-channel transmission with varying symbol-rate 56GBd, 28GBd, 14GBd, 7GBd and 3.5GBd was considered first.

Table 14: Spectral efficiency and net-bitrate per channel for a given symbol-rate and modulation format

			PS-QPSK	PDM-QPSK	PDM-8PSK	PDM-8QAM	PDM-16QAM
SPECTRAL EFFICIENCY (bit/s/Hz)			1.5	2	3	3	4
BIT PER SYMBOL			3	4	6	6	8
	SYMBOL RATE	OPTICAL FILTER BW					
NET-BITRATE (Gbit/s)	56GBd	100GHz	150	200	300	300	400
	28GBd	50GHz	75	100	150	150	200
	14GBd	25GHz	37.5	50	75	75	100
	7GBd	12.5GHz	18.75	25	37.5	37.5	50
	3.5GBd	6.25GHz	9.375	12.5	18.75	18.75	25

In every case, it was assumed that the payload of up to 400 Gbit/s (see net bitrates per channel in Table 14) is accompanied by a 4% overhead for the Ethernet frame and 7% overhead for forward error correction (FEC) which adds up to a 12% overhead to the payload (e.g. 104Gbit/s+7%=111.28Gbit/s). Each WDM-channel was modulated with 2^{15} symbols using a different random symbol sequence drawn from a uniform probability distribution rendering every symbol equally probable, as shown in Figure 58. Single channel propagation has been modelled with 8 temporal samples per symbol, to

allow for sufficient bandwidth to accommodate the spectrum and excess bandwidth to cover nonlinearity induced spectral broadening.

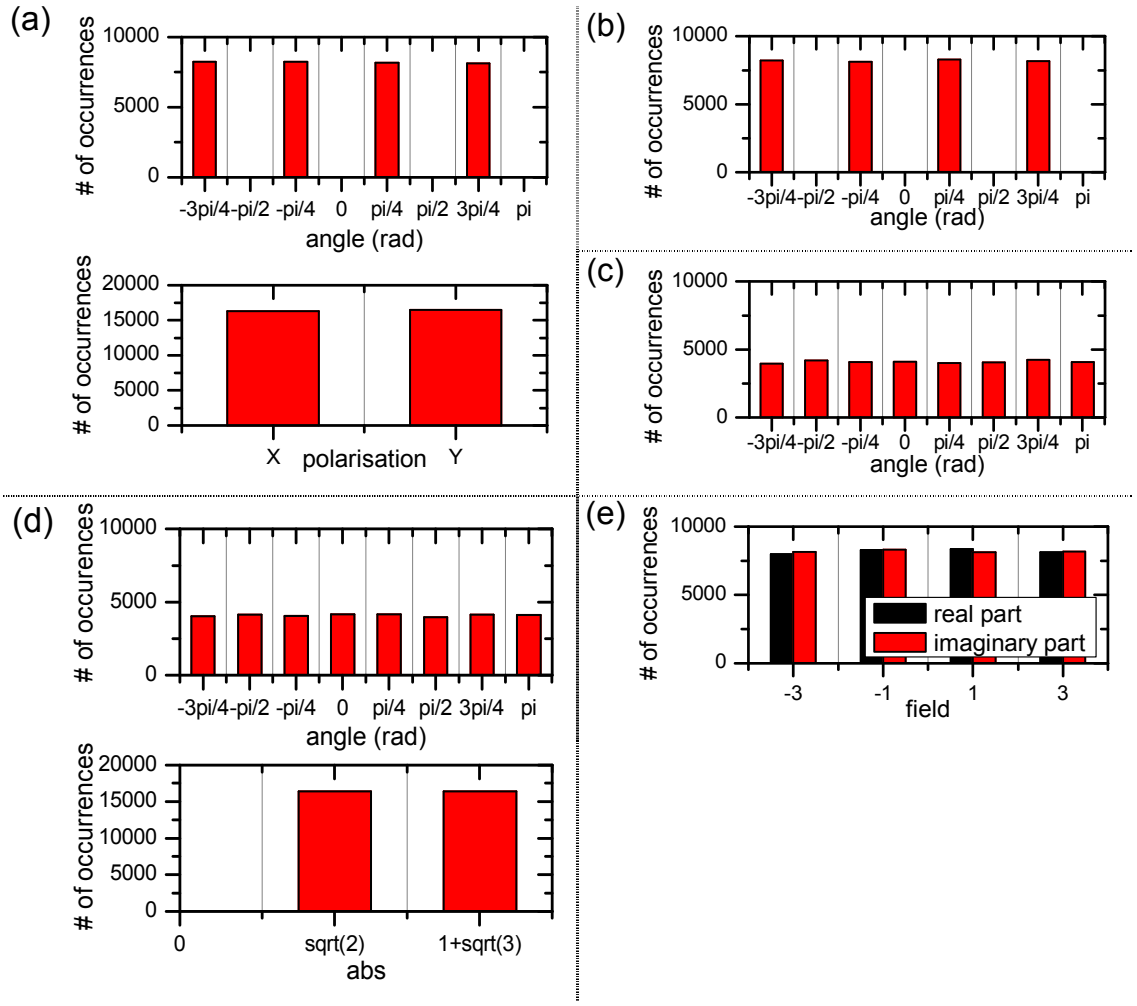

Figure 58: Uniform probability distributions of 2^{15} symbols for (a) PS-QPSK (phase and polarisation), (b) QPSK, (c) 8PSK (phase), (d) 8QAM (phase and amplitude) and (e) 16QAM (real and imaginary part)

In the simulation tool developed, QPSK was generated by an IQ-modulator which enables the modulation of in-phase and quadrature components of the optical field with different binary signals (as described section 3.1.1). 8PSK was obtained by inserting another phase-modulator which varies the phase between 0 and π/4, as determined by a third driving signal. PS-QPSK was generated with an IQ-modulator to obtain a QPSK constellation and a polarisation switching stage consisting of two parallel Mach-Zehnder modulators. The polarisation switching stage is used to extinguish one polarisation while the other one is in transmit state (see section 3.1.4). To generate 8QAM the driving signal for one arm of an IQ-modulator is attenuated and the in-built phase shifter is set to a constant phase-shift of π/4. A subsequent phase-modulator varies the optical phase between 0 and π/4 to obtain the desired 8-symbol constellation (see section 3.1.2). The last modulation format under investigation is

16QAM, which is generated by driving an IQ-modulator with 4-level driving signals, leading to 16 different symbols in the complex plane as described in section 3.1.3. In every case, the limited transmitter bandwidth was emulated by applying a 5^{th}-order electrical Bessel filter with a 3dB bandwidth of 0.8 × symbol-rate and the laser line-width of the transmitter was set to 100 kHz, corresponding to a standard external cavity laser (ECL). Note that the electrical bandwidth of the transmitter is usually dominated by the modulator bandwidth and the highest 3dB electrical bandwidth needed would be 0.8 × 56GHz = 44.8GHz. Commercially available Lithium Niobate phase modulators [1] and IQ modulators [2] have a 3dB electrical bandwidth around 30GHz, however, due to the shallow roll-off of the frequency transfer function, they are suitable for modulation bandwidths beyond their 3dB bandwidth. To reduce the number of optical components, all modulation formats have NRZ pulse-shape, because RZ pulseshapes require another pulse carver and additional driving electronics, even though pulse carving has been shown to improve nonlinear transmission performance [3]. After modulation, the signals were polarisation-multiplexed with another random symbol-pattern and finally passed through an optical interleaver consisting of 2^{nd} order Gaussian filters with a 3dB-bandwidth, as shown in Table 14. Section 7.2 provides an example of the MATLAB code that was used to generate WDM-signals of arbitrary modulation format, wavelength-spacing and symbol-rate.

At the receiver, the signal is detected with a single ended coherent receiver. The linewidths of transmitter- and LO-laser are both 100 kHz, while the frequency offset between the two was assumed to be 0 GHz. To suppress the direct-detection terms the LO-signal-ratio was set to 20 dB. The limited receiver bandwidth was modelled with 5^{th} order Bessel filters, employing a 3dB bandwidth of 0.8×symbol rate and resampled to 2 samples/symbol. The specifications of a maximum receiver bandwidth of 44.8GHz and a required ADC speed of 112Gsample/s are reasonable assumptions for future digital coherent receivers, considering today's state of the art oscilloscopes offer an electrical bandwidth of up to 45GHz and up to 120Gsample/s [4]. After digitisation the signal was normalised to unit power and chromatic dispersion was compensated in the frequency domain (see section 3.4.1). Adaptive equalisers were implemented to compensate for PMD and de-skew the linear impulse response of the channel. While a standard CMA–equaliser could be used on QPSK and 8PSK, a polarisation switch CMA is implemented for PS-QPSK [5]. A radially-directed equaliser needed to be implemented for 8QAM and 16QAM, to accommodate for the multiple intensity rings of these formats (see section 3.3.5). For the same reason a decision directed PLL had to be implemented to recover the carrier phase for QAM formats, while for PSK-formats the

Viterbi & Viterbi algorithm and for PS-QPSK a decision directed version of the Viterbi & Viterbi algorithm is used (see section 3.3.6). After differential decoding and symbol to bit mapping, Monte-Carlo error counting was performed to determine the BER.

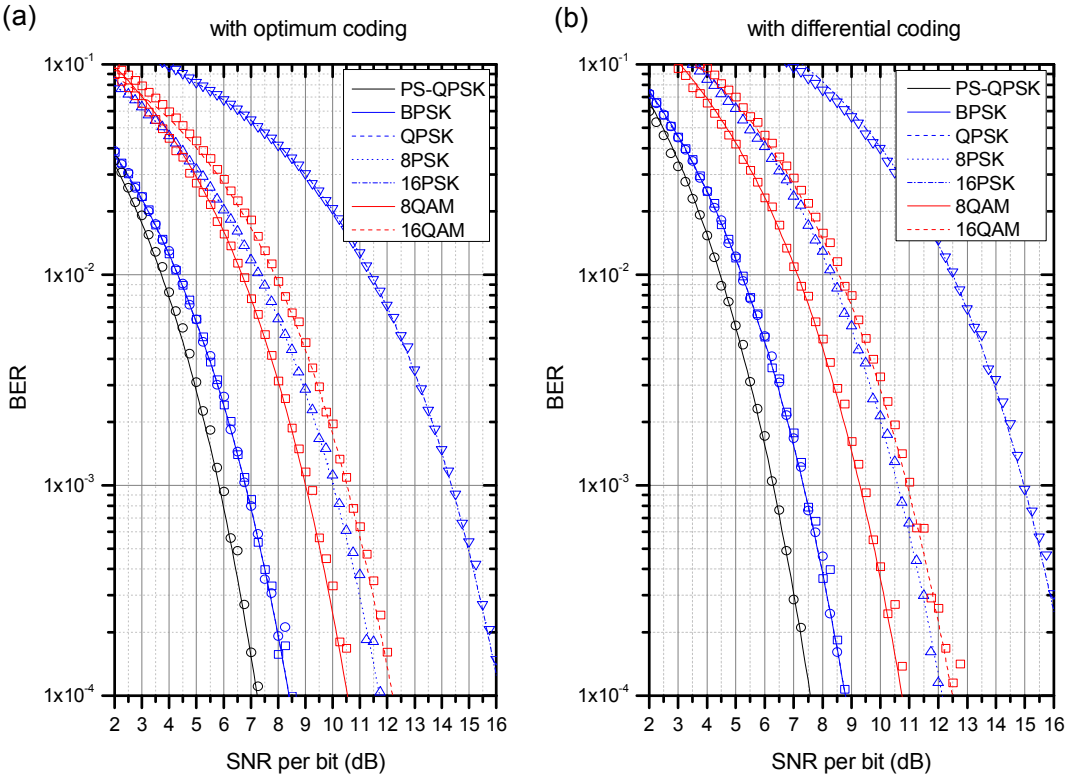

Figure 59: Receiver sensitivities for PS-QPSK, BPSK, QPSK, 8PSK, 16PSK, 8QAM and 16QAM with (a) optimum coding and (b) differential coding. Lines show analytical equations (8QAM: numerical approximation) and symbols results of Monte-Carlo simulations.

The simulation tool was tested against well-known theoretical values for the receiver sensitivity in presence of additive white Gaussian noise. Figure 59 shows the BER vs. the signal-to-noise ratio (SNR) per bit, comparing Monte-Carlo simulations (symbols) and analytical approximations to the BER performance for optimum and differential coding (see section 3.2.1 and 3.2.2). The SNR per bit is related to the optical-signal-noise ratio (OSNR) as follows:

$$\mathrm{SNR}_{\mathrm{bit}} = \frac{2B_{Ref}}{F_B} OSNR \tag{69}$$

With B_{Ref} referring to the noise reference bandwidth (0.1nm or 12.5GHz in this case) and the overall bitrate F_B.

Excellent agreement between analytical approximation and simulations employing ideal matched filters with a root-raised cosine frequency response at the transmitter and receiver has been achieved, especially in the region of high SNR. At low SNR values,

the assumption that errors occur only between neighbouring symbols is not necessarily true anymore.

Most analytical approximations are based on the Marcum Q-function [6]:

$$Q(x) = \frac{1}{2}\operatorname{erfc}\left(\frac{x}{\sqrt{2}}\right) \quad \textbf{(70)}$$

The following equations have been used to obtain the bit error probabilities of BPSK[6]:

$$\mathrm{BER_{BPSK}} = Q\left(\sqrt{2 \cdot \mathrm{SNR_{bit}}}\right) \quad \textbf{(71)}$$

QPSK [6]:

$$\mathrm{BER_{QPSK}} = Q\left(\sqrt{2 \cdot \mathrm{SNR_{bit}}}\right)\left(1 - \frac{1}{2}Q\left(\sqrt{2 \cdot \mathrm{SNR_{bit}}}\right)\right) \quad \textbf{(72)}$$

8PSK and 16PSK [6]:

$$\mathrm{BER_{MPSK}} = \frac{2}{\log_2(\mathrm{M})}Q\left(\sqrt{2 \cdot \log_2(\mathrm{M}) \cdot \sin^2\left(\frac{\pi}{\mathrm{M}}\right) \cdot \mathrm{SNR_{bit}}}\right) \quad \textbf{(73)}$$

as well as 16QAM [6]:

$$\mathrm{BER_{16QAM}} = \left(1 - \frac{1}{\sqrt{16}}\right)Q\left(\sqrt{\frac{12}{15} \cdot \mathrm{SNR_{bit}}}\right)\left(1 - \left(1 - \frac{1}{\sqrt{16}}\right)Q\left(\sqrt{\frac{12}{15} \cdot \mathrm{SNR_{bit}}}\right)\right) \quad \textbf{(74)}$$

Note that an analytical approximation of the BER for PS-QPSK requires the numerical solution of an integral [7] :

$$\mathrm{BER_{PS-QPSK}} = \frac{1}{2\sqrt{\pi}}\int_{-\infty}^{\infty}\operatorname{erfc}(x)\left(3 - 3\operatorname{erfc}(x) + \operatorname{erfc}^2(x)\right)\exp(-(x - 3 \cdot \mathrm{SNR_{bit}})^2)dx \quad \textbf{(75)}$$

Furthermore, 8QAM requires an entirely numerical approach, which is due to the complicated ideal decision boundaries as shown in [8].

In case of differentially coded field in Figure 59 (b) the analytical approximations in equation (81)-(84) are not valid anymore, because in the event of a symbol error the following symbol will be erroneous as well. As a consequence the resulting BER will be higher than in case of optimum coding e.g. by a factor of 2 for phase shift keying as shown in Table 15. However, differential coding is still likely to be implemented in

commercial systems, because it prevents catastrophic error bursts due to cycle slipping. As a result differential coding is employed throughout the investigation described in this chapter.

Table 15: Correction factors for BER in case of a differentially coded field

M-PSK	8QAM	16QAM	PS-QPSK
2	1.4545	1.625	2.222

Table 16 summarises the SNR per bit at the FEC rate of BER=3×10^{-3} as inferred from Figure 59 (a) for optimum coding and Figure 59 (b) for differential coding.

The spectral efficiency assuming that both polarisations of the optical field are utilised is given as well and it is easy to see that the receiver sensitivity reduces monotonically with increasing spectral efficiency. Once the spectral efficiency of the modulation format increases, more energy must be invested to keep the symbol points separate, given the same amount of additive white Gaussian noise. Notable exception to this rule is BPSK with a spectral efficiency of 2bit/s/Hz, which does not utilise the 4 available dimensions (in-phase- and quadrature components in two polarisations) by using only one dimension per polarisation.

Table 16: required SNR per bit at an FEC rate of BER = 3×10^{-3} for various modulation formats

	PS-QPSK	BPSK	QPSK	8QAM	8PSK	16QAM	16PSK
SPECTRAL EFFICIENCY (bit/s/Hz)	3	2	4	6	6	8	8
OPTIMUM CODING (dB)	4.9	5.8	5.8	8.0	8.9	9.4	13.2
DIFFERENTIAL CODING (dB)	5.5	6.4	6.4	8.4	9.6	9.9	13.9

The following investigation focuses on the transmission performance of PS-QPSK, PDM-QPSK, PDM-8PSK, PDM-8QAM and PDM-16QAM. The transmission line, used in all the simulations described in this chapter, consists of 13x80km SSMF spans without any inline dispersion compensation. EDFAs, with a noise figure of 4.5dB, are used to compensate for the loss of the optical fibre. These EDFAs were set to operate in saturation with a fixed output power of 17dBm; attenuators were used to obtain the required power levels. Note that the noise was added at each amplifier along the link to model the interaction between ASE noise and nonlinearity (see Gordon Mollenhauer

noise in section 2.2.5), which is an important nonlinear limitation especially in long and ultra-long haul transmission systems beyond 3,000km [9]. Signal propagation in the fibre is modelled with the symmetrical split-step Fourier method including the effect of chromatic dispersion, dispersion slope, polarization mode dispersion, power dependence of the refractive index (Kerr effect) and nonlinear polarization scattering (see section 2.3). The step size of 100m was used to ensure a valid representation of PMD via the waveplate model and accurate modelling of the peak nonlinear phase shift per step Δh (see section 2.3). Table 17 summarises the link parameters used in the simulations described in this chapter.

Table 17: Fibre- & Link parameters

α [dB/km]	0.2
D [ps/km/nm]	16
S [ps/km/nm^2]	0.06
γ [1/W/km]	1.2
PMD COEFFICIENT [ps/$\sqrt{\text{km}}$]	0.1
SPAN LENGTH [km]	80
NUMBER OF SPANS	13
EDFA NOISE FIGURE [dB]	4.5

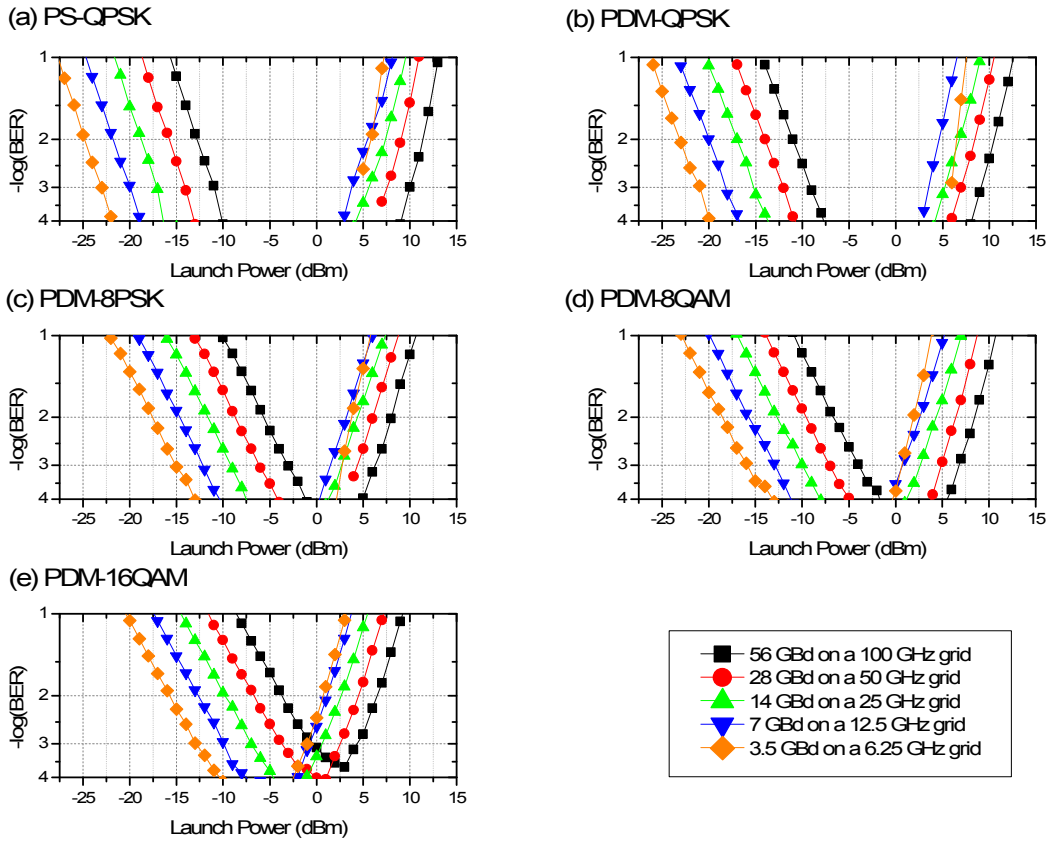

Figure 60: BER vs. launch power in single channel transmission of coherently detected PS-QPSK, PDM-QPSK, PDM-8PSK, PDM-8QAM and PDM-16QAM, as a function of baud rate

Figure 60 shows the variation of BER vs. of input launch power for PS-QPSK, PDM-PDM-QPSK, PDM-8PSK, PDM-8QAM and PDM-16QAM, plotted for different baud rates. It can be seen that the linear parts of the curves at low input powers are shifted to the left by 3dB as the symbol rate is halved. This seems intuitively correct if one considers that in half the spectral width only half of the in-band ASE-power is detected, so that only half the signal power is required to achieve the same SNR at the receiver. Figure 61 highlights this effect by showing SNR per bit for the transmission link under investigation with a separate launch power axis in blue for each spectral width.

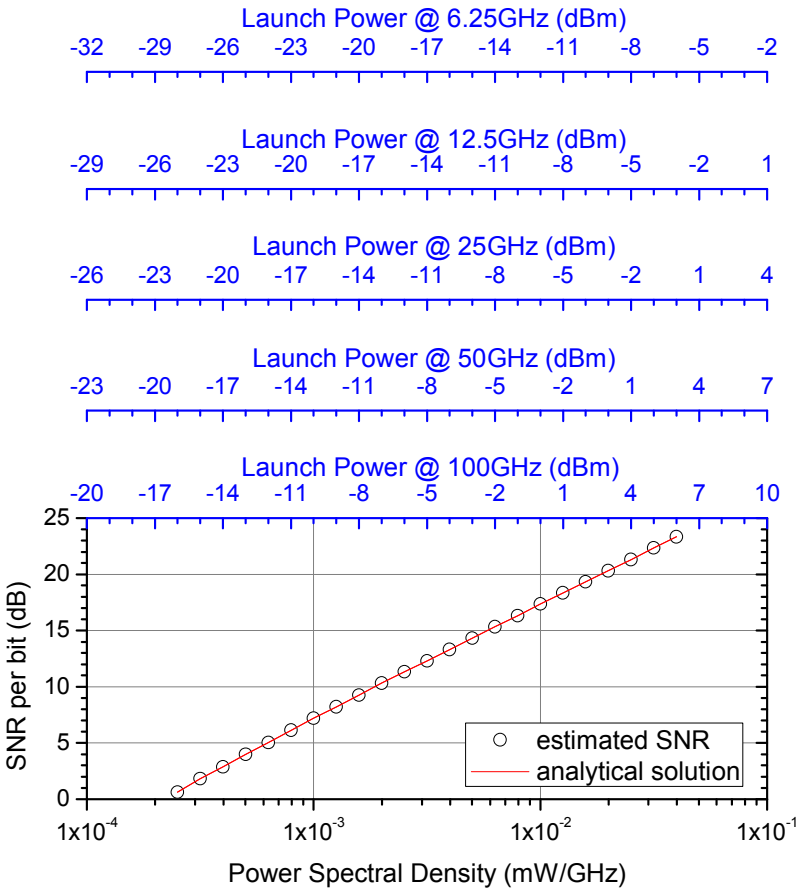

Figure 61: received SNR per bit as a function power spectral density (PSD) for a 13 x 80 km standard single mode fibre link with EDFA amplification. Blue axes show the power per channel depending on the spectral width.

However, the effect of varying in-band ASE-power can be neglected when plotting the received SNR per bit as a function of the power spectral density (PSD), defined by the launch power per channel normalised to the channel spacing (see Figure 61). In this case, different symbol rates can be compared at the same SNR and curves of the same spectral efficiency and modulation format overlap in the linear transmission regime and have the same BER as shown in Figure 62. Therefore, the power spectral density was selected as the basis for comparing transmission performance at different symbol-rates.

Note that, the PSD should not be given in dBm/Hz, because in this case the power would scale logarithmically while the frequency spacing scales linearly, again leading to a biased estimation of the linear and nonlinear performance. Instead it should be used in mW/GHz as in this work.

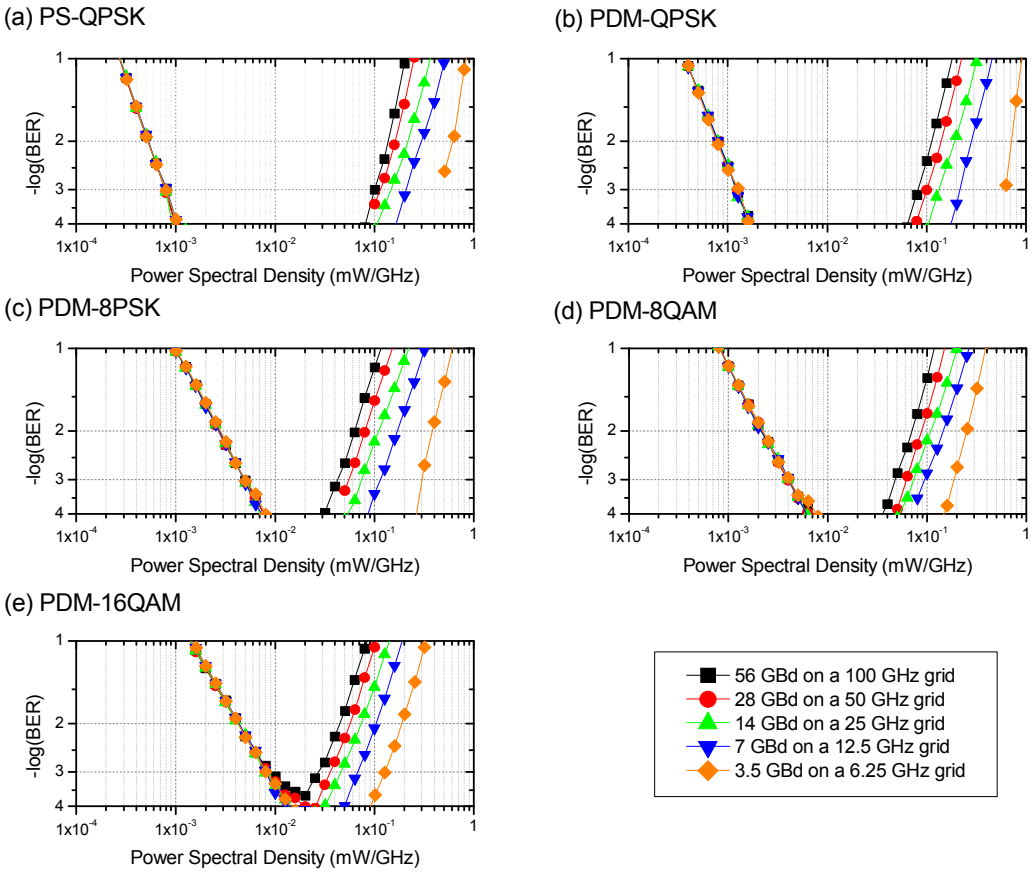

Figure 62: BER vs. power spectral density for single channel transmission of coherently detected PS-QPSK, PDM-QPSK, PDM-8PSK, PDM-8QAM and PDM-16QAM, for different values of baud rate.

Figure 63 shows the maximum power spectral density (PSD) at BER=3×10^{-3} (corresponding to –log(BER)=2.52), which has been chosen as a figure of merit to compare the transmission performance of all modulation formats in the nonlinear regime. The maximum PSD was taken as a slice through the nonlinear part of the waterfall curves at BER=3×10^{-3} in Figure 62. All the modulation formats show a clear improvement in nonlinear performance when the symbol-rate is reduced, which agrees very well with recent experimental results comparing PDM-QPSK and PS-QPSK at different symbol-rates [10, 11] as well as simulation results obtained Piyawanno et al. [12] comparing PDM-QPSK, PDM-16QAM and PDM-64QAM. The improved transmission performance with lower symbol-rate can be attributed to a significantly reduced pulse-overlap during transmission.

Intra-channel four-wave mixing (IFWM) is the limiting nonlinear effect for single-channel phase shift keyed formats and its severity increases with the number of pulses that are involved in the nonlinear mixing process [13]. While a pulse propagating at 3.5GBd only affects 3 neighbouring pulses, this number increases to 745 pulses at 56GBd.

As already mentioned in 2.2.1, intra-channel self-phase modulation (ISPM) and intra-channel cross phase modulation (IXPM) depend on the signals pulse shape and, therefore, result in a constant nonlinear phase shift for every pulse for phase shift keyed formats. This phase-shift will not degrade performance, since the digital phase recovery is able to mitigate it. However, in case of modulation formats with multiple intensity rings, like 8QAM and 16QAM, an increased de-rotation of the constellation rings due to different nonlinear phase shifts depending on the intensity can be observed [3]. This effect becomes more significant with reduced symbol rate and, therefore, reduced pulse-spread, which can clearly be seen when comparing 8PSK to 8QAM. For modulation formats with multiple intensity rings, the derotation cannot be mitigated by the digital phase recovery, since the phase shift varies between adjacent symbols of different intensity. However, a simple intensity-dependent phase shift at the receiver can improve performance in this case [14].

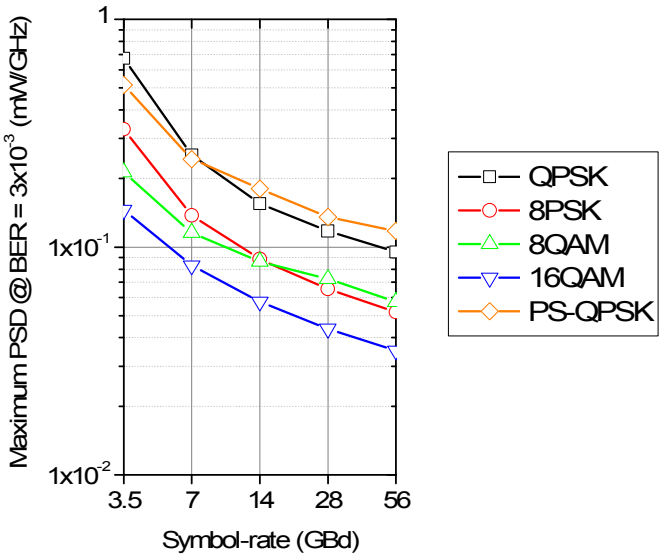

Figure 63: Maximum power spectral density @ BER=3×10^{-3} versus symbol-rate for single channel transmission of PDM-QPSK, PDM-8PSK, PDM-8QAM, PDM-16QAM and PS-QPSK

PS-QPSK shows better performance than all other formats, which can be explained with the absence of cross phase modulation (XPM) between the orthogonal polarisations which is characteristic of every polarisation multiplexed modulation format.

The severity of nonlinear distortions increases with increasing spectral efficiency, similarly to the case of linear distortions due to additive white Gaussian noise (see section 2.1.4). Recently, Carena et al. [15] showed that in uncompensated transmission the nonlinear distortion can be reasonably well approximated with a

Gaussian noise process whose variance is proportional to the square of the launch power.

5.2 Single Channel Digital Backpropagation

We now investigate the potential performance improvement that can be gained from applying optimum digital backpropagation to a single channel polarisation multiplexed signal. The split-step Fourier method is implemented with the Manakov equation as explained in section 3.3.2. The nonlinear step is according to equation (58):

$$\widehat{N}(t) = -j\gamma\varphi\frac{8}{9}(|E_Y|^2 + |E_X|^2)P_{in}10^{\left(-\left[\frac{s}{n}-1\right]\frac{\alpha L}{10}\right)}$$

where P_{in} denotes the input power per span, while $10^{\left(-\left[\frac{s}{n}-1\right]\frac{\alpha L}{10}\right)}$ accounts for the varying power profile along the span, with n being the number of steps per span, s the index of the step within a span, L the span length in km and α the fibres attenuation coefficient in dB/km.

φ is a variable that converges with increasing number of computational steps towards 1, but has to be optimised for a realistic number of steps. φ and the number of steps per transmitted span has been optimised to minimise the error vector magnitude (EVM), which is defined as root mean square value of the Euclidian distance between detected symbol $\mathrm{x_j}$ and the closest member of the symbol alphabet $\mathrm{s_j}$:

$$\mathrm{EVM} = 100\% \cdot \sqrt{\frac{\frac{1}{\mathrm{N}}\sum_{\mathrm{j}=1}^{\mathrm{N}}\left|\mathrm{s_j} - \mathrm{x_j}\right|^2}{\frac{1}{\mathrm{N}}\sum_{\mathrm{j}=1}^{\mathrm{N}}\left|\mathrm{s_j}\right|^2}} \quad \textbf{(76)}$$

Here, the EVM will be used as a percentage value. In this optimisation, the BER is not an appropriate performance metric. This is because given a fixed number of symbols to count errors on, at the accuracy at low values of BERs reduces, due to the small number of counted errors.

The optimisation φ and the number of steps per span was performed in the nonlinear transmission regime at 11dBm, 9dBm, 7dBm, 5dBm and 7dBm for 56GBd, 28GBd, 14GBd, 7GBD and 3.5GBd, respectively (see Figure 64). The accuracy of the digital backpropagation was monotonically increased by increasing the number of steps per span from 1 to 25, while varying φ between 0 and 1.

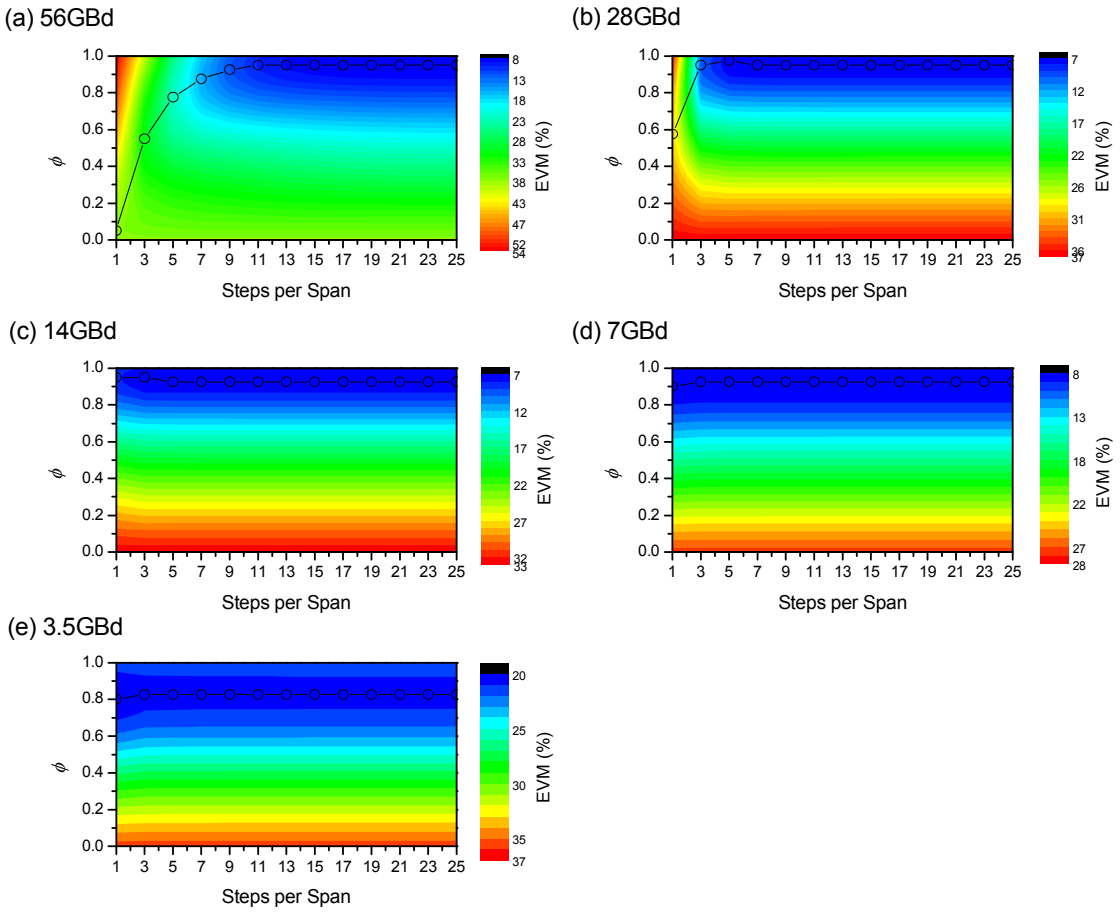

Figure 64: Backpropagation optimisation for different symbol rates of PDM-QPSK. The parameters φ and steps per span are optimised with EVM as a performance metric. Open symbols show the decent of the optimum parameters towards lowest EVM.

Generally, the performance improvement achieved by digital backpropagation increases with a higher number of steps per span, since the representation of the waveform within the optical fibre, allowing for a more accurate estimation of the nonlinear phase shift. Of interest in this work is what is ultimately achievable with digital backpropagation and, therefore, the optimum number of steps per span was chosen. This value corresponded to the point at which a significant reduction of the EVM (<0.1% EVM) was no longer achievable.

The optimum values are the same for every modulation format:

- 25 steps per span for 56GBd
- 7 steps per span for 28GBd
- 3 step per span for 14GBd
- 1 step per span for 7GBd
- 1 step per span 3.5GBd

with $\varphi = 0.9 - 0.95$.

Note that the achievable performance improvement can be traded-off against lower hardware complexity by reducing the number of computational steps. Recently Du and Lowery [16] showed that by applying a filtered nonlinear phase shift, the performance of the backpropagation algorithm can be improved, and the complexity was reduced by a factor of 4. Another, conclusion is that the optimum number of steps per span scales with DR_S^2 where D is the accumulated dispersion within a span and R_S the symbol rate. The faster the low and high frequency components walk off from each other, the faster the waveform evolves during fibre propagation. Hence, an accurate representation of the waveform requires more samples, or steps per span, for signals with a higher bandwidth, or symbol-rate.

As mentioned earlier, in an ideal case the parameter φ converges towards 1 with increasing number of steps per span, so that the nonlinear phase shift in equation (58) becomes the original nonlinear term of the Manakov equation. However, it has to be noted that the digital backpropagation algorithm is limited by a lot of factors, related to transmission distortions and the non-ideal implementation of the coherent receiver:

- Gordon Mollenhauer noise [17]
- Out of Band nonlinear noise (XPM, XPolM) [18, 19]
- PMD [19], PDL
- Frequency Response of the Receiver (Optical Filter, Electrical Front end ...)
- ADC sample rate [20]
- Quantisation noise
- LO laser phase noise [21]

While in full field DBP Gordon Mollenhauer noise [17] has been identified as the dominant limitation, out of band nonlinear noise has been shown to dominate [18] the achievable efficiency of the DBP algorithm when only a portion of the transmitted spectrum is backpropagated. Note that, in real systems it will only be possible to apply DBP to the received channel, since the neighbouring WDM-channels may be added and dropped along the link, causing unpredictable nonlinear distortions [22].

Figure 65 shows the BER as a function of input power density for transmission of PS-QPSK, PDM-QPSK, PDM-8PSK, PDM-8QAM and PDM-16QAM with and without optimum numbers of steps and full-field digital backpropagation. The curves, with and without digital backpropagation, overlap in the linear transmission regime, since the

nonlinear phase shift is negligible and digital backpropagation compensates only for chromatic dispersion in this case.

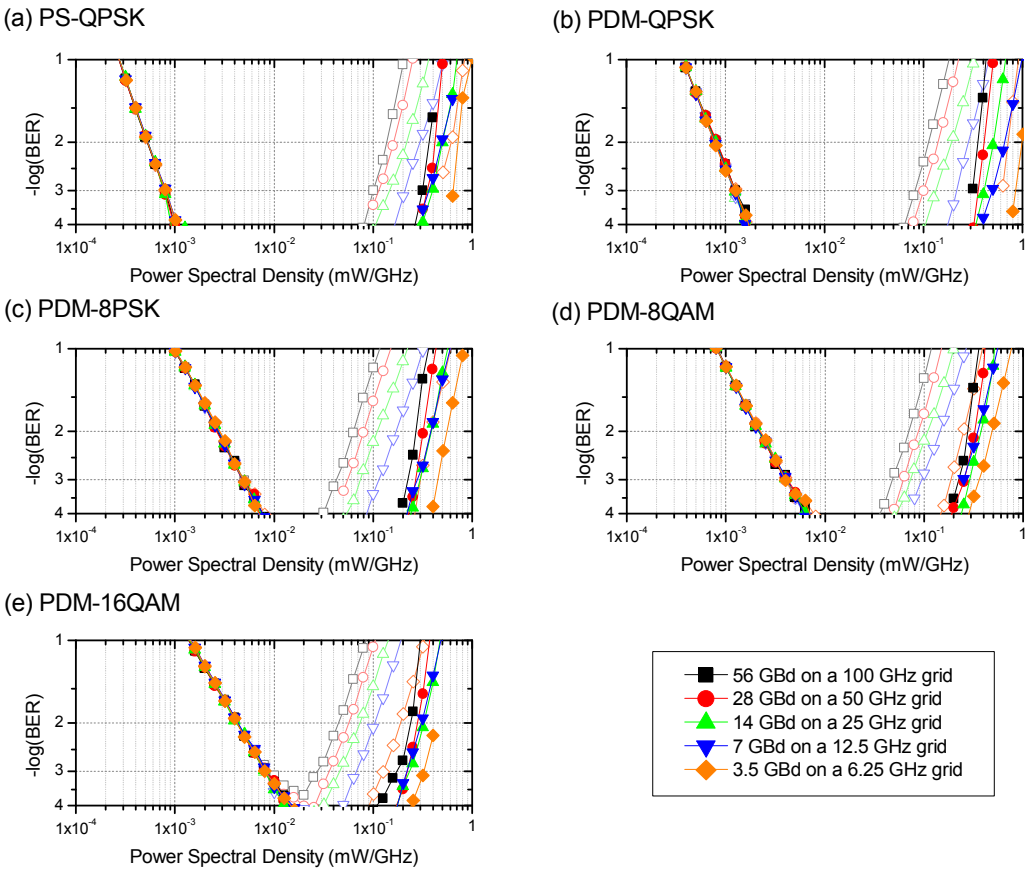

Figure 65: BER as a function power spectral density for single channel transmission of coherently detected PS-QPSK, PDM-QPSK, PDM-8PSK, PDM-8QAM and PDM-16QAM. Open symbols denote transmission without nonlinear compensation, while filled symbols show transmission with optimum digital backpropagation.

Similarly to the previous section the nonlinear transmission performance can be compared more easily among different modulation formats by looking at the maximum power spectral density at BER=3×10^{-3}. Figure 66 (a) shows the maximum PSD for transmission with (filled symbols) and without optimum nonlinear compensation (open symbols). It can be seen that lower symbol rates show an improved transmission performance than higher symbol rates, irrespective of whether nonlinear compensation is applied or not. PDM-QPSK shows the best nonlinear performance throughout all the symbol rates, while PS-QPSK is the only modulation format to match performance at 56GBd and 28GBd. PDM-8QAM and PDM-8PSK have a similar maximum PSD for 56GBd, 28GBd and 14GBd, while PDM-8PSK outperforms PDM-8QAM at lower symbol rates. PDM-16QAM exhibits the worst nonlinear performance, among all the modulation formats.

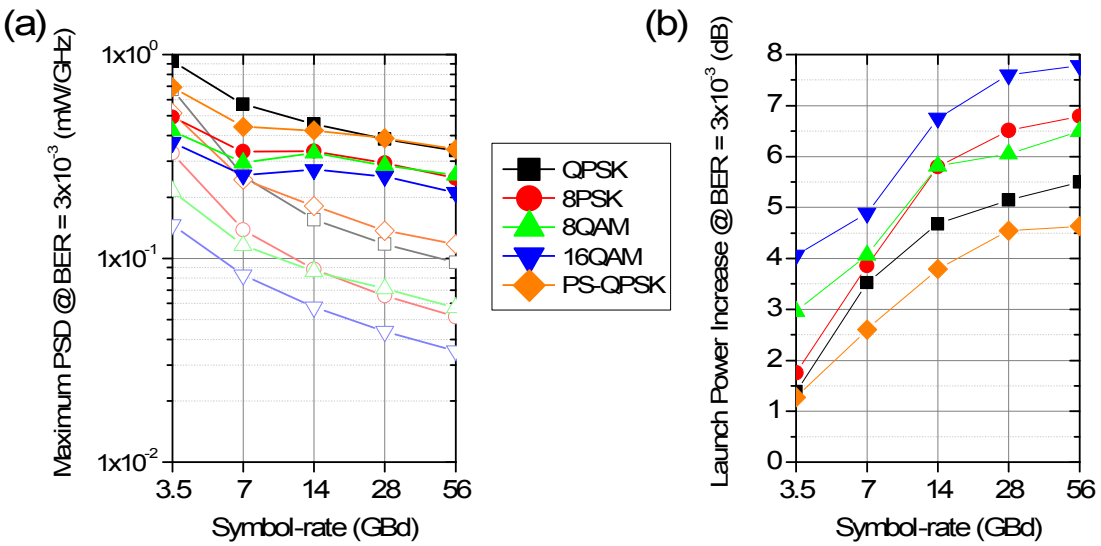

Figure 66: Figure (a) depicts the maximum power spectral density @ BER=3×10^{-3} versus symbol-rate for single channel transmission with (filled symbols) and without optimum digital backpropagation (open symbols). Figure (b) shows the resulting increase in maximum launch power @ BER=3×10^{-3}.

However, more spectrally efficient modulation formats benefit the most (up to 7.75dB for PDM-16QAM) from nonlinear compensation as shown in Figure 66 (b), which translates the maximum PSD into the equivalent increase in maximum launch power at BER=3×10^{-3}. This effect can be explained as follows: since the denser constellations suffer more from nonlinear distortions due to the higher proximity of the constellation points, the improvement in BER tends to be more significant when this distortion is compensated for. Another observation is that higher symbol rates benefit more from digital backpropagation. Nonlinear mixing processes between signal frequencies and ASE-noise, which is usually denoted as Gordon Mollenhauer noise (see section 2.2.5) is the effect which ultimately limits digital backpropagation in a single channel regime [17]. For a narrower spectrum, signal components show a lower phase variation across the spectrum, which facilitates mixing processes between neighbouring signal components, which are already affected by Gordon Mollenhauer noise.

Multi ring modulation formats such as PDM-8QAM and PDM-16QAM benefit more from digital backpropagation at lower symbol rates, because the de-rotation between adjacent rings, which dominated the BER in the nonlinear regime, is mitigated by the digital backpropagation.

5.3 WDM Transmission Performance

In this section, the attention focuses on WDM-transmission of coherently detected PS-QPSK, PDM-QPSK, PDM-8PSK, PDM-8QAM and PDM-16QAM. In WDM transmission

systems with polarisation multiplexing, SPM is not the only severe nonlinear distortion, since cross phase modulation (see section 2.2.2) and cross polarisation modulation (see section 2.2.4) also limit transmission. These nonlinear impairments are known to grow in severity with reduced frequency spacing due to reduced walk off between neighbouring channels [23]. However, as described in the previous section, it was found that in case of SPM-limited transmission the nonlinear degradation reduces with a narrower spectrum for every modulation format. Consequently, by changing the frequency spacing and symbol-rate intra-channel nonlinearities and inter channel nonlinearities can be traded-off against each other, leading to optimum transmission performance at a specific symbol-rate.

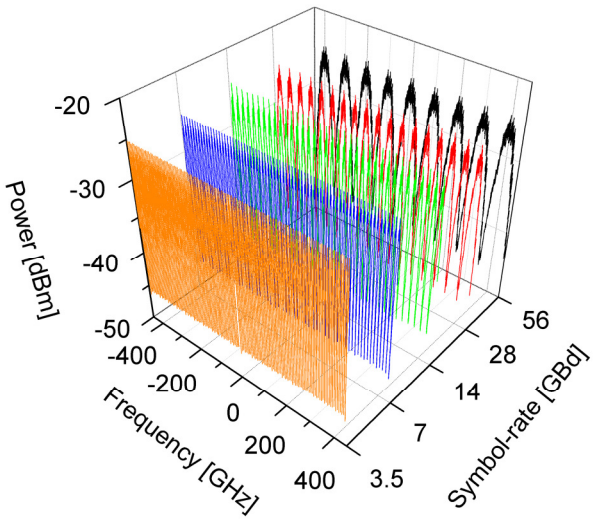

Figure 67: Optical power spectra for QPSK at 56GBd (black), 28GBd (red), 14GBd (green), 7GBd (blue) and 3.5GBd (orange)

Similarly to the previous section, the investigation was conducted at a fixed spectral efficiency per modulation format and we compared different symbol-rates in terms of the power spectral density (PSD). The use of the PSD facilitates comparison between different symbol-rates, because signals with the same signal to noise ratio have the same PSD, but not the same launch power per channel. As shown in Table 14, the spectral efficiency varies from 1.5bit/s/Hz in case of PS-QPSK, to over 2bit/s/Hz for QPSK, 3bit/s/Hz for 8PSK and 8QAM, and up to 4bit/s/Hz for 16QAM. The symbol-rate has been varied between 3.5Gbd and 56Gbd, corresponding to varying net-bitrates, again as listed in Table 14. The channel spacing has been varied between 100GHz and 12.5GHz according to the symbol-rate, while the number of channels had to be increased from 9 in the case of 56GBd up to 144 in the case of 3.5GBd to ensure a full occupation of the optical bandwidth that has been investigated (Figure 67). Note that all WDM channels as well as X- and Y-polarisation contain completely decorrelated

symbol patterns based on pseudo random symbol sequences with different seeds. This particularly important when investigating ultra-dense frequency grids below 25GHz, since WDM-channels walk-off much slower from each other leading to correlated distortions. Note that WDM propagation was modelled with 16, 32, 64, 128 and 256 temporal samples per symbol for 56GBd, 28GBd, 14GBd, 7GBd and 3.5GBd, respectively. This poses a good trade-off between simulation time (in the order of weeks for 3.5GBd) and accuracy, because it allows for sufficient bandwidth to accommodate the spectrum and excess bandwidth to cover nonlinearity induced spectral broadening.

Transmitter and receiver architecture as well as the transmission link are identical to the previous section, apart from the fact that instead of a single channel, multiple WDM channels are transmitted now.

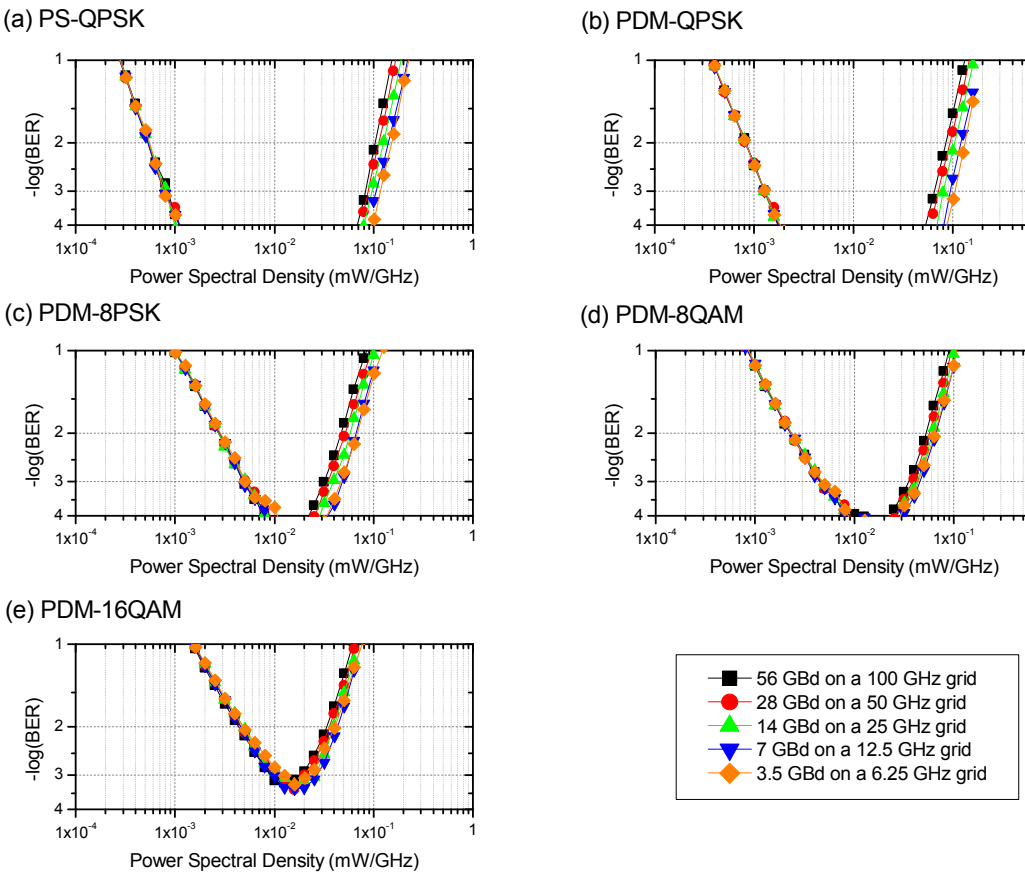

Figure 68: BER as a function power spectral density for WDM- transmission of coherently detected PS-QPSK, PDM-QPSK, PDM-8PSK, PDM-8QAM and PDM-16QAM.

To compare the differences in nonlinear performance of WDM-systems it is useful to plot the BER as a function of the power spectral density (PSD), similar to the previous section. Figure 68 shows the BER as a function of the PSD for all modulation formats

that have been investigated. In the linear transmission regime curves of different symbol rates overlap because signals with the same PSD have the same SNR and consequently the same BER, similarly to the single channel case (see Figure 62).

To compare transmission performance in the nonlinear regime the maximum PSD at BER=3×10^{-3} is shown in Figure 69. In the case of WDM transmission (Figure 69 (a)), all modulation formats follow the same trend of improved performance for lower symbol-rates down to 7GBd. However, at lower symbol rates the performance starts to be dominated by inter-channel XPM and FWM, as the gap between nonlinear performance of single channel and WDM-transmission widens (compare Figure 69 (a) and (b)). Additionally, an increased impact on higher density constellations can be observed, which confirms the findings in [12].

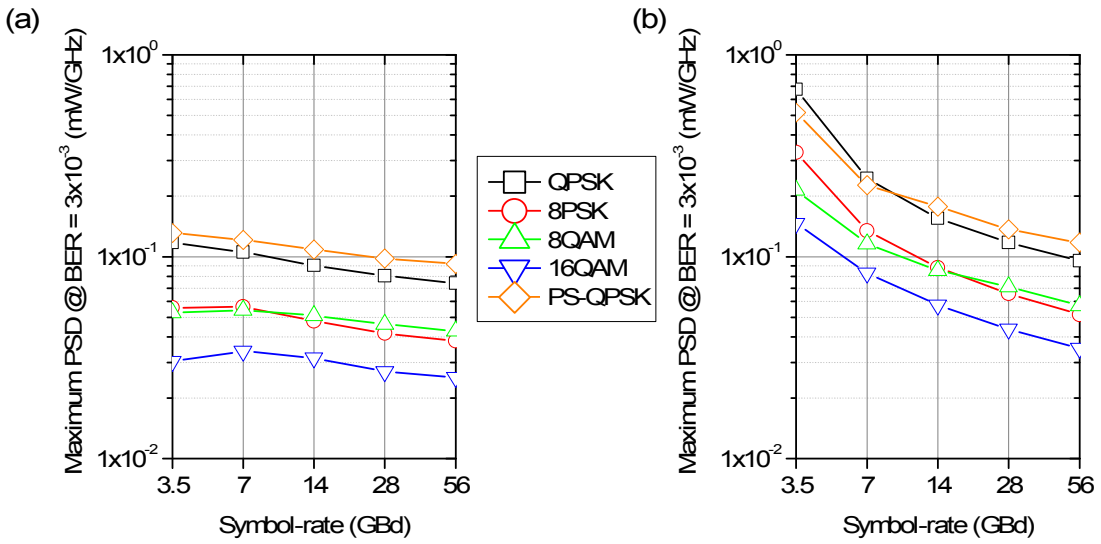

Figure 69: Figure (a) depicts the maximum power spectral density @ BER=3×10^{-3} versus symbol-rate for WDM transmission, while figure (b) shows single channel transmission

It can be seen that PS-QPSK exhibits the best nonlinear performance with a maximum PSD of 0.13 mW/GHz at 3.5GBd. PDM-QPSK shows nearly the same maximum PSD (0.12 mW/GHz at 3.5GBd), while PDM-8PSK and PDM-8QAM tolerate only half the maximum PSD with 0.056 and 0.055 mW/GHz at 3.5GBd and 7GBd, respectively. The maximum PSD for PDM-16QAM is 0.034 mW/GHz at 7GBd. The improvement that can be gained by reducing the symbol-rate with respect to 56GBd ranges from 2dB for QPSK and 1.6dB for 8PSK to 1.5dB for PS-QPSK, 1.3dB for 16QAM and 1dB for 8QAM. The benefit of reducing the symbol rate in reducing intra-channel nonlinear distortion as depicted for single channel transmission in Figure 69 (b), is largely offset by the increased inter-channel XPM and FWM resulting from the reduced channel spacing.

Despite the knowledge about the linear and nonlinear performance on the 13×80km transmission link investigated, it is still unclear into what maximum transmission distance an increased nonlinear tolerance translates. To obtain the answer to this question, the link was extended, on a span by span basis, until the BER exceeded the value 3×10^{-3}. Figure 70 shows the achievable transmission distance for a WDM-system as a function of the input power spectral density, modulation format and symbol rate. A higher nonlinear tolerance was observed at lower symbol rates for all the modulation formats (similarly to a fixed link length in Figure 69 (a)). This increased nonlinear performance translates into an equivalent increase in transmission distance, listed in Table 18.

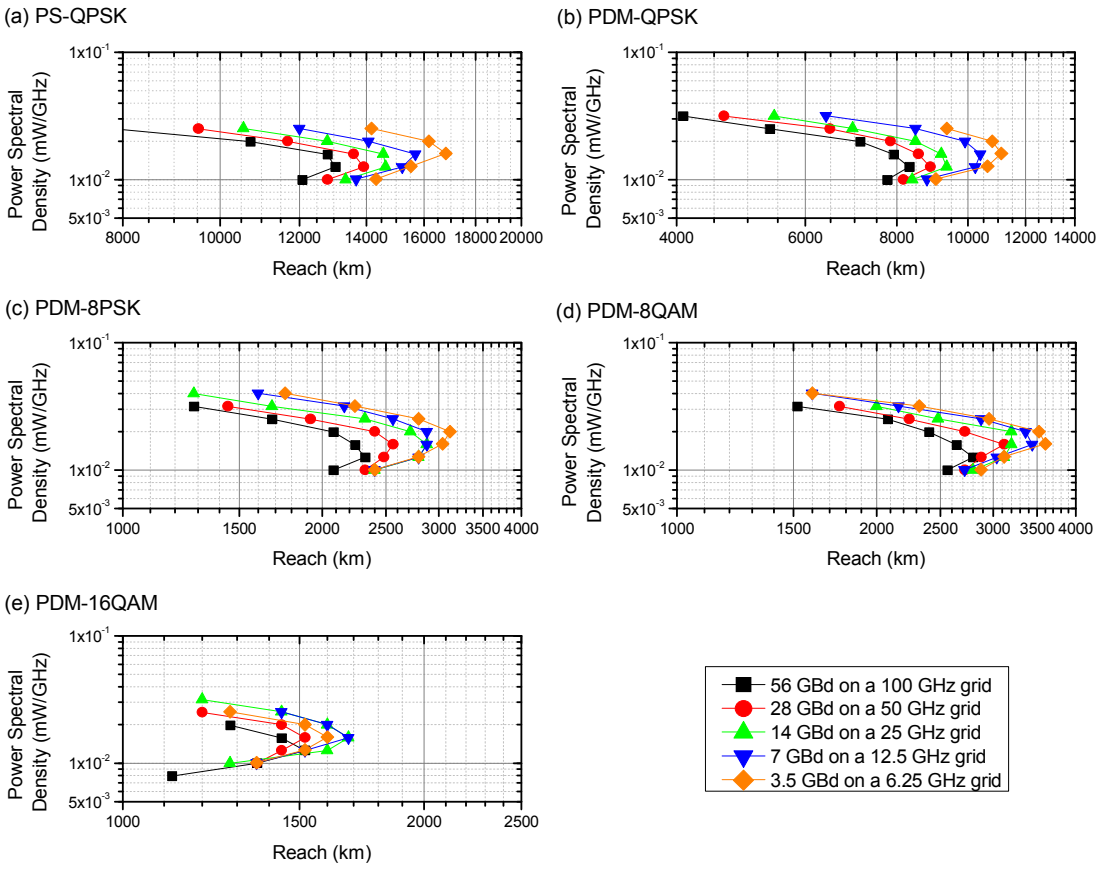

Figure 70: Achievable transmission reach @ BER=3×10^{-3} as a function of power spectral density for WDM transmission of (a) PS-QPSK, (b) PDM-QPSK, (c) PDM-8PSK, (d) PDM-8QAM and (e) PDM-16QAM.

Table 18: Maximum transmission distance in kilometres, assuming FEC can correct for BER=3×10^{-3} (largest transmission distances per modulation format are highlighted)

SYMBOL RATE	PS-QPSK	PDM-QPSK	PDM-8PSK	PDM-8QAM	PDM-16QAM
56GBd	13,040	8,320	2,320	2,800	1,520
28GBd	13,920	8,880	2,560	3,120	1,520
14GBd	14,640	9,360	2,880	3,200	1,680
7GBd	15,680	10,400	2,880	3,440	1,680
3.5GBd	16,800	11,120	3,120	3,600	1,600

Due to the highest linear and nonlinear tolerance, the longest transmission distance with up to 16,800km for 3.5GBd was achieved with PS-QPSK, while PDM-QPSK was second with up to 11,120km at 3.5GBd. PS-QPSK and PDM-QPSK have recently been experimentally investigated at 20GBd on a 50GHz grid [10] and at 15GBd on a 25GHz grid [11], confirming the higher transmission reach for PS-QPSK in this region. Furthermore, 28GBd PDM-QPSK can be compared to the experimental results for an equivalent system in section 4.4.3. The experimental maximum transmission distance was more than 1,400km lower (7,382 km compared to 8,800km), due to additional implementation penalty and an increased amount of ASE noise. The direct comparison between PDM-8PSK and PDM-8QAM at 3.5GBd shows a 480km higher transmission reach of 3,600km for PDM-8QAM compared to 3,120km for PDM-8PSK. The highest transmission distance for PDM-16QAM has been observed at 7 and 14GBd: 1,680km, in line with recent simulation results of Piyawanno et al. [12]. However, it is worth noting that all maximum transmission distances for 16QAM lie within 3 spans, ranging from 1,520km to 1,680km. In case of 28GBd PDM-16QAM, the simulated maximum reach was more than 300km higher compared to an equivalent system investigated in [18] (1,520km compared to 1,200km), again due to additional implementation penalty and higher levels of ASE-noise.

Generally, the symbol rates with highest transmission distances correspond very well to the nonlinear performance on the fixed link displayed in Figure 69 (a). A notable exception is the relative performance of PDM-8PSK and PDM-8QAM, where PDM-8QAM shows worse nonlinear performance on the fixed link, but a higher maximum transmission reach at the lowest symbol rate of 3.5Gbd. This inconsistency can be explained by taking into account, that 8QAM can show a 1.2dB better linear performance at BER=3×10^{-3} as shown in Figure 59(b). This benefit in the linear region,

combined with better nonlinear performance at higher symbol rates, leads to higher transmission reach for every symbol rate.

Table 19: Optimum power spectral density in mW/GHz, assuming FEC can correct for BER=3×10^{-3} (highest power spectral densities per modulation format are highlighted)

SYMBOL RATE	PS-QPSK	PDM-QPSK	PDM-8PSK	PDM-8QAM	PDM-16QAM
56GBd	0.013	0.013	0.013	0.013	0.013
28GBd	0.013	0.013	0.013	0.016	0.016
14GBd	0.013	0.013	0.016	0.016	0.016
7GBd	0.016	0.016	0.016	0.016	0.016
3.5GBd	0.016	0.016	0.020	0.016	0.016

Note that the optimum symbol-rate for WDM transmission of a particular modulation format is not only determined by the trade-off between inter- and intra-channel nonlinearities, but is also influenced by practical considerations such as cost effectiveness (governed by the trade-off between number of transceivers required and the operating speed of the electronics) and the most convenient WDM channel spacing for network routing.

The optimum launch power spectral density lies in the same, relatively narrow range between 0.013 and 0.02 mW/GHz for all modulation formats (see Table 19). The maximum transmission reach is correlated with the optimum power spectral density: the higher the optimum PSD the larger the tolerance to nonlinearities will be, when comparing symbol rates of the same modulation format. However, when comparing transmission among different modulation formats this correlation is masked by different tolerances to ASE noise, which affect the optimum PSD.

5.4 Digital Backpropagation of the Central Channel

In this section we investigate the potential gain of the digital backpropagation algorithm based on the Manakov equation described in section 3.3.2. As for the investigation of single channel transmission in section 5.2, we focus on optimum backpropagation of one channel at different symbol-rates, but now in a WDM environment.

The optimum number of steps per span and the value of optimisation parameter φ have been found to be similar as in the single channel case (see Figure 64), which is logical since these parameters only depend on the backpropagated spectrum and not on adjacent channels. The optimum values are identical irrespective on the modulation

format: 25 steps per span for 56GBd, 7 steps per span for 28GBd, 3 step per span for 14GBd and 1 step per span for 7GBd and 3.5GBd with $\varphi = 0.9 - 0.95$.

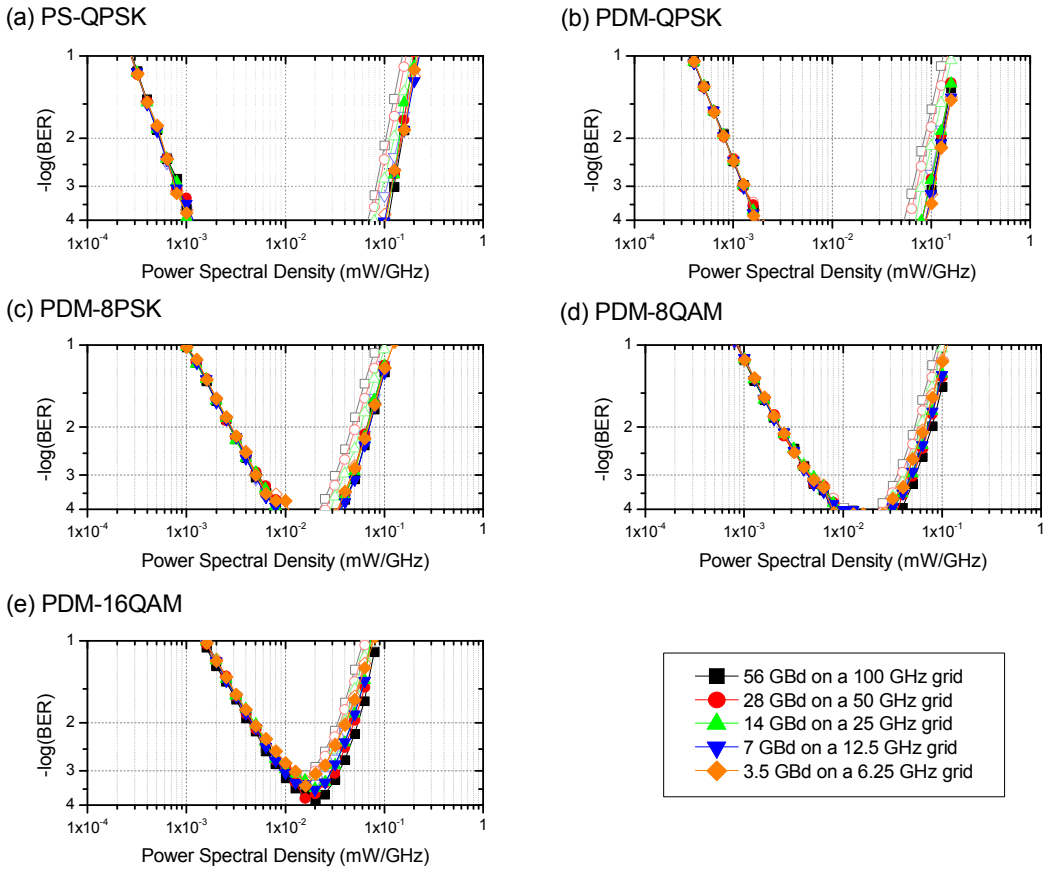

Figure 71: BER as a function power spectral density for WDM-transmission of coherently detected PS-QPSK, PDM-QPSK, PDM-8PSK, PDM-8QAM and PDM-16QAM. Open symbols denote transmission without nonlinear compensation, while filled symbols show transmission with digital backpropagation of the central channel.

Figure 71 shows the calculated BER for all modulation formats and symbol rates, as a function of the PSD. Filled symbols denote transmission with digital backpropagation at the receiver, while open symbols show transmission with chromatic dispersion compensation only for comparison. It can be seen that curves in the linear region overlap as before, because nonlinear compensation does not improve performance in regions with negligible nonlinear phase shift.

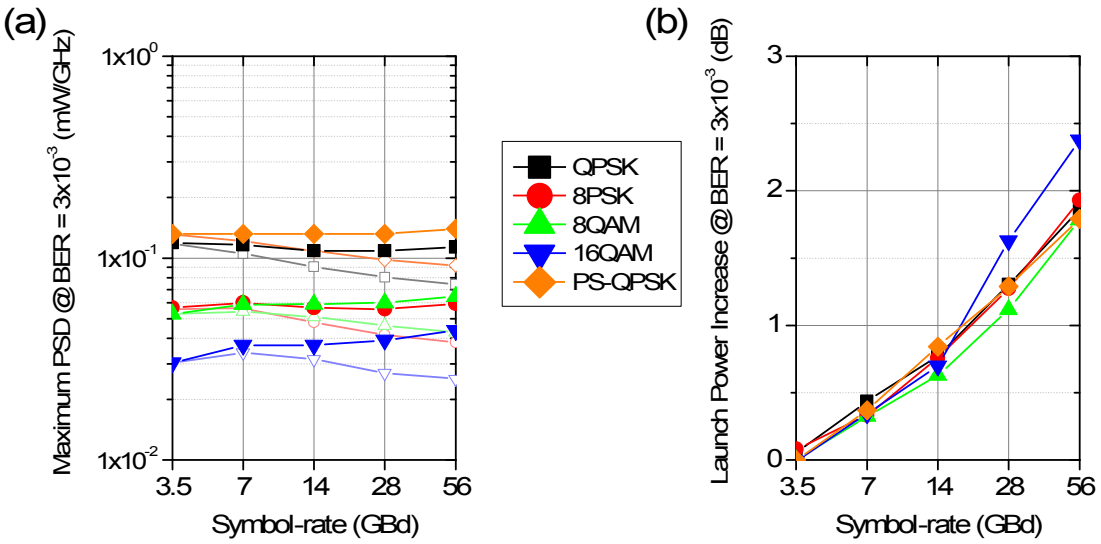

Figure 72: Figure (a) depicts the maximum power spectral density @ BER=3×10^{-3} versus symbol-rate for WDM transmission with (filled symbols) and without optimum digital backpropagation of the central channel (open symbols). Figure (b) shows the resulting increase in maximum launch power at @ BER=3×10^{-3}.

Figure 72 shows the maximum PSD @ BER=3×10^{-3} and resulting launch power increases in the nonlinear transmission regime. PS-QPSK performs best for every symbol rate that has been investigated and shows the nearly same performance of 0.13-0.14mW/GHz. PDM-QPSK shows same flat performance over all symbol rates with a maximum PSD of 0.11-0.12mW/GHz. Modulation formats with 3bit/symbol like 8PSK and 8QAM show similar performance in the region of 0.06mW/GHz for all symbol rates. In the case of 16QAM the best nonlinear performance of 0.044mW/GHz can be seen at the highest symbol rate 56GBd.

Figure 72 (b) translates the improvement that can be gained by digital backpropagation from maximum PSD into launch power in dB. All modulation formats show a clear trend of higher benefit from digital backpropagation for higher symbol-rates similar to the single channel case in Figure 69 (b). However, there is significantly less improvement to be gained, which can be attributed to the nonlinear phase shift from adjacent channels (cross phase modulation (XPM)). Figure 73 (a) illustrates, how the nonlinear distortion depends on the symbol-rate R_S. The nonlinear distortion due to SPM increases with the symbol-rate (as described in section 2.2.1 and 5.1), while the XPM distortion reduces with increased frequency spacing/symbol-rate. Although SPM is fully compensated, since the full spectrum of the channel of interest is backpropagated (see Figure 73 (b)-(f)), XPM is not compensated for and acts as additional distortion that limits the efficiency of digital backpropagation, so that the benefit is negligible in case of a low symbol-rate of e.g. 3.5GBd on a 6.25GHz grid. At 7GBd the launch power can be increased by 0.4dB and at 14GBd by 0.6-0.8dB. 16QAM shows a higher benefit than

all other modulation formats at 28GBd (1.6dB compared to 1.1-1.3dB) and at 56GBd (2.4dB compared to 1.8-1.9dB), respectively.

An increased improvement for spectrally more efficient modulation formats has been already observed in the single channel case (see section 5.2). This effect can be attributed to the higher density of constellation points - denser constellations suffer more from nonlinear distortions, therefore the improvement in BER tends to be more significant when this distortion is compensated for. However, this effect is heavily masked by the degrading impact of XPM which limits the efficiency of the digital backpropagation algorithm and can only be seen at higher symbol rates for PDM-16QAM [22].

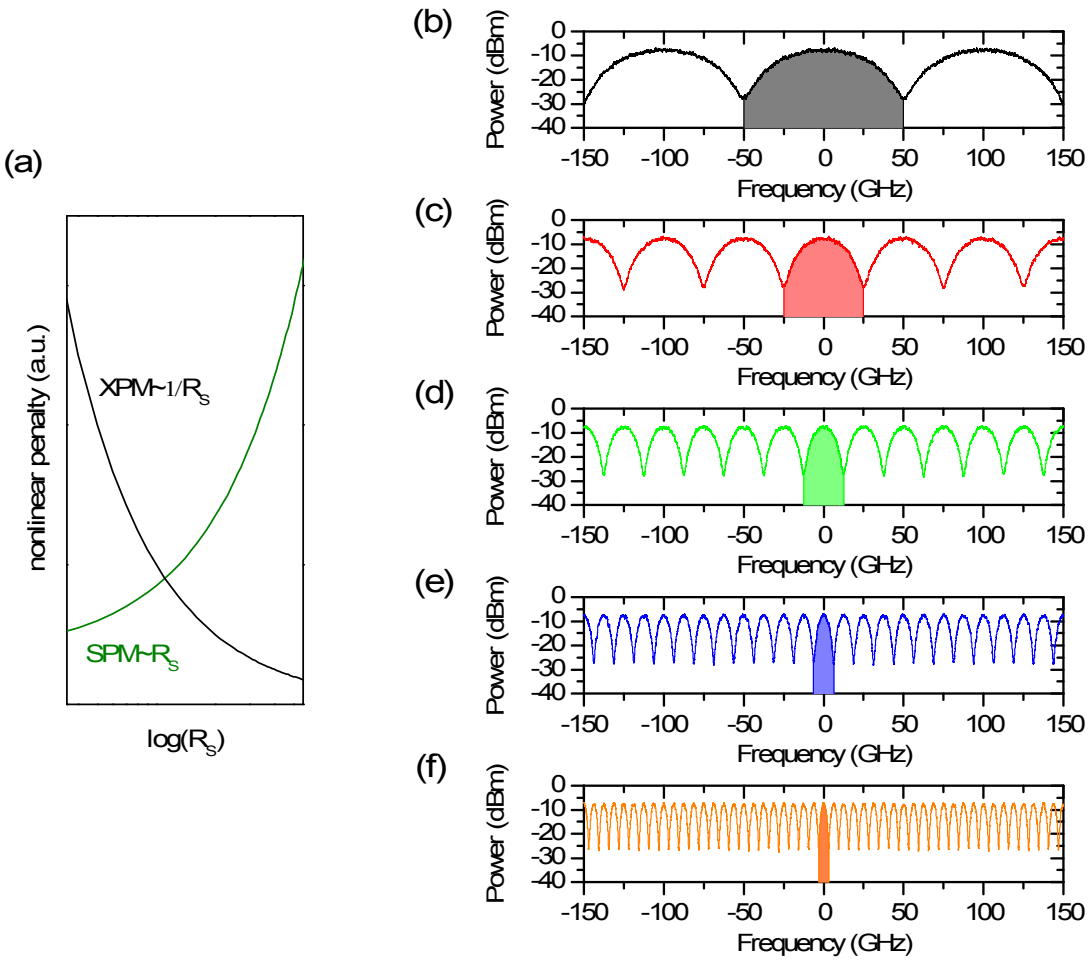

Figure 73: (a) schematic of the symbol-rate dependency of SPM and XPM as well as backpropagated spectral content for (b) 56GBd, (c) 28GBd, (d) 14GBd, (e) 7GBd and (f) 3.5GBd

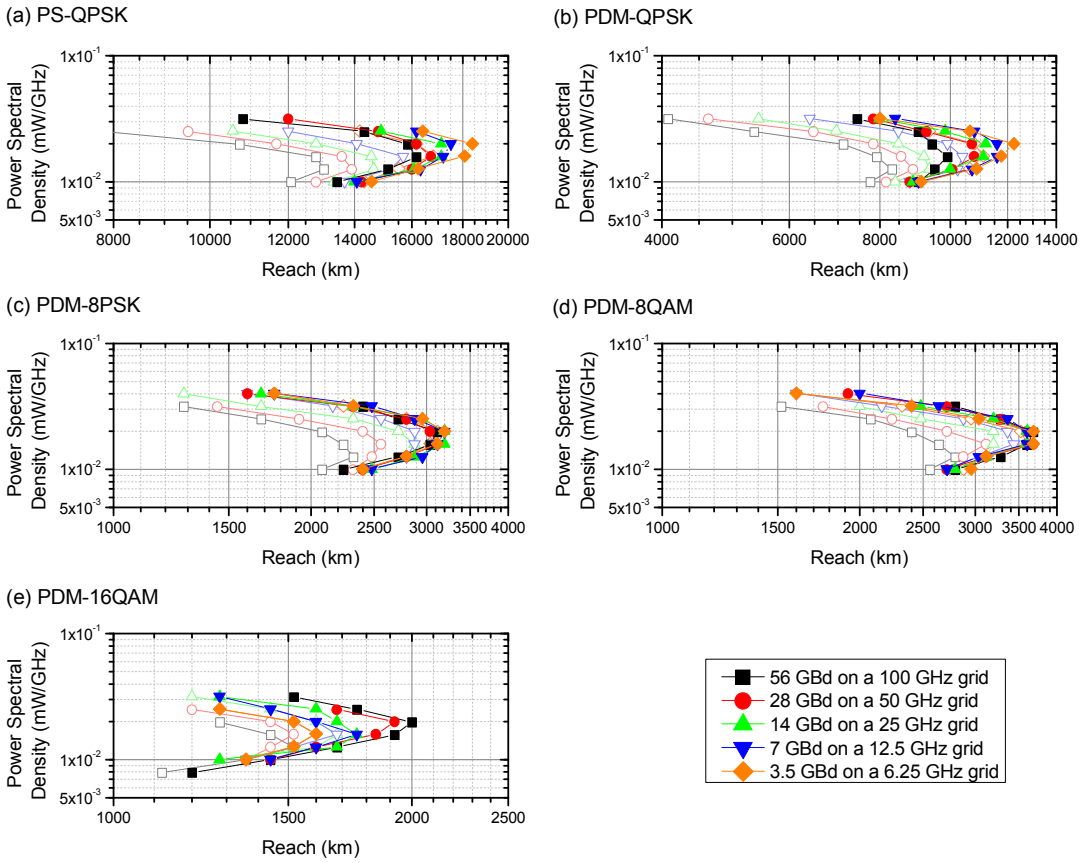

Figure 74: Achievable transmission reach @ BER=3×10^{-3} with (filled symbols) and without digital backpropagation (open symbols). WDM transmission of (a) PS-QPSK, (b) PDM-QPSK, (c) PDM-8PSK, (d) PDM-8QAM and (e) PDM-16QAM is investigated at varying symbol rates.

To determine into what maximum transmission distances the increased nonlinear performance documented in Figure 72 translate, the maximum achievable transmission reach is investigated for PS-QPSK, PDM-QPSK, PDM-8PSK, PDM-8QAM and PDM-16QAM (see Figure 74 for a comparison between transmission with and without digital backpropagation).

Surprisingly, despite a very small performance improvement on the 13×80km link at lower symbol rates (see Figure 72 (b)), the maximum achievable transmission reach can still be increased significantly (up to 1,840km in case of PS-QPSK). This can be attributed to the fact, that on all amplified transmission links degradations tend to accumulate in a logarithmical fashion (e.g. SNR increases with launch power in dB – see Figure 61). As a consequence, small differences in nonlinear performance after a few spans can lead to significant differences in maximum achievable reach.

It must be noted that the symbol rate with the best nonlinear performance on the fixed link is not necessarily the symbol rate with the highest maximum reach, especially for PS-QPSK and PDM-QPSK. The disparity between the two sets of results can be

explained by the high value of power spectral density at which the results are obtained. For the BER vs. PSD simulations on the 13×80km link, changing SNR conditions are characteristic. First the SNR increases in the linear regime and then reduces in the nonlinear regime, whereas maximum reach curves are taken at a fixed BER and, therefore, at a fixed SNR. This can negatively affect equalisation convergence and phase recovery algorithms, especially when an increased amount of nonlinear noise is present and the length of averaging windows have been designed for high SNR regions.

Table 20: Maximum transmission distance with digital backpropagation in kilometres, assuming FEC can correct for BER=3×10^{-3} (largest transmission distances per modulation format are highlighted)

SYMBOL RATE	PS-QPSK	PDM-QPSK	PDM-8PSK	PDM-8QAM	PDM-16QAM
56GBd	16,160	9,920	3,120	3,680	2,000
28GBd	16,720	10,800	3,120	3,680	1,920
14GBd	17,120	11,200	3,200	3,600	1,760
7GBd	17,520	11,600	3,200	3,600	1,760
3.5GBd	18,400	12,240	3,200	3,680	1,600

PS-QPSK achieves the highest transmission distance with 18,400 km at 3.5GBd and PDM-QPSK performs second best with 12,240km at 3.5GBd as documented in Table 20. Similar to the results for the fixed link (see Figure 72 (b)), an increased benefit of digital backpropagation for higher symbol rates can be observed consistently for all modulation formats. In the case of PS-QPSK, digital backpropagation increases reach by 1,600km for 3.5GBd, 1,840km for 7GBd, 2,480km for 14GBd, 2,800km for 28GBd and 3,120km for 56GBd.

However, the absolute transmission reach shows a very different picture across the different modulation formats. While PS-QPSK and PDM-QPSK exhibit their maximum transmission reach at the lowest symbol rate of 3.5GBd (18,400km and 12,240km), a similar maximum transmission distance for all symbol rates can be observed at PDM-8PSK and PDM-8QAM (~3,200km and ~3,700km). The trend even reverses with PDM-16QAM, for which the maximum transmission distance of 2,000km can be achieved at 56GBd. This behaviour can be explained by an increased nonlinear penalty induced by neighbouring WDM channels modulated with higher order modulation formats such as 16QAM compared to e.g. PDM-QPSK [22]. The increased nonlinear crosstalk is more detrimental to the efficiency of the digital backpropagation algorithm in the case of a

narrow grid such as 6.25GHz than in case of a 100GHz grid. This suggests, that if the interfering channels had been modulated consistently with e.g. PDM-QPSK (or another modulation format with low spectral efficiency), digital backpropagation would provide a greater benefit for more spectrally efficient modulation formats at all symbol rates. However, it is worth noting that this benefit comes at the cost of reduced capacity of the neighbouring WDM channels. Rafique et al. [22] pointed out, that the increased degradation induced by more spectrally efficient modulation formats is a result of the higher peak-to-average power ratio at low values of accumulated dispersion and could be mitigated by appropriate dispersion pre-compensation.

Improvements of the DBP algorithm can be compared for 28GBd PDM-QPSK between simulation and the experiment described in section 4.4.3. In case of the experiment it was possible to extend the maximum achievable reach by +20% (corresponding to 1400km from 7382km to 8826km) with a 1 step per span algorithm, while in case of the simulation transmission reach was extended by +23% (corresponding to 2000km from 8800km to 10800km) with a 7 step per span algorithm. Comparing the simulation of 28GBd PDM-16QAM to a similar experiment [24], it appears that in experimental transmission reach has been extended by only +13% (160km from 1,200km to 1,360km) with a 1 step per span algorithm, as opposed to +26% (400km from 1,520km to 1,920km) with 7 step per span algorithm. However, it should be noted that a simulation study [18] based on the experiment in [24] revealed that a +30% improvement (1 span more than in the simulations described in this thesis) would be more characteristic for this system. At this symbol-rate, a single step per span seems to be sufficient to enjoy the major part of the improvement offered by DBP.

5.5 Multi-channel Digital Backpropagation

In the previous section DBP has been investigated for backpropagation of a single channel. However, especially for low symbol-rate signals (<28GBd) the ADC speed is sufficient to digitise larger bandwidths covering adjacent WDM-channels. Therefore, it is possible to compensate not only for intra-channel nonlinearities, but for inter-channel nonlinearities such as XPM as well. Let us now assume that for every symbol rate investigated a coherent receiver with a 3dB electrical bandwidth of 0.8×56 = 44.8GHz (corresponding to the 56GBd receiver) is available. In this case the full available bandwidth would be digitised at 112Gsamples and digitally backpropagated. For symbol rates below 56GBd, more than one channel is backpropagated and, therefore, cross-phase modulation is compensated for, additionally to self-phase modulation. Digital backpropagation based on the Manakov equation, was applied, as described in

section 3.3.2. The optimum number of steps per span is 25, which is identical to the value used for 56GBd single channel and WDM transmission, since the backpropagated spectral width is 100GHz in all cases. The overall power of the backpropagated waveform at the beginning of backpropagation is the sum of the power of all channels that have been digitised. However, due to the roll-off of the optical filter at the receiver, spectral content of the channels in the roll-off region is cut out. The optimisation parameter φ must reflect this, and is correspondingly smaller. After backpropagation the central channel was selected by resampling the signal to 2 samples per symbol and an equaliser, a phase recovery circuit and a differential decoder is applied, before errors are counted.

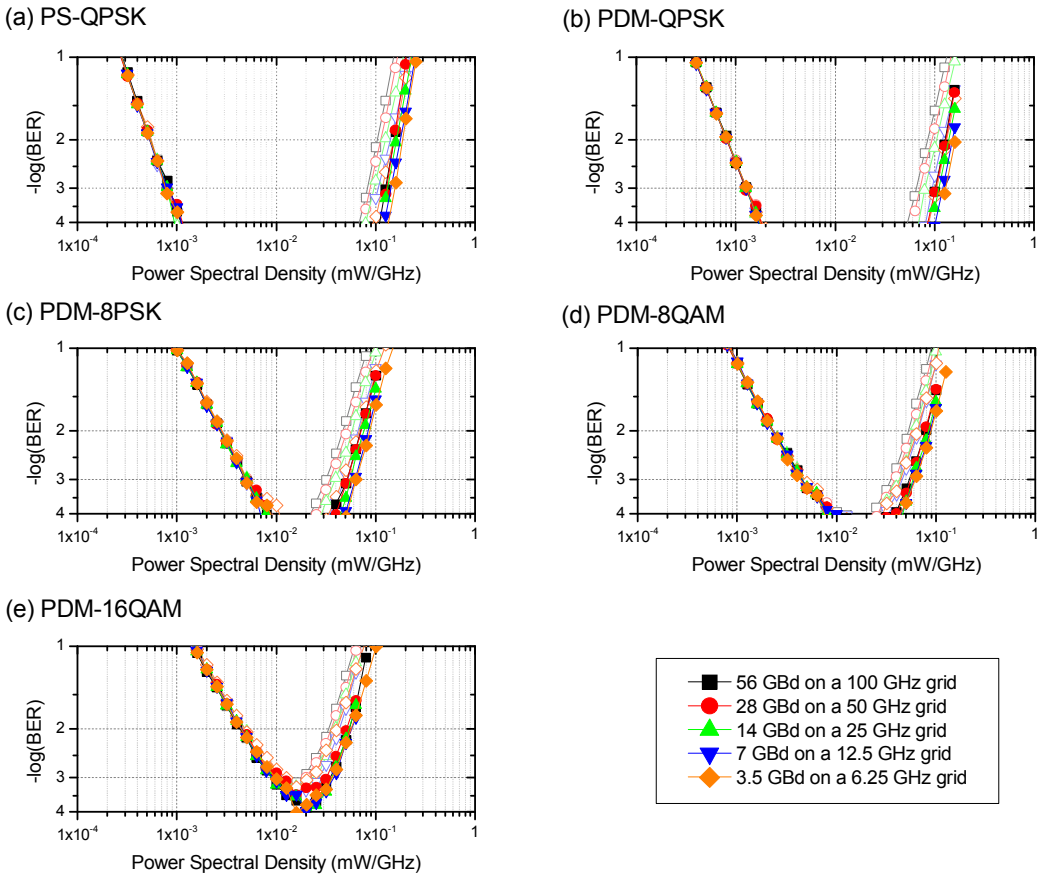

Figure 75: BER vs. power spectral density for WDM-transmission of coherently detected PS-QPSK, PDM-QPSK, PDM-8PSK, PDM-8QAM and PDM-16QAM. Open symbols denote transmission without nonlinear compensation, while filled symbols show transmission with digital backpropagation covering 100GHz.

Figure 75 shows the resultant BER for all modulation formats and symbol rates as a function of the PSD. Filled symbols denote transmission with full digital backpropagation covering 56GHz at the receiver, while open symbols show transmission with chromatic dispersion compensation only for comparison. Again,

curves in the linear region overlap, because nonlinear compensation does not improve performance in regions with negligible nonlinear phase shift.

Figure 76 shows the maximum PSD @ BER=3×10^{-3} and resulting launch power increases in the nonlinear transmission regime. PS-QPSK performs best for every symbol rate, similarly to the previous section, where only the central channel was backpropagated. However, when backpropagating a 100GHz portion of the spectrum, 3.5GBd shows the best performance with a maximum PSD of 0.17mW/GHz compared to 0.13mW/GHz, when only the central channel (6.25GHz) is backpropagated. PDM-QPSK shows the same performance improvement towards lower symbol rates with a maximum PSD of 0.14mW/GHz at 3.5GBd. PDM-8QAM and PDM-8PSK show similar performance in the region of 0.06-0.07mW/GHz, with slightly better performance at lower symbol rates. In the case of 16QAM the maximum PSD is nearly flat across the symbol rates in the region of 0.044-0.045mW/GHz.

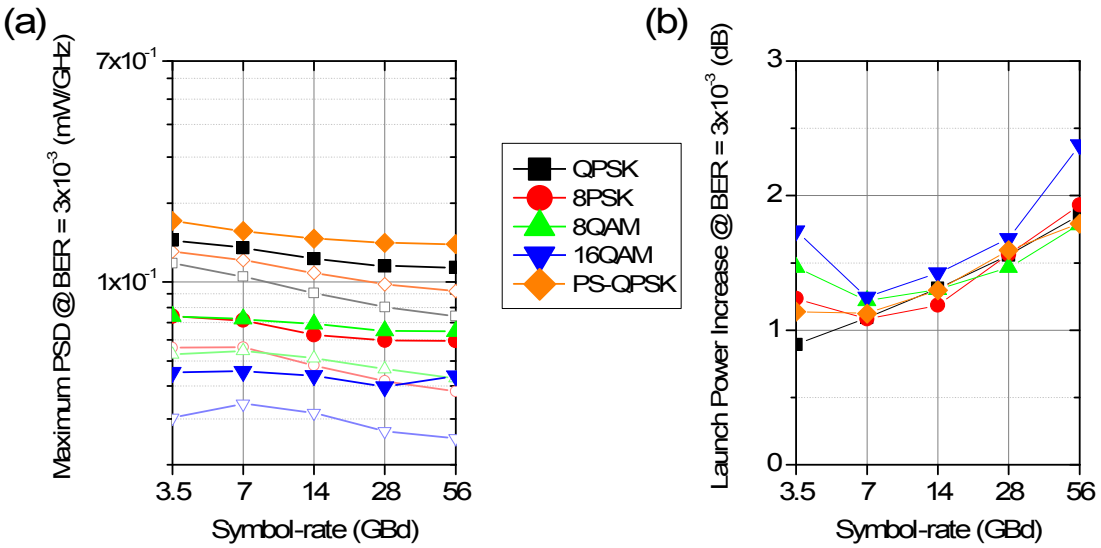

Figure 76: Figure (a) depicts the maximum power spectral density @ BER=3×10^{-3} versus symbol-rate for WDM transmission with (filled symbols) and without optimum digital backpropagation covering 100GHz (open symbols). Figure (b) shows the resulting increase in maximum launch power

Figure 76 (a) translates the improvement that can be gained by digital backpropagation from maximum PSD into launch power in dB. As expected, all modulation formats show better performance at lower symbol-rates compared to digital backpropagation of the central channel (see Figure 72), since a larger proportion of the spectrum is backpropagated (see Figure 77 (b)-(f)). However, the benefit from digital backpropagation remains different at different symbol rates, even though the same spectrum of 100GHz is backpropagated in every case.

As already discussed in the previous section, Figure 77 (a) shows how the impact of SPM increases with symbol-rate, while the distortion due to XPM is reduced with increased frequency spacing or symbol-rate. However, because a fixed bandwidth of 100GHz is backpropagated, not only SPM is compensated but at lower symbol-rates increasing amounts of XPM are compensated as well. The DBP-algorithm is now limited by XPM induced by the channels outside the backpropagated bandwidth. The influence of this uncompensated XPM increases with reduced symbol-rate and frequency spacing (Figure 77 (a)), resulting as before in higher benefit for DBP at higher symbol-rates as displayed in Figure 76 (a).

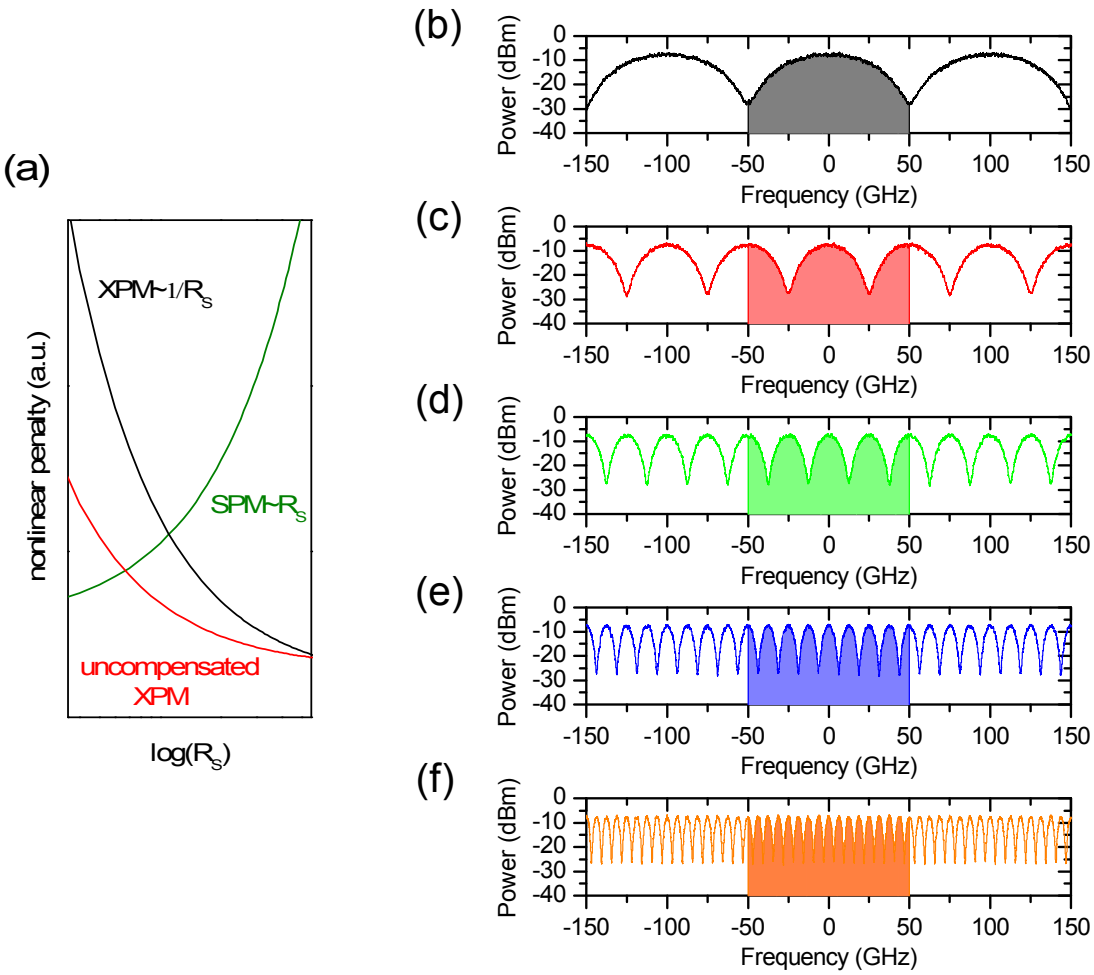

Figure 77: (a) schematic of the symbol-rate dependency of SPM, XPM and uncompensated XPM as well as backpropagated spectral content (100GHz) for (b) 56GBd, (c) 28GBd, (d) 14GBd, (e) 7GBd and (f) 3.5GBd

Similarly to previous sections, the maximum achievable transmission reach has been investigated when 100GHz is backpropagated.

Figure 78 shows the reach curves for (a) PS-QPSK, (b) PDM-QPSK, (c) PDM-8PSK, (d) PDM-8QAM and (e) PDM-16QAM (filled symbols) comparing it to transmission without DBP (open symbols).

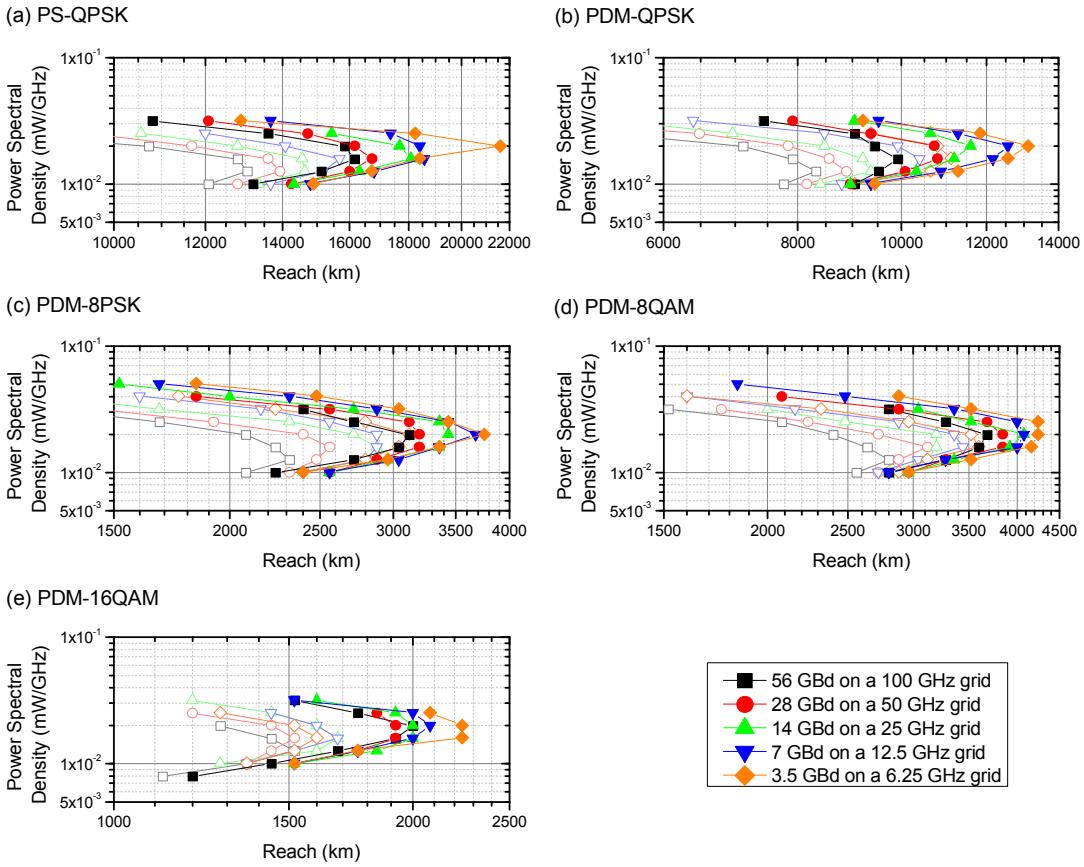

Figure 78: Achievable transmission reach @ BER=3×10^{-3} with (filled symbols) and without 100GHz digital backpropagation (open symbols). WDM transmission of (a) PS-QPSK, (b) PDM-QPSK, (c) PDM-8PSK, (d) PDM-8QAM and (e) PDM-16QAM is investigated at varying symbol rates.

Table 21 displays the maximum achievable transmission distances for all modulation formats with 100GHz DBP, highlighting the trend of increased reach for lower symbol-rates similarly to what has been observed without DBP (see Table 18). Again, PS-QPSK outperforms all other modulation formats by achieving a maximum transmission distance of 21,600km at 3.5GBd (+28.6% with respect to no DBP and +17.4% compared to central channel DBP), which is more than 7,000km more compared to the second best modulation format PDM-QPSK (+17.9% with respect to no DBP and +7.2% compared to central channel DBP) at the same symbol-rate. PDM-8QAM outperforms PDM-8PSK by more than 400km irrespective of the symbol rate. At 3.5GBd PDM-8PSK gains +20.5% reach compared to no DBP and +17.5% compared to central channel DBP, while PDM-8QAM gains +17.8% and +15.2%, respectively. PDM-16QAM shows a +40% improvement compared to the case without DBP or central channel DBP.

Table 21: Maximum transmission distance with 100GHz digital backpropagation in km, assuming FEC can correct for BER=3×10^{-3} (largest transmission distances per modulation format are highlighted)

SYMBOL RATE	PS-QPSK	PDM-QPSK	PDM-8PSK	PDM-8QAM	PDM-16QAM
56GBd	16,160	9,920	3,120	3,680	2,000
28GBd	16,800	11,040	3,200	3,840	1,920
14GBd	18,080	11,600	3,440	4,080	2,000
7GBd	18,560	12,560	3,680	4,080	2,080
3.5GBd	21,600	13,120	3,760	4,240	2,240

5.6 Summary

The impact of varying the symbol-rate and frequency grid has been investigated for single-channel and WDM transmission of PS-QPSK, PDM-QPSK, 8PSK, 8QAM and 16QAM for a fixed spectral efficiency per modulation format.

A trade-off between intra- and inter-channel nonlinearities was observed. With increasing symbol-rate inter-channel nonlinear distortions show a reduced impact, which is due to the wider frequency spacing. At the same time however, inter-channel nonlinearities show a more severe impact with increasing symbol rate, since the pulse overlap within the system increases with spectral width. The optimum symbol-rate can be found to balance these effects and shifts from 3.5GBd to 7GBd when increasing the density of the constellation e.g. from QPSK to 16QAM, indicating that higher order modulation formats lead to more severe inter-channel distortions.

Initially digital backpropagation was investigated for a scenario in which only intra-channel nonlinearities are compensated for by backpropagating the central channel. The optimum number of computational steps per span was used for the DBP algorithm, in contrast to Chapter 4, where the complexity was restricted to 1 step per span. Higher symbol-rate signals such as 56Gbd and higher order modulation formats such as PDM-16QAM have been found to benefit more from digital backpropagation. However, low symbol-rates such as 3.5GBd and spectrally less efficient modulation formats such as PS-QPSK still show a higher maximum transmission reach in single channel transmission. Even though deterministic nonlinearities are now compensated for, nonlinear interactions between signal and ASE noise limit the efficiency of the DBP algorithm. These tend to be less harmful for signals with a narrower spectrum (lower symbol-rate) since less ASE power is picked up along the transmission link. Adding

more WDM channels to the signal leads to an increased amount of uncompensated inter-channel nonlinearities, which is particularly harmful in a narrower grid (lower symbol-rate). Under these conditions the optimum symbol-rate is the result of a trade-off between nonlinear signal-ASE interactions and uncompensated inter-channel nonlinearities. While less spectrally efficient modulation formats such as QPSK and PS-QPSK have their optima at 3.5GBd, 8QAM and 8PSK show a similar transmission reach for all symbol rates and 16QAM clearly favours 56GBd, which is due to an increased influence of inter-channel nonlinearities induced by spectrally more efficient modulation formats.

In the final investigation described in section 5.5 the receiver provides a fixed electrical bandwidth of 100GHz and is therefore capable of backpropagating adjacent channels as well for symbol rates smaller than 56GBd. Under these conditions, the trade-off between nonlinear signal-ASE interactions and uncompensated inter-channel nonlinearities described in the previous paragraph is notably relaxed towards lower symbol-rates. As a consequence increased transmission distances have been observed for lower-symbol rates, irrespective of the modulation format.

However, for selecting the optimum symbol-rate in a real system one has to take into account practical considerations, such as cost effectiveness (governed by the trade-off between number of transceivers required and the operating speed of the electronics) and the most convenient WDM channel spacing for network routing.

5.7 References

[1] Covega Co. (2011, March). Available: http://www.covega.com/products/pdfs/LN%20027-066%20Rev%20F.pdf

[2] Fujitsu Optical Components Ltd. (2011, November). Available: http://jp.fujitsu.com/group/foc/downloads/services/100gln/ln100gdpqpsk-e-111102.pdf

[3] C. Behrens, R. I. Killey, S. J. Savory, M. Chen, and P. Bayvel, "Nonlinear Distortion in Transmission of Higher-Order Modulation Formats," *Photonics Technology Letters,* 2010.

[4] Le Croy Co. (2011, December). Available: http://cdn.lecroy.com/files/pdf/lecroy_labmaster_9_zi_datasheet.pdf

[5] D. S. Millar and S. J. Savory, "Blind Adaptive Equalization of Polarization Switched QPSK Modulation," *Optics Express,* vol. 19, pp. 8533-8538, 2011.

[6] J. D. Proakis and M. Salehi, *Digital Communications*: McGraw-Hill, 2008.

[7] E. Agrell and M. Karlsson, "Power-Efficient Modulation Formats in Coherent Transmission Systems," *Journal of Lightwave Technology,* vol. 27, pp. 5115-5126, 2009.

[8] E. Ip and J. M. Kahn, "Carrier synchronization for 3- and 4-bit-per-symbol optical transmission," *Journal of Lightwave Technology,* vol. 23, pp. 4110-4124, 2005.

[9] P. Serena, N. Rossi, and A. Bononi, "PDM-iRZ-QPSK vs. PS-QPSK at 100Gbit/s over dispersion-managed links," *Optics Express,* vol. 20, pp. 7895-7900, March 2012.

[10] M. Sjödin, B. J. Puttnam, P. Johannisson, S. Shinada, N. Wada, P. A. Andrekson, and M. Karlsson, "Transmission of PM-QPSK and PS-QPSK with different fiber span lengths," *Optics Express,* vol. 20, pp. 7544-7554, March 2012.

[11] M. Sjödin, B. J. Puttnam, P. Johannisson, S. Shinada, N. Wada, P. A. Andrekson, and M. Karlsson, "Comparison of PS-QPSK and PM-QPSK at Different Data Rates in a 25 GHZ-spaced WDM System," in *Proc. Conference on Optical Fiber Communication and the National Fiber Optic Engineers Conference OFC/NFOEC 2012*, Los Angeles, 2012, p. OTu2A.3.

[12] K. Piyawanno, M. Kuschnerov, B. Spinnler, and B. Lankl, "Optimal Symbol Rate for Optical Transmission Systems with Coherent Receivers," in *Proc. SPPCom 2010*, Karlsruhe, Germany, 2010, p. SPWA2.

[13] K.-P. Ho, *Phase Modulated Optical Communication Systems*: Springer, 2005.

[14] K. Kikuchi, "Electronic Post-compensation for Nonlinear Phase Fluctuations in a 1000-km 20-Gbit/s Optical Quadrature Phase-shift Keying Transmission

System Using the Digital Coherent Receiver," *Optics Express,* vol. 16, pp. 889-896, 2008.

[15] A. Carena, G. Bosco, V. Curri, P. Poggiolini, M. Tapia Taiba, and F. Forghieri, "Statistical Characterization of PM-QPSK Signals after Propagation in Uncompensated Fiber Links," in *Proc. European Conference on Optical Communications ECOC 2010*, Torino, 2010, p. P4.07.

[16] L. B. Du and A. J. Lowery, "Improved single channel backpropagation for intra-channel fiber nonlinearity compensation in long-haul optical communication systems," *Optics Express,* vol. 18, pp. 17075-17088, August 2010.

[17] D. Rafique and A. D. Ellis, "The Impact of Signal-ASE Four-Wave Mixing in Coherent Transmission Systems," in *Proc. Conference on Optical Fiber Communication and the National Fiber Optic Engineers Conference OFC/NFOEC 2011*, 2011, p. OthO2.

[18] C. Behrens, S. Makovejs, R. I. Killey, S. J. Savory, M. Chen, and M. Bayvel, "Pulse-shaping versus digital backpropagation in 224Gbit/s PDM-16QAM transmission," *Optics Express,* vol. 19, pp. 12879-12884, 2011.

[19] E. Ip, "Nonlinear Compensation Using Backpropagation for Polarization-Multiplexed Transmission," *Journal of Lightwave Technology,* vol. 28, pp. 939-951, March 2010.

[20] E. Ip and J. M. Kahn, "Compensation of dispersion and nonlinear effects using digital backpropagation," *Journal of Lightwave Technology,* vol. 26, pp. 3416-3425, 2008.

[21] I. Fatadin and S. J. Savory, "Impact of phase to amplitude noise conversion in coherent optical systems with digital dispersion compensation," *Optics Express,* vol. 18, pp. 16273-16278, 2010.

[22] D. Rafique and A. D. Ellis, "Nonlinear penalties in long-haul optical networks employing dynamic transponders," *Optics Express,* vol. 19, pp. 9044-9049, May 2011.

[23] T. K. Chiang, N. Kagi, T. K. Fong, M. E. Marhic, and L. G. Kazovsky, "Cross-phase modulation in fiber links with multiple optical amplifiers and dispersion compensators," *Journal of Lightwave Technology,* vol. 14, pp. 249-259, 1996.

[24] S. Makovejs, "High-speed optical fibre transmission using advanced modulation formats," PhD thesis, Electrical and Electronic Engineering, University College London, London, 2011.

Chapter 6

CONCLUSIONS AND FUTURE WORK

6.1 Conclusions

Next-generation optical networks will rely on increased capacity enabled by higher-order modulation formats, which use the available optical bandwidth more efficiently than binary modulation formats. Unfortunately, higher-order modulation formats are characterised by increased OSNR requirements, limiting the achievable transmission reach in the presence of linear and nonlinear distortions. The research work, described in this thesis, was devoted to the investigation of the generation and performance of higher-order modulation formats, in conjunction with a coherent receiver-based nonlinear compensation algorithm known as digital backpropagation (DBP).

Long haul and ultra-long haul transmission of PDM-BPSK, PS-QPSK, PDM-QPSK, PDM-8PSK, PDM-8QAM and PDM-16QAM modulation were studied experimentally in single-channel and 7 channel WDM transmission systems. The investigation focused on the most ubiquitous fibre type: standard single mode fibre (SSMF) and the most widespread amplification solution: erbium doped fibre amplifiers (EDFA) as well as a digital coherent receiver, which is the most promising receiver solution for future optical transport networks.

A simulation system based on MATLAB has been written, supporting the generation, transmission and coherent detection of PDM-BPSK, PDM-QPSK, PDM-8PSK, PDM-8QAM, PDM-16QAM and PS-QPSK. The simulation system was capable of modelling a variety of transmitter-side impairments: such as laser phase noise, electrical and optical filtering and electrical noise; receiver-side impairments such as local oscillator phase noise, local oscillator frequency offset, electrical and optical filtering and

quantisation noise; as well as transmission impairments such as ASE-noise, chromatic dispersion, dispersion slope, Kerr nonlinearity and PMD. At the receiver, digital signal processing algorithms for nonlinear compensation, chromatic dispersion compensation, equalisation and phase estimation were implemented for all modulation formats.

The 4-dimensional modulation format PS-QPSK was compared, for the first time, experimentally and by simulation, against PDM-BPSK and PDM-QPSK at 42.9Gbit/s. Whilst outperforming both conventional formats in the linear transmission regime, PS-QPSK was found to suffer 1.5dB more from nonlinear distortions than PDM-BPSK and 1.5dB less than PDM-QPSK. As a result, the maximum transmission distance of 14,042km for WDM transmission of PDM-BPSK (which is currently the only commercially available option for transpacific transmission) reduces to 13,640km for PS-QPSK and 10,350km for PDM-QPSK. Nonlinear compensation was not investigated for this scenario, because the achieved transmission distances were in excess of 10,000km, covering most of submarine and terrestrial transmission system requirements.

However, at 112Gbit/s it was shown that a DBP algorithm becomes useful in increasing the transmission distance. A single computational step per transmitted fibre span was, yielding a higher benefit for higher-order modulation formats. In a single-channel regime at 112Gbit/s maximum transmission distance was extended by +20.7% for PS-QPSK (3bits/symbol), +31.6% for PDM-QPSK (4bits/symbol), +59.3% for PDM-8PSK, +69.7% for PDM-8QAM (both 6bits/symbol) and +63.4% for PDM-16QAM (8bits/symbol). Two reasons have been identified for the increased gain. Firstly, higher order modulation formats show a lower tolerance to nonlinear distortions due to their denser constellation diagrams – therefore, it is reasonable to assume that they experience a higher gain when these distortions are compensated for. Secondly, the DBP will give a more accurate interpretation of the waveform within the effective length of the fibre for signals with a lower symbol rate (higher spectral efficiency), given a fixed number of computational steps per span is used. At this point it is worth noting that a lower symbol rate has other positive implications for the complexity of the digital coherent receiver. It relaxes bandwidth requirements of the electrical circuitry and reduces the length of FIR filters which are used to compensate for chromatic dispersion in time domain (number of taps is proportional to symbol-rate^2). Additionally, a narrower spectrum increases tolerance to optical filtering, making the signal more robust to ROADM cascades. From the perspective of receiver complexity the optimum modulation format to pick for a specific transmission distance may be the one that maximises capacity while still achieving the required margin after transmission over the link.

In the single-channel scenario the DBP algorithm is mostly limited by nonlinear signal ASE interactions, which cannot be compensated due their stochastic nature. However, adding additional WDM channels leads to a large amount of uncompensated inter-channel nonlinearity, which further reduces the efficiency of DBP. In a 7-wavelength WDM system transmission distance could be extended by +19.6% for PDM-QPSK, +20% for PDM-8PSK, +17.8% for PDM-8QAM and +25% for PDM-16QAM (only 3 WDM channels).

After focussing on the potential gains from DBP for optical transport networks carrying 42.9Gbit/s or 112Gbit/s on a fixed 50GHz grid on, transmission systems with increased spectral efficiency up to a capacity of 448Gbit/s within 100GHz were investigated, using computer simulations. Here, channels spaced by as little as 6.25GHz, far below the current ITU standard of 50 and 100GHz, were considered to accommodate new data rates and a more flexible network management to raise bandwidth efficiency in future optical networks. Investigations of nonlinear transmission performance revealed a trade-off between inter- and intra-channel nonlinearities with the optimum symbol rate to be found at lower symbol rates (3.5-7GBd), irrespective of the modulation format. However, for selecting the optimum symbol-rate in a real system one has to take into account practical considerations, such as cost effectiveness (governed by the trade-off between number of transceivers required and the operating speed of the electronics) and the most convenient WDM channel spacing for network routing.

In the course of the work, an optimum DBP algorithm compensating for intra-channel nonlinear effects has been developed and applied at the receiver and it has been confirmed that higher order modulation formats, indeed, benefit more from nonlinear compensation, confirming earlier findings in Chapter 4. Furthermore, it was found that under WDM conditions the optimum symbol rate shifts with increased constellation density towards 56GBd. This behaviour is related to the fact that higher-order modulation formats induce worse inter-channel nonlinear distortions, which have been found to be the dominant limitation for the DBP algorithm (see Chapter 4). As a consequence, performance improvement is unlikely to exceed +10% transmission reach if DBP is applied to higher-order modulation formats such as 8QAM and 16QAM, for wavelength spacings denser than 50GHz.

However, the DBP algorithm was shown to be capable of compensating for inter-channel nonlinearities as well, given that sufficient bandwidth can be digitised by the ADCs at the receiver. It was demonstrated that a receiver with an electrical bandwidth of 100GHz (consistent with the current state-of-the-art ADCs) can dramatically improve the performance of a DBP algorithm and the maximum transmission reach was

extended by up to +40% for PDM-16QAM on 6.25GHz grid. Furthermore it was shown that under these circumstances the DBP is limited uncompensated XPM originating from the WDM channels outside the compensation bandwidth.

Nevertheless, applying nonlinear compensation algorithms such as digital backpropagation in a commercial product is currently prohibitive due the large number of logic gates that would be required on an ASIC. However, it is conceivable that with the scaling of CMOS technology and further reduction in complexity of the DSP algorithms, it is likely that nonlinear compensation will be applied in the future. Upgrading terminal equipment with a receiver-based SPM compensation scheme might be implemented, especially if in face of increasing data traffic the only viable alternative would be to install new fibre with all the associated costs.

6.2 Future Work

6.2.1 DBP performance for OFDM and Nyquist WDM

The research described in this thesis focussed on the investigation of single-carrier transmission, where a single optical carrier is modulated and transmitted in wavelength window, significantly broader than the symbol rate. To increase spectral efficiency it is possible to pack channels at a symbol rate spacing, which is denoted OFDM or Nyquist WDM. Although, nonlinear compensation algorithms have been already applied to OFDM, Nyquist WDM has not been investigated and a comprehensive study on potential performance improvement is not available in either case.

6.2.2 Increased FEC overhead versus DBP

As FEC technology continues to evolve it becomes increasingly difficult to consider modulation formats isolated from coding. An example that illustrates this notion was brought forward recently: PS-QPSK can be regarded as a low complexity code applied to PDM-QPSK, which can be outperformed by more complex codes like LDPC codes [1]. Therefore, one fruitful area for future research might be to investigate gains in achievable transmission reach as a function of correctable BER. Is it possible to gain more transmission distance by increasing FEC overhead or by applying DBP? How does the implementation complexity compare between nonlinear compensation algorithms and increased overhead FEC?

6.2.3 Trade-off between Modulation Format and FEC

SNR requirements can be traded-off against spectral efficiency by adjusting the FEC overhead or by changing the modulation format. With the use of soft FEC, correctable

BERs can be as high as 2×10^{-2} while SNR requirements for different modulation formats tend to converge at higher BERs as illustrated in section 5.1, Figure 59. This raises the interesting question of what is the optimum modulation format/FEC combination for a given link configuration? Although some initial work has been done on theoretical capacity limitations of the optical channel [2], the relationship between spectral efficiency and SNR requirements still requires a lot of study especially in the context of optimum combination of FEC and modulation format as well as implementation complexity.

6.2.4 Spectrally-efficient 4D Modulation Formats

Recently, various 4-dimensional constellations have been proposed as the most power efficient modulation formats for the optical channel [3, 4]. Although transmission of PS-QPSK has already been demonstrated [5-7], more-spectrally efficient 4D modulation formats such as 128-SP-QAM have only attracted little attention so far [8]. These constellations might provide increased transmission performance, due to their superior SNR requirements compared to constellations of equivalent spectral efficiency optimised for a 2 dimensional channel. With recent advances in digital transponder design it has become possible to modulate these formats onto an optical carrier and investigate their transmission performance. However, it has to be noted that reliable polarisation and phase estimation algorithms still have to be developed to detect 4D modulation formats with a digital coherent receiver.

6.3 References

[1] B. Krongold, T. Pfau, N. Kaneda, and S. C. J. Lee, "Comparison Between PS-QPSK and PDM-QPSK With Equal Rate and Bandwidth," *Photonics Technology Letters,* vol. 24, pp. 203-205, February 2012.

[2] R. J. Essiambre, G. Kramer, P. J. Winzer, G. J. Foschini, and B. Goebel, "Capacity Limits of Optical Fiber Networks," *Journal of Lightwave Technology,* vol. 28, pp. 662-700, February 2010.

[3] E. Agrell and M. Karlsson, "Power-Efficient Modulation Formats in Coherent Transmission Systems," *Journal of Lightwave Technology,* vol. 27, pp. 5115-5126, 2009.

[4] M. Karlsson and E. Agrell, "Which is the most power efficient modulation format in optical links?," *Optics Express,* vol. 17, pp. 10814-10819, 2009.

[5] E. Masalkina, R. Dischler, and H. Buelow, "Experimental Study of Polarization-Switched-QPSK Subcarrier Modulation and Iterative Demapping on Optical OFDM Systems," in *Proc. Conference on Optical Fiber Communication and the National Fiber Optic Engineers Conference OFC/NFOEC 2004*, Los Angeles, 2011, p. OThO6.

[6] M. Sjödin, P. Johannisson, H. Wymeersch, P. A. Andrekson, and M. Karlsson, "Comparison of polarization-multiplexed QPSK at 30 Gbit/s," *Optics Express,* vol. 19, pp. 7839-7846, April 2011.

[7] D. S. Millar, D. Lavery, S. Makovejs, C. Behrens, B. C. Thomsen, P. Bayvel, and S. J. Savory, "Generation and long-haul transmission of polarization switched QPSK at 42.9Gbit/s," *Optics Express,* vol. 19, pp. 9296-9302, 2011.

[8] M. Sjödin, P. Johannisson, J. Li, E. Agrell, P. A. Andrekson, and M. Karlsson, "Comparison of 128-SP-QAM with PM-16-QAM," *Opt. Express,* vol. 20, pp. 8356-8366, 2012.

Chapter 7

APPENDIX

7.1 Perturbational Approach to the Nonlinear Schrödinger Equation

This chapter contains an analytical approach to assess the impact of a variance of the duty-cycle on the nonlinear distortion caused by intra-channel Four-wave-mixing (IFWM) [1, 2].

The nonlinear Schrödinger equation (NLSE) is given by:

$$\frac{\partial U}{\partial z} + \frac{\alpha}{2}U + j\frac{\beta_2}{2}\frac{\partial^2 U}{\partial T^2} = j\gamma|U^2|U \tag{77}$$

With $T = t - z/\vartheta_G \equiv t - \beta_1 z$ being a frame of reference moving with the pulse at the group velocity ϑ_G. The transmission fibre has the attenuation coefficient α and the chromatic dispersion coefficient β_2. Considering that $U^{(l)}$ satisfies the linear Schrödinger equation:

$$\frac{\partial U^{(l)}}{\partial z} = -\frac{\alpha}{2}U^{(l)} - j\frac{\beta_2}{2}\frac{\partial^2 U^{(l)}}{\partial T^2} \tag{78}$$

The perturbation approach is justified, assuming that nonlinearity causes only a small distortion $\Delta U(z,T)$ to the linear solution.

$$U(z,T) \cong U^{(l)} + \Delta U(z,T) \tag{79}$$

Suppose the transmission of a sequence of k Gaussian pulses with a $1/e$-width T_0, related to the full-width-half-maximum (FWHM) by $T_{FWHM} = 1.66 \cdot T_0$, separated by T_S. The modulation information of each pulse is given by X_k.

$$U^{(l)}(z,T) = \sum_k \underbrace{\frac{T_0 \cdot exp(-\alpha z/2)}{\sqrt{T_0^2 - j\beta_2 z}} exp\left\{-\frac{(T-kT_S)^2}{2(T_0^2 - j\beta_2 z)}\right\}}_{U_k} \cdot \underbrace{A_k exp(j\varphi_k)}_{X_k} \quad (80)$$

The perturbation term satisfies:

$$\frac{\partial \Delta U}{\partial z} + \frac{\alpha}{2}\Delta U + j\frac{\beta_2}{2}\frac{\partial^2 \Delta U}{\partial T^2} = j\gamma \left|U^{(l)2}\right| U^{(l)} = j\gamma \sum_{l,m,n} U_l U_m U_n^* \cdot X_l X_m X_n^* \quad (81)$$

Now it is possible to separate different nonlinearities. Intra-channel Self-phase modulation (ISPM) is a modulation of the pulses phase by its own intensity ($l = m = n$). Intra-channel Cross-phase modulation (IXPM) involves the phase-modulation induced by the intensity of another pulse (on pulse m: $l = n \neq m$, on pulse l: $m = n \neq l$ or on pulse n: $m = l \neq n$), whereas in the presence of large pulse overlap intra-channel Four-wave-mixing (IFWM) involves pulses satisfying $k = l + m - n$.

Since pure phase-modulation does not change the pulse shape, SPM and IXPM are neglected in the following because they affect every pulse in the same way. If we concentrate on the distortion incident on the pulse in slot $k = 0$, we can set $n = l + m$.

$$\frac{\partial \Delta U_0}{\partial z} + \frac{\alpha}{2}\Delta U_0 + j\frac{\beta_2}{2}\frac{\partial^2 \Delta U_0}{\partial T^2} = j\gamma \left|U^{(l)2}\right| U^{(l)} = j\gamma \sum_{l,m\neq 0} U_l U_m U_{l+m}^* \cdot X_l X_m X_{l+m}^* \quad (82)$$

Assuming superposition principle for all contributions to the nonlinear distortion leads to:

$$\Delta U_0 = \sum_{l,m\neq 0} \Delta U_{l,m,l+m} \quad (83)$$

and eventually to:

$$\frac{\partial \Delta U_{l,m,l+m}}{\partial z} + \frac{\alpha}{2}\Delta U_{l,m,l+m} + j\frac{\beta_2}{2}\frac{\partial^2 \Delta U_{l,m,l+m}}{\partial T^2} = \underbrace{j\gamma U_l U_m U_{l+m}^* \cdot X_l X_m X_{l+m}^*}_{F(z,T)} \quad (84)$$

The nonlinear force $F(z,T)$ can be normalised to:

$$F(z,T) = j\gamma A(z) exp\{-a(z)T^2 + b(z)T \cdot T_S - c(z)T_S^2\} \quad (85)$$

Containing the following terms:

$$A(z) = \frac{T_0^3 \cdot X_l X_m X_{l+m}^* \cdot exp(-3\alpha z/2)}{\sqrt{|r|^2 r}} \quad (86) \qquad a(z) = \frac{1}{2}\left(\frac{1}{r^*} + \frac{2}{r}\right) \quad (87)$$

$$b(z) = \frac{l+m}{r^*} + \frac{l+m}{r} \quad (88) \qquad c(z) = \frac{1}{2}\left[\frac{(l+m)^2}{r^*} + \frac{l^2+m^2}{r}\right] \quad (89)$$

with $r = T_0^2 - j\beta_2 z$. Transforming (85) into the frequency domain yields:

$$\tilde{F}(z,\omega) = j\gamma A(z)\sqrt{\frac{\pi}{a(z)}}exp\left\{-c(z)T_S^2 - \frac{[b(z)T_S - j\omega]^2}{4a(z)}\right\} \quad (90)$$

Now, we assume large pulse overlap $|\beta_2|z \gg T_0^2 \rightarrow r \sim -j\beta_2 z$, which considerably simplifies (86)-(89) :

$$A(z) = \frac{T_0^3 \cdot X_l X_m X_{l+m}^* \cdot exp(-3\alpha z/2)}{-|\beta_2|z \cdot \sqrt{j\beta_2 z}} \quad (91) \qquad a(z) \sim \frac{1}{2r} \quad (92)$$

$$b(z) \sim 0 \quad (93) \qquad c(z) \sim -\frac{lm}{r} \quad (94)$$

Consequently (90) can be rewritten as:

$$\tilde{F}(z,\omega) \sim j\gamma A(z) \cdot \sqrt{2\pi r} \cdot exp\left(\frac{lm}{r}T_S^2 - \frac{r}{2}\omega^2\right) \quad (95)$$

After propagating through a single span the waveform is dispersion compensated and amplified. Therefore, at $z = L$ the IFWM distortion accumulates to a field, which is given in the time domain:

$$\Delta U_0(L,T) = \int_0^L \sum_{l,m\neq 0} \mathcal{F}^{-1}\left\{\tilde{F}(z,\omega) \cdot exp\left(\underbrace{\frac{\alpha}{2}z}_{\substack{ideal \\ amplification}} \underbrace{-j\frac{\beta_2}{2}z\omega^2}_{\substack{ideal\ dispersion \\ compensation}}\right)\right\} dz \quad (96)$$

Herein, inverse Fourier transform is given by:

$$\mathcal{F}^{-1}\left\{\tilde{F}(z,\omega) \cdot exp\left(\frac{\alpha}{2}z - j\frac{\beta_2}{2}z\omega^2\right)\right\} = \frac{j\gamma A(z)}{\sqrt{1 + j2\beta_2 z a(z)}} \cdot exp\left(-\frac{a(z)T^2}{1 + j2\beta_2 z a(z)} - c(z)T_S^2\right) \cdot exp\left(\frac{\alpha}{2}z\right) \quad (97)$$

Inserting (91)-(94) and (97) into (96) leads to an expression for the nonlinear distortion caused by IFWM:

$$\Delta U_0(L,T) = \sum_{l,m\neq 0} j\gamma\, exp\left(-\frac{T^2}{6T_0^2}\right)\cdot X_l X_m X_{l+m}^* \cdot \int_0^L \frac{exp(-\alpha z)}{\sqrt{1+j\,2\beta_2 z/T_0^2 + 3(\beta_2 z/T_0^2)^2}} \cdot exp\left\{-\frac{3(2T/3 - lT_S)(2T/3 - mT_S)}{T_0^2 + j3\beta_2 z} - \frac{(m-l)^2 T_S^2}{T_0^2[1+j\,2\beta_2 z/T_0^2 + 3(\beta_2 z/T_0^2)^2]}\right\} dz \quad \textbf{(98)}$$

For lossless fibre ($\alpha = 0$) one can approximate the integral in (98) with the exponential integral function $\mathrm{E}_1(x) = \int_1^\infty T^{-1}\exp(-xT)\,dT$ yielding:

$$\Delta U_0(L,T) = \sum_{l,m\neq 0} j\gamma\, exp\left(-\frac{T^2}{6T_0^2}\right)\cdot X_l X_m X_{l+m}^* \cdot \frac{T_0^2}{\sqrt{3}|\beta_2|}\cdot \mathrm{E}_1\left(-j\frac{lmT_S^2}{\beta_2 L}\right) \quad \textbf{(99)}$$

From equation (99) you can see, that the IFWM-distortion is a Gaussian shaped pulse with a pulse-width of $\sqrt{3}T_0$. The average input power of the optical pulse train is given by:

$$\mathrm{P}_0 = \sqrt{\pi}\mathrm{A}_0^2\frac{\mathrm{T}_0}{\mathrm{T}_\mathrm{S}} \quad \textbf{(100)}$$

Therefore the amplitude distortion relative to A_0 is proportional to the pulse-width and input power of the signal.

$$\frac{\Delta U_0(L,0)}{A_0} \sim \mathrm{P}_0 T_0 \quad \textbf{(101)}$$

Figure 79 shows the normalised peak phase shift induced to a pulse at $t = 0$ by considering contributions of $l = \mp 1$ and $m = \pm 1$. The integration of equation (98) and (99) has been done assuming a lossless (α=0 dB/km) SSMF fibre (D=16 ps/(km·nm), γ=1.2 W/km) with a length L of up to 800 km. The modulation format was BPSK with a bitrate of 40 Gbit/s and pulse-widths of $T_0 = 5.02$ ps, $T_0 = 7.53$ ps and $T_0 = 10.1$ ps are equivalent to RZ-67, RZ-50 and RZ-33, respectively.

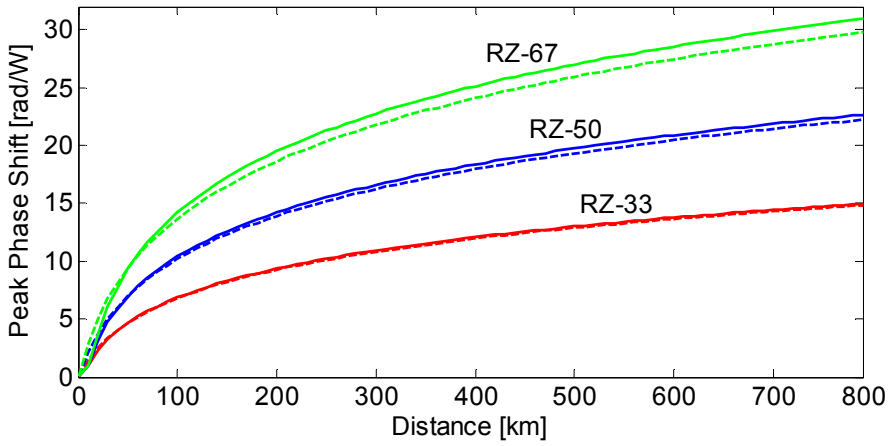

Figure 79: Peak Phase Shift involving contributions of $l = \mp 1$ and $m = \pm 1$ over a distance of lossless 800 km SSMF. The solid lines denote exact integration (98) and the dashed lines approximation by the exponential integral function (99) [2].

A full characterisation of the nonlinear behaviour of higher order modulation formats is very time consuming, since every possible contribution of overlapping pulses has to be taken into account. This leads to M^n symbol-sequences to be simulated, for a modulation format with M different symbols. For a signal with symbol-rate R_S, bandwidth Δf experiencing a maximum accumulated dispersion of D_{max}, n is defined as follows [3]:

$$n \geq |D_{max}| \lambda^2 R_S \frac{\Delta f}{c} \tag{102}$$

with λ being the optical transmission wavelength and c the speed of light. For QAM-16 transmission at 10 GBd (40 Gbit/s) over 800 km of electronically compensated SSMF (D_{max}=12800 ps/nm) n would be 11, leading to more than 4 million different sequences to be simulated.

7.2 MATLAB Code

In this section an example of the MATLAB code used to generate WDM-signals of arbitrary modulation format, wavelength spacing and symbol-rate is given. It should be noted that previous work has concluded that most of the nonlinear penalty is obtained from the neighbouring channels so that in most cases the simulation of a subset of channels is sufficient to quantify the total penalty. For example, to model a 40-channel system, the simulations can be carried out for 3, 5, 7…channels until no further significant penalty is obtained from adding more channels. However, with reduced wavelength-spacings it is important to model an increasing number of WDM-channels and maintain a minimum simulation bandwidth as illustrated in section 5.3.

```
load('RandomNumberSeed')
CentralChannel=ceil(P.NumberOfChannels/2);

%% loop for Polmux
for Pol=1:Signal.Polmux+1
    FieldBuffer=zeros(2,Signal.Nt);

    %% Generate laser combs
    for ChannelNo=1:P.NumberOfChannels

        disp(strcat('processing polarisation',num2str(Pol),' channel
        #',num2str(ChannelNo),''))

        %% CW laser
        P.CW.Offset=(ChannelNo-P.NumberOfChannels/2)*P.OptFilt.BW-
        P.OptFilt.BW/2;     %GHz
        SignalCW=CWLaser(Signal,P.CW);

        if ChannelNo~=CentralChannel
            Seed=RandomNumberSeed(ChannelNo,Pol);
        else
            Seed=Signal.Seed(Pol);
        end

        %% Modulate
        switch Signal.ModFormat
            case 'BPSK'
                %% Generate driving signals
                if ChannelNo==CentralChannel
                    if Signal.Differential
                        Drive=coderDBPSK(Signal,Seed);
                    else
                        Drive=coderBPSK(Signal,Seed);
                    end
                else
                    Drive=coderBPSK(Signal,Seed);
                end

                %% Low pass filter to simulate limited bandwidth of
                electronics
                Drive=BesselLowPassFilter(Drive,P.ElectrFilt);

                %% MZI
                SignalMod=PushPullMZModulator(Drive,SignalCW,P.MZI);

            case 'QPSK'
                %% Generate driving signals
                if ChannelNo==CentralChannel
                    if Signal.Differential
                        [Qdrive,Idrive]=coderDQPSK(Signal,Seed);
                    else
                        [Qdrive,Idrive]=coderQPSK(Signal,Seed);
                    end
                else
                    [Qdrive,Idrive]=coderQPSK(Signal,Seed);
                end

                %% Low pass filter to simulate limited bandwidth of
                electronics
                Qdrive=BesselLowPassFilter(Qdrive,P.ElectrFilt);
                Idrive=BesselLowPassFilter(Idrive,P.ElectrFilt);

                %% IQ Modulator
                SignalI=PushPullMZModulator(Idrive,SignalCW,P.MZI);
                SignalQ=PushPullMZModulator(Qdrive,SignalCW,P.MZI);
                SignalQ.Et=SignalQ.Et.*exp(1i*pi/2);
                SignalMod=SignalI;
```

```
        SignalMod.Et=SignalI.Et+SignalQ.Et;

    case '8PSK'
        %% Generate driving signals
        if ChannelNo==CentralChannel
            if Signal.Differential
                [Qdrive,Idrive,PMdrive]=coderD8PSK(Signal,Seed);
            else
                [Qdrive,Idrive,PMdrive]=coder8PSK(Signal,Seed);
            end
        else
            [Qdrive,Idrive,PMdrive]=coder8PSK(Signal,Seed);
        end

        %% Low pass filter to simulate limited bandwidth of
        electronics
        Qdrive=BesselLowPassFilter(Qdrive,P.ElectrFilt);
        Idrive=BesselLowPassFilter(Idrive,P.ElectrFilt);
        PMdrive=BesselLowPassFilter(PMdrive,P.ElectrFilt);

        %% IQ Modulator
        SignalI=PushPullMZModulator(Idrive,SignalCW,P.MZI);
        SignalQ=PushPullMZModulator(Qdrive,SignalCW,P.MZI);
        SignalQ.Et=SignalQ.Et.*exp(1i*pi/2);
        SignalIQ=SignalI;
        SignalIQ.Et=SignalI.Et+SignalQ.Et;

        %% Phasemodulator
        SignalMod=PhaseModulator(SignalIQ,PMdrive,P.MZI);

    case '16PSK'
        %% Generate driving signals
        if ChannelNo==CentralChannel
            if Signal.Differential
         [Qdrive,Idrive,PM45drive,PM22drive]=coderD16PSK(Signal,Seed);
            else
         [Qdrive,Idrive,PM45drive,PM22drive]=coder16PSK(Signal,Seed);
            end
        else
         [Qdrive,Idrive,PM45drive,PM22drive]=coder16PSK(Signal,Seed);
        end

        %% Low pass filter to simulate limited bandwidth of
        electronics
        Qdrive=BesselLowPassFilter(Qdrive,P.ElectrFilt);
        Idrive=BesselLowPassFilter(Idrive,P.ElectrFilt);
        PM45drive=BesselLowPassFilter(PM45drive,P.ElectrFilt);
        PM22drive=BesselLowPassFilter(PM22drive,P.ElectrFilt);

        %% IQ Modulator
        SignalI=PushPullMZModulator(Idrive,SignalCW,P.MZI);
        SignalQ=PushPullMZModulator(Qdrive,SignalCW,P.MZI);
        SignalQ.Et=SignalQ.Et.*exp(1i*pi/2);
        SignalIQ=SignalI;
        SignalIQ.Et=SignalI.Et+SignalQ.Et;

        %% Phasemodulator 45deg
        SignalPM=PhaseModulator(SignalIQ,PM45drive,P.MZI);

        %% Phasemodulator 22deg
        SignalMod=PhaseModulator(SignalPM,PM22drive,P.MZI);

    case '8QAM'
        %% Generate driving signals
        if ChannelNo==CentralChannel
            if Signal.Differential
              [outerDrive,innerDrive,PMdrive]=coderD8QAM(Signal,Seed);
```

```
            else
              [outerDrive,innerDrive,PMdrive]=coder8QAM(Signal,Seed);
            end
        else
            [outerDrive,innerDrive,PMdrive]=coder8QAM(Signal,Seed);
        end

        %% Low pass filter to simulate limited bandwidth of
        electronics
        outerDrive=BesselLowPassFilter(outerDrive,P.ElectrFilt);
        innerDrive=BesselLowPassFilter(innerDrive,P.ElectrFilt);
        PMdrive=BesselLowPassFilter(PMdrive,P.ElectrFilt);

        %% IQ Modulator
        SignalI=PushPullMZModulator(innerDrive,SignalCW,P.MZI);
        SignalQ=PushPullMZModulator(outerDrive,SignalCW,P.MZI);
        SignalI.Et=SignalI.Et.*exp(1i*(pi/4));
        SignalIQ=SignalI;
        SignalIQ.Et=SignalI.Et+SignalQ.Et;

        %% correcting phase offset (cosmetic effect)
        SignalIQ.Et=SignalIQ.Et.*exp(1i*(pi/2-0.2604));

        %% phasemodulator
        SignalMod=PhaseModulator(SignalIQ,PMdrive,P.MZI);

    case '16QAM'
        %% Generate driving signals
        if ChannelNo==CentralChannel
            if Signal.Differential
                [Qdrive,Idrive]=coderD16QAM(Signal,Seed);
            else
                [Qdrive,Idrive]=coder16QAM(Signal,Seed);
            end
        else
            [Qdrive,Idrive]=coder16QAM(Signal,Seed);
        end

        %% Low pass filter to simulate limited bandwidth of
        electronics
        Qdrive=BesselLowPassFilter(Qdrive,P.ElectrFilt);
        Idrive=BesselLowPassFilter(Idrive,P.ElectrFilt);

        %% IQ Modulator (odd channels)
        SignalI=PushPullMZModulator(Idrive,SignalCW,P.MZI);
        SignalQ=PushPullMZModulator(Qdrive,SignalCW,P.MZI);
        SignalQ.Et=SignalQ.Et.*exp(1i*pi/2);
        SignalMod=SignalI;
        SignalMod.Et=SignalI.Et+SignalQ.Et;

    case 'PSQPSK'
        Signal.Polmux=0;
        %% Generate driving signals
        if ChannelNo==CentralChannel
            if Signal.Differential
                [Qdrive,Idrive,PolDrive]=coderDPSQPSK(Signal,Seed);
            else
                [Qdrive,Idrive,PolDrive]=coderPSQPSK(Signal,Seed);
            end
        else
            [Qdrive,Idrive,PolDrive]=coderPSQPSK(Signal,Seed);
        end

        %% Low pass filter to simulate limited bandwidth of
        electronics
        Qdrive=BesselLowPassFilter(Qdrive,P.ElectrFilt);
        Idrive=BesselLowPassFilter(Idrive,P.ElectrFilt);
        PolDrive=BesselLowPassFilter(PolDrive,P.ElectrFilt);
```

```
                %% IQ Modulator
                SignalI=PushPullMZModulator(Idrive,SignalCW,P.MZI);
                SignalQ=PushPullMZModulator(Qdrive,SignalCW,P.MZI);
                SignalQ.Et=SignalQ.Et.*exp(1i*pi/2);
                SignalMod=SignalI;
                SignalMod.Et=SignalI.Et+SignalQ.Et;

                %% Polshift stage
                PolDriveX = PolDrive;
                PolDriveY = PolDrive;
                PolDriveY.Et = 0.5-1*(PolDriveY.Et-0.5);
                P.AM.Vpi = 1;
                P.AM.Vbias=0;

                %% PBS
                SignalModX = PushPullMZModulator(PolDriveX,SignalMod,P.AM);
                SignalModY = PushPullMZModulator(PolDriveY,SignalMod,P.AM);

                %% PBC
                SignalMod = SignalModX;
                SignalMod.Et(2,:)=SignalModY.Et(1,:);

            end

            %% Construct WDM signal
            FieldBuffer=FieldBuffer+SignalMod.Et;
            if ChannelNo==CentralChannel
                InfoBuffer=SignalMod;
            end
        end

        Signal=InfoBuffer;
        Signal.Et=FieldBuffer;

        %% pulse carver
        sinus=Signal;
        sinus.Et=Bias + Amplitude.*sin(2*pi*Frequency*1e-3.*sinus.TT + Phase);
        Signal=PushPullMZModulator(sinus,Signal,P.MZI);

        if P.NumberOfChannels>1
            %% MUX
            if Pol==1
                SignalMux=AWGmux(Signal,P);
            else
                SignalMuxY=AWGmux(Signal,P);

                SignalMux.Et(2,:)=SignalMuxY.Et(1,:);
                SignalMux.Data(2,:)=SignalMuxY.Data(1,:);
                SignalMux.CodedData(2,:)=SignalMuxY.CodedData(1,:);
            end
        else
            %% Gaussian Optical Filter
            if Pol==1
                SignalMux = GaussianOpticalFilter(Signal,P.OptFilt);
            else
                SignalMuxY = GaussianOpticalFilter(Signal,P.OptFilt);

                SignalMux.Et(2,:)=SignalMuxY.Et(1,:);
                SignalMux.Data(2,:)=SignalMuxY.Data(1,:);
                SignalMux.CodedData(2,:)=SignalMuxY.CodedData(1,:);
            end
        end
    end
```

7.3 References

[1] A. Mecozzi, C. B. Clausen, and M. Shtaif, "Analysis of intrachannel nonlinear effects in highly dispersed optical pulse transmission " *Photonics Technology Letters,* vol. 12, pp. 392-394, 2000.

[2] K.-P. Ho, *Phase Modulated Optical Communication Systems*: Springer, 2005.

[3] L. K. Wickham, R. J. Essiambre, A. H. Gnauck, P. J. Winzer, and A. R. Chraplyvy, "Bit pattern length dependence of intrachannel nonlinearities in pseudolinear transmission," *Photonics Technology Letters,* vol. 16, pp. 1591-1593, 2004.

Chapter 8

LIST OF ACRONYMS

ADC	Analogue to Digital Converter
AM	Amplitude Modulator
AOM	Accousto Optic Modulator
(D)16PSK	(Differential) 16 Phase Shift Keying
(D)16QAM	(Differential) 16 Quadrature Amplitude Modulation
(D)8PSK	(Differential) 8 Phase Shift Keying
(D)8QAM	(Differential) 8 Quadrature Amplitude Modulation
(D)BPSK	(Differential) Binary Phase Shift Keying
(D)QPSK	(Differential) Quadrature Phase Shift Keying
(I)FWM	(Intra-channel) Four Wave Mixing
IMDD	Intensity Modulation Direct Detection
(I)XPM	(Intra-channel) Cross Phase Modulation
(O)SNR	(Optical) Signal to Noise Ratio
APSK	Amplitude Phase Shift Keying
ASE	Amplified Spontaneous Emission
ASIC	Application Specific Integrated Circuit
BASK	Binary Amplitude Shift Keying
BER	Bit Error Rate
CMA	Constant Modulus Algorithm
CMOS	Complementary Metal-Oxide Semiconductor
CW	Continuous Wave
DAC	Digital to Analogue Converter
DBP	Digital Backpropagation
DC	Direct Current
DCA	Digital Communications Analyzer
DCF	Dispersion Compensating Fibre

DFB	Distributed Feedback Laser
DFE	Decision Feedback Equaliser
DGD	Differential Group Delay
DLI	Delay Line Interferometer
DSO	Digital Sampling Oscilloscope
DSP	Digital Signal Processing
EAM	Electro Absorption Modulator
ECL	External Cavity Laser
EDFA	Erbium Doped Fibre Amplifier
FEC	Forward Error Correction
FFE	Feed Forward Equaliser
FFT	Fast Fourier Transform
FIR	Finite Impulse Response Filter
FSR	Free Spectral Range
FWHM	Full Width Half Maximum
GFF	Gain Flattening Filter
ISI	Inter-Symbol-Interference
LMS	Least Mean Square Algorithm
LO	Local Oscillator
LSPS	Loop Synchronous Polarisation Scrambler
MAP	Maximum a Posteriori
MIMO	Multiple Input Multiple Output
MLSE	Maximum Likelihood Sequence Estimation
MZI	Mach Zehnder Interferometer
NLPN	Nonlinear-Phase-Noise
NLSE	Nonlinear-Schrödinger-Equation
NRZ	Nonreturn to Zero
NZDSF	Non-Zero Dispersion Shifted Fibre
OFDM	Orthogonal Frequency Domain Multiplex
OOK	On Off Keying
OTDM	Optical Time Domain Multiplex
PBC	Polarisation Beam Combiner
PBS	Polarisation Beam Splitter
PDL	Polarisation Dependent Loss
PDM	Polarisation Division Multiplex
PM	Phase Modulator
PMD	Polarisation Mode Dispersion
PPG	Pulse Pattern Generator

PRBS	Pseudo Random Binary Sequence
PS-QPSK	Polarisation Switched Quadrature Phase Shift Keying
PSD	Power Spectral Density
PSK	Phase Shift Keying
QAM	Quadrature Amplitude Modulation
RDE	Radially Directed Equaliser
rOSNR	required Optical Signal to Noise Ratio
RZ	Return to Zero
SER	Symbol Error Rate
SOP	State of Polarisation
SDM	Spatial Division Multiplex
SPM	Self-Phase Modulation
SSMF	Standard Single Mode Fibre
VOA	Variable Optical Attenuator
WDM	Wavelength Division Multiplex
XPolM	Cross Polarisation Modulation